An assessment of the mechanics of protected and unprotected head impacts in cricket using representative impact conditions and a sport-specific anthropomorphic test device

AN ASSESSMENT OF THE MECHANICS OF PROTECTED AND UNPROTECTED HEAD IMPACTS IN CRICKET USING REPRESENTATIVE IMPACT CONDITIONS AND A SPORT SPECIFIC ANTHROPOMORPHIC TEST DEVICE

A doctoral thesis submitted in partial fulfilment of the requirements for the award of Doctor of Philosophy of Loughborough University

by

Ben William Stone

Wolfson School of Mechanical, Electrical and Manufacturing Engineering

Loughborough University

United Kingdom

November 2019

ABSTRACT

The fundamental aim of the research presented in this thesis was to investigate the mechanics of protected and unprotected head impacts in Cricket through the development of enhanced, laboratory-based projectile tests. In order to develop an improved test methodology, research was conducted to; (1) establish the properties of cricket balls at realistic loading rates, (2) determine appropriate impact conditions to represent those seen in real-life impacts, and (3) develop a novel, sport-specific headform (LU headform), that could be used in protected and unprotected impacts. An additional aim was to assess the validity of the impact attenuation test currently specified in the British Standard for head protectors for cricketers (BS 7928:2013), by comparing the mechanics of the impacts observed in these drop tests to those observed in more realistic projectile impacts.

The properties of two elite level Cricket balls (Dukes Special County and Kookaburra Turf) and one Cricket training ball (BOLA) were assessed at three nominal initial loading rates c. 4.5, 18 and 31 m/s). This study found that Cricket balls exhibit different characteristics based on the construction and materials used, the orientation of the ball at impact, and the level of wear. The Dukes ball were at least 15% stiffer than the Kookaburra balls, and the Kookaburra balls were at least 9% stiffer when impacted perpendicular to the seam than when impacted parallel to the seam. The BOLA ball was found to be at least three times more compliant than the two Cricket balls tested. After 20 repeated high-speed impacts, the Dukes and Kookaburra balls were found to be at least 36.3 and 20.5% more compliant respectively. As a result of these findings, the Kookaburra ball was selected for future impact tests due to improved ball to ball variation and reduced ball degradation. Non-destructive 4.5 m/s impact tests were also integrated into projectile tests to ensure that the ball properties remained within 5% of the pre impact stiffness.

A representative impact speed was determined by using ball tracking data collected during match play. A database containing measured release speeds of 447 elite level bowlers was used to identify the maximum observed release speed (43 m/s). Ball tracking data was also used to determine the release speed and the speed at which the ball passed the batsman (inception speed) from a sample of short length deliveries. A ~worst case impact speed was determined by dividing the highest release speed in the database by the lowest percentage change in speed from release to inception. This resulted in a nominal impact speed of 34.7 m/s. Three anatomically anchored impact locations were defined to generate linear and angular motion in six degrees of freedom. Each headform was suspended using bungee cords to simulate the passive stiffness of the human neck and therefore a ~worst-case scenario with respect to the observed dynamic response.

Due to the construction and materials used in commercially available headforms, the development of a headform that was capable of producing realistic first order dynamic responses during projectile impacts was deemed necessary for the assessment of protected and unprotected scenarios (LU headform). External soft tissue, bone and brain components were modelled in Siemens NX 10.0 based on CT and MRI scans. The geometry of the model was manipulated to match that reported for a 50th percentile UK male, and tissue thicknesses were measured to be within previously reported ranges. The inertial properties (including principal moment of inertia, Moment of inertia about axes at the centre of gravity and location of the Centre of Gravity) were theoretically calculated and empirically measured to be closer to the average values reported for human heads than commercially available headforms. The inherent validity of the LU headform was established through material tests which showed each component to be comparable to values reported for human tissue. In addition, the resonance frequency of the skull component of the LU headform was found to be comparable to that reported for dry human skulls. The response of the LU headform during drop test and projectile impact tests was found to be within the range reported in human cadaver responses with similar impact conditions.

This research facilitated the development of a test methodology to investigate the mechanics of head impacts observed in Cricket, that was superior to that achieved in previous research. Four headforms (EN 960, Hybrid-III, NOCSAE and LU) were instrumented with a ±2000 g triaxial linear accelerometer and ±6000 deg/sec triaxial angular rate sensor and subjected to projectile impacts at three locations, when protected by two helmet types used at the professional level in the 2018 season. The Hybrid-III and LU headforms were also subjected to unprotected impacts at the same three impact locations.

Headform type and impact location was found to significantly influence the observed dynamic response during the projectile impacts. The EN 960 headform was found to be unsuitable in this impact scenario as the sensor mounting block introduced non-biofidelic frequency artefacts that could not be removed without significant signal distortion. When using the LU headform, frequency artefacts were also evident in the measured signal that were in line with the measured resonance frequency of the skull component. This concurs with the findings of previous research using human cadavers with similar impact conditions (Raymond et al., 2008) and was therefore considered a legitimate response phenomenon. The NOCSAE headform produced a response comparable to the LU headform. Alternatively, the Hybrid-III responded predominantly as a rigid body and therefore overlooked the potentially important resonance frequency excitation. As a result of the resonance frequency excitation, the LU and NOCSAE headforms produced higher peak resultant linear acceleration, impulse, head injury criteria (HIC), maximum angular velocity and brain injury criteria (BrIC) values, in addition to longer contact times.

This study is the first of its kind to assess unprotected head impacts in Cricket and therefore the first opportunity to compare the true performance of helmets relative to unprotected scenarios. Both helmet types tested were found to reduce the linear and angular response observed during impact, and prevent skull fracture that was observed at one location when using the LU headform. When using the Hybrid-III headform, the peak resultant linear acceleration, maximum angular velocity, HIC and BrIC values were reduced by at least 39.9, 37.9, 69.6 and 32.3% respectively when helmeted. When using the LU headform, peak resultant linear acceleration, maximum angular velocity, HIC, BrIC calculated using maximum angular velocity and BrIC calculated using steady state angular velocity were reduced by at least 32.9, 25.7, 15.0, 32.05 and 13.86% respectively when helmeted. When using the LU headform the HIC values were found to be alarmingly high, even in the helmeted scenarios. However, as the HIC was not developed for short duration impacts where resonance frequency excitation is likely to occur, this metric should be used with caution. These results highlight the need for further investigations into injury mechanisms in projectile head impacts and the development of injury metrics specifically for this impact scenario. Repeated impacts at one impact location on the helmets were found to significantly reduce their ability to attenuate the observed linear and angular response, despite minimal external damage.

Drop test were also conducted as specified in the current British Standard (BS 7928:2013) with the same helmet types and impact locations used in the projectile tests. The drop tests were found to produce contact time and time to peak resultant linear acceleration at least 61.4 and 59.9% longer than the projectile tests respectively. With the exception of one helmet type at one impact location, peak resultant linear acceleration was at least 161.8% lower in the standard drop tests. From these results it can be concluded that although the standard tests achieved what it intended to (i.e. preventing skull fracture), the mechanics of these impacts are unrepresentative of those seen in real-life impacts.

Overall, the research presented in this study facilitated the assessment of laboratory-based head impacts representative of those seen in Cricket and highlighted the importance of suitable human surrogates during testing. The results presented in this thesis can be used in future work to; improve helmet design (through access to more realistic response data), develop and validate finite element models to investigate injury mechanisms, and in the development of impact specific injury metrics.

ACKNOWLEDGEMENTS

I would like to thank my supervisors, Professor Andy Harland and Dr Sean Mitchell who were always forthcoming with advice and expertise, and pushed me to be better. Thanks also to Dr Ben Halkon who started the project before making the move down under. Furthermore, a huge thanks must also go to Steve Carr and Max Farrand who went above and beyond to supply unrivalled craftsmanship and technical assistance.

Thank you to my Sports Tech colleagues who provided advice, support and an extra pair of hands when needed.

Finally, I am most grateful to my family and friends who have been a constant source of support and an outlet away from it all.

PUBLICATIONS ARISING FROM THIS RESEARCH

STONE BW, AR HARLAND, JA JONES, SR MITCHELL, P SHERRATT, C RANSON, BJ HALKON. 2017. On the dynamic response of an instrumented headform for alternative mounting stiffness when subjected to ballistic impacts. *Proceedings of the Institution of Mechanical Engineers Part P Journal of Sports Engineering and Technology*. 231(4). 324-335.

STONE BW, SR MITCHELL, Y MIYAZAKI, N PEIRCE, AR HARLAND. 2019. Development of a frangible headform for the assessment of protected and unprotected impacts typical of those observed in sports. *Submitted to Proceedings of the Institution of Mechanical Engineers Part P Journal of Sports Engineering and Technology – Special Issue Physical (Mechanical) Models for Sports Equipment Research, Development and Testing.*

STONE BW, SR MITCHELL, BJ HALKON, N PEIRCE, AR HARLAND. 2019. The dynamic properties of Cricket and Cricket training balls. *Submitted to Sports Engineering.*

STONE BW, BJ HALKON, AR HARLAND. 2016. Headform Mounting Performance in Cricket Standard Testing. *Procedia Engineering 147. 11th Conference of the International Sports Engineering Association ISEA 2016.* 401-406

STONE BW, BJ HALKON, AR HARLAND. 2016. An explorative study into the mechanics of projectile impacts to the head. *Proceedings of the International Research Council on the Biomechanics of Injury IRCOBI Conference 2016.*

TABLE OF CONTENTS

LIST OF FIGURES

LIST OF TABLES

ABBREVIATIONS

PPE – Personal Protective Equipment
ECB – England and Wales Cricket Board
ATD – Anthropomorphic test device
BS – British Standard
AIS – Abbreviated Injury Scale
mTBI – Mild Traumatic Brain Injury
RFU – Rugby Football Union
NFL – National Football League
CTE – Chronic Traumatic Encephalopathy
US(A) – United States (of America)
UK – United Kingdom

NCAA – National Collegiate Athletic Association
FIH – International Hockey Federation
ICC – International Cricket Council
CoG – Centre of Gravity
EAM – External Auditory Meatus
IMO – Inferior Margin of the Orbit
SD – Standard Deviation
MoI – Moment of inertia
PMHS – Post Mortem Human Subjects
FE – Finite Element
MLB – Major League Baseball
HIC – Head Injury Criteria
MCC – Marylebone Cricket Club
CT – Computerised Tomography
MRI – Magnetic Resonance Imaging
UCDBTM – University College Dublin Brain Trauma Model
DOF – Degrees of Freedom
WSTC – Wayne State Tolerance Curve
GSI – Gadd Severity Index
GAMBIT – Generalised Head Acceleration Model for Brain Injury Threshold
HIP – Head Impact Power
BrIC – Brain Injury Criterion
$BrIC_{SS}$ – BrIC value calculated using steady state angular velocity
$BrIC_{MAX}$ – BrIC value calculated using maximum angular velocity
PAIS*n* – Probability of sustaining AIS *n* injury
NOCSAE – National Operating Committee on Standards for Athletic Equipment
CoR – Coefficient of Restitution

fps – Frames per Second
HSV – High-Speed Video
LU – Loughborough University
GBP – Great British Pound
USD – United States Dollar
CAD – Computer Aided Design
PTFE – Polytetrafluoroethylene
PETG - Polyethylene Terephthalate Glycol
PLA - Polyactic Acid
ABS - Acrylonitrile Butadiene Styrene
FDM – Fused Deposition Modelling
EPS – Expanded Polystyrene

ω – Angular Velocity
α – Angular Acceleration
V and v – Velocity
m – Mass
k – Stiffness
ω_n – Natural Frequency
$\dot{x}$ – Initial Deformation Rate
ε_t – Tensile Strain
σ_t – Tensile Stress
ε_f – Flexural Strain
σ_f – Flexural Stress
ε – Engineering Strain
σ – Engineering Stress
Is – Inception speed
Rs – Release speed
T – Torque
I – Moment of inertia (used in equations)

CHAPTER 1

Introduction

1.1. Background

In recent times, head injuries in sport have become a prevalent topic, with much media attention and a number of high-profile lawsuits. Measures intended to prevent injury are therefore an important aspect of many sports (McIntosh and McCrory, 2005). As such, research has focussed on the mechanics of impacts, mechanisms of injury and the efficacy of Personal Protective Equipment (PPE) with varied impact conditions observed in sport. These studies have however focussed on relatively high-mass and low-velocity collisions, similar to those seen in American Football, Rugby and other contact sports. There is however limited research into impacts similar to those seen in Cricket, that have significantly different impact characteristics (i.e. a hard, low-mass ball with relatively high-velocity). As a result, the impact mechanics of these collisions may be significantly different to those observed in contact sports.

Cricket is played on a field, with boundaries of varied dimensions. All bowling and batting occurs in the middle of the field, on a pitch which is rectangular area that the Laws of Cricket (MCC) specify as 20.12 m long and 3.05 m wide. A designated member of the fielding team bowls a hard, leather bound ball towards a batsman who aims to score runs without losing his wicket. Prior to 1932, bowlers would predominantly aim at or around the stumps (71 cm tall and 22.8 cm wide). As a result, risk of injury from the ball impacting the upper body was minimal. However, during the infamous ‘bodyline tour’ of 1932-33, England bowlers adopted the controversial tactic of aiming directly at the body of the Australian batsmen by bowling a shorter length (making the ball bounce closer to the bowler). These shorter length deliveries, known as ‘bouncers’, have now been accepted as a legitimate tactic, and as a result the risk of impact injury to the upper body, neck and head has increased.

PPE is now commonplace in the game, with batsmen wearing protection on the lower and upper legs, groin, chest, arms, hands and neck, as well as helmets to protect the head and face. Although Patsy Hendren was initially ridiculed for wearing a self-designed ‘helmet’ in the 1930s, the potentially catastrophic consequence of a head impact has meant that, in modern Cricket, the helmet is considered a fundamental component of safe play which is utilised by batsmen, wicket keepers and closely positioned fielders. Indeed, the England and Wales Cricket Board (ECB) now mandate helmet use in professional Cricket when batting,

wicket keeping at the stumps and fielding within eight yards of the batsman's middle stump. In order to be worn in the professional game, helmets must pass the tests specified in the British Standard for head protectors worn by cricketers (BS 7928:2013), which includes a penetration test (intended to assess the helmets ability to prevent facial contact occurring) and drop test (intended to assess a helmets ability to attenuate impact energy).

Laboratory reconstructions are an important means of assessing the mechanics of an impact, and the performance of associated PPE in a controlled environment – an approach that has been used to good effect in a number of scenarios including sports, falls, automotive crashes and environments involving the emergency services (Allsop et al., 1988a; Gilchrist and Mills, 1996; McIntosh et al., 2000; R A Oeur et al., 2019; Post et al., 2016, 2013; Viano et al., 2005a). Anthropomorphic test devices (ATDs), also known as human surrogates, are an artificial representation of the human form (or components thereof) that offer a solution to the numerous challenges associated with using human cadavers (when referring to ATDs that represent the human head, the term 'headform' is commonly used). The ultimate goal of laboratory-based testing is to create reconstructions that are as close to those observed in real life as possible, through the use of appropriate strikers, impact conditions, and human surrogates with a suitable level of biofidelity (which is the term used to describe how closely the dynamic response of the surrogate approximates the response of a human during comparable loading conditions (Crandall et al., 2011)). However, if laboratory reconstructions are a poor representation those seen in real-life, the understanding of impacts mechanics, development of appropriate PPE, and representative standards tests are limited to observations made in potentially injurious, real-life events. In Cricket, the paucity of laboratory-based research into head impacts using realistic impact scenarios means the PPE development process is limited to the ineffective cycle shown in Figure 1 – based on limited observations made on real-life impacts and potentially unrealistic standard tests. Additionally, this cycle relies on the mass design and manufacture of varied helmet designs, thereby resulting in unnecessary time and financial expenditure (which is often passed to the consumer).

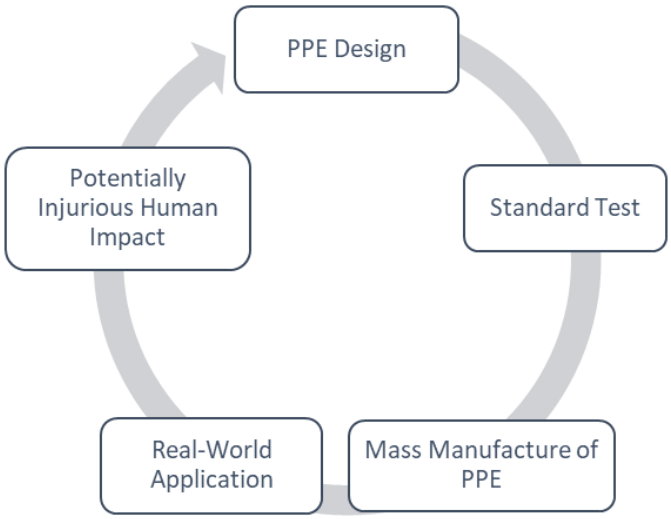

Figure 1. Current development cycle for Cricket helmets.

1.2. Research Aims

It is hypothesised that it is possible to develop improved laboratory-tests representative of those observed in Cricket. Improved laboratory-based tests would facilitate investigations into the mechanics of head impacts in Cricket and provide better means of assessing PPE performance and provide novel and important information to improve PPE design, and facilitate an assessment of the current impact attenuation test specified in the British Standard (BS 7928:2018). As such, the aims and objectives of the research presented in this thesis are to:

1) *Enhance laboratory test methods for the assessment of head impacts in Cricket*
   a) *Improve the understanding of the dynamic properties of Cricket balls at realistic loading rates*
   b) *Identify impact conditions representative of those seen in head impacts in Cricket*
   c) *Develop a sport specific headform surrogate, that is a better representation of the human form than those currently available*
2) *Improve the understanding of the mechanics of head impacts in Cricket in protected and unprotected scenarios*
3) *Assess the mechanics of the impact attenuation test currently specified in the British Standard for head protectors for cricketers (BS 7928:2013), relative to more realistic projectile impacts.*

As a result of the research aims and objectives, a series of key research questions have been formulated to provide structure and an objective means of assessing the success of the research presented in this thesis.

I. *What are the dynamic properties of Cricket balls at realistic loading rates?*
II. *What are appropriate impact conditions for the assessment of head impacts in Cricket?*
III. *Is the production of a headform with improved biofidelity, appropriate for potentially destructive projectile tests, possible considering time and financial constraints?*
IV. *Is the observed linear and angular response of a headform influenced by headform type and impact location during projectile impacts representative of those seen in Cricket?*
V. *How do currently available Cricket helmets influence the linear and angular response of the head during impacts in Cricket, relative to unprotected scenarios?*
VI. *Is the current impact attenuation test specified in BS 7928:2013 a suitable representation of real-life head impacts?*

CHAPTER 2

Literature Review

2.1. Categorising Head Injury

There are many different types of head injury that can occur in sport, ranging from extremely mild to life threatening. Superficial injures such as minor bruising or laceration of the face or scalp may be inconvenient, and at times painful, but are unlikely to be life changing. Traumatic brain injury, which is a result of external force(s) acting on the brain, can also range from temporary and mild to permanent and life threatening and be categorised based on severity or mechanism of injury. When considering mechanisms of injury, head injuries can be broken down into open or closed, with the former resulting from penetration of the scalp and skull, while in the latter, the skull and scalp remain intact.

The abbreviated injury scale (AIS) is widely used to classify traumatic brain injury, and has undergone a number of updates since its original development in 1971 (Rogers and Trickey, 2017). The AIS classifies injuries from 1 to 6, where AIS1 does not require hospitalisation and AIS6 is fatal (Gennarelli and Wodzin, 2008). Descriptions of AIS1-6 for brain injury can be found in Table 1.

Table 1. Description of AIS (Rogers and Trickey, 2017)

AIS 1	Cerebral injury, headache/dizziness, no loss of consciousness
AIS 2	Cerebral injury, with/without skull fracture, >15 mins loss of consciousness, no post event amnesia
AIS 3	Cerebral injury with/without skull fracture, <15 mins loss of consciousness, no severe neurological abnormalities, <3 hours post-event amnesia
AIS 4	Cerebral injury with/without skull fracture, <15 mins loss of consciousness, definite neurological abnormalities, 3-12 hours post event amnesia
AIS 5	Cerebral injury with/without skull fracture, >24 hours loss of consciousness, >12 hours post event amnesia, intracranial haemorrhage
AIS 6	Death

The term concussion is often used when describing brain injuries in sport. This term is however quite ambiguous, and an absolute definition is often debated (Hammond et al., 2015; McCroy et al., 2017). It is generally accepted that the term concussion refers to a temporary disruption of normal brain function as a result of mechanical force transmission to the brain and does not have to include a period of unconsciousness (Hammond et al., 2015). In this thesis, due to the potential ambiguity of the term concussion, mild traumatic brain

injury (mTBI) will be used as an umbrella term that encompasses concussion but does not exclude other related mild brain injuries. When ‘concussion’ is used in this thesis, it is limited to describing previous work that has used the term. When describing mTBI in sport, AIS1 would correspond to low end mTBI, whereas AIS2 would correspond to a moderate-severe mTBI.

2.2. Head injury Epidemiology in sport

2.2.1. Contact Sports

In contact sports such as American Football and Rugby, mechanisms such as player-player and player-ground impacts may lead to head injury. Brooks et al. (2005) monitored injuries to rugby union players over a two-year period and reported that player-player collisions were the most common mechanism of injury, accounting for 72% of all injuries. Of all injuries, mTBI were reported to be the third most common injury type, accounting for 4.4 injuries per 1000 player hours. Injury monitoring by the Rugby Football Union (RFU, 2015), concurred with Brooks et al. (2005) stating that the tackle was the most common match event leading to injury during the 2013-2014 Premiership season. It was also reported that head and neck injuries were the most common type of injury leading to player retirement.

Pellman et al. (2003) monitored mTBI in the National Football League (NFL) over a six-year period (1996-2001) and found mTBI to be a relatively common event, with 0.41 mTBIs occurring per NFL game. 68% of these mTBIs were caused by helmet-helmet collisions, 21% resulted from striking another region of another player and 11% resulted from contact with the ground. A follow up study by Casson et al. (2010) compared mTBI rates from 1996-2001 with those from 2002-2007. This study showed that the incidence of mTBI remained very similar over this period, however the percentage of players returning to play in the same game after sustaining an injury was significantly lower, and the time players were prevented from returning to play was longer. This suggests that although developments in PPE had little effect on the incidence of mTBI, the management of those that sustained mTBI were more conservative. Repeated mTBI and potentially sub-mTBI impacts in American Football have also been linked to the development of Chronic Traumatic Encephalopathy (CTE) (Omalu et al., 2005; Stern et al., 2011), a progressive degenerative disease that can affect the quality life of sportsmen in later life. The prevalence of CTE in deceased American Footballers was reported by Mez et al. (2017) who found CTE in 14.3% (n=14) of high school players, 90.6% (n = 53) of college players and 99% (n = 111) of NFL players assessed. These results are however likely to be skewed towards increased

prevalence, since those concerned about the presence of the disease would be more likely to donate deceased family members to the study.

2.2.2. Combat Sports

In combat sports such as boxing and the martial arts, inflicting physical harm to the opponent often results in success. In these sports the head is a legitimate target of tactical significance, and as a result, it is not surprising that mTBI is common in these sports. The highest rate of mTBI occurrence in combat sports has been reported in professional Boxing where values between 93 and 125.6 mTBIs per 500 rounds boxed have been reported (Zazryn et al., 2003 and Bledsoe et al., 2005). In Kickboxing and Taekwondo, mTBIs have been reported to be lower with values of 9.6 and 6.7 mTBIs per 500 rounds respectively (Pieter et al., 1995; Zazryn et al., 2003b). Shirani et al. (2010) investigated the prevalence of facial injuries in Boxing, Taekwondo, Kickboxing and Muay-thai, from 2005-2009. This study reported that facial lacerations, bone fractures, dental injuries and mandible dislocations occurred in 69.2%, 45.1%, 44.2% and 6.7% of participants respectively. It was also reported that different sports tended to result in different injuries, with Kickboxing causing the most frequent facial fractures, but Muay-thai causing the most facial lacerations. This suggests that the mode of impact influences the type of injury sustained, due to the differing mechanics of any given impact.

2.2.3. Projectile Sports

In sports such as Baseball, Hockey and Cricket, player-ball impacts can result in injury. Nicholls et al. (2004) reported that impact injury rates in Baseball are higher than many other sports, with the primary cause of impact injury occurring through a ball impact after it has been hit, pitched or thrown. In the US, the fatality rate in children aged 5 – 14 playing Baseball and Softball is the higher than any other sport (Rutherford et al., 1984). However, the rates of catastrophic injury in collegiate and professional players are much lower (Nicholls et al., 2004), perhaps due to the greater skill level and ability to avoid impacts. The National Centre for Catastrophic Sports Injury Research (2002) reported a direct fatal injury rate of 0.1 per 100,000 participants between 1983 and 2001 for collegiate and high-school players, as well as a non-fatal/serious injury rate of 2 per 100 participants. It was reported that most of the catastrophic injuries were a result of ball impacts to the head or chest. Zagelbaum et al. (1994) reported that head injuries occur at a rate of 170,000 per year. However, the type of injury is not reported and, at the current time, no study has provided a comprehensive analysis of mTBI rate in professional Baseball (Athiviraham et al., 2012).

As a contact sport that utilises a small projectile ball, there are various potential injury mechanisms in Field Hockey, including player-player, player-ground, player-ball and player-stick impacts. The National Collegiate Athletic Association (NCAA) (2010) reported that between the 2004/05 – 2008/09 seasons the overall injury rate for collegiate players in the USA was 6.3 per 1,000 athlete exposures. The most common specific types of injury were Quadricep strains (6.8%), ankle sprains (6.6%) and mTBI (6.3%), however the mechanisms of injury were not reported. Murtaugh (2001) investigated the prevalence and mechanism of injury in 158 high school, collegiate and national level female Field Hockey players. Of the 469 reported injuries, the most common site of injury was the lower limb (51%), followed by the head/face (34%). Of these head/face injuries, the most common type of injury was bruising (43%), with mTBI accounting for 22% of all head and face injuries. Player-ball collisions accounted for the most head/face injuries (42%) followed by player-stick (36%), player-player (18%) and player-ground (4%). However, most of the mTBIs were caused by player-player collisions (47%), whereas 60% of the bruises/black eyes were a result of player-ball impacts. Theilen et al. (2016) assessed International Hockey Federation (FIH) injury records for men's and women's major tournaments and reported that head/face injuries were the most common region of injury, and ball impact was the most frequent mode of injury.

2.2.4. Cricket

Historically, Cricket has been classified as a sport with 'moderate' injury risk (Weightman and Browne, 1971). Brukner et al. (2018) reviewed the number of on-field deaths in Australian Cricket and reported 174 deaths between 1858 and 2016, with five deaths in from 1986-2016. In Cricket, impact injuries are mainly limited to player-ball collisions, although player-bat impacts have occurred and player-bail impacts have led to career ending injuries (Moonda, 2012). Cricket varies from other projectile sports in that the bowler can legally target the batsman with the ball in order to intimidate or draw them into a shot likely to lead to the fall of a wicket. Recently the introduction of shorter formats of the sport (One-Day and Twenty over), where the emphasis is on scoring runs quickly, has led to a more aggressive batting style (Orchard et al., 2006). This has mean that batsmen attempt to play a shot more frequently than their historical counterparts, potentially leaving them open to a head impact should they misjudge/miss the ball. For club Cricketers in England, an injury rate of 2.6 per 10,000 hours played has been previously reported (Corrigan, 1984; Crisp, 1990). Frost and Chalmers (2014) reported a higher injury rate of 51.6 injuries per 10,000 playing hours during international matches. However, both these values are much lower than the value of 333 per 10,000 playing hours as reported by Payne et al. (1987) for first class Australian Cricketers. The discrepancy in reported injury rates may be due to a number of factors,

mainly, the difficulty in determining the amount of time a player is actively involved in a game, inconsistent diagnosis of injury, or may be due to the different levels of performance. Indeed the overall incidence of injury per season for schoolboy, club and provincial Cricketers has been reported to be 49.1%, 28.4% and 71.6% respectively (Stretch, 1995, 1993).

The reported frequency of head, neck and facial injuries in Cricket has varied between 1.9 and 25% of all injuries (Stretch, 2001, 1995, 1993, 1989; Temple, 1982), with mTBI, contusions, lacerations and nosebleeds reported as the most common injuries. These studies are however relatively old and may not account for more contemporary changes to the game, such as the continued development of PPE or the growth in popularity of the shorter formats of the sport. A more recent study completed by Ranson et al. (2013) investigated the types of head and facial injuries based on data collected by the International Cricket Council (ICC). Of the 35 injuries assessed in this study, all were caused by a ball impact to the head whilst batting, and comprised of 29% facial fractures, 23% mTBI, 20% lacerations, 20% contusions, 6% eye injuries and 3% dental injuries. This research led to a revision of the British Standard for head protectors for cricketers (BS 7928:2013), in an attempt to reduce the occurrence of facial injuries.

The most serious and high-profile Cricket injury in recent times occurred in November 2014, when Philip Hughes died following a ball impact to the back of his head/neck while batting. Although this tragic event was highly unlikely, it sparked much media attention into Cricket safety and in, particular, the PPE being used. The independent review of the incident, commissioned by Cricket Australia (Curtain, 2016), reported that although fatal events resulting from head impacts in Cricket are extremely rare, blows to the head are relatively common, with mTBI reported or suspected in many cases. Figure 2 shows injury surveillance data form all forms of first-class Cricket played in England from 2007 – 2017, with a clear increase in the frequency of reported or suspected mTBI over this period. Figure 3 shows the breakdown of reported or suspected mTBI frequency with activity. It can be seen that in every year other than 2014, batting was the most common activity resulting in mTBI, followed by fielding. As discussed previously, a variety of factors may contribute to this apparent rise in the frequency of mTBI, including a change in playing style (more aggressive batting and bowling), a change in helmet design as a result of the revision of the British standard for head protectors for cricketers (BS 7928:2013), and the increased awareness and recording of mTBI and the associated screening procedures.

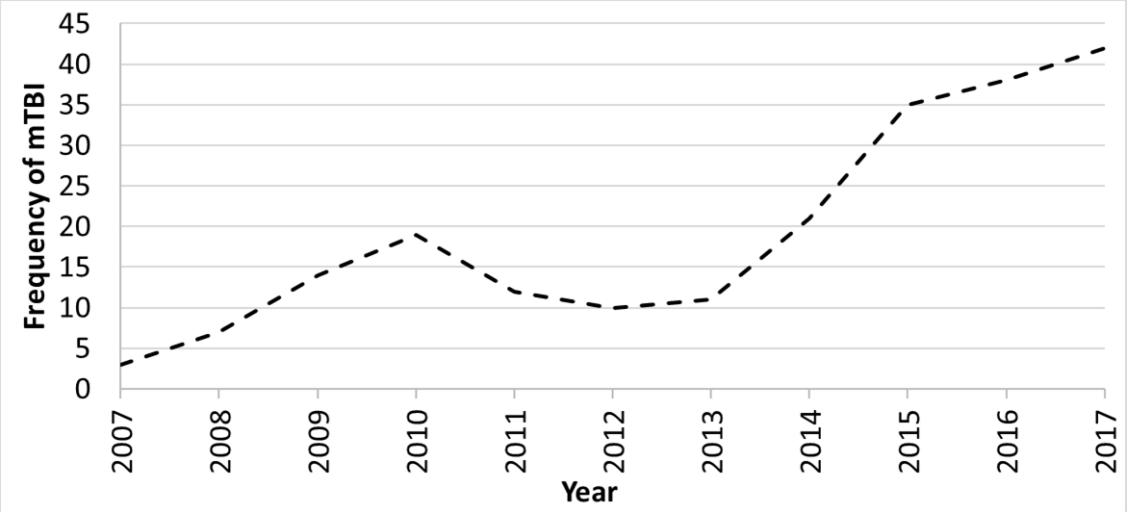

Figure 2. Frequency of reported and suspected mTBI in English County Cricket from 2007 to 2017 (data obtained from the England and Wales Cricket Board (ECB)).

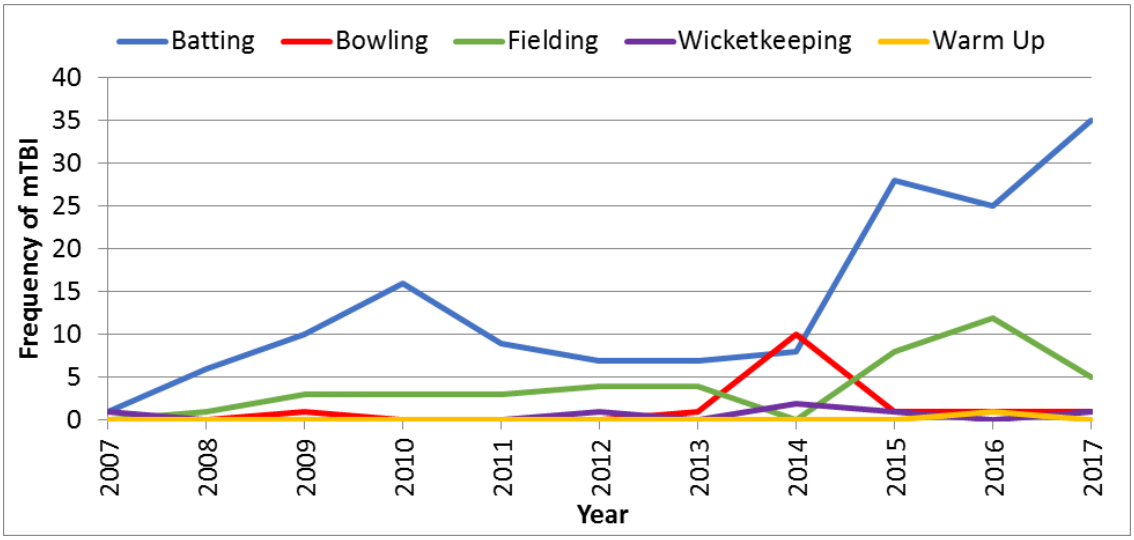

Figure 3. Breakdown of reported and suspected mTBI frequency in Cricket from 2007 to 2017 by activity (data obtained from ECB).

It is apparent that in Cricket, the risk of head injury and in particular mTBI is relatively low compared to other contact and combat sports. However, it remains an important aspect of the game, and a concern of the ECB, as evidenced through the recent publication of the head injury and concussion guidelines (ECB, 2015). This is not only due to the potential short-term damage that can be caused, but also because of the longer-term effects on player availability and performance, financial implications, health effects and the potential

misconception of an unsafe sport which may result in a decrease in mass participation. As such, research into this area now, may mitigate future problems in the sport.

2.2.5. Limitations of Epidemiology Studies

Although epidemiology studies can provide important information regarding the prevalence of particular injuries in sport, thereby leading to important and necessary changes in PPE or regulations (a good example being the work of Ranson et al. (2013), which led to the revision of BS 7928:2013), the limitations of the studies should also be considered. As epidemiology studies often rely on the correct definition, diagnosis and reporting of injuries, any developments in these factors can influence the results. Recent increases in awareness of head injury in sport and medical techniques have led to more thorough injury reporting and as such the comparability of historical and current injury rates may be questionable.

2.3. Anatomy of the Head

The components of the head are some of, if not the most, complex structures in the human body. The head itself is made up of various tissues including the skin, muscle/adipose, connective tissues, skeletal structures and the brain which can be broken down into distinct regions (see Figure 4), with varied material properties in each.

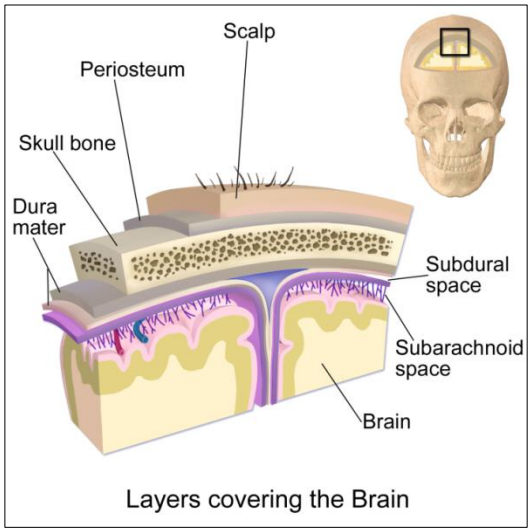

Figure 4. Structural components of the head (Blausen (2014))

2.3.1. Definition of a Co-Ordinate System

In this thesis, the co-ordinate system defined for the head has the origin (0, 0, 0) at the centre of gravity (CoG) of the head. The positive x axis runs posterior-anteriorly, the positive y axis runs medio-laterally to the left and the positive z axis runs inferior-superiorly, as shown in Figure 5. With respect to angular motion, angular about the x and z axis to the left will be defined as positive, and flexion of the head about the y axis will be defined as positive. With respect to planes of motion, the frontal plane bisects the body from front to back, the sagittal plane bisects the body laterally, and the transverse plane divides the body horizontally.

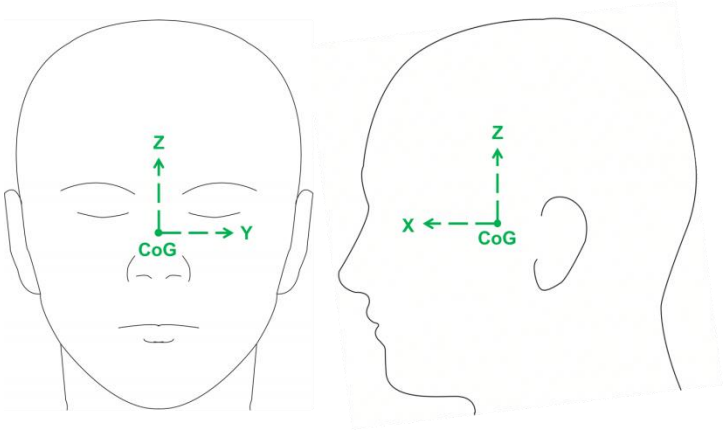

Figure 5. Co-ordinate system defined and used in this thesis.

2.3.2. Anatomical Landmarks

A number of anatomical landmarks can be defined on the human head (Peebles and Norris, 1998; Snell, 2003; Standring et al., 2008; van Sint Jan, 2007), as shown in Figure 6 which can be used to define a neutral position and geometrical measurements. Descriptions of the landmarks shown in Figure 6, as defined by Peebles and Norris (1998), Snell (2003), Standring et al. (2008) and van Sint Jan, (2007) can be found in Table 2. The Frankfort plane, as shown in Figure 6, is the direct line connecting the external auditory meatus (EAM) and the inferior margin of the orbit (IMO). The anatomic position, or neutral orientation, of the head is defined as the orientation where the Frankfort plane lies in the transverse plane.

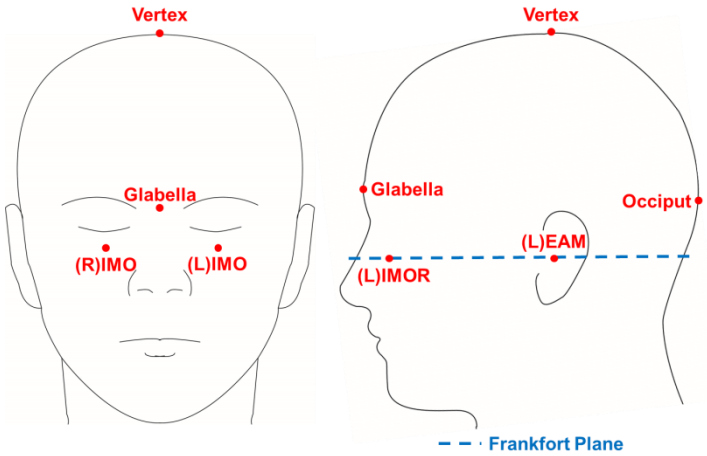

Figure 6. Graphical representation of surface landmarks on the head as defined by Peebles and Norris (1998), Snell (2003), Standring et al. (2008) and van Sint Jan (2007)

Table 2. Definitions of surface landmarks of the head as defined by Peebles and Norris (1998), Snell (2003), Standring et al. (2008) and van Sint Jan (2007).

Landmark	Definition
Vertex	The most superior aspect of the head in the sagittal plane
Occiput	The most posterior aspect of the head in the sagittal plane
Glabella	Protuberance located on the frontal bone, above the nasal bones, between the brow
External Auditory Meatus (EAM)	Ear canal leading from the outside of the head to the ear drum
Inferior margin of orbit (IMO)	Most inferior edge of the orbital bone surrounding the eye

2.3.3. External Soft Tissue

The external soft tissue of the head consists of the skin, the subcutaneous layer, and some muscle/fascia. The external soft tissue covers the skull and is 3 to 8 mm thick, depending on the exact location (Lin et al., 2008), and can slide a limited distance on the skull and provides some, albeit limited, protection to the skull from direct impacts to the head (Robinovitch et al., 1995).

2.3.4. The Skull

The Skull can be broken down into the neurocranium, which forms the protective cranial cavity and the mandible, and the viscerocranium which is formed by the bones supporting the face. The neurocranium consists of eight bones including the frontal, parietal (x2), occipital, temporal (x2), sphenoid and ethmoid bones which are fused together (Snell, 2003)

(see Figure 7). The thickness of the skull can vary between 4 and 9.35 mm, depending on location and physiological factors (Hodgson et al., 1970; Lynnerup, 2001; Mahinda and Murty, 2009; McElhaney et al., 1970).

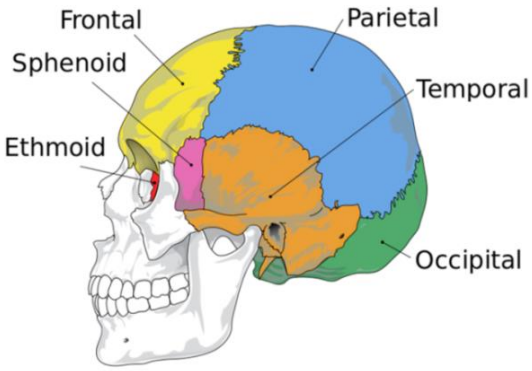

Figure 7. Bones of the neurocranium.

2.3.5. The Brain

The largest area of the brain is the cerebrum which is divided through the frontal plane into the left and right hemispheres, connected by the corpus callosum. The cerebrum can then be divided into a number of lobes, with other regions of the brain including the cerebellum and the brainstem (as shown in Figure 8). The brain is covered by membranes called the meninges. The outer most of these membranes (the dura mater) adheres to the inner surface of the skull. Two structures, the falx cerebri and tentorium cerebelli, are created by folds in the dura mater. The falx cerebri separates the left and right hemispheres, while the tentorium cerebelli separates the cerebrum (specifically the inferior portion of the occipital lobe) from the cerebellum. These are thin, but relatively stiff structures that help prevent linear and angular motion of the brain (Glaister et al., 2017). Between the dura mater and the underlying arachnoid membrane there is a narrow subdural space (see Figure 4), which is filled with fluid, which acts as a lubricant between the two membranes. The subarachnoid space (see Figure 4) holds most of the cerebrospinal fluid, which acts to isolate the brain from the skull and reduce shock transfer from the skull to the brain (Kleiven, 2002).

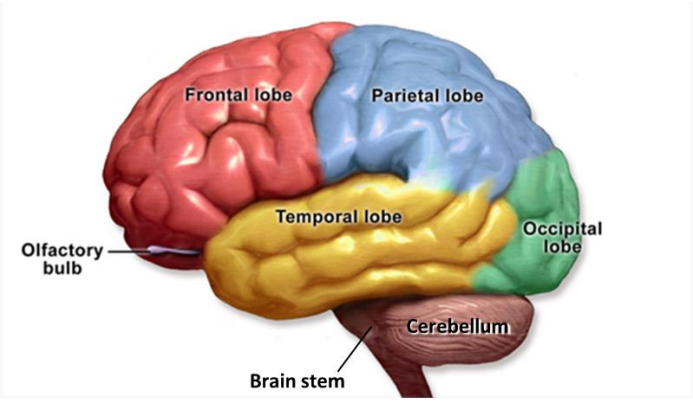

Figure 8. Lobes of the brain (Blausen (2014).

2.3.6. Geometric properties

A comprehensive collection of human anthropometric data is presented by Peebles and Norris (1998). Here various measurements are presented using anatomical landmarks for 5^{th}, 50^{th} and 95^{th} percentile males and females from the UK, USA, Brazil, France, Japan, Poland, Sri Lanka, Sweden and the Netherlands. This is a useful source of data that allows the assessment of human head geometry and variations based on geographic location. Table 3 shows mean and standard deviations of geometric measurements from the UK and USA, as these are pertinent to the impacts being investigated and currently available commercial headforms.

Although the USA population dimensions presented by Peebles and Norris (1998) are slightly greater than those of the UK population, these differences are small and, based on the standard deviation values, likely to be insignificant. More prominent differences are seen between males and females in both countries, with the former showing significantly larger heads than the latter.

Table 3. Selected 50th percentile head dimensions with standard deviations for males and females from the UK and USA (Peebles and Norris, 1998).

	UK		USA		
	Male	**Female**	**Male**	**Female**	**Description**
	Mean (SD)	**Mean (SD)**	**Mean (SD)**	**Mean (SD)**	
Head length	200.2 (7.6)	184.3 (7.5)	200.9 (7.7)	185.1 (8.2)	Measured horizontally from the glabella to the occiput
EAM to occiput	98.5 (7.6)	97.0 (8.5)	98.8 (7.7)	97.4 (9.3)	Measured horizontally from the EAM to the occiput
Head breadth	143.8 (6.3)	128.6 (6.0)	144.2 (6.4)	129.2 (9.5)	Measured Horizontally across the head where the head is widest
Head height	228.5 (11.3)	196.6 (11.5)	229.2 (11.5)	197.4 (12.5)	Measured vertically from the bony tip of the chin to the vertex
EAM to vertex	130.4 (8.5)	121.3 (7.5)	130.8 (8.6)	121.8 (8.2)	Measured from the EAM to the vertex
Head circumference	575 (16.8)	547.4 (15.6)	576.8 (17.1)	549.7 (17)	Measured around the maximum circumference of the head

2.3.7. Inertial Properties

Properties such as mass, CoG and moment of inertia (MoI) of the human head will influence the dynamic response of a head during an impact. These parameters have been previously investigated, but for obvious reasons, have had to use post-mortem human specimens (PMHS). It was important that in these studies, the head separation technique is defined and consistent. In the literature reviewed here, the head was separated from the neck superior to the first cervical vertebrae, as shown in Figure 9. As the raw data relating to inertial properties was not available in the studies assessed here, an 'All Study average' was calculated for each parameter, based on the reported means and standard deviations.

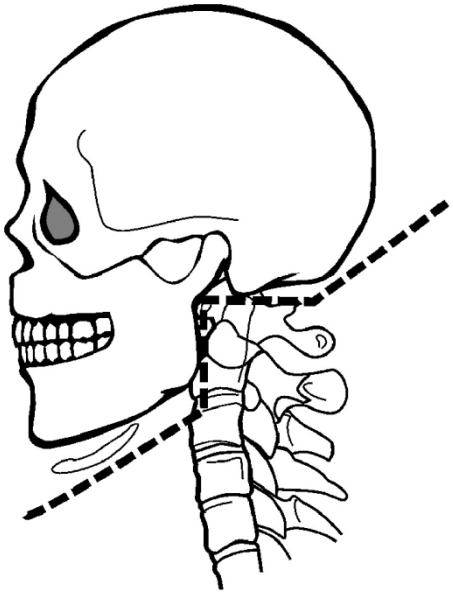

Figure 9. Head separation planes (from Yoganandan et al. (2009)).

Table 4 details the mean human head mass with standard deviations from specific studies. Hodgson et al. (1972) reported the mass of 13 male high school American Football players. Becker et al. (1972) reported the average mass of six cadavers, but unfortunately failed to report specific details on the origin of the subjects. Walker et al. (1973) reported the mass of 18 embalmed male cadavers, between the ages of 20 and 50 that were not 'wasted' by disease, and were of 'normal weight and stature'. Chandler et al. (1975) reported the mass of six male cadavers that exhibited no congenital abnormalities, major surgical alterations, general or localized structural atrophy, excessive wasting or obesity. Beier et al. (1980) reported the mass of 19, unpreserved male cadavers between the ages of 19 and 64, where the mass measurement was taken at most 86 hours post mortem. Albery and Whitestone (2003) reported the mass of eight male cadaver heads, aged between 16 and 80

years old, with a mean age of 55±22. As can be seen here, these report the range of human head masses to be relatively wide, potentially due to variations in PMHS origin, storage and preservation. The All Study average was found to be 4.14 ± 0.32 kg.

Table 4. Mean head mass and standard deviations from literature.

	Hodgson et al. (1972)	Becker et al. (1972)	Walker et al. (1973)	Chandler et al. (1975)	Beier et al. (1980)	Albery & Whitestone (2003)
Mean mass (kg)	4.6	3.88	4.38	3.99	4.32	3.68
SD (kg)	0.8	0.47	0.59	0.53	0.4	0.53

When considering the CoG of the human head, previous studies have reported the position of this relative to the EAM. In almost all the reported studies, the CoG was located very close to the centre line of the head as divided by the sagittal plane, with greater variation in the x and z axes. Figure 10 shows a graphical representation of the previously reported location of the CoG of the human head. As with the mass results, these can be seen to be widely variable, particularly in the x axis. The average location of the CoG from all these studies was found to be 7.7 mm anterior to the EAM in the x axis and 2.74 mm superior to the EAM in the z axis.

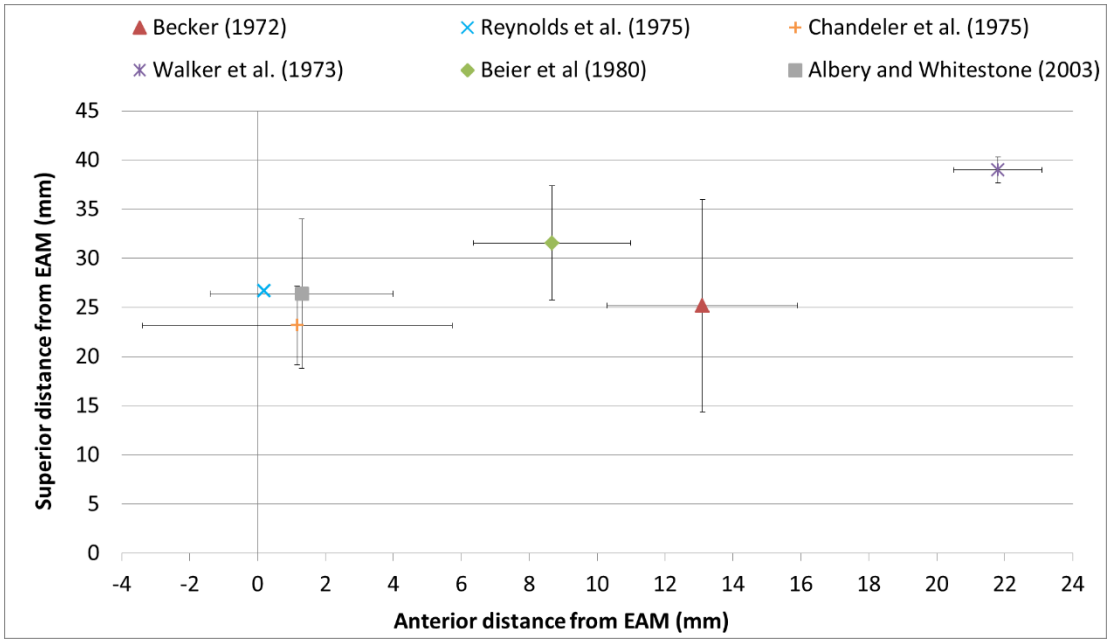

Figure 10. Graphical representation of the location of the CoG of the human head.

Previous studies have reported the MoI of the human head using principal MoI, MoI about anatomical axes at the centre of gravity, and MoI about imposed axes. Principal MoI were reported by Becker (1972), Beier et al. (1980) and Chandler et al. (1975), but again these showed relatively high variation, as can be seen in the standard deviation values show in Table 5. The average principal moments were 215.95 ± 48.31, 192.2 ± 44.9 and 149.2 ± 135.6 kg/cm^2 for I_1, I_2 and I_3 respectively.

Table 5. Average principal moments of inertia with standard deviations from literature.

	I_1 (kg/cm^2) (mean (SD))	**I_2 (kg/cm^2) (mean (SD))**	**I_3 (kg/cm^2) (mean (SD))**
Becker (1972)	221 (51.1)	198.5 (57.6)	133.8 (16.7)
Chandler et al. (1975)	200.8 (61.2)	170.8 (42.8)	164 (37.9)
Beier et al. (1980)	226.05 (32.6)	207.32 (34.3)	149.68 (25.7)

MoI about the x, y and z axes at the CoG of the head have been reported by Albery and Whitestone (2003) and Becker (1972), whereas Hodgson et al. (1972) reported the moment of inertia about just the x axis. These values can be seen in Table 6. These values again show large variation with the average of all three studies being 175.5 ± 47.4, 196.5 ± 44.5 and 160.5 ± 38.8 kg/cm^2 about the x, y and z axes respectively.

Table 6. Average moments of inertia about the x, y and z axes at the centre of gravity of the human head from literature.

	I_{xx} (kg/cm^2) (mean (SD))	I_{yy} (kg/cm^2) (mean (SD))	I_{zz} (kg/cm^2) (mean (SD))
Hodgson et al. (1972)	225.0 (67.2)	-	-
Becker (1972)	174.9 (45.2)	219.3 (50.8)	159.0 (25.7)
Albery and Whitestone (2003)	126.6 (29.7)	173.6 (38.3)	162.0 (51.8)

Walker et al. (1973) reported the moment of inertia about a lateral axis connecting the left and right EAM to be 233.2 ± 36.6 kg/cm^2. This however is the only study that has reported such a parameter.

2.3.8. Organic Tissue Properties

The mechanics of an impact and the observed dynamic response of the head during an impact are influenced by the mechanical properties of the scalp, bone and brain tissue that make up the human head. Due to the difficulties in practically obtaining good quality in-vivo data using material test methods, many studies have been conducted in-vitro, using PMHS. However, the measured mechanical properties of PMHS are influenced by the degradation of tissue due to the time between death and mechanical testing and from the storage conditions used. As a result, there are very few studies that report good mechanical data from human tissue (Balaraman et al., 2012).

The material properties of skin are commonly tested in tension (Wu et al., 2003), usually using quasi-static loading conditions (Ankerson et al., 1999; Ni Annaidh et al., 2012), although some dynamic tests have been conducted (Gallagher et al., 2012). Porcine and human skin tissues have been assessed in tension by Lim et al. (2011) and Gallagher et al. (2012) respectively. In these studies, a modified Split Hopkinson Pressure Bar was used, and significant strain rate dependencies were observed. More recently, Falland-Cheung et al. (2018) reported that, the mechanical properties of human scalp skin in tension varies depending on the area from which it has been harvested (eg, frontal/parietal etc…). Few studies have reported skin tissue properties in compression. Shergold et al. (2006) tested porcine rump skin in uniaxial compression at strain rates from 0.004s^{-1} to 4000s^{-1}, and Wu et al. (2003) tested porcine skin from the neck and back. Representative data from a number of studies is show in Figure 11.

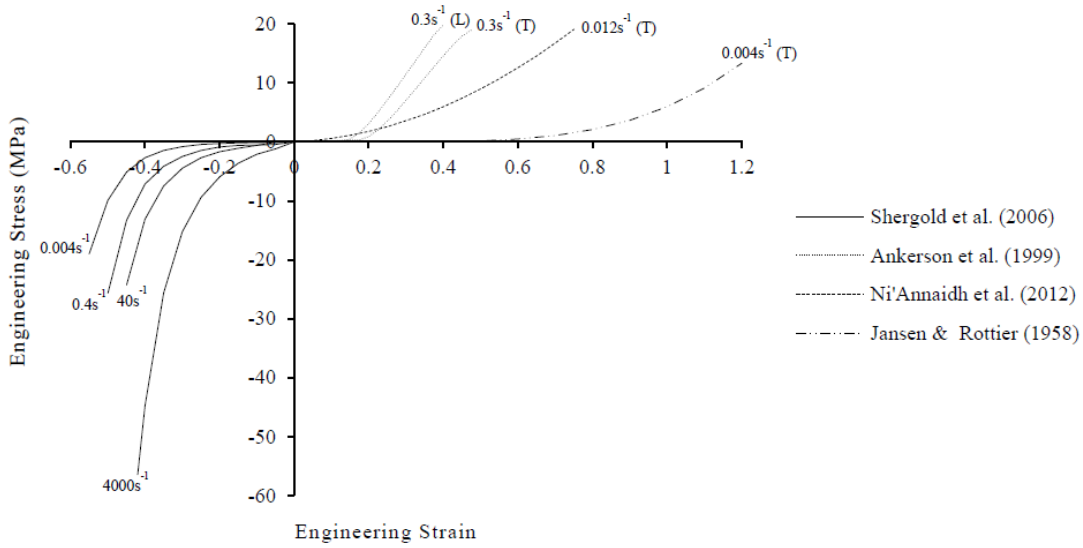

Figure 11. Representative engineering stress vs strain graphs from a range of studies investigating organic skin samples at different strain rates. T = transverse, L = Longitudinal (from (Payne, 2015)).

The density of skin is reported by CES Edupack (2017) to be between 1110 and 1270 kg/m^3. The Young's modulus and yield strength were also reported to be between 1 and 4 MPa and 0.53 and 1.2 MPa respectively.

The properties of bone have been found to vary based on the type of bone (i.e. long, short, flat etc…), and based on the location within the same bone (Li et al., 2013). The bones of the neurocranium generally consist of a layered structure, where cancellous bone is sandwiched between two layers of compact cortical bone (Hubbard, 1971). Blanton and Biggs (1968) and Yeni et al. (1998) reported that the density of cortical bone is around 1850 and 1880 kg/m^3 respectively. CES Edupack (2017) concurred with the findings for cortical bone, as it reported that the density of this is between 1800 and 2000 kg/m^3, whereas cancellous bone was reported to have a higher range of 300 – 975 kg/m^3. The mechanical properties of the different bones of the neurocranium have been assessed in tension, compression, flexion and torsion. As discussed with respect to skin properties, the studies assessing bone properties have a number of limitations, including the variety (sometimes unreported) in tested strain rates, dependence on testing PMHS and the associated degradation with time, preservation and storage technique.

Hubbard (1971) and Wood (1971) investigated the flexural properties of embalmed parietal bones, and temporal, frontal and parietal bones of PMHS aged 25 to 95 using a three point bend test. Delille et al. (2007) used a three point bend test and reported the

flexural elastic modulus of frontal, parietal, temporal and occipital bones, while Motherway et al. (2009) used the same technique to test frontal and parietal bones of PMHS aged 81 ±11, preserved by freezing, and reported strain rate dependent variations in bone properties. Mechanical properties of parietal and occipital bones in flexion, compression, tension and torsion of specimens aged between 56 and 73 have been reported by McElhaney et al. (1970), and Robbins and Wood (1969) reported the tensile strength of samples harvested from different bones of the skull. The average results from these studies can be found in Table 7Table 8Table 9.

CES Edupack (2017) reported that the Young's modulus of compact bone ranged from 10 to 26 GPa, whereas cancellous bone ranged from 0.07 to 1.5 MPa. The yield strength of compact and cancellous bone was reported to be between 45 to 144 MPa and 2 to 10 MPa respectively.

Table 7. Average flexural elastic modulus and flexural strength of skull bone from literature.

	Flexural Elastic Modulus (GPa) (mean (SD))	Flexural Strength (MPa) (mean (SD))	Info
Hubbard (1971)	11.73 (0.95)	82 (25.5)	Embalmed parietal bones
Delille et al. (2007)	5.21	-	Frontal, parietal, temporal and occipital bones
Motherway et al. (2009)	7.46 (5.39) to 15.54 (10.29)	-	Frozen parietal and frontal bones aged 81 ±11

Table 8. Average tensile elastic modulus and tensile strength of skull bone from literature.

	Tensile Elastic Modulus (GPa) (mean)	Tensile Strength (MPa) (mean (SD))	Info
Robbins and Wood (1969)	-	67.73 (17.8)	
McElhaney et al. (1970)	1.23 to 5.38	-	Parietal and Occipital bones aged 56 - 73

Table 9. Average compressive and torsional elastic modulus of skull bone from literature.

	Compressive elastic modulus (GPa) (mean)	Torsional elastic modulus (GPa) (mean)	Info
McElhaney et al. (1970)	2.41 to 5.58	1.38	Parietal and Occipital bones aged 56 - 73.

A number of studies have investigated the properties of human brain tissue using PMHS and animals and employing in vivo, in vitro, indentation, relaxation, and dynamic loading tests (Fallenstein et al., 1969; Gefen and Marguiles, 2004; Leung et al., 2006; Lippert and Grimm, 2003; MacManus et al., 2018, 2017; Miller et al., 2000; Miller and Chinzei, 2002; van Dommelem et al., 2010). The complex shear modulus of brain tissue has been reported to vary widely, with the values of 0.75 to 1.5 kPa reported by Fallenstein et al. (1969) being approximately the average. As the brain is approximately 80% water (Keep et al., 2012) it is almost incompressible, with a bulk modulus of 2.19 GPa and a density of ~1000 kg/m^3.

2.4. Head Impact Mechanics

When considering head injuries in sport, automotive crashes and military applications, the dynamic linear and angular response of the head observed during impacts have been used directly and/or used to drive finite element (FE) models, in an attempt to determine the likelihood and severity of injury. Mechanical parameters such as contact time, peak linear/angular response, time to peak linear/angular response and change in energy, to name a few, are likely to be important aspects of the observed dynamic response. Importantly the dynamic response observed is dependent upon the mechanics of an impact which are likely to vary in different sporting contexts due to differences in mass, stiffness and damping of the colliding bodies as well as variations in impact characteristics such as speed, location and angle (Clark et al., 2019; Karton, 2012; Oeur, 2012; R A Oeur et al., 2019; R Anna Oeur et al., 2019; Post et al., 2013)

In order to research the mechanics of head impacts in sports, two approaches have been used. The first approach is to directly instrument athletes or PPE to collect data during real-life competition. This approach is useful in providing direct access to data from impacts known to cause mTBI, and as such can be useful in the determination of injury thresholds and may be used to validate FE models. However, this approach is limited by the

unrepeatable nature of the impacts and the potentially problematic and/or inaccurate analysis due to independent PPE movement relative to the head.

The second approach, which is more commonly used in research, is to instrument a surrogate headform in a laboratory test environment. This approach is more repeatable and, as the control afforded to the researcher is greatly increased, individual parameters can be isolated. Additionally, the use of headforms allows multiple impacts to be completed relatively quickly and without endangering human participants. However, in order to provide accurate results, a suitably biofidelic headform must be used – that is, that the dynamic response of the headform during an impact must representative of that observed in humans. This can be challenging, and as a result, multiple headforms have been developed for specific types of impact testing.

2.4.1. Contact Sports

High-mass, low-velocity collisions are likely to occur in contact sports such as rugby, American Football and Australian Rules Football, where players often collide with each other and the ground. In American football, player-player contact can occur at various body locations (such as helmet-helmet, helmet-shoulder etc…) which have differing stiffnesses specific to each impact and influences the dynamic response of the head (Hoshizaki et al., 2014). The velocity of an impact in American Football can vary from 4 – 11 m/s, with some studies reporting that the effective mass can vary between 15 and 25 kg for full body collisions (Pellman et al., 2003 and Pellman et al., 2005). Greenwald et al. (2008) reported that the contact duration of impacts occurring in American football ranged from 5.5 to 13.7 ms.

A number of studies have attempted to recreate impacts in a laboratory setting with an instrumented headform, using video recordings of real-life American Football impacts. Pellman et al. (2003) and Zhang et al. (2004) utilised this type of approach to reconstruct helmet to helmet impacts that resulted in mTBI. These studies reported varied peak resultant linear accelerations of 61 to 144 g and peak resultant angular accelerations of 4,168 to 12,832 rad/sec^2 for impacts resulting in mTBI. Zanetti et al. (2013) reconstructed head impacts in American Footballers playing in three positions. As in the previous studies, these reconstructions utilised an instrumented, helmeted Hybrid-III head and neckform, with a pendulum and pneumatic striker system to recreate recorded real-life impacts. The impact velocity varied between 3.28 and 11 m/s, and the impact mass varied between 13.1 and 28 kg. Due to the varied impact velocities, energies and locations, this study reported significantly different peak linear accelerations for the three playing positions with peak

resultant linear accelerations between 32 and 160g and resultant angular acceleration between 1,951 and 10,362 rad/s^2.

Although these studies are useful in comparing the relative severity of impacts in this sport and in different playing positions, they do not isolate individual impact parameters, such as energy, location or angle and therefore are not useful in identifying how specific characteristics influence the dynamic response of the headform. It is also important to note that all these studies utilised helmeted headforms during reconstructions. This does not give insights into the baseline response observed in an unprotected headform and as a result it is difficult to gauge the true effect of a helmet as the reduction in impact severity cannot be determined.

The influence of impact location and angle in American Football impacts was investigated by Walsh et al. (2011), who utilised a instrumented Hybrid-III headform and linear impactor (13.1 kg) to investigate linear and angular accelerations. This study reported that impact location and angle had a significant effect on both linear and angular accelerations with some combinations resulting in levels above previously reported thresholds for mTBI. In most cases, the angular acceleration values showed a higher risk of injury than the linear acceleration values, suggesting that helmets that are capable of reducing linear acceleration may not be capable of reducing angular acceleration.

In Rugby, King et al. (2014) utilised an instrumented mouth guard to assess the dynamic response of player's heads during impacts in real-life situations. This study reported mean peak linear and angular accelerations of 22 ±16 g and 3,990 ±3,949 rad/s^2. However, for impacts that resulted in mTBI the peak resultant linear and angular accelerations were found to be higher than the reported average, at 55 to 95 g, and 5,319 to 9,935 rad/s^2 respectively. The mean values reported here were lower, but more inconsistent, than those previously reported for American Football. This may be expected however, as the previous American Football reconstructions were conducted in a controlled, laboratory environment. Frechede and McIntosh (2009) used video recordings of real-life collisions occurring in Australian Rules Football and Rugby Union that resulted in mTBI and utilised a numerical simulation technique to model these impacts. This study reported peak resultant linear acceleration of 103 g and peak angular acceleration of 8,020 rad/s^2, which are values comparable with those reported by (King et al., 2014), but slightly lower than the most severe American football impacts reported by Pellman et al. (2003), Zanetti et al. (2013) and Zhang et al. (2004) despite the absence of protective headgear. This may be due to the varied impact characteristics such as energy, speed, location and angle.

2.4.2. Combat Sports

A punch can be characterised by an effective mass of the hand and arm of 1 – 8 kg (additional weight of, for example, a Boxing glove can reach 0.283 kg), which contacts the head at a velocity of 1 – 12 m/s (Atha et al., 1985; Kendall et al., 2012a; Walilko et al., 2005). The stiffness and damping characteristics of the impact are dependent on the material properties of the hand and any added materials such as gloves. An initial study into the dynamics of a punch, conducted by Atha et al. (1985) investigated the response of a cylindrical mass (7kg) representing the human head when subjected to a punch from an elite Boxer. This study reported a peak resultant linear acceleration of 53 g, which is similar to the low to average values reported in American Football and Rugby, with a time of 14 ms from initial contact to peak resultant linear acceleration. Although this study proved useful as an initial step to develop the research within this area, it is limited by the nature of the impact mass and does not consider the angular response during the impact.

Walilko et al. (2005) utilised an instrumented Hybrid-III dummy to assess the dynamic response of the headform when subjected to punches from 8 Olympic Boxers from 5 weight categories. Although the results varied somewhat based on the weight class of the Boxers, the average contact duration of 11.4 ±1.4 ms was shorter than that reported by Atha et al. (1985), but comparable to those observed in American Football impacts. The dynamic response of the headform was similar to that reported by Atha et al. (1985), as the peak resultant linear acceleration was reported to be 58 ±13 g. The peak angular acceleration was reported to be 6,343 ±1,789 rad/s^2, with a relatively weak correlation between linear and angular acceleration. This study is however limited by the impact characteristics, as only direct punches to the face were investigated. Therefore, the effect of impact location and angle on the dynamic response of the headform were not established.

Viano et al. (2005) compared the mechanics of different types of Boxing punches at different impact locations, to the mechanics of impacts in American Football that resulted in mTBI. In this study, hand mass and fist width were measured using anthropometric and volumetric measurements and reported to be 1.67 ±0.28 kg and 8.9 ±0.4 cm respectively. The mass of the hand was found to increase with boxer weight and, importantly, is greater than an order of magnitude smaller than that of the effective mass that Pellman et al. (2005) reported in American Football impacts. The dynamic response of the headform was found to vary based on punch type. The uppercut was found to produce the lowest peak resultant linear and angular accelerations (24.1 ±12.5 g and 1,486 ±910 rad/s^2 respectively), whereas the hook was found to produce the highest values for these parameters (71.2 ±32.2 g and 9,306 ±4,485 rad/s^2 respectively). This difference is likely a consequence of a combination of

the Boxer's ability to generate more force through this style, and the influence of impact location.

The linear and angular accelerations observed in Boxing punches are similar to the values reported to result in mTBI in helmeted American Football impacts. However, there are differences between the two types of impact. Specifically, the proportion of angular acceleration to linear acceleration is greater in Boxing punches compared to American Football impacts and the effective radius of the impact is smaller in Boxing punches.

2.4.3. Projectile Sports

In sports that use a projectile, this can be an additional or primary injury threat and due to the nature of projectile sports, impacts can occur at a variety of speeds, locations and angles. The defining mechanical properties of a projectile impact are different to those observed in high-mass, low-velocity collisions and combat sports. In most projectile sports, the projectiles are stiff, relatively low-mass bodies moving with a relatively high-velocity that result in a very short contact duration (Hoshizaki et al. (2014) observed contact durations of 1 – 2 ms in puck impacts). In Baseball, ball velocities can reach 37 m/s when pitched and are even higher (~47 m/s) when hit with the bat (Greenwald et al., 2001; Urbin et al., 2013). The properties of the projectile are also important factors as Crisco et al. (1997) showed that Baseball mass and stiffness significantly influenced the dynamic response of a headform during impact, as balls with reduced mass and stiffness produced a lower magnitude dynamic response. Major League Baseball (MLB) regulations state that the ball must have a mass of 142 – 149 grams and a diameter of 75 mm (MLB, 2016).

Post et al. (2016) reported linear and angular parameters, and compared the performance of Baseball helmets at different impact locations, using a Hybrid-III headform and neck. They reported significant variation in both peak resultant linear acceleration (73.1 ±18.4 – 207.5 ±57.9 g) and peak resultant angular acceleration (7 ±2.1 – 21.1 ±7 krad/s^2) due to variations in impact location. Yang et al. (2014) also assessed the response of a Hybrid-III 50th percentile male headform during unprotected and helmeted impacts. At a frontal location with an impact speed of 34 m/s, peak linear acceleration, Head Injury Criteria (HIC) and angular acceleration values ranged from 104-161g, 36-100 and 6.3-10.8 krad/s/s respectively when helmeted. When unprotected, values of 262-276g, 357-405 and 25.2-26.8 krad/s/s were observed. At a location defined as the 'left temple', helmeted impacts resulted in peak resultant linear acceleration, HIC and peak angular acceleration values of 68-115g, 23-50 and 6.6-11 krad/s/s respectively. The unprotected impacts at this location resulted in 259-273 g, 381-424 and 39.5-41.6 krad/s/s. Clark (2015) assessed the performance of Ice Hockey goaltenders' helmets in impacts representative of falls, collisions and projectile

impacts. In the projectile impacts at 35.8 m/s, the peak resultant linear acceleration varied between 37.9 ±1.7 to 44.5g ±0.4 whereas the angular acceleration and velocity values ranged from 3.47 ±0.26 to 4.88 ±0.28 krad/sec^2 and from 4 ±0.1 to 6.8 ±0.9 rad/s respectively. Although these studies are useful in identifying the magnitude of linear and angular accelerations during unprotected and helmeted impacts representative of those seen in other projectile sports, they are potentially limited by the properties of the headform surrogate, and due to the potential variations in impact conditions, do not increase the understanding of the mechanics of protected or unprotected head impacts in Cricket.

Ball velocities in Cricket are similar to those observed in Baseball, however the ball has a slightly greater mass of 156 – 163 grams, and a slightly smaller diameter of 71 – 73 mm (MCC). Fuss (2008) reported that generally, Cricket balls were inconsistent in terms of construction and stiffness values. Indeed, of the balls tested, only Kookaburra balls were found to be consistent in terms of construction, but still varied in regard to stiffness. Carré et al. (2004), Fuss (2008) and Subic et al. (2005) report varying stiffness values from around 300 N/mm to 1,000 N/mm for Cricket balls. The variations in reported stiffness values may be due to the strain rate dependencies of Cricket balls (reported by Fuss (2008)), as these studies used quasi-static and drop techniques, and therefore varied loading characteristics. Importantly, no studies have investigated the properties of Cricket balls at loading rates close to those observed in real-life impacts.

Research into head impacts in Cricket is limited. Stretch (2000) investigated the impact absorption characteristics of 6 different Cricket batting helmets at the right temple, forehead and back locations, using a wooden headform and a 5 kg drop mass to create an impact with equivalent energy to that of a 156 g Cricket ball travelling at 44.4 m/s. The peak resultant linear acceleration was found to vary within and between helmets, based on impact location. The peak resultant linear accelerations reported in this study were higher than those reported in the previously discussed American Football, Rugby and Boxing impacts, as the right temple location produced values of 216.2 – 322 g, the rear impact site displayed a range of 263 – 334 g and the forehead site produced a range of 246.5 – 315.7 g. Despite producing acceleration levels close to the acceptable level (>250 g) specified in the British standard (BS 7928:2013), the performance of the Cricket helmets tested appeared to be poorer than those used in American Football. This study is however limited by the sole use of linear acceleration to quantify helmet performance, and a potentially inappropriate test method.

McIntosh and Janda (2003) compared the performance of Cricket helmets to those used in Baseball and Ice Hockey, using drop and air cannon testing methods. Air cannon

tests using a Cricket ball on an unprotected 5th percentile female Hybrid-III headform and neck showed peak linear acceleration of the headform to be 278 and 347 g for impact speeds of 19 and 27 m/s respectively. These were slightly lower than the values observed for the same impact speeds using a baseball which produced values of 316 and 426 g. Although impacts were arranged to occur at the front, side and back of the headform during helmeted impacts, individual results were not reported. Instead, combined results were presented and can be seen in Table 10.

Table 10. Peak acceleration values of a headform protected by a Cricket helmet during a projectile impact.

Impact Speed (m/s)	Peak resultant linear acceleration (mean (SD))
19	67 (25)
27	160 (59)
36	316 (86)
45	438 (161)

Helmet performance was deemed to be adequate at low impact velocities where acceleration was reduced by ~80%, but as impact velocity increased the performance of Cricket helmets decreased (~40% reduction at 27 m/s), particularly when compared to Baseball and Ice Hockey helmets. McIntosh and Janda (2003) went on to compare air cannon and drop test results and reported little correlation between the values obtained through the different test methods. Although this study utilised unprotected headform tests to provide a baseline measurement, it did not consider the effect of impact location, nor the role of angular motion, and may produce erroneous results due to the nature of the Hybrid-III head and neck surrogates (Raymond, 2008). In terms of test methods, Pang et al. (2013) concurred with McIntosh and Janda (2003) and reported that drop tests and air cannon tests produce significantly different results in terms of peak linear acceleration.

It is clear from this research that although previous studies have attempted to gauge the performance of Cricket helmets using peak linear acceleration, no studies have reported angular motion in Cricket specific impacts. It is also clear that the studies that have investigated unprotected head impact scenarios in projectile sports have done so using the Hybrid-III headform, which may influence the observed response due to its construction. As a result of the limited research surrounding head impacts in Cricket, the dynamic response during these impacts, and the performance of currently available PPE remains unclear.

2.4.4. Finite Element Modelling

Computational models using the FE technique have been used in the assessment of head injury for many years to predict the response of specific structures and/or identify areas of high stress and strain. In the FE method, a system is separated into constitutive structures (i.e. the head could be broken down into the brain, skull and soft tissue components, each of which could be broken down further into connective tissue, blood vessels etc…). Each structure is made up of individual areas or volumes (elements) and, as the size and shape of these elements is not limited, there are no restrictions on the complexity of an FE model (Friswell and Mottershead, 1995). However, more complex models may be limited by the computing power required to process them. A system of matrix equations representing the stiffness and mass of each structure are constructed and boundary conditions are assigned to areas where structures interact. When using this method to assess impacts, two approaches can be taken. One approach is to model both colliding bodies, apply appropriate material properties and impact characteristics and model the impact as a whole. A more common approach is to measure the response of a headform in six degrees of freedom (DOF) and use this to drive a FE model of the head from which the motion of the brain contained within can be predicted (Clark et al., 2016a; Post et al., 2012; Zhang et al., 2001). Although there have been many models produced, a number of FE models commonly used in the sports context will be discussed here.

Kleiven (2002) developed an FE model of the human head, with geometry derived from computerised tomography (CT) and magnetic resonance imaging (MRI) scans. The total mass of the model was 4.52 kg and consisted of 11,158 eight node brick elements making up the scalp, skull, brain (differentiating between white and grey matter), meninges, cerebrospinal fluid and bridging veins. A hyper-elastic constitutive law was applied to the tissues, and the model was validated using displacement data derived from cadaver head impacts (Hardy et al., 2001). The model has been used to simulate head impacts in American Football (Hernandez et al., 2015; Kleiven, 2007), where output parameters such as peak principal strain, 1st principal Green-Lagrange, cumulative strain damage and minimum/maximum pressure were reported as important injury predictors.

Similar to the model produced by Kleiven (2002), the University College Dublin Brain Trauma Model (UCDBTM) (described by Horgan and Gilchrist (2003) and Gilchrist (2003)) was based on geometry derived from CT scans. The model consists of 26,000 hexahedral elements and includes the scalp, skull (outer and inner tables and diploe), dura, cerebrospinal fluid, meninges, cerebral hemispheres, cerebellum and brain stem. The material properties of the brain tissues are modelled as viscoelastic in shear and elastic in

compression. The UCDBTM was validated using data from cadaveric pressure responses during impact, reported by Nahum et al. (1977). Although the model was first developed to investigate injury mechanism to pedestrians during automotive crashes (Horgan and Gilchrist, 2003), it has since been used extensively to investigate brain injury in American Football, Ice Hockey and Baseball (Clark et al., 2019, 2016b; Anna Oeur et al., 2019; R Anna Oeur et al., 2019; Post et al., 2017, 2016; Post and Hoshizaki, 2012; Zanetti et al., 2013). In these studies, the model was driven by accelerations measured in six DOF, with maximal principal strain in various structures of the brain commonly reported as injury predictors.

Ghajari et al. (2017) presented a model using geometry from high resolution MRI scans of a healthy 34-year-old male. This model is more complex than the models developed by Horgan and Gilchrist (2003) and Kleiven (2002) as it consists of nearly one million hexahedral elements and a quarter of a million quadrilateral elements. The model incorporates the scalp, skull, meninges and subarachnoid space, as well as including anatomical features such as the sulci (grooves on the brain). A hyper-viscoelastic material model, based on the non-linear response of brain tissue with deformation rate (Donnelly and Medige, 1997; Franceschini et al., 2006) was applied. The non-linear, volume preserving response of brain tissue was modelled using the Ogden hyper-elastic model with a strain energy function, and the model is validated against brain displacement (Hardy et al., 2001) and intracranial pressure (Nahum et al., 1977). Ghajari et al. (2017) use the model to predict maximum principal strain of the Green-Lagrange strain tensor and the maximum principal value of the total time derivative of the Green-Lagrange strain tensor in laboratory-reconstructed American Football impacts. It was also reported that the areas with largest strain in the model, matched the areas affected by CTE in American footballers.

Despite the detail and complexity of the FE models discussed here, the quality of the results gained from such simulations are dependent on the data used to determine drive them. Where both colliding bodies are simulated, it is important that appropriate material and inertial properties are utilised – at present, this is not possible in Cricket, given that ball property data at realistic strain rates is not yet available. It would also be beneficial to have a FE model of the surrogate headform (without the extreme complexity of components of the brain), and with measured material properties. This would allow the validation of the simulated response against the measured laboratory experiments, thereby adding to the work of Hardy et al. (2001) and Nahum et al. (1977) and provide additional confidence in the computational model before progressing to more complex models using human structures. Alternatively, when the simulations are driven by accelerations in six DOF, derived from

laboratory reconstructions, it is imperative that surrogates used in the laboratory reconstructions display appropriate biofidelity (e.g. mass, MoI, skull compliance etc…).

2.5. Injury Mechanisms and Proposed Injury Thresholds

A head impact results in a complex series of mechanical and physical effects which can result in local bending of the skull, volume changes to the cranial cavity, pressure wave propagation through the brain and inertial effects, all of which may result in micro-damage to blood vessels and cellular networks (Meaney and Smith, 2011). This can result in neuronal signalling difficulties, neuronal dysfunction and neuronal death due to mechanical load, and the resulting biochemical cascades.

Although there is considerable evidence that shows mTBI is primarily caused by the amount of acceleration experienced by the brain during an impact (Meaney and Smith, 2011), other factors that are not yet clear may also contribute to the development of the injury. During almost all real-life head impacts, a combination of both linear and angular acceleration will occur. As discussed previously, FE modelling techniques have been developed to predict the mechanical load and acceleration of the brain using measurable head accelerations. This has been used to assess the relative importance of linear and angular motion in the development of mTBI and propose thresholds in these responses (or calculated metrics) that are related to injury.

2.5.1. Linear Response

Linear acceleration has, for a long time, been a commonly used metric to assess the likelihood and severity of brain injuries resulting from head impacts. Early animal studies into the mechanisms of mTBI reported that intracranial damage occurred due to deformation of the skull and intracranial pressure gradients that resulted from acceleration of the head, with linear acceleration considered to be the most important mechanism. Angular acceleration, negative pressure and cavitation were initially judged to be of little importance (Gurdjian et al., 1963, 1961, 1955; Gurdjian and Webster, 1945). In conjunction with these animal studies, other research attempted to establish a tolerance curve in humans (Gurdjian et al., 1950, 1949, 1947). These tests utilised drop tests using PMHS filled with gelatine. Although these studies could not establish an mTBI threshold, they did measure the relative onset of skull fracture. The resulting Wayne State Tolerance Curve (WSTC) provided a foundation that subsequent research built on, aimed at correlating physical parameters with head injury. Indeed, many test standards for PPE across sports now utilise linear acceleration as a

metric as a result of these initial studies, and the relatively ease with which linear acceleration can be measured.

During an impact, relative brain movement creates an area of high, positive pressure local to the impact location (coup), this relative movement also generates an area of low, negative pressure at the location distal to the impact location (contrecoup) (Post and Hoshizaki, 2012). While the positive component of intracranial pressure has been suggested to be influential in this injury mechanism, the negative pressure, and resulting cavitation has also been investigated. It has been suggested that cavitation may result in damage through the creation of vacuum bubbles within the brain, which collapse and cause injury (Lubock and Goldsmith, 1980). However, the negative pressure theory has not been widely accepted as other researchers have reported that negative pressure shows little contribution to mTBI in animal testing (Nuscholtz et al., 1984; Stalhammar and Olsson, 1975). Indeed, Gurdjian and Gurdjian (1975) showed that the damage expected through cavitation did not occur, and Gurdjian and Gurdjian (1980) suggested that the energy required to generate cavitation is unachievably high.

Since these early studies, advancements in computing power have allowed the development of complex FE models that estimate the magnitude, timing and location of strains within the brain that result from acceleration. Zhang et al. (2004; 2001) used FE models and showed that linear acceleration does indeed correlate well with intracranial pressure gradients, suggesting that if the high, positive component of the intracranial pressure does lead (or at least contribute) to injury, then this is likely a result of the linear acceleration experienced by the skull.

Linear acceleration has also been used as a means of predicting fracture injuries. As radial impacts produce greater contact forces (and therefore greater linear acceleration), this increases the stress in the skull bone (Kleiven, 2013; McIntosh et al., 2011). Although consistent fracture forces of 4.8 – 5.8 kN and 3.5-3.6 kN have been reported for the frontal and tempo-parietal bones respectively (Allsop et al., 1988b; Nahum et al., 1968; Schneider and Nahum, 1972), these forces, and the relation with skull fracture are also dependent on impactor area and hardness (Hodgson and Thomas, 1973).

2.5.2. Angular Response

Although some initial studies focussed on the linear acceleration of the head during an impact, Holbourn (1943) suggested that angular motion may be important in the development of mTBI. Due to the material properties of the brain, it is particularly susceptible

to damage from shear strains (Prange et al., 2000; Takhounts et al., 2003) and therefore any motion that is likely to induce this form of strain is potentially injurious.

Gennarelli et al. (1972, 1971) conducted animal studies and applied purely linear or angular acceleration and observed the resulting symptoms. They concluded that non-contact linear acceleration could not produce symptoms conforming with mTBI, whereas non-contact angular acceleration could. Gennarelli et al. (1983) utilised the same device to isolate angular acceleration and reported that the direction of rotation was important in determining both the severity and type of injury. It is important to note however, that although these studies highlight the importance of angular acceleration in the development of mTBI, since no impact occurred, they may neglect other important parameters that may be present during an impact that contribute to the development of mTBI.

The relationship between angular velocity and brain injury has also been suggested as a useful metric in defining head injury, particularly in short duration impacts (Holbourn, 1943). Hardy et al. (2008; 2001) and Takhounts et al. (2013) also reported angular velocity is an important parameter when considering brain injury, and has been used as an injury metric when considering the development of brain injury in sports related head impacts (Clark et al., 2016b).

FE models have also been used to investigate the effect of angular motion on the strains experienced by the brain during an impact. Zhang et al. (2006) assessed the influence of linear and angular acceleration in isolation and found that angular acceleration strongly influenced the magnitude of the observed shear strain. Similarly, Zhang et al. (2004), found that angular acceleration is highly correlated with shear strains within core regions of the brain, but poorly correlated with intracranial pressure. Conversely, linear acceleration is highly correlated with intracranial pressure gradients, but poorly correlated with shear strains. In addition to these studies that suggest the importance of angular acceleration, Bradshaw et al. (2001), Fijalkowski et al. (2009) and Takhounts et al. (2008) concluded that angular kinematic measures are correlated with injurious levels of strain within the brain during an impact. The findings from these studies have led to the now commonly held belief that angular motion is the predominant cause of mTBI (Kleiven, 2013; Meaney and Smith, 2011).

As previously stated, in almost every real-life situation a combination of linear and angular motion will occur during any impact. It is therefore likely that although angular motion may be the dominant cause of mTBI in some types of impact, the specific combination of both linear and angular motion produced from a given impact ultimately leads to the development of this type of injury (Post and Hoshizaki, 2012). Additionally, the primary

cause of brain injury may also be specific to a given set of impact conditions (including, but not limited to, striker properties, impact speed and contact duration). It may also be the case that other factors such as contact pressure, or others that are not immediately apparent at the moment, also influence the development of mTBI in given impact scenarios.

2.5.3. Proposed Injury Thresholds

Many researchers have attempted to define a level or magnitude of insult that would result in injury. This has led to the development of numerous injury thresholds based on the dynamic response of the headform observed during impact. Historically, the common use of linear acceleration in injury thresholds, and the knock on effect that this has on PPE design, has led to a reduction in the number of focal injuries (e.g. skull fracture) in sport (Hoshizaki and Brien, 2004), but the occurrence of injuries such as mTBI has yet to be resolved (Post and Hoshizaki, 2012).

The WSTC provided the basis for early injury thresholds. This curve proposes that high acceleration may not cause injury if it occurs over a very short duration, however, lower levels of acceleration may cause injury should they occur over a longer duration. One such metric is the Gadd Severity Index (GSI) which was produced in order to provide a value that could be easily applied in the automotive industry to predict the likelihood of skull fracture. The GSI is an integrated acceleration pulse, with a weighting factor to give more influence to higher levels of response, while reducing the influence of lower level responses. This was seen as an improvement on the initial technique of using the singular peak acceleration value, as the GSI accounts for differing curve shapes (Post and Hoshizaki, 2012). A value of 1000 was proposed as the injury threshold, based on data from Wayne State. The HIC was developed in an attempt to improve the GSI (Versace, 1971). HIC is calculated by selecting a period of the acceleration time pulse to integrate (Eq. 1) where HIC would be maximised. Again, a value of 1000 was proposed as the threshold for injury.

$$HIC = \left(\left[\frac{1}{t_2 - t_1} \int_{t_1}^{t_2} a(t)dt \right]^{2.5} (t_2 - t_1) \right)_{max} \quad \text{Eq. 1}$$

It is important to note the limitations of these thresholds. Firstly, they are derived from cadaver data obtained through drop tests, so the validity of these in relation to human injury and alternate impact scenarios may be questionable. Secondly, they were developed to predict the likelihood of severe brain injury, and not mTBI (Prasad and Mertz, 1985). Thirdly, they only consider frontal impacts and should not be used in impacts at other locations

(Fenner et al., 2005). Finally, they do not consider angular motion and therefore may be erroneous in their estimation of the likelihood of brain injury. Indeed, Nahum and Smith (1976) attempted to correlate GSI and HIC with brain injury severity and found a weak correlation, indicating that, as previously discussed, other factors should also be considered. Overall, the HIC and GSI are considered inadequate when used in isolation due to these limitations (Fernandes and Sousa, 2015; Goldsmith, 1981).

Injury thresholds have also been developed that attempt to incorporate angular acceleration with the traditional linear acceleration metrics. The generalised head acceleration model for brain injury threshold (GAMBIT) (Newman, 1986) was the first threshold to utilise both forms of acceleration. GAMBIT uses instantaneous linear and angular acceleration with constants to derive the metric value. This differs from the previous techniques which integrate the acceleration pulses, as it provides a critical value in linear and angular acceleration above which injury would occur, but was never extensively validated. Newman et al. (2000a, 2000b) further developed the GAMBIT to produce the Head Impact power (HIP) metric, which was validated for mTBI. This metric is based on the concept that brain injury would occur if the rate of change of kinetic energy passes a critical value (the authors reported a 50% chance of mTBI at 12.8 kW) and incorporated coefficients to scale power in different directions. This was the first (and so far, only) metric that utilises measurements made in six DOF.

Assessment of GSI, HIC, GAMBIT and HIP found that those techniques utilising both linear and angular acceleration showed the highest correlation with injury (Newman et al., 2000a). Despite the focus on linear and angular acceleration, recent studies have shown that angular velocity may be better correlated with brain injury in some impact scenarios (Clark et al., 2016b), as suggested by Holbourn (1943). Indeed, a relatively recent measure, termed Brain Injury Criterion (BrIC) (see Eq. 2) (Takhounts et al., 2013), uses maximum angular velocities about each axis during impact and incorporates a critical value in each direction. The resulting value can be compared to injury curves to predict the likelihood and severity of brain injury. Although this measure focuses on just angular motion, the authors suggest that, if used in conjunction with HIC, the criteria may be able to capture most brain injuries and skull fractures (Takhounts et al., 2013).

$$BrIC = \sqrt{\left(\frac{\omega_x}{\omega_{xC}}\right)^2 + \left(\frac{\omega_y}{\omega_{yC}}\right)^2 + \left(\frac{\omega_z}{\omega_{zC}}\right)^2} \quad \text{Eq. 2}$$

where ω_{iC} are critical angular velocities (rad/s) and ω_i are maximum measured angular velocities (rad/s) in each direction. ω_{xC} = 66.25 rad/s, ω_{yC} = 56.45 rad/s and ω_{zC} = 42.87 rad/s

It should be noted that, regardless of the complexity of injury thresholds, all suffer from limitations. Goldsmith (1981) discussed the use of injury thresholds and concluded that it is unlikely that a single metric would be sufficient to capture the tolerance levels of different populations. This is an important point, as it is likely that variation in gender, age, physical fitness, fatigue and injury history would all contribute to influence the tolerance levels of any given individual. It is also important to understand that all injury thresholds have been developed and validated using different types of impact, none of which focus on projectile impacts. As a result, although the injury thresholds discussed here may give an appreciation of the severity of projectile impacts relative to other impact modalities, they should be used in conjunction with mechanical parameters such as contact time, peak linear/angular acceleration and velocity, time to peak acceleration and impulse to give a more complete understanding of the mechanics of an impact.

2.6. Standard Tests

As previously mentioned, PPE is commonly worn in sports where head impacts may occur. In many respects, the introduction of PPE into sports has achieved the initial goal, which was to reduce severe, focal and catastrophic injuries (McIntosh et al., 2011). Despite this, the efficacy of helmets in reducing more minor head and brain injuries like mTBI remains poor (Hoshizaki et al., 2014; McIntosh et al., 2011). This may be, at least in part, due to the standards used to certify PPE. In many cases PPE must be certified in order to be legally sold, and as a result manufacturers design product to pass these tests. Therefore, if standard tests do not accurately represent the true threat in a given sporting context, either through using inadequate metrics and/or inappropriate test methods, disparity between testing and actual use may lead to injury, despite the best intentions of manufacturers.

In the USA, the National Operating Committee on Standards for Athletic Equipment (NOCSAE) develops and implements standards for testing PPE. The NOCSAE standards utilise a combination of drop, linear impactor and projectile tests to determine the performance of PPE in terms of impact attenuation and facial protection. In these standards, the test method is determined by the type of impact that is likely to occur in the given sport.

For example, the American Football standard (NOCSAE, 2015a) utilises a drop test, the Baseball/Softball standard (NOCSAE, 2015b) utilises a projectile test and the Ice Hockey standard (NOCSAE, 2016) utilises both methods. Although these standards may use relatively realistic test methods, the pass or fail criteria for the impact attenuation tests is based entirely on the calculated peak GSI and therefore only considers linear acceleration.

In Cricket, the globally accepted standard is the British Standard specification for head protectors for cricketers (BS 7928:2013). This standard uses a drop test method to assess impact attenuation and a projectile test method that aims to ensure that no facial contact can occur, either through direct contact with the ball, or from deformation of the grille onto the face. Although the drop test method is used to assess impact attenuation, the energy of this impact is just 18.24 J and equivalent to a 156 g Cricket ball travelling at a velocity of just 15.7 m/s (~35 mph). A more realistic impact velocity of 34 m/s (~75 mph) would produce an impact energy of 90.2 J, suggesting that the current test method may be both inappropriate (as suggested by Pang et al. (2013)) and at an unrepresentative level. In order to pass the standard, peak deceleration must be less than 250 g – this, similarly to the NOCSAE standards, neglects the potential importance of angular motion.

2.7. Headforms used in Standards and Research

2.7.1 Headform Properties

The most commonly used headforms in standards testing and research are the 50th percentile Hybrid-III, medium size NOCSAE and EN 960:2006 (EN 960), size 575. These headforms aim to represent the average male (generally from the USA) and have been developed for different impact scenarios and applications in mind. As such, each have advantages and disadvantages that should be considered before engaging in research.

The current impact attenuation test of the BS7928:2013 specifies the use of the EN 960 headform. This is a fully metallic headform, made of magnesium alloy. Although fully metallic headforms benefit from high repeatability, the increased stiffness of the metal relative to human tissue has been shown to result in clear differences between these headforms and human cadaver impacts (Kendall et al., 2012). As a result, FE models driven by loading curves gained laboratory testing using such headforms are likely to be erroneous due to the unrealistic interaction between the impacting body, the helmet and the headform (Post et al., 2012). In addition, during high shock, short duration impacts, such as a projectile Cricket ball strike, the hollow, metallic construction of these types of headform may excite

the resonance frequency of the headform which could compromise acceleration measurements.

The Hybrid-III headform, which was developed for the automotive industry but has been used extensively in sports impacts, incorporates a vinyl layer over a steel skull component, in an attempt to account for the soft tissue of the human head. However, in some impacts, the steel skull of the Hybrid-III may introduce similar problems to those seen in the EN 960. Indeed, Raymond (2008) reported that during impacts that result in high-pressure, the vinyl layer may bottom out and result in an unrealistic response due to the overly stiff steel skull.

The NOCSAE headform, which was developed for the assessment of head impacts in American Football, is the most widely used headform in sports impacts (Raymond, 2008). This headform consists of a urethane external soft tissue component and a more compliant skull component made of nylon. The NOCSAE headform also incorporates a cavity that is filled with glycerine to simulate the inertial presence of the brain. Although this should produce a more realistic inertial element of the headform, the cavity is closed and is unlikely to allow brain displacement that has been reported in a variety of impacts (Al-Bsharat et al., 1999; Feng et al., 2010; Zou et al., 2007) which should be considered as a limitation. Due to the compliant nature of the skull component of the NOCSAE headform, the manufacturers advise that an unprotected, high-speed impacts may cause permanent damage to this headform. Representative material properties of components in the EN 960, Hybrid-III and NOCSAE headforms obtained from CES EduPack (2017) can be seen in Table 11.

Table 11. Representative material properties for the components of the EN 960, Hybrid-III and NOCSAE headforms, obtained from CES EduPack (2017).

	EN 960	**Hybrid-III**		**NOCSAE**	
	Skull (Magnesium Alloy)	**Soft Tissue (Vinyl)**	**Skull (Steel)**	**Soft Tissue (Urethane)**	**Skull (Nylon)**
Density (kg/m^3)	1800	1303 - 1580	2670 - 2733	1020 - 1250	1120 - 1140
Young's Modulus (GPa)	45	2.14 - 4.14	71 - 75	0.002 - 0.03	2.62 - 3.2
Flexural Strength (MPa)	130	35.4 - 52.1	124 - 137	25 - 51	50 - 94.8
Tensile Strength (MPa)	220	40.7 - 65.1	200 - 221	25 - 51	90 - 165

The dimensions of the EN 960, Hybrid-III and NOCSAE headforms can be compared to the average values presented by Peebles and Norris (1998) to ensure that these are

appropriate representations of human geometry. As can be seen from Table 12, all three headforms are within one standard deviation with respect to head length, and circumference, but are slightly larger with respect to head breadth. More limited data is available for the headforms with respect to measurements based on the EAM. It can be seen that the NOCSAE headform is accurate from the EAM to the occiput, but is smaller than the reported values for the EAM to vertex. The EN 960 headform is accurate with respect to head height, but, like the NOCSAE, is smaller than the reported values for the EAM to vertex.

Table 12. Comparison of EN 960, Hybrid-III and NOCSAE headform dimensions with those reported by (Peebles and Norris, 1998).

	UK Male Mean (SD) (mm)	USA Male Mean (SD) (mm)	EN 960 (mm)	Hybrid-III (mm)	NOCSAE (mm)
Head length	200.2 (7.6)	200.9 (7.7)	201.6	203.0	200.0
EAM to occiput	98.5 (7.6)	98.8 (7.7)	-	-	98.0
Head breadth	143.8 (6.3)	144.2 (6.4)	158.0	155.0	152.0
Head height	228.5 (11.3)	229.2 (11.5)	225.0	-	-
EAM to vertex	130.4 (8.5)	130.8 (8.6)	121.0	124.0	115.0
Head circumference	575.0 (16.8)	576.8 (17.1)	575.0	572.0	576.0

The reported inertial properties of the headforms can also be compared to published human data. Figure 12 shows the reported mass of the headforms and values from cadaveric studies. The mass of all three headforms lies within the range of reported values for at least one study, however when the average head mass from all studies is considered, all three headforms are greater than the average plus one standard deviation.

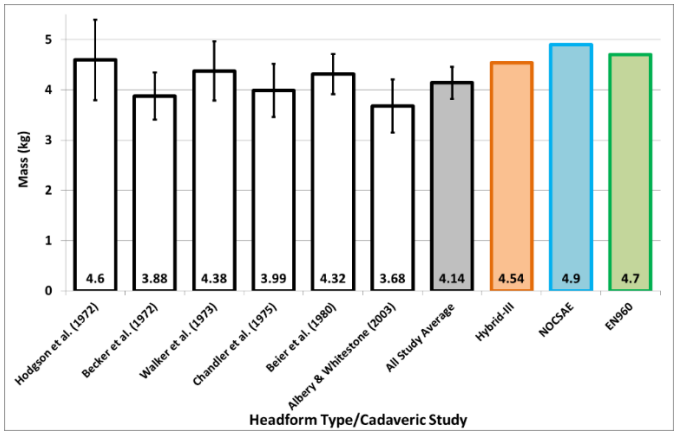

Figure 12. Reported average head mass and standard deviations from caderveric studies and headform masses.

In terms of MoI, the only data available for the headforms is at the CoG about the x (I_{xx}), y (I_{yy}) and z (I_{zz}) axes. This however can be compared to the published values from Albery and Whitestone (2003), Becker (1972) and Hodgson et al. (1972), as shown in Figure 13. The Hybrid-III matches well with the average cadaveric data in all three axes. While the NOCSAE is within the range of the average plus one standard deviation in all three axes, it is close to the upper limit of this range in I_{yy}. For the EN 960 headform, only the I_{zz} MoI is within one standard deviation of the mean reported in the cadaveric studies. The I_{xx} and I_{yy} values are above the average reported in the cadaveric studies.

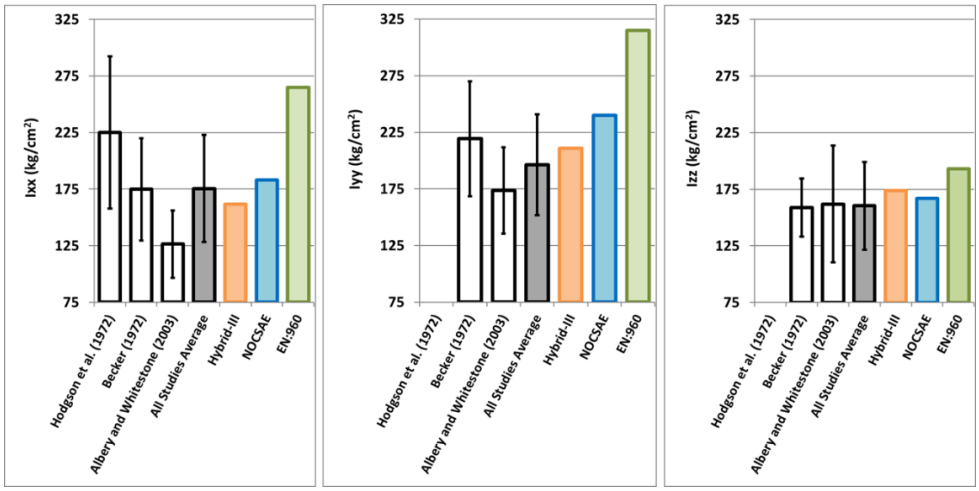

Figure 13. Average I_{xx}, I_{yy} and I_{zz} from cadaveric studies and reported headforms.

2.7.2. Head and Neck Complex

The headform mounting technique is another important factor as this may influence the observed dynamic response of the headform. The Hybrid-III neckform has been used extensively in sports research (Athiviraham et al., 2012; Beyer et al., 2012; Clark et al., 2016b; McIntosh and Janda, 2003; Pellman et al., 2003; Post et al., 2016; Viano et al.,

2005a; Walsh et al., 2011; Zanetti et al., 2013). However, as this was developed for crash tests in the automotive industry, the development only considered flexion and extension of the neck about the y axis and in this particular impact scenario where the occupant is likely to be braced in anticipation of an impact. Indeed McElhaney et al. (1988) reported that, when in slight compression, the stiffness of the Hybrid-III neck was 18.6, 43.8 and 61.2 times that of the passive stiffness of the human cervical spine in flexion, extension and lateral loading respectively. When in slight tension, the Hybrid-III neck stiffness was found to be 13.45, 13.5 and 17.4 times that of the passive stiffness of the human cervical spine in flexion, extension and lateral loading respectively.

As a result, simply applying this mounting technique to impacts where motion in six DOF is expected and/or the energy of an impact is far lower than that expected in the automotive industry, may be inappropriate. Indeed, until a suitable alternative for the Hybrid-III neckform is available, a mounting arrangement that suspends the headform relatively freely may be useful for considering a worst-case scenario, where the stiffness of this suspension is similar to that of the passive stiffness of a human neck.

2.8. Framework to Define Appropriate Impact Conditions

In order to accurately observe the mechanics of a given impact in a laboratory environment, realistic impact conditions must be achieved. In order to ensure that the laboratory experiments accurately reflect real-life impacts, the impact system as a whole can be broken down into constituent components – each of which is made up of a number of important parameters that should be considered prior to testing. In Cricket, the impact system can be broken down into three pre-impact components that influence the observed mechanical response during impact. These can be seen in Figure 14, with an overview of the constituent parameters for this particular application defined in Table 13.

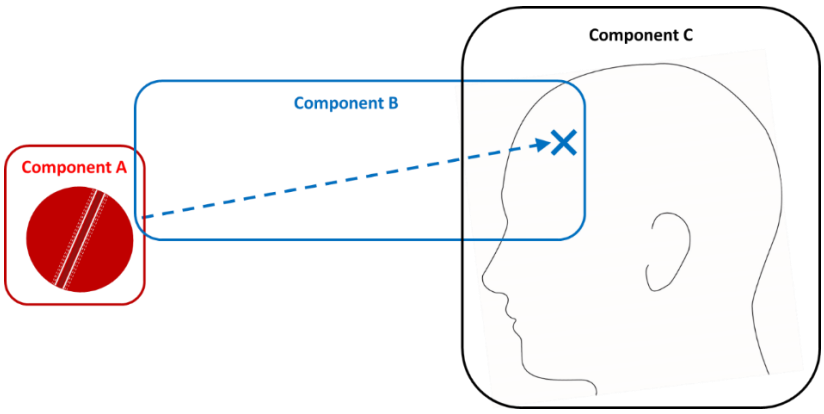

Figure 14. Components of impact system in Cricket.

Table 13. Definition and constituent parameters of the components of impact identified in Figure 14.

Component	Definition	Constituent Parameters
A	Cricket ball properties	Mass Stiffness Damping Strain rate dependency Global and local geometry
B	Impact Conditions	Speed Angle Spin Orientation Impact location
C	Head(form) Properties	Inertial properties Material properties Global and local geometry

Component A is made of parameters concerning the properties and orientation of the striker – in this case, a Cricket ball. As discussed previously, the construction and material properties of the ball are likely to influence parameters such as mass, stiffness, impact force, loading rate and contact time, all of which are potentially important parameters that may influence the impact mechanics observed when assessing the system as a whole. Additionally, Carré et al. (2004) and Fuss (2008) reported that in some cases, these parameters can vary based on the orientation of the Cricket ball. Clearly, these parameters differentiate Cricket from contact and combat sports and will therefore likely produce different impact mechanics. Due to the unique design of Cricket balls, this component is also different to other projectile sports such as Baseball, where subtle differences in ball properties may produce differences in the observed dynamic response. However, as previously discussed, Cricket ball properties have, as yet, only been investigated in quasi-static, bilateral conditions or unilaterally at unrealistically low impact speeds. An improved

understanding of Cricket ball properties at realistic loading rates is therefore necessary to fully define the parameters in this component.

Component B consists of the impact conditions including ball speed, angle and impact location. As discussed previously, in Cricket these parameters are dissimilar to those observed in combat and contact sports and will likely influence the observed impact mechanics. Although a number of studies have investigated the release speed that bowlers at various levels of performance can achieve (Elliot et al., 1993; Penrose et al., 1976; Stockill and Bartlett, 1992), there are limited studies that assess impact speed or the ball speed as it reaches the batsman – thereby accounting for speed loss due to air resistance and during contact with the ground. Due to the variety of bowling strategies used in Cricket combined with the variety of environmental conditions that influence speed loss, the range of potential impact speeds is likely to be relatively large. As such, an appropriate means of determining an impact speed for laboratory testing should be defined. Impact angle and location are also important parameters that are likely to significantly influence the impact mechanics and observed dynamic response. A limited number of studies have investigated these parameters in professional Cricket (Ranson et al., 2013), and the approach taken to determine appropriate laboratory tests can be based on a number of techniques that will be discussed in more detail in Chapter 4.

Component C consists of parameters related to the object colliding with the striker – in this case the human head. Important parameters in this component include the inertial, geometric and material properties of the head, and in some impact scenarios the head and neck complex. The inertial properties of Component C (mass, CoG, MoI) are key parameters that determine the linear and angular response of a body when subjected to a given Force/Torque and the geometric properties define the structure of the body and the local geometry at the impact location. There are multiple structures in the human head that each have material properties (such as density, stiffness and strength) that influence the mechanics of a given impact to varying degrees, dependent on the impact characteristics. In real-life, these parameters show significant individual variation, and as a result it is difficult for laboratory tests using physical surrogates to fully replicate any single impact observed in real life. As a result, laboratory tests should utilise physical surrogates that suitably represent the population in question. Although the structure of the human head is complex, physical surrogates should aim to achieve a suitable level of complexity, as over simplification may reduce biofidelity and potentially overlook legitimate response phenomenon that is pertinent in the development of injury. The relative importance of the inertial, geometric and material properties parameters is influenced by the specific impact scenario being assessed. For example, in sports such as Rugby, where the striker is likely to have much lower stiffness

and velocity compared to those seen in Cricket, negligible local deformation would be expected and as such component C may be assumed to respond as a rigid body. In these types of impact, the specific material properties of each element of the surrogate are likely to be less important than the inertial and geometric properties. Considering this, the parameters in component C should be compared with those in Component A and B, to ensure that a suitable surrogate is used in laboratory testing.

Overall, there are important parameters in each component highlighted in Figure 14 and Table 13 that distinguish impacts in Cricket from those seen in other projectile, contact and combat sports. Understanding the important parameters in each component of a given impact scenario is critical in determining appropriate laboratory test conditions prior to investigating the mechanics of the impact system as a whole. The paucity of research into each component of the framework highlighted in Figure 14, and the mechanics of head impacts as a whole, led to the development of the research aims, objectives and questions discussed in Chapter 1, which are addressed in the following chapters.

CHAPTER 3

Ball Characterisation

3.1. Introduction

In professional, International Cricket, the most commonly used ball is the Kookaburra Turf, which is used in Australia, New Zealand, South Africa, Pakistan and Sri Lanka. The Dukes Special County ball is used in England and the West Indies, whereas, in India, the SG ball is used. The materials and manufacturing processes used when producing Cricket balls varies from brand to brand, each with varied construction and subtle differences in finish. Along with good ball to ball consistency, a unique expectation of Cricket balls is that they should degrade throughout a game due to wear. This, anecdotally at least, leads to a change in the balls properties which may influence the dynamic response of PPE and the human body during an impact. Indeed Crisco et al. (1997) modelled the effect of baseball modulus and mass on head and chest impacts and reported that the likelihood and severity of skull and brain injuries may be reduced by using more compliant baseballs as a result of longer contact durations and lower peak accelerations.

Within a game, a Cricket ball undergoes highly intensive and rapid loading and unloading in various situations. Although some previous work has attempted to characterise Cricket balls, no studies have thoroughly investigated the dynamic properties of Cricket balls at deformation rates representative of those seen in match play. Fuss (2008) and Subic et al. (2005) used quasi-static compression tests done slowly (5 – 500 mm/min) which are not necessarily indicative of real-life impacts where the loading occurs rapidly and from a single side. Carré et al. (2004) modelled a Cricket ball impact with the ground and used experimental testing to validate this model. In this study, an unused Readers 'Grade 1 county' Cricket ball was dropped onto a load cell in two orientations (face and seam) with impact velocities up to c. 6 m/s. It was reported that, unsurprisingly, greater impact speed resulted in greater impact force and ball deformation. For an impact force of ~2 kN, seam impacts produced deformation of 2.7 mm (stiffness ~740 N/mm) whereas face impacts of the same impact force produced deformation of 1.8 mm (stiffness ~1,111 N/mm). Whilst this study utilised a more realistic impact method, the deformation rate was again limited to 6 m/s and much lower than those experienced during a direct impact with a bat or PPE during match play.

Currently, a Cricket training ball (BOLA) is specified for use in the penetration test annexe of the current British Standard for head protectors for cricketers (BS 7928:2013) due to its perceived consistency and durability relative to actual Cricket balls. This perception stems from the construction of the different ball types. The BOLA ball is an injection moulded ball made from homogenous polyurethane (as shown in Figure 15 c). The diameter of a BOLA ball is 71 mm in diameter and therefore comparable to cricket balls. The surface of the BOLA ball has a number of dimples that are around 8 mm in diameter, and 3 mm deep. Alternatively the Kookaburra ball has a core (~40 mm in diameter) made from ground natural cork and rubber, surrounded by five layers of woven yarn and cork, as shown in Figure 15 a. The casing is made of leather, coated in nitrous cellulose lacquer, and is ~4 mm thick. The Dukes ball differs from the Kookaburra in that the core is made of just compacted, ground natural cork, as shown in Figure 15 b. The casing is also made of leather, but is polished with a synthetic grease. Although the seam is hand stitched in both types of ball, the seam of the Kookaburra ball is more prominent than that of the Dukes. Although both types of cricket ball must have a diameter of 71 – 73 mm, the differences in construction, materials and manufacturing processes may manifest in variations in observed ball properties. As yet, no studies have investigated the properties of BOLA or Cricket balls at realistic loading rates. As a result, the type of ball used in laboratory and standards tests cannot be fully defined and variations in their properties cannot be limited or accounted for.

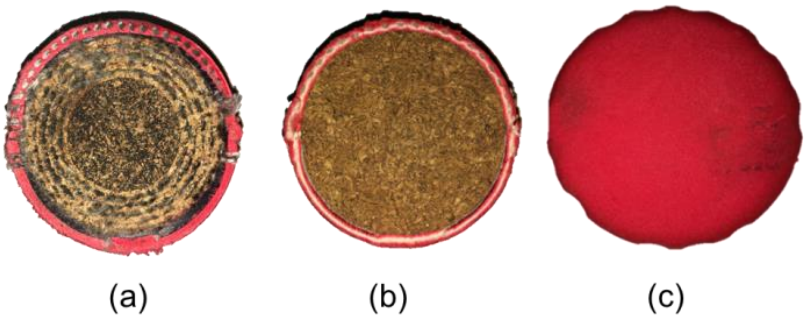

Figure 15. Examples of the varied constructions of a Kookaburra Turf (a), Dukes Special County (b) and BOLA (c) ball.

Although some work has looked into the properties of Cricket balls, the paucity of research conducted at realistic loading rates means that the understanding of these properties remains poorly understood. There are also no studies that have investigated ball degradation as a result of repeated impacts, despite anecdotal evidence of ‘ball softening’ (Fuss, 2008). This has potentially important ramifications relating laboratory and standards testing and FE modelling of such impacts.

Due to the varied constructions and use of organic materials used in the manufacture of Cricket balls, these may show intra and inter ball variations in ball properties which, in turn, may influence the mechanics of a head impact in Cricket (Crisco et al., 1997). It is therefore imperative that, when designing test methods to assess head impacts in Cricket, the striker is representative of real-life scenarios to provide meaningful data, and consistent enough to allow impact by impact comparisons.

The aims of the study reported in this chapter were to:

1) *Investigate the dynamic impact properties of two of the most commonly used elite level Cricket balls and a Cricket training ball at realistic loading rates*
2) *Investigate the effect of repeated impacts on the observed ball properties.*
3) *Determine an appropriate ball for future laboratory tests when assessing head impacts in Cricket.*

In order to investigate the dynamic properties of these balls, and the potential implications of test ball selection on laboratory reconstructions of head impacts, a number of parameters are required across representative balls. These include:

- Mass
- Coefficient of restitution (CoR)
- Contact time
- Peak force
- Time to peak force
- Maximum ball deformation
- Stiffness

3.2. Methodology

In this study, the properties of three ball types were assessed. Two of these were the Kookaburra Turf and Dukes Special County (as used in international Cricket around the world in 2017/2018), and the other was a BOLA Cricket training ball (currently specified for use in the penetration test included in BS 7928:2013) (as shown in Figure 15).

Prior to all testing all balls were stored at 22 ± 2 ^{o}C with a relative humidity of 15 ±5 % for at least 24 hours. The mass of each ball was measured using a calibrated Kern 572 set of scales (measurement resolution ±0.001 g). A short repeatability test confirmed that the mass measurement varied by, at most 0.001 g and therefore repeated mass measurements were deemed to be unnecessary.

When attempting to experimentally determine the properties of balls at realistic deformation rates, the fundamental governing principles should be assessed in order to confirm validity. In all collisions between two non-rigid bodies, deformation occurs in both of the colliding objects. Depending on the relative inertia, stiffness and damping exhibited by both bodies, the initial deformation rate of either will be a fraction of the relative approach velocity. Simplifying, a two-body system, with each body having associated mass (m_1, m_2), stiffness (k_1, k_2) and velocity (v_1, v_2) has a relative velocity of approach, V given by Eq. 3.

$$V = v_1 - v_2 \qquad \text{Eq. 3}$$

Assuming, as done by (Ankrah and Mills, 2003), both bodies achieve a common velocity at maximum deformation (v_c), conservation of momentum requires:

$$v_c = \frac{m_1 v_1 + m_2 v_2}{m_1 + m_2} \qquad \text{Eq. 4}$$

Conservation of energy then requires that the deformation energy absorbed during impact at the point of maximum deformation (E_e) is given by:

$$E_e = \frac{m_1 m_2 (v_1 - v_2)^2}{m_1 + m_2} \qquad \text{Eq. 5}$$

$$\Rightarrow \frac{1}{2} \mu V^2 \qquad \text{Eq. 6}$$

$$\text{where: } \mu = \frac{m_1 m_2}{m_1 + m_2}$$

Initial deformation rates for either body, and estimates for a more complex Cricket ball system, can be calculated by considering the two-mass system with k_1 and k_2 perfectly linearly elastic. Upon contact the two bodies become a two-mass oscillating system. The stiffnesses act in series with total (k_T) given by:

$$k_T = \frac{k_1 k_2}{k_1 + k_2} \qquad \text{Eq. 7}$$

The natural frequency (ω_n) of the two-mass system can be defined using Eq. 6 and Eq. 7 as:

$$\omega_n = \sqrt{\frac{k_T}{\mu}} \qquad \text{Eq. 8}$$

Body 1 will oscillate at ω_n with amplitude a_1, while body 2 will oscillate at ω_n with amplitude a_2 and will exert an equal and opposite force on each other so that:

$$k_1 a_1 = k_2 a_2 \qquad \text{Eq. 9}$$

The total strain energy (E_s) stored in both springs at maximum deformation is equal to the effective impact energy, so that:

$$E_s = \frac{1}{2} k_1 {a_1}^2 + \frac{1}{2} k_2 {a_2}^2 = \frac{1}{2} \mu V^2 \qquad \text{Eq. 10}$$

a_1 can then be predicted by continuing Eq. 8 and 10:

$$a_1 = \sqrt{\frac{\mu k_2}{k_1(k_1 + k_2)}} \times V \qquad \text{Eq. 11}$$

The individual initial deformation rate of body 1 ($\dot{x}_1$) is given at contact by:

$$\dot{x}_1 = \omega_n a_1 \qquad \text{Eq. 12}$$

If $\lambda = \frac{k_1}{k_2}$, consolidating Eq 7, 8 and 12 gives:

$$\dot{x}_1 = \frac{1}{(1 + \lambda)} \times V \qquad \text{Eq. 13}$$

By symmetry of equations:

$$\dot{x}_2 = \frac{1}{(1 + \lambda_{21})} \times V \qquad \text{Eq. 14}$$

where $\dot{x}_2$ is the initial deformation rate of body 2 and $\lambda_{21} = \frac{k_2}{k_1}$.

Thus, given the masses, stiffnesses and velocities of the two bodies, Eq. 13 and Eq. 14 can be used to estimate the initial deformation rate seen in each body. However, to experimentally determine the dynamic stiffness of a Cricket ball at a realistic deformation

rate, the stiffness of the ball must be known in order to determine the realistic deformation rate, which poses a circular problem.

A solution to this problem is to measure ball stiffnesses when colliding with rigid objects of extremely large mass and high stiffness. As the stiffness of the ball is much less than that of the rigid surface, the initial deformation rate of the ball is approximately equal to the impact speed. By testing balls at multiple impact speeds, a curve that describes the ball stiffness at varied deformation rates can be developed.

This approach was taken in this study to assess the three ball types at three nominal impact speeds and initial deformation rates. These were; 4.4 m/s (9.84 mph) (low speed), 17.9 m/s (40 mph) (medium-speed) and 31.3 m/s (70 mph) (high-speed). Impact tests were conducted in two orientations one where the impact occurred at a point furthest from the seam, with the line of force applied perpendicular to the seam (Face), and one where the point of impact occurred on the seam, with the line of force applied parallel to the seam (Seam). As initial tests at all impact speeds using the BOLA balls revealed no significant differences between the two orientations, impacts were only conducted in one orientation.

Following the initial high-speed impact tests, one representative ball from each ball type was selected and subjected to 15 additional high-speed impacts to assess ball degradation. Although this is an accelerated measure of ball degradation relative to that observed in a real-life game (since the intensity of each impact is likely greater than that seen in actual impacts due to the mass and stiffness of the colliding bodies in real-life scenarios) it provides a time-efficient means of assessing ball degradation.

3.2.1. Low-Speed Impacts

A 1m drop test was used to assess the dynamic properties of five of each ball type at the low impact speed. Each ball was dropped five times on the Face, and five times on the Seam with a minimum of five minutes between concurrent impacts on a given ball. A vacuum drop system was used to hold each ball in the desired orientation, 1m above a Kistler 9367B force link. The force link was connected to a Bruel and Kjaer conditioning amplifier, set to the known sensitivity of 3.8 pC/N and, following conditioning, a Picoscope 5000 series digital oscilloscope was used to record the impact force at 1 MHz. A Photron Mono Fastcam was positioned level and perpendicular with the impact surface to record the impact at 40,000 fps. Two Arri pocket Parr lights were used to provide additional lighting and allowed the background and impact plate to be fully saturated in the image, with the ball appearing as a darker body. The camera focal plane was adjusted to contain the motion of the ball centre and was calibrated using a precise metric scale placed in this plane (calibration factor 4.05

pixels/mm). Two laser timing gates were positioned 100 mm apart to measure the time interval, from which the inbound and outbound ball speed could be calculated using equations of constant acceleration. The laser timing gate closest to the force link was one ball diameter from the impact surface and used to simultaneously trigger force and high-speed video (HSV) data collection (experimental setup shown in Figure 16).

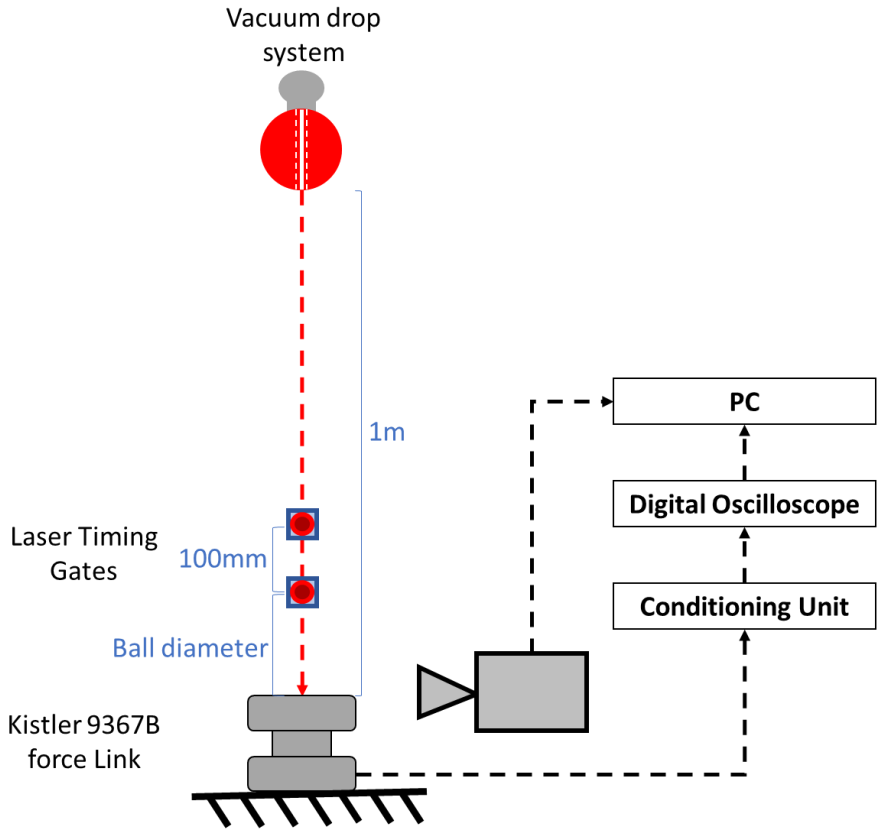

Figure 16. Schematic of the low speed experimental setup.

3.2.2. Medium- and High-Speed Impacts

The medium and high-speed impacts were conducted by propelling balls onto a rigid plate mounted onto a concrete block (c. 250 kg). Three screws and an araldite epoxy resin were used to bond a 15 mm thick steel plate at the required location. Three PCB 208C05 ICP force sensors were mounted onto the concrete block in a triangular arrangement with 45 mm separation and connected to a Picoscope 5000 series digital oscilloscope recording at 1 MHz. A 130x125x15 mm steel plate was then screw mounted onto the three force sensors. The concrete block was then positioned and secured onto a weight bearing column to further increase the effective mass of this system (schematic of this sandwich arrangement can be found in Figure 17). The block and column system were assumed to be of sufficient mass, relative to that of a Cricket ball, that any movement of the block during impact would be

negligible. The stiffness of the system was also assessed and considered to be suitably high (modal analysis revealed the lowest natural frequency of the whole structure to be c. 10 kHz). An approach similar to this has used to good effect in previous studies to assess baseball and softball properties (Biesen and Smith, 2007; Duris and Smith, 2004; Smith, 2008; Smith et al., 2010; Smith and Duris, 2009; Smith and Faber, 2011).

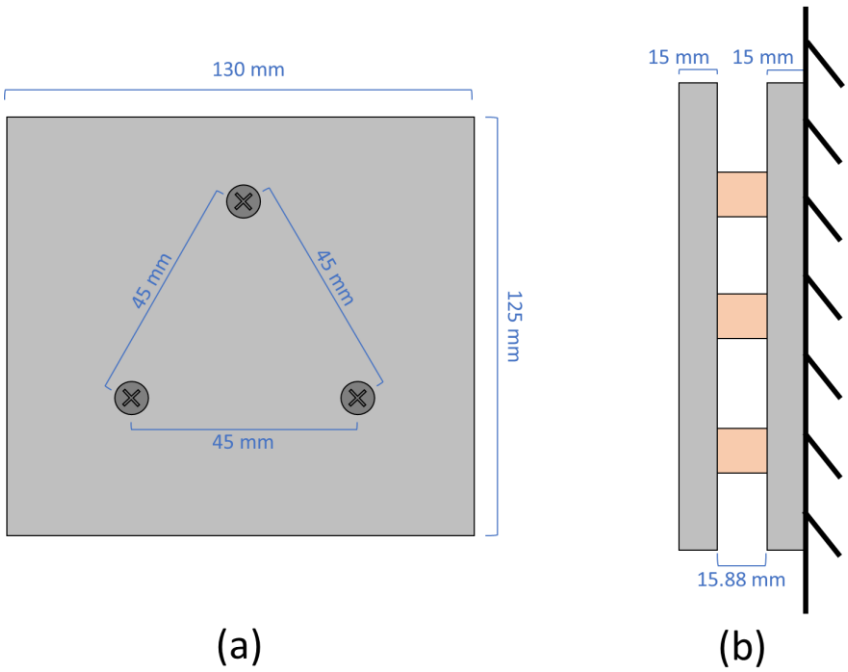

Figure 17. Schematic of the sensor arrangement used to measure force during the medium- and high-speed impacts.

A pressurised air cannon was used to propel five unused balls of each type at a nominal speed of 17.88 m/s (40 mph), and five different, unused balls of each type at nominal impact speeds of 31.29 m/s (70 mph). All trials were within ±0.5 m/s of the nominal impact speed. Following each impact, the Cricket balls were rotated through 90^{o} through an axis perpendicular to the line of flight, until five impacts were completed with the in the Face and Seam orientations. During all testing, a recovery period of at least five minutes was included between each concurrent impact on a given ball in order to minimise the effect of internal frictional heating, as described by Smith et al. (2010). Following this, a single representative Cricket ball of each type was selected and impacted a further 15 times on the face and 15 on the seam, at a nominal impact speed of 31.29 m/s with a recovery period of at least five minutes between each impact. A representative BOLA ball was also selected and impacted 15 times on the face with the same nominal impact speed and recovery period between each impact.

The air cannon was positioned so that the ball would impact the rigid plate at the centre of the three force sensors. A Photron Mono Fastcam was positioned perpendicular to the face of the front steel plate (schematic shown in Figure 18). The spatial resolution allowed a view of the rigid plate, the full ball diameter and around 40mm of ball flight. A 40,000 fps sampling frequency was achieved through additional lighting (2 Arri Pocket Parr lights). The additional lights allowed full saturation of the background and rigid plate in the image, meaning that the ball was outlined as a darker object on the recording (still images throughout the impact sequence for each ball are shown in Figure 19). The entire field of view was calibrated using a precise metric scale in the plane perpendicular to the impact plate at the point of impact. Due to the limited field of view, there was no measurable effect of lens distortion and the calibration factor was determined to be 4.15 pixels/mm throughout the entire capture area. Two laser timing gates were positioned 100 mm apart were used to calculate the inbound and outbound ball velocity over this distance. As in the low speed impacts, synchronised data capture on the oscilloscope and HSV was achieved by using the laser closest to the rigid plate to synchronously trigger both systems.

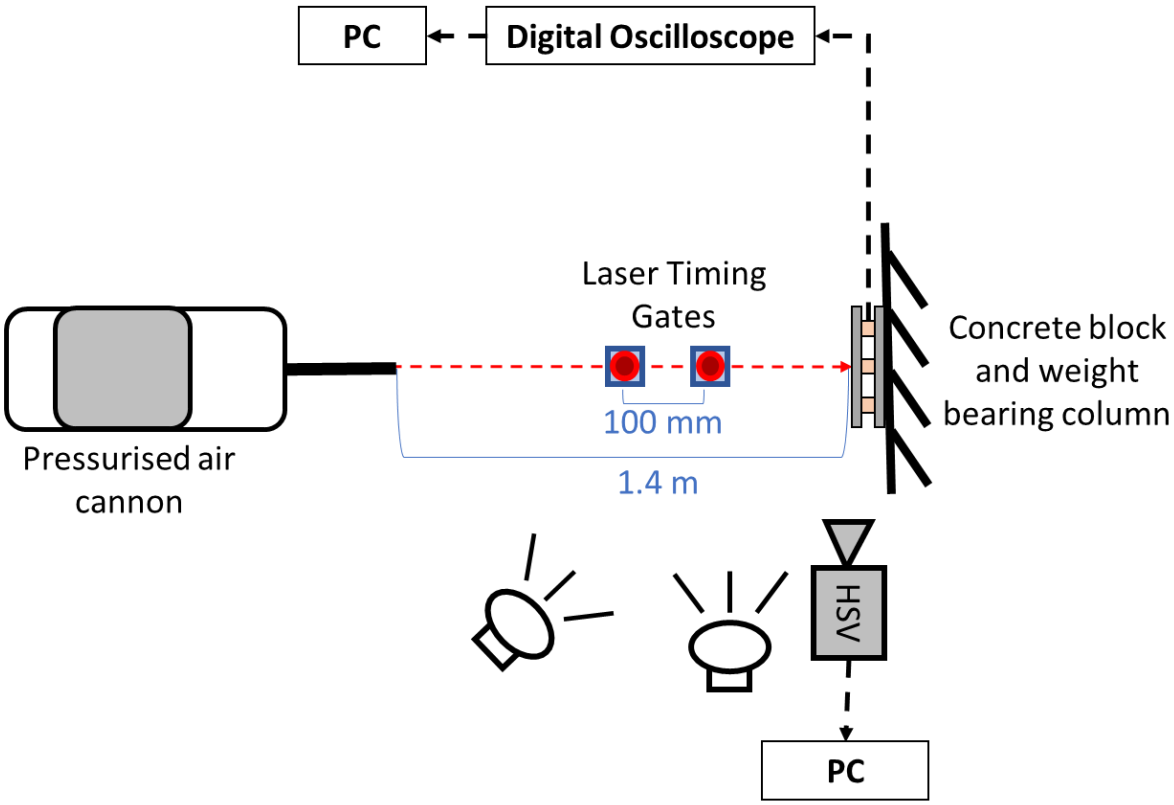

Figure 18. Schematic of the medium and high-speed experimental setup.

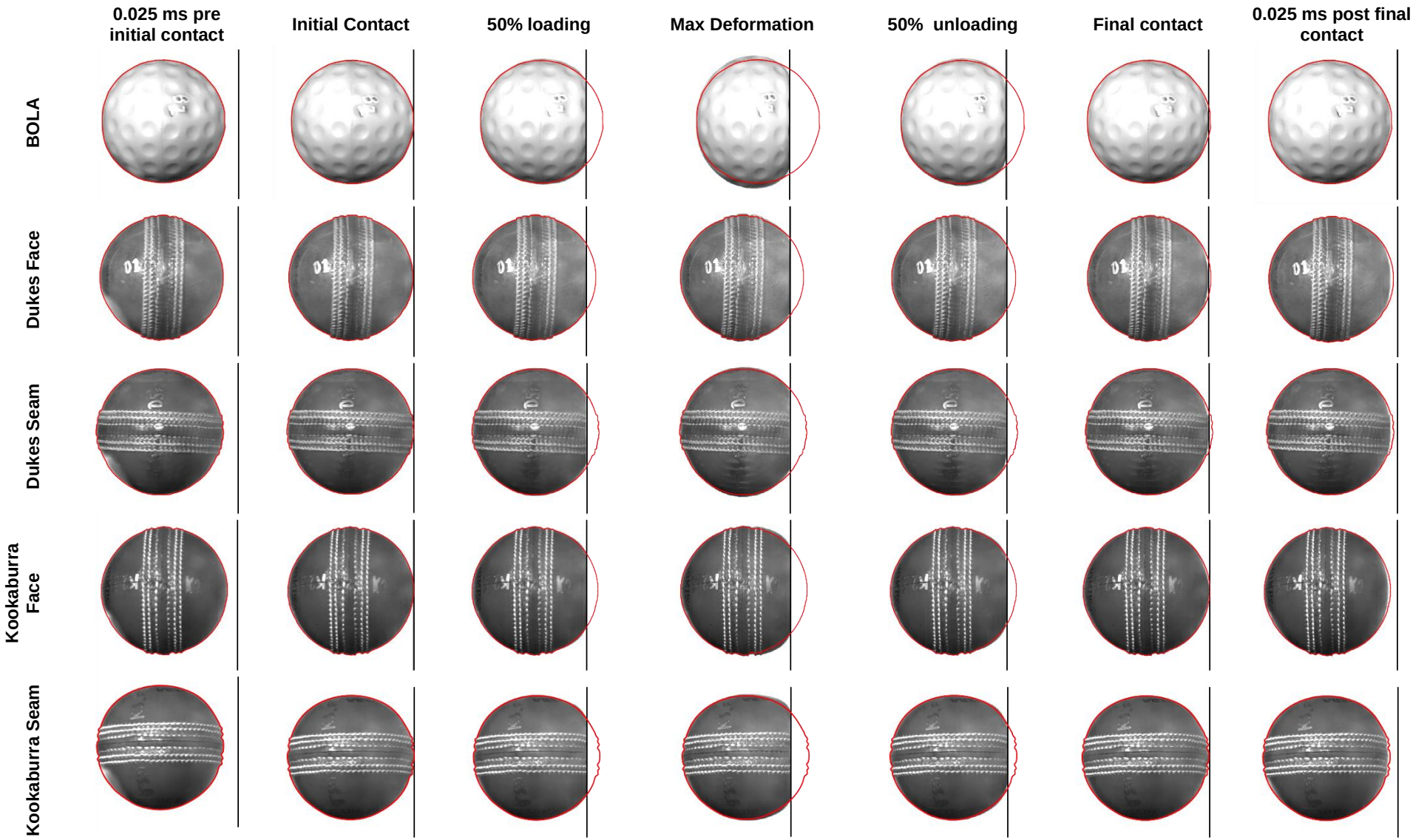

Figure 19. Still images from the deformation sequence of each ball. Outlines of the initial ball shape are shown as red outlines, and the impact surface is referenced as the solid black line.

3.2.3. Post Processing

A custom MATLAB script was written to process the HSV and force data for all three impact speeds. Edge detection techniques were used to identify the leading and trailing edges of the ball, and the calibration factor was applied to convert the pixel difference between these measures into mm (Figure 20), thereby directly measuring ball deformation using the diameter compression technique (Collins, 2011). The contact time was identified as the period where the position of the leading edge was constant (as per Figure 20a). Image-Pro Analyzer 7.0 was used to manually measure initial diameter, maximum deformation and contact time of 10 randomly selected trials to verify the MATLAB image processing script.

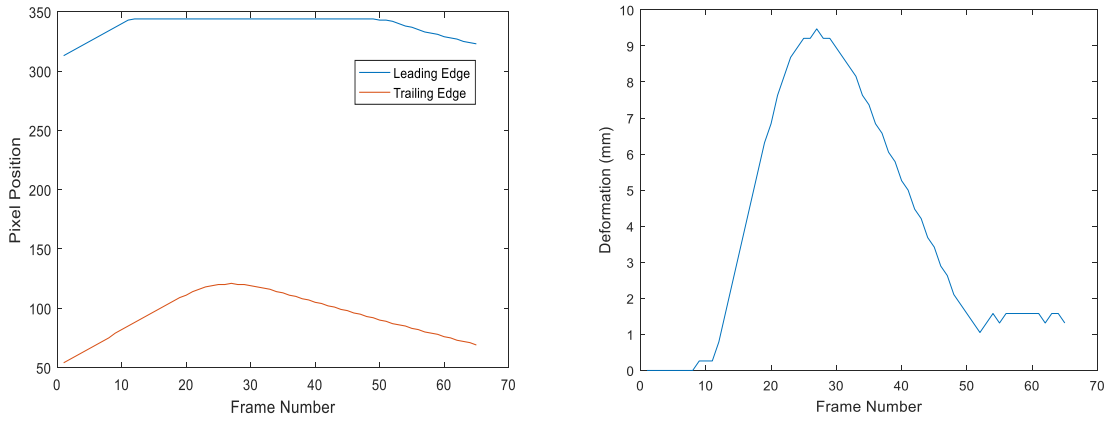

(a) (b)

Figure 20. Examples of identification of leading and trailing edges (a) and ball deformation (b).

The force output was converted from millivolts (mV) to Newtons (N) by applying the known sensitivity (0.217 mV/N) to each force sensor output. The total force was determined by summing the output of all three force sensors. Any zero offset was accounted for by subtracting the mean of the first 5,000 data points (prior to any contact) from the whole signal. In order to remove the very high frequency noise, potentially introduced through resonant excitation of the force measurement/block structure from the signal, a 4th order low pass Butterworth filter set at 8 kHz was applied. The HSV frames identified as initial and final contact were used to isolate the contact period from the whole force trace (see Figure 21 for examples of typical filtered and unfiltered force data). Variations in actual impact velocity will produce proportionally different forces in the same contact time. As such, this was accounted for by multiplying the measured force by the measured impact velocity divided by the nominal impact velocity (referred to as ‘corrected force’). As variations in impact speed

would also influence the maximum ball deformation, this parameter was also corrected by applying the same procedure (referred to as 'corrected maximum deformation').

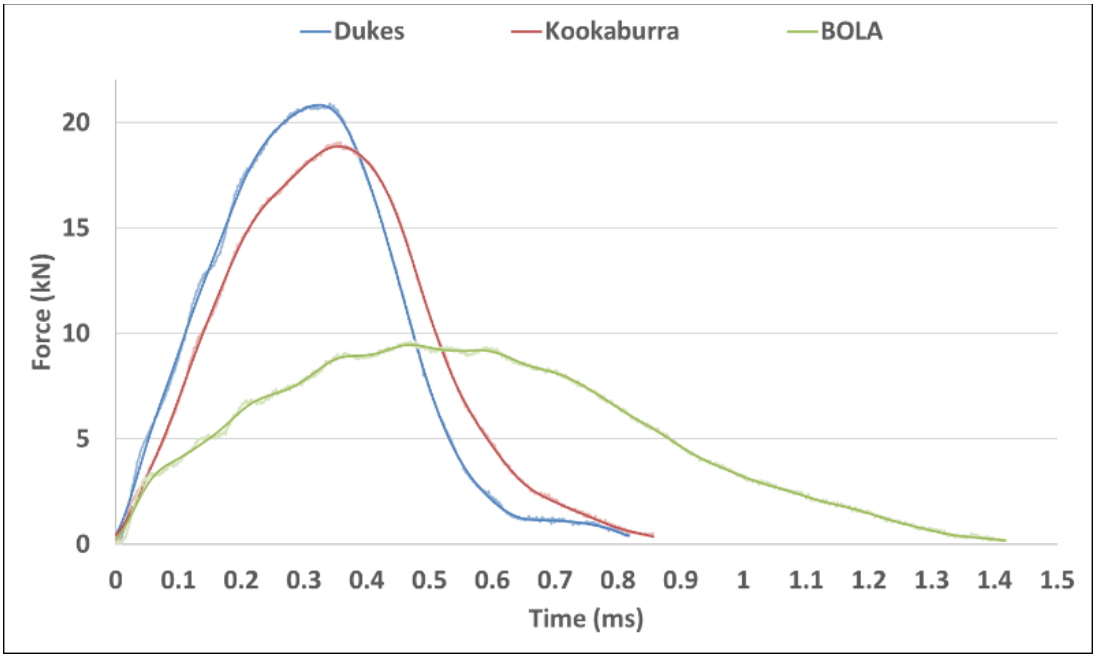

Figure 21. Examples of typical filtered (darker) and unfiltered (lighter) force traces from individual impacts, from initial to final contact at 31.29 m/s.

The peak force and time to peak force were extracted from the isolated force traces. Although the force and HSV recordings were synchronised, the sampling frequency of the HSV was lower than that of the force transducers. As such, the force signal was down sampled by a factor of 25 to produce force deformation curves (see Figure 22 for typical examples of these). As the loading phase of the force deformation curves for the Dukes and Kookaburra balls was found to be relatively linear, secant stiffness was determined by identifying the magnitude of the peak force and dividing this by the measured deformation at the corresponding time point (see Figure 21 representation of this measure). Although the BOLA balls displayed non-linear stiffness during loading (see Figure 22), the same technique was used to determine an average, overall stiffness during loading and allow comparison with the Dukes and Kookaburra balls. In addition to the calculation of the CoR, the measured inbound and outbound ball speeds were used to determine the change in momentum, which was compared to the area under the force curve as a means of validating the force measurement. In all impacts the area under the curve was found to be slightly greater than the change in momentum – however, these differences were small, with an average difference of just 1.85% and a maximum difference of 3.36%.

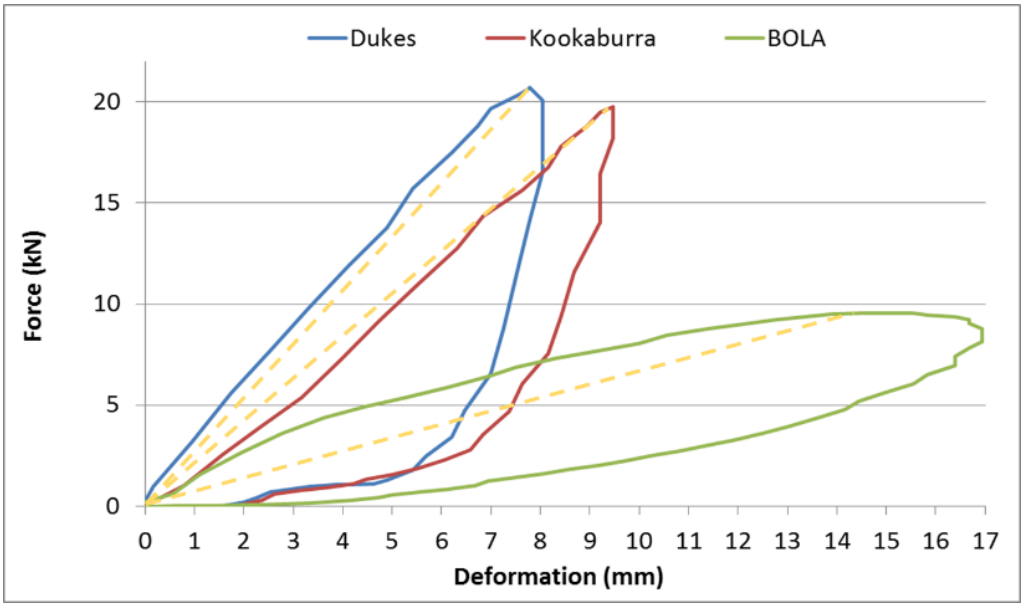

Figure 22. Examples of typical force deformation from individual impacts from initial to final contact at 31.29 m/s. Yellow dashed lines indicate the calculated secant stiffnesses.

In the medium and high-speed impacts non-linear relationships between impact number and various parameters were observed. This suggested that the first impacts that caused significant deformation resulted in a permanent change in the balls properties, and that further severe impacts caused the ball properties to tend to a steady state – similar to the Mullins effect in rubber materials (Mullins, 1969). Multiple regression equations were applied to the repeated impact data, but a power regression showed the highest R^2 value for each parameter and ball brand/orientation. These regressions were then used to predict the number of high-speed impacts required for each ball type to reach a 'steady state' – defined here as the impact at which the difference between concurrent impacts was less than or equal to 1%.

Statistical analysis was completed using IBM SPSS version 23. Following confirmation of normal distribution and homogeneity of variance, using Shapiro-Wilk and Levene's test respectively, One-way ANOVAs (with a Bonferroni post-hoc) and T-tests were completed where appropriate, with the significance threshold set at $p \leq 0.05$.

3.3. Results

3.3.1. Mass

The measured masses of the balls tested can be seen in Table 14. The Laws of Cricket (MCC) specify that the mass of a Cricket ball should be between 156 and 163 gm. The mean and standard deviations of the Dukes and Kookaburra (159.9 ±2.4 and 159.4 ±2.8 gm

respectively) sit within the specified maximum and minimum. However, one Dukes ball (155.7 gm) and two Kookaburra balls (both 155.5 gm) and were found to have masses slightly below the specified minimum. Although they are not required to meet any performance standards, all of the BOLA balls were well below the minimum mass specified in the Laws of Cricket (MCC), with a mean mass of 144.9 ±1.1 gm. As expected, the Dukes and Kookaburra balls did not show a statistically significant difference ($p = 1$). Statistically significant differences were found between the BOLA balls and the two Cricket ball types ($p < 0.001$). The greatest variation in mass was seen in the Kookaburra balls (SD = 2.83 gm), closely followed by the Dukes (SD = 2.37 gm) and BOLA (SD = 1.1 gm).

Table 14. Measured masses of the Dukes, Kookaburra and BOLA balls.

Ball Type	Mass (gm) (mean (SD))
Dukes	159.9 (2.4)
Kookaburra	159.4 (2.8)
BOLA	144.9 (1.1)

3.3.2. Impact Properties

As discussed previously, some parameters were found to change on an impact by impact basis during the medium and high-speed impacts, potentially due to permanent alterations resulting from the large deformations experienced by the balls. Although this was not the case for the low speed impacts, all results are presented on a ball type and impact number basis.

3.3.2.1. Contact Time

Mean contact time on an impact by impact basis for each nominal impact speed is presented in Figure 23. As reported by Bridge (1998) and Goldsmith (1960) shorter contact times were found as impact speed increased. For the medium and high-speed impacts, performance of the Dukes balls showed little difference between the Face and Seam orientations across all five impacts (statistically insignificant ($p > 0.887$)). In the low speed impacts, the difference between the Dukes face and seam was greater showing a trend towards significance, but remained statistically insignificant ($p = 0.056$). The Kookaburra balls displayed significantly ($p < 0.001$) longer contact durations in the Seam impacts than the Face at the low, medium and high impact speeds. As can be seen in Figure 23, the Dukes balls showed a statistically significant ($p < 0.001$) shorter contact time than the Kookaburra balls at all three impact speeds in both orientations. The BOLA balls show statistically significant ($p < 0.001$) longer contact durations than the Dukes and Kookaburra balls at each impact speed. As can be

seen in the standard deviations presented in Figure 23, there is greater intra-ball variability in the Dukes and BOLA balls than in the Kookaburra balls (the standard deviation was found to be maximally 5.85%, 3.26% and 2.76% of the mean for the Dukes, BOLA and Kookaburra respectively).

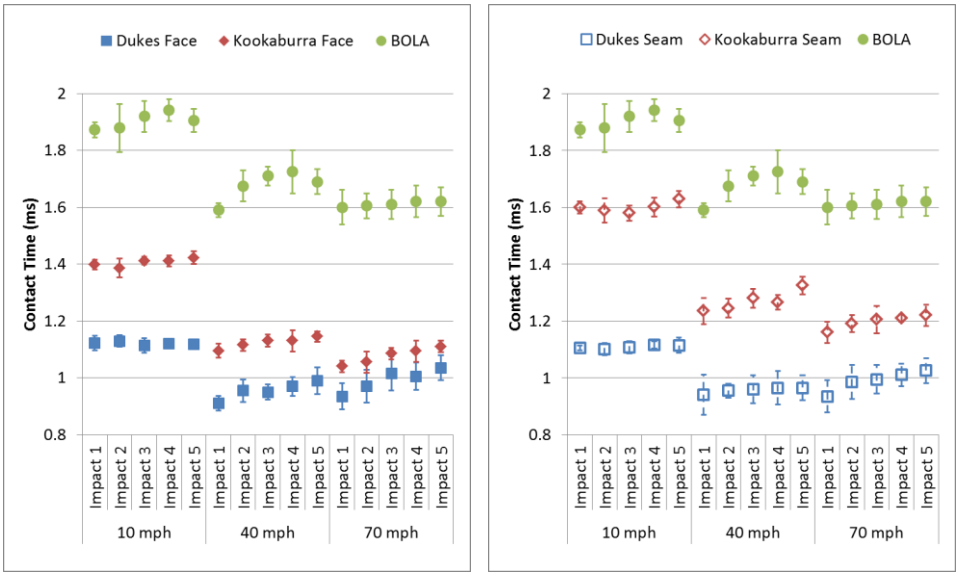

Figure 23. Mean of the measured contact times on an impact by impact basis.

In the high-speed impacts, contact duration increased slightly with impact number in each ball type and impact orientation. In the Dukes and Kookaburra balls the mean change in contact time was around 0.1 ms from the first impact to the fifth, whereas the BOLA showed lower deviation. Although 0.1 ms appears relatively low, it does correspond to ~10% of the total contact time. Figure 24 shows the 20 repeated impacts on a representative Dukes, Kookaburra and BOLA ball. In both orientations, similar to Figure 24, the initial impacts produced the shortest contact times in the Dukes and Kookaburra balls. However, the change in contact time appears to plateau as impact number increases. The BOLA ball also showed slightly longer contact time with increased impact number, however this change was less pronounced than in the Dukes or Kookaburra balls. Based on the power regressions, all ball types and orientations showed strong relationships with the measured results (R^2 values – Dukes face: 0.92, Dukes seam: 0.92, Kookaburra face: 0.87, Kookaburra seam: 0.91, BOLA: 0.8). The Dukes ball took longer to reach 'steady state' (10 and 7 impacts for the Face and Seam respectively), than the Kookaburra (6 impacts for both the Face and Seam), whereas the BOLA ball took just 4 impacts.

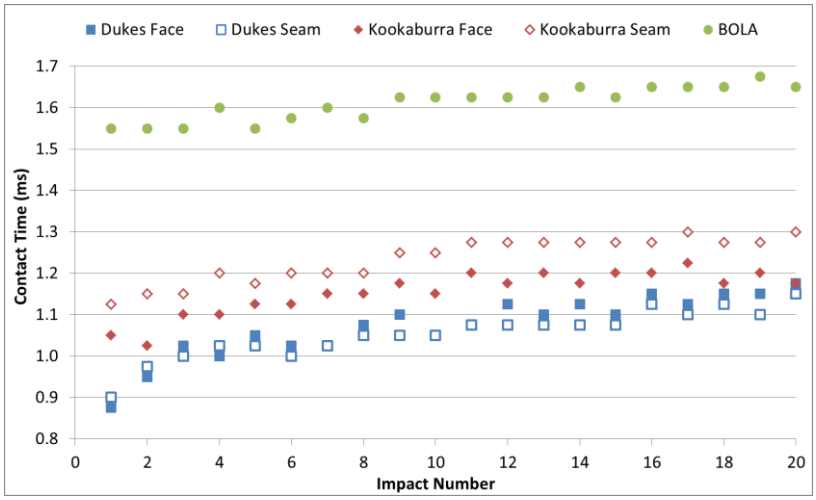

Figure 24. Measured contact time of the repeated 70 mph impacts on a representative ball of each type.

3.3.2.2. Coefficient of Restitution

The impact by impact mean CoR of the Dukes, Kookaburra and BOLA balls for each impact speed can be found in Figure 25. Statistically significant ($p < 0.01$) differences were observed between the Face and Seam impacts, in all impact scenarios other than the Dukes balls at the medium impact speed ($p = 0.58$). All ball type comparisons showed statistically significant differences ($p < 0.03$), other than the medium speed Kookaburra face – BOLA face ($p = 1$) and the low speed Dukes seam – Kookaburra seam ($p = 1$) impacts. Generally, the Kookaburra showed a higher CoR than the Dukes, but a slightly lower CoR than the BOLA balls at all three impacts speeds. The effect of impact speed on CoR is clear in Figure 25, as in each ball type and orientation CoR reduces with impact speed. This has previously been reported in other sports balls (Carré et al., 2004; Collins, 2011; Smith and Duris, 2009).

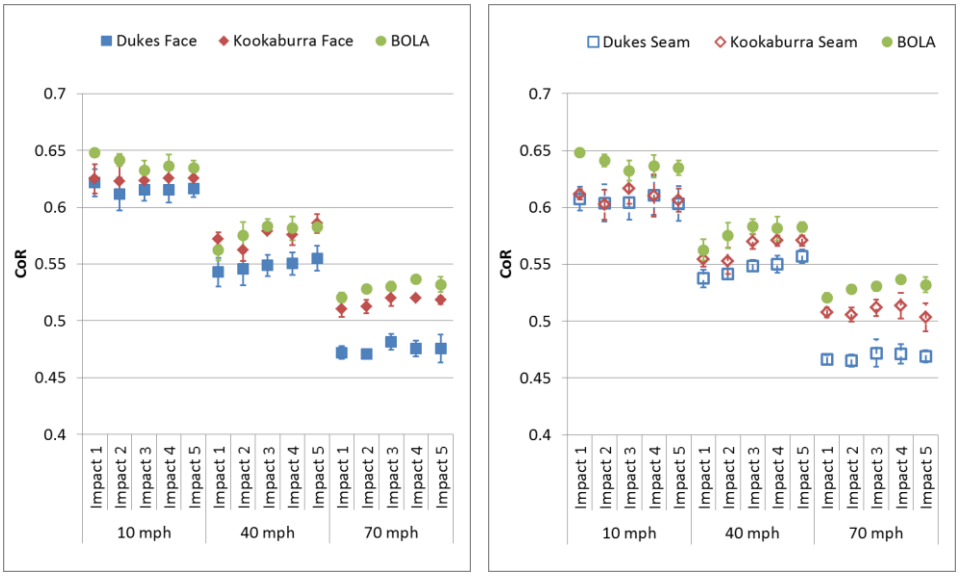

Figure 25. Mean measured CoR on an impact by impact basis.

Repeated high-speed impacts appear to have a limited effect on CoR, as only small changes from impact 1 to 20 can be seen (Figure 26). The CoR of the Dukes balls reduced with impact number, whereas the Kookaburra balls showed a slight increase. The BOLA balls showed a more pronounced increase. Indeed, the only impact conditions where the R^2 values of the power regression were reasonable were the Dukes face (0.67) and the BOLA (0.8). Both impact conditions showed 'steady state' after 3 impacts.

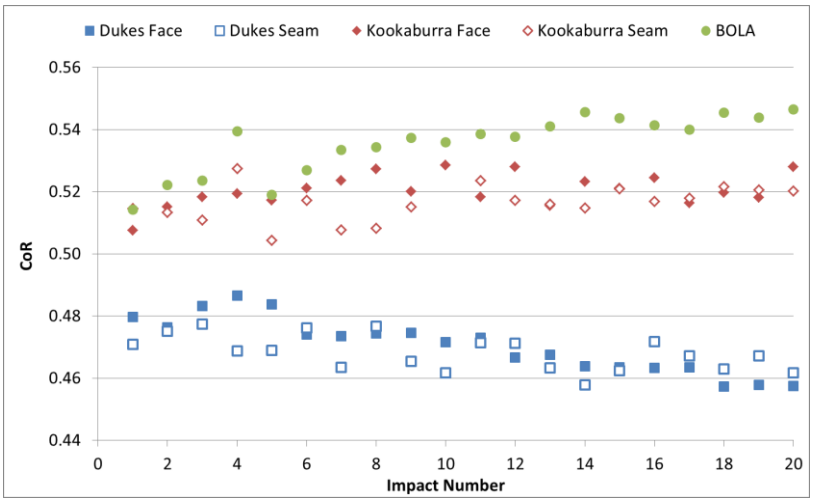

Figure 26. Measured CoR for the repeated 70 mph impacts on a representative ball of each type.

3.3.2.3. Maximum Ball Deformation

Figure 27 shows an impact by impact mean of the corrected maximum ball deformation at each impact speed. As expected, higher impact speeds resulted in greater ball deformation. In all three impact speeds the Dukes balls showed slightly lower corrected maximum ball deformation than the Kookaburra, particularly in the Seam orientation. When considering all five impacts at each speed, statistically significant differences were found between the Dukes and Kookaburra balls in the Seam orientation ($p < 0.001$). In the Face orientation, significant differences were found at the low and medium impact speeds ($p < 0.001$), but not at the high impact speed ($p = 0.117$). The BOLA balls showed almost double the corrected maximum deformation observed in the Dukes and Kookaburra balls and, unsurprisingly, these differences were found to be statistically significant ($p < 0.001$).

When comparing the effect of impact orientation within a specific ball type, the Kookaburra balls showed greater corrected maximum ball deformation in the Seam orientation than in the Face at each impact speed, which were found to be statistically significant in each case ($p < 0.001$). The Dukes balls show no statistically significant differences at high impact speeds ($p = 0.944$), whereas at the medium and low impact speeds the Seam orientation showed significantly greater corrected maximum ball deformation ($p < 0.045$).

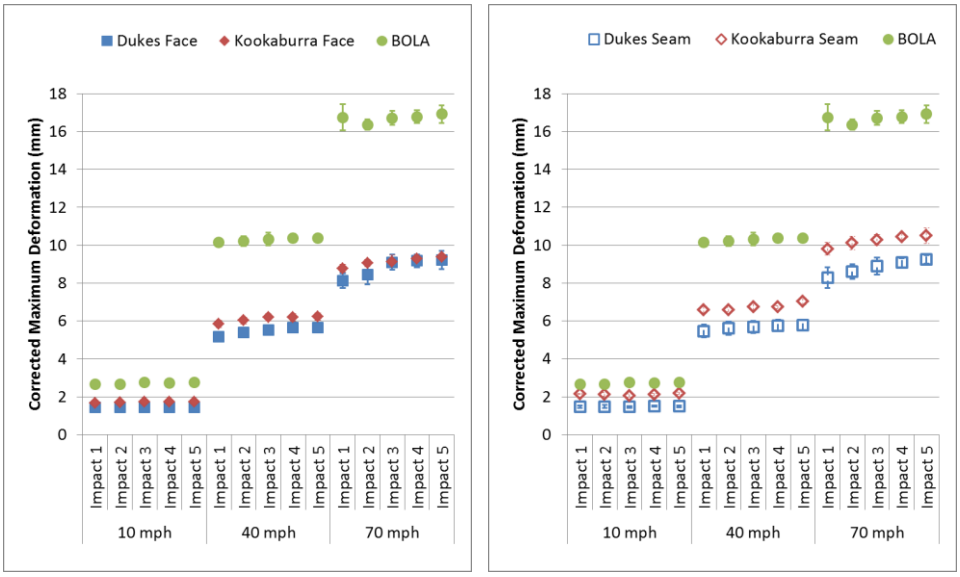

Figure 27. Mean corrected maximum ball deformation for each ball type and impact speed.

Similar to the contact time results presented previously, in every ball type and orientation, corrected maximum ball deformation increased with impact number during the high-speed impacts. Figure 28 shows the repeated high-speed impacts for an individual

Dukes, Kookaburra and BOLA ball. There was little difference between the impact orientations for the Dukes ball, and in both orientations there was a fairly rapid initial increase in the corrected maximum ball deformation before plateauing. For the Kookaburra ball, the Seam showed greater corrected ball deformation than the Face, and both orientations show a consistent increase in ball deformation as impact number increased. In addition to showing much greater deformation than both Cricket ball types, the BOLA ball showed increased deformation as impact number increased (albeit at a slower rate than the Dukes and Kookaburra balls). The applied power regressions all showed strong relationships between impact number and corrected maximum ball deformation (R^2 values – Dukes face: 0.93, Dukes seam: 0.95, Kookaburra face: 0.89, Kookaburra seam: 0.8, BOLA: 0.83). As observed in the contact time results, the Dukes balls took a greater number of impacts to reach 'steady state' (13 and 12 impacts for the face and seam respectively) than the Kookaburra ball (7 and 8 impacts for the face and seam respectively). The BOLA ball reached 'steady state' after just 4 impacts.

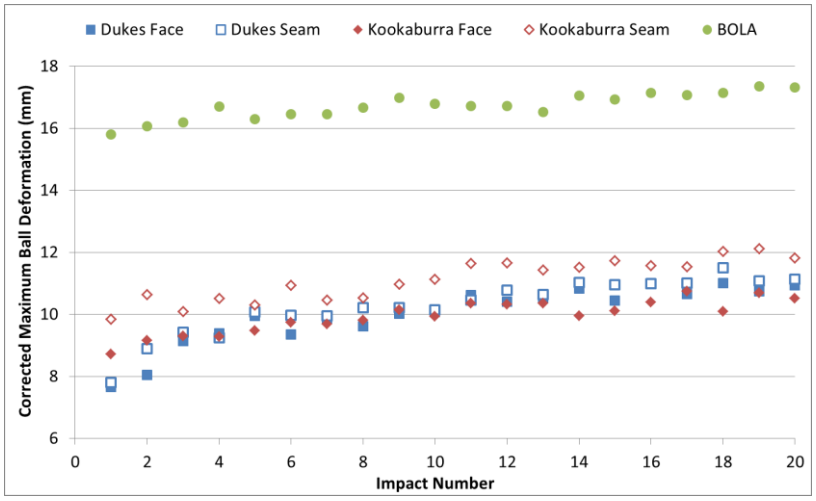

Figure 28. Corrected maximum ball deformation for the repeated 70 mph impacts in each ball type.

3.3.2.4. Peak Force

Figure 29 shows the mean corrected peak force on an impact by impact basis at each impact speed. The corrected peak forces measured in this study are comparable to those predicted by the model presented by Fuss (2008). As expected, corrected peak force measurements increased with impact speed. When considering all five impacts at each impact speed, the Dukes balls showed significantly greater corrected peak force for the face and seam orientations ($p < 0.01$). Again, unsurprisingly, the BOLA balls show significantly

lower corrected peak force than both Cricket ball brands and orientations, in all the tested impact speeds ($p > 0.001$).

No statistically significant differences were observed based on orientation in either the Dukes or Kookaburra balls at the medium or high impact speed ($p > 0.258$). However, at the low impact speed, the Face showed significantly greater corrected peak force than the Seam orientation in both ball brands ($p < 0.012$).

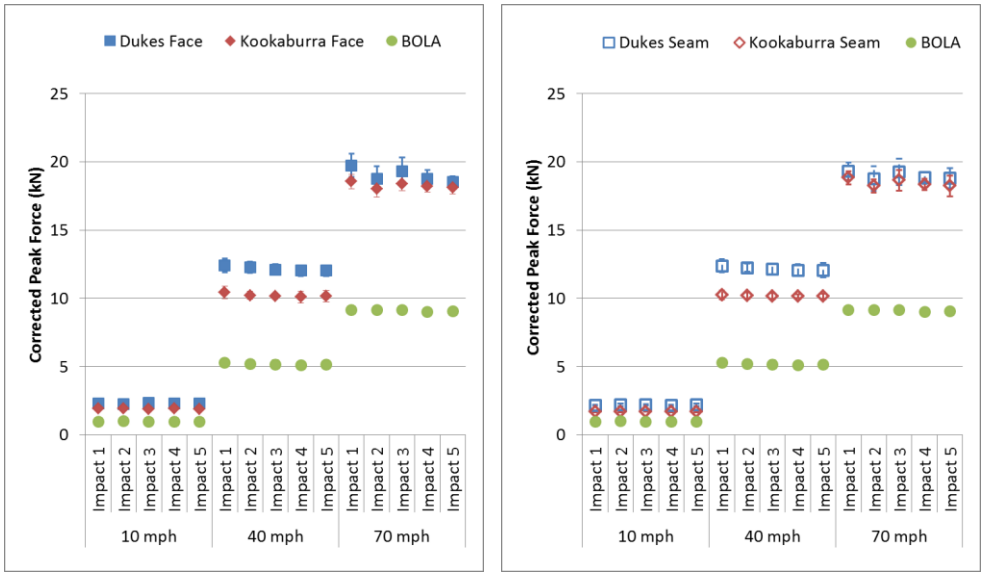

Figure 29. Mean corrected peak force for each ball type and impact speed.

In all ball brands and orientations, the mean corrected peak force measured during the high-speed impacts reduced with impact number (see Figure 29). Figure 30 shows the repeated impacts on a representative Dukes, Kookaburra and BOLA ball. Although the Dukes ball initially showed greater corrected peak force than the Kookaburra, the Dukes showed a relatively rapid reduction, resulting in corrected peak forces very similar to the Kookaburra. As discussed, the BOLA ball showed considerably lower corrected peak force, which decayed at a similar rate to that of the Kookaburra ball. With respect to the power regressions, the Dukes Face and Seam showed strong correlations (R^2 values – 0.8 for both), with both orientations reaching 'steady state' after 6 impacts. The Kookaburra Face and Seam, and the BOLA ball all showed moderate correlations (R^2 values – 0.67, 0.69 and 0.7 respectively). The Kookaburra ball reached steady state after 3 and 4 impacts in the Face and Seam orientations respectively, and the BOLA ball reached 'steady state' after 3 impacts.

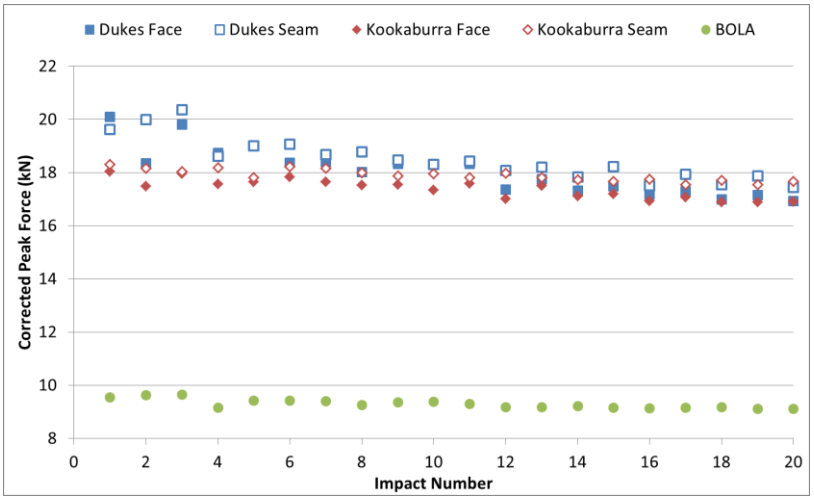

Figure 30. Corrected peak force for the repeated 70 mph impacts on a representative ball of each type.

3.3.2.5. Time to Peak Force

Figure 31 shows an impact by impact comparison of the mean time to peak force at each impact speed. In each impact speed and orientation, the Kookaburra balls showed a significantly greater time to peak force than the Dukes ($p < 0.001$), with a greater difference in the Seam orientation. The Kookaburra balls also showed orientation dependent differences, with greater time to peak force in the Seam orientation than the face – a difference most pronounced in the low speed impacts, but still statistically significant in the medium and high-speed impacts ($p < 0.001$). Significant differences were found between the Dukes Face and Seam at the low and medium impact speeds ($p < 0.01$), but not at the high impact speeds ($p = 0.371$). The BOLA balls show significantly greater time to peak force than the Dukes and Kookaburra balls in every impact condition ($p < 0.001$).

The effect of repeated impacts on the time to peak force can be found in Figure 32. The Dukes showed little difference between the Face and Seam. The Kookaburra balls showed a slightly longer time to peak force than the Dukes, and the Seam showed a consistently longer time to peak force than the Face. As would be expected from the results presented in Figure 32, the BOLA ball showed significantly longer time to peak force than the Dukes and Kookaburra balls ($p < 0.001$). The power regression analysis showed weak relationships with the Dukes Face and Seam (R^2 values – 0.158 and 0.2717 respectively). The Kookaburra Face and Seam and BOLA ball regressions showed stronger, R^2 values (0.64, 0.76 and 0.93 respectively), with all three impact conditions reaching steady state in 6 impacts.

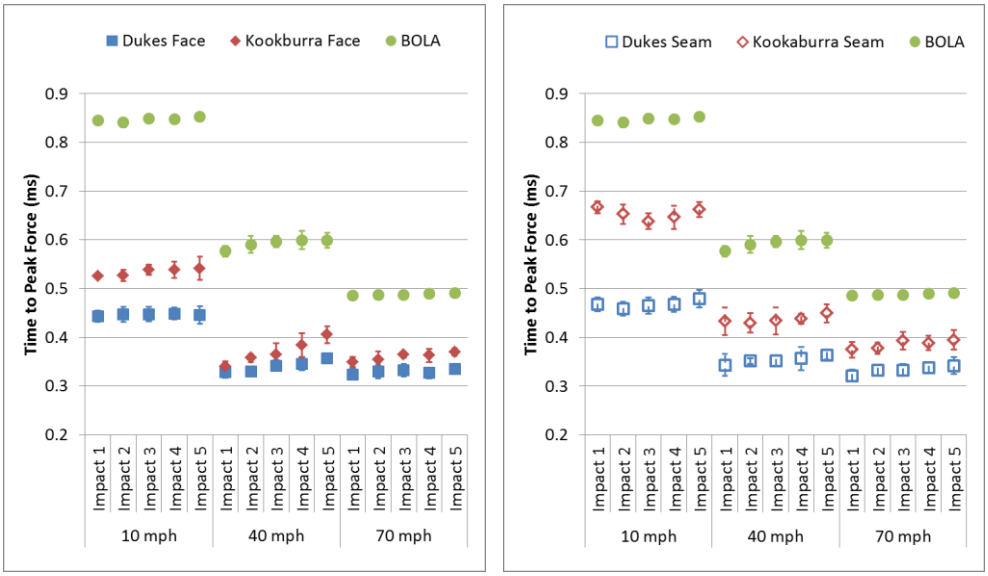

Figure 31. Mean time to peak force for each ball type on an impact by impact basis.

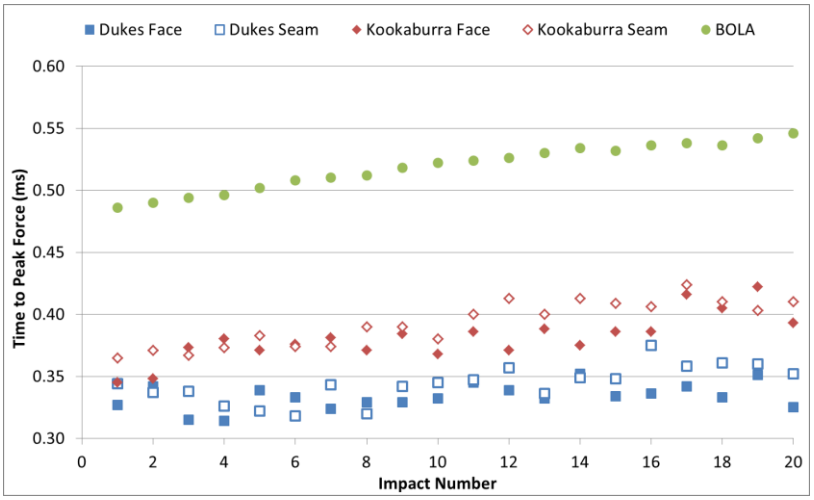

Figure 32. Time to peak force for a representative ball of each type during the repeated 70 mph impacts.

3.3.2.6. Stiffness

Figure 33 shows the impact by impact mean stiffness at each impact speed. The Dukes were found to be significantly stiffer than the Kookaburra balls in both impact orientations at each impact speed ($p < 0.001$). The difference between the Dukes and Kookaburra balls were most pronounced at the low and medium impact speeds. In the low speed impacts, the Dukes balls were 43 and 84% stiffer than the Kookaburra balls in the Face and Seam orientations respectively. When considering the first impact at the medium speed (before degradation), the Dukes balls were, on average, 34 and 46% stiffer than the Kookaburra balls in the Face and Seam orientations respectively. In the first high speed impact, the

Dukes balls were found to be 15 and 22% stiffer than the Kookaburra balls in the Face and Seam orientations respectively. The Dukes balls showed no statistically significant orientation dependent differences at the medium and high impact speeds ($p > 0.209$), however at the low impact speed the Face was significantly stiffer than the Seam ($p = 0.003$). In the Kookaburra balls, the Seam orientation was found to be significantly stiffer than the Face at all impact speeds ($p < 0.001$). The BOLA balls were found to be considerably more compliant than both the Dukes and Kookaburra balls (77 and 74% less stiff than the first high speed impact on the Dukes face and Kookaburra face respectively). Unsurprisingly, the BOLA ball was found to be significantly less stiff than both Cricket ball types and orientations ($p < 0.001$).

The standard deviations suggest that the highest intra-ball variability was shown by the Dukes, followed by the Kookaburra, and then the BOLA which may be expected due to the construction and manufacturing processes involved. There is also a clear reduction in stiffness at the low impact speed for all ball types and orientations – likely due to strain rate dependencies. When comparing the mean stiffnesses at the low impact speed to the first high-speed impact, the Dukes were found to be 35 and 37% less stiff during the low speed impacts in the Face and Seam orientations respectively. The Kookaburra balls were found to be 47 and 58% less stiff during the low speed impacts in the Face and Seam respectively. Although the Kookaburra and BOLA balls showed statistically significant differences between each impact speed ($p > 0.001$), the Dukes ball showed no statistically significant differences between the medium and high-speed impacts in either orientation ($p > 0.932$).

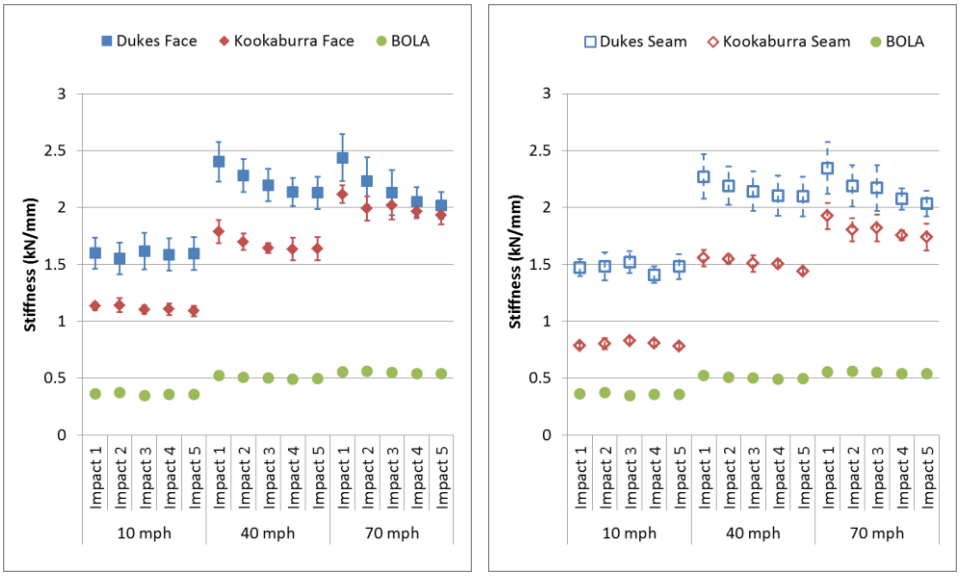

Figure 33. Mean stiffness for each ball type and impact speed.

Figure 34 shows the power regressions fitted to the mean stiffness obtained for each ball brand and impact orientation from the first impact at each tested ball speed. Although other regressions were fitted to these data, the power regressions showed the highest R^2 values, all of which showed a strong relationship and were greater than or equal to 0.94 (see Figure 34). The equations of these regressions (see Table 15) can therefore be used to predict the stiffness (k) of a ball brand and orientation from a given impact speed/initial deformation rate ($\dot{x}$).

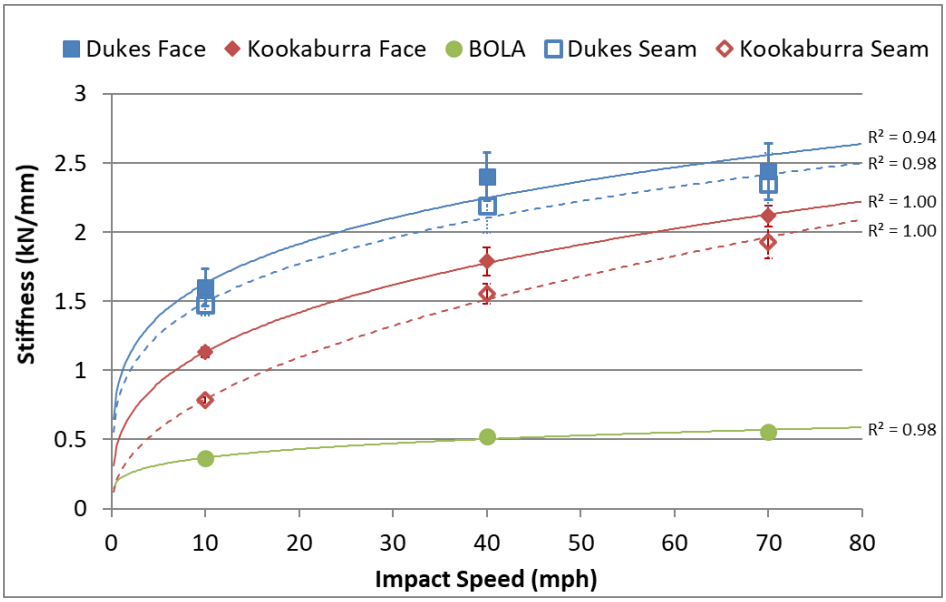

Figure 34. Power regression fitted to the mean stiffness of each ball type at impact 1 of each impact speed.

Table 15. Regression equations for each ball brand and orientation, to predict stiffness (k) from initial deformation rate ($\dot{x}$).

Ball Brand/Orientation	Equation
Dukes Face	$k = 0.96 \times \dot{x}^{0.23}$
Dukes Seam	$k = 0.84 \times \dot{x}^{0.25}$
Kookaburra Face	$k = 0.54 \times \dot{x}^{0.32}$
Kookaburra Seam	$k = 0.27 \times \dot{x}^{0.47}$
BOLA	$k = 0.22 \times \dot{x}^{0.22}$

The effect of repeated impacts on the stiffness of the balls can be seen in Figure 35. Although the Dukes ball had a higher initial stiffness in the Face and Seam orientations, this reduced more rapidly than the Kookaburra balls, and was similar to the Kookaburra face after around 5 impacts and similar to the Kookaburra seam after around 14 impacts. Although there are no significant differences between orientations for the Dukes ball, the Kookaburra seam is consistently slightly less stiff than the Kookaburra face. Although the BOLA ball has a significantly lower stiffness, a small reduction in stiffness throughout the 20 impacts (605 kN/mm at impact 1 compared to 526 kN/mm at impact 20) was observed. The regression analysis showed strong relationships between high-speed impact number and stiffness (R^2 values: Dukes face – 0.97, Dukes seam – 0.98, Kookaburra face – 0.91, Kookaburra seam – 0.83, BOLA – 0.84). Based on the regression model, the Dukes ball would reach 'steady state' after 18 and 17 impacts for the Face and Seam respectively. The Kookaburra took just 9 impacts for the Face and Seam to reach the same state, and the BOLA ball only 6 impacts.

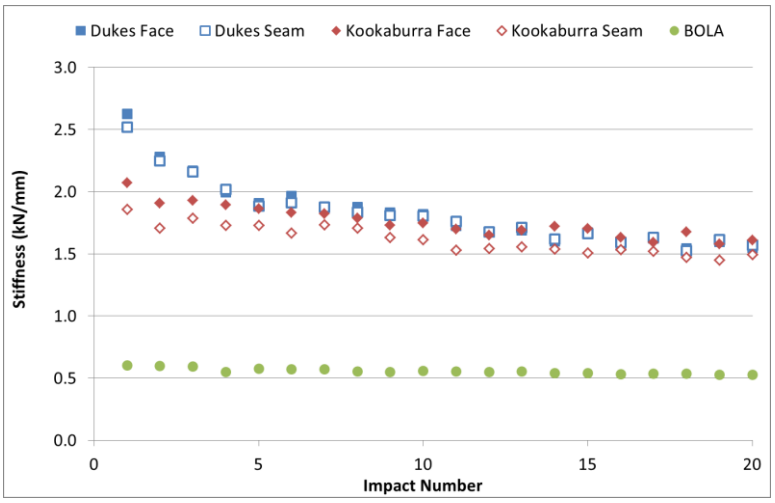

Figure 35. Stiffness for the repeated high speed impacts for a representative ball of each type.

3.4. Discussion

The dynamic properties of two types of elite level Cricket balls and a Cricket training ball have been assessed at realistic deformation rates. The ball properties are an important factor when considering player safety and the assessment of PPE since parameters such as peak force, time to peak force, contact time and stiffness all influence the mechanics of a collision between the ball and the human body/PPE. Indeed, mechanical failure of organs, bone, connective tissue, muscle and blood vessels has been shown to be influenced by peak load and strain rate (Kennedy et al., 1976; McElhaney et al., 1970; Miller and Chinzei, 2002; Rashid et al., 2012; Reilly and Burnstein, 1974; Saraf et al., 2007). Albeit in a simplified, theoretical study, Crisco et al. (1997) reported that modified, more compliant baseballs were less likely to induce injuries associated with high forces and accelerations. Viano et al. (1993) also presented experimental data showing that more compliant baseballs reduced the dynamic response of a 5th percentile Hybrid III headform. Importantly though, as each type of ball that was tested was from the same batch, batch-to-batch variations that may be introduced through the manufacturing processes and/or organic materials used in the construction of cricket balls has not been assessed. This should be considered a limitation that should be addressed in future studies.

In this study, clear differences were observed between the between the Dukes, Kookaburra and BOLA balls in a number of parameters, at all three deformation rates. Although the BOLA balls were found to show better ball to ball consistency, it is clear that, during an impact, the properties observed in BOLA balls are significantly different from those observed in the two types of Cricket ball assessed here (though the high-speed impact stiffness values presented for the BOLA balls are similar to those previously reported for sliotars used in Hurling (Collins et al., 2010)). This is particularly evident when considering stiffness, where the BOLA balls were found, on average, to be 77 and 74 % more compliant than the Dukes and Kookaburra balls during the first high speed impact in the Face orientation respectively. The findings of this study suggest that the BOLA ball should be considered an inappropriate substitute for an actual Cricket ball during laboratory reconstructions when investigating the mechanics of head impacts in Cricket.

Although no studies have investigated the properties of Cricket balls at the medium and high deformation rates assessed in this study, the results of the low speed impacts compare well with those previously reported by Carré et al. (2004). When considering the medium- and high-speed impacts, the contact time observed in the Cricket balls was similar to that reported for baseballs (Cheng et al., 2008), and slightly shorter than softballs (Smith et al., 2010). Hendee et al. (1998) reported that the average CoR of traditional baseballs at

60 mph was 0.56. This is higher than the medium-speed results for the Dukes balls, and comparable to the medium-speed Kookaburra results, despite the higher impact speed tested by Hendee et al. (1998). The Cricket balls tested here displayed greater stiffness than the value reported for softballs by Smith et al. (2010) (~1.375 kN/mm), despite the softballs being tested a higher impact speed (110 mph). Smith and Faber (2011) reported that the stiffness of an MLB baseball was ~2.1 kN/mm in a 95 mph impact – a value similar to the high-speed Kookaburra impacts presented here. However, at 95 mph, the regression model predicts a slightly greater stiffness of 2.35 and 2.28 kN/mm for the Kookaburra face and seam respectively. At all three deformation rates, there were measurable differences between the two types of Cricket ball tested in this study. Generally, the Dukes balls were found to exhibit shorter contact time and time to peak force, lower maximum deformation, and higher peak force and stiffness values than the Kookaburra balls at all three deformations rates. Although the differences were found to decrease as deformation rate increased, there remained statistically significant differences between the two Cricket ball types at the highest deformation rate (31.3 m/s (70 mph)).

The Kookaburra balls displayed a number of measurable differences based on the impact orientation, which were less evident in the Dukes balls. Orientational differences in some ball brands have been reported by Fuss (2008), using a quasi-static technique and at low speed unilateral impacts by Carré et al. (2004). In this study, the orientation dependent differences observed in the Kookaburra balls were more pronounced at the low and medium impact speeds, where the Face of the Kookaburra balls produced shorter contact time and time to peak force, lower maximum deformation and higher peak force and stiffness relative to the Seam. This is likely due to the construction of the Kookaburra balls, that use layered cork and twine, as opposed to the solid core used in the Dukes balls.

The repeated impacts used in this study to assess degradation give a good, representative insight into degradation trends. However, in a test match game of Cricket, an individual ball is used for at least 80 overs (480 individual deliveries) and is therefore subjected to more than 20 impacts. In this respect, limiting the number of repeated impacts to 20 seems inappropriate. However, many of the impacts observed in real-life are of low magnitude. Indeed, the number of impacts with a magnitude comparable to that observed in the laboratory tests (that is, a single high-speed impact against a rigid, immovable plate) are likely to be limited to the deliveries that score six runs. Narayan (2016) assessed 715 test match matches from 200-2015 and reported that, on average, 3.5 deliveries per innings resulted in six runs being scored – significantly fewer than the 20 used in the repeated impacts here. As such, due to the impact conditions used in the repeated impacts, it is important to note that the absolute impact number presented in this study is unlikely to

directly link to real-life events, but presents an accelerated and pragmatic means of assessing ball degradation in a laboratory environment. Indeed, future work may look to determine the upper limit on the number of high-speed impacts that a Cricket ball can sustain before the degradation observed renders it unfit for play.

The BOLA ball showed relatively consistent performance during the repeated impact testing, indicating a low level of ball degradation. Alternatively, both types of Cricket ball showed more pronounced changes in a number of parameters with increased impact number. For example, the Dukes ball showed the highest initial change in ball stiffness, as by the fifth high-speed impact the ball stiffness was found to be on average 20% more compliant than that observed in the first impact (see Figure 33). Repeated impacts also resulted in a change in the stiffness observed in the Kookaburra balls. However, this was less pronounced than that observed in the Dukes, and as such, the stiffness of the Dukes and Kookaburra Cricket balls converged after around five high-speed impacts (see Figure 35).

As the Dukes ball produced greater peak force, shorter contact time and displayed greater stiffness than the Kookaburra balls, head impacts with an unused Dukes ball may be considered the worst-case scenario. Theoretically then, PPE proven to be effective against an unused Dukes ball is likely to be effective against a Kookaburra ball – suggesting that the Dukes ball should be used in product development and laboratory testing. However, the Dukes ball also displayed greater ball to ball variation in stiffness (Figure 33) and a more rapid reduction in stiffness during repeated impacts (Figure 35) than the Kookaburra ball. The change in properties of the Dukes ball may influence the mechanics of a head impact in Cricket and make it difficult to establish whether observed differences are a result of variations in PPE performance/impact parameters or a change in ball properties.

When considering laboratory testing, it is likely that, regardless of the ball type selected, any individual ball is likely to be subjected to multiple impacts since using a fresh, un-used ball for every impact is impractical and likely to be financially unviable during laboratory-based PPE testing. When considering the ball types tested in this study, the Kookaburra ball in the Face orientation was selected for future laboratory tests for pragmatic reasons, given that this was a good representation of real-life impacts and that this ball type displayed superior consistency and degradation relative to the Dukes ball. However, as the properties of the Kookaburra ball have been shown in this study to change with repeated impacts, non-destructive 1m drop tests should be conducted after a pre-determined number of impacts to ensure that the measured ball properties remain within reasonable tolerances to ensure that dynamic observations are comparable across multiple impacts.

CHAPTER 4

Determination of Appropriate Impact Speed and Location for the Assessment of Head Impacts in Cricket

4.1. Introduction

As discussed in Chapter 2, it is necessary to establish the impact characteristics representative of the specific impact scenario being investigated, to facilitate ecologically valid laboratory-based assessments of sporting head impacts. As such, this chapter details research that investigates parameters that define the impact conditions (identified as component B in Figure 14). As previously discussed, in contact sports such as American Football, Rugby Union and Australian Rules Football, video recordings of real life events are commonly used to estimate impact speed, location, angle and effective mass of the colliding bodies (Frechede and McIntosh, 2009; Pellman et al., 2003; Zhang et al., 2004). This approach can provide useful information regarding specific injurious incidents and is particularly useful in scenarios where the general mechanics of impacts are well understood. This however, is not the case in Cricket as the paucity of research means the general mechanical responses of the human head during impact are not well understood. As such, a useful first step is to establish this understanding through the assessment of impacts in specified locations that are likely to produce motion through and about each axis of motion.

4.2. Ball Speed

To enable ecologically valid laboratory tests of head impacts in Cricket, the expected range of impact speeds must be determined. The most dangerous bowlers to face, from an impact injury perspective, are fast bowlers who often open the bowling attack and therefore use a new and, as shown in Chapter 3, stiffer ball. It is also not uncommon for these types of bowler to utilise a ‘bouncer’ technique (a short length delivery intended to bounce up at the batsman’s head/chest) to intentionally intimidate the batsman and/or draw them into a shot likely to lead to the loss of a wicket.

4.2.1. Previous Studies

Various studies have investigated the bowling release speeds of cricketers at different performance levels (summarised in Table 16). Elliot et al. (1993) assessed 24 junior fast bowlers (average age 13.7) and reported that the average ball release speed was 24.6 m/s ±

1.8 (55 mph ± 4.0). Prior to this, Elliot et al. (1992) reported that the average ball release speed of 20 slightly older (average age 18) junior fast bowlers was 31.7 m/s ±1.9 (~71 mph). At the senior level, Davis and Blanksby (1976) reported that low ability fast bowlers could achieve an average ball release speed of 31.7 m/s (c. 71 mph), whereas high ability senior fast bowlers could achieve an average ball release speed of 36.4 m/s (c. 81.5 mph). Stockill and Bartlett, (1992) reported that elite senior fast bowlers could achieve average ball release speeds of 37.1 m/s (c. 84 mph). Penrose et al. (1976) evaluated the performance of 6 international seniors and reported that the average ball release speed was 40 m/s ± 2.76 (c. 89.5 mph ± 6.2), with one bowler's release speed reaching 44.3 m/s (c. 99 mph).

Table 16. Average release speed of fast bowlers at various levels of performance (Elliot et al., 1993; Penrose et al., 1976; Stockill and Bartlett, 1992).

Level	Average release speed range (m/s (mph))
Junior	24.6 (55.0) - 31.7 (71.0)
Senior	31.7 (71.0) - 36.4 (81.5)
Elite/International	37.1 (84.0) - 40 (89.5)

These studies utilised video analyses to determine the average release speeds of various groups of bowlers, based on a limited number of subjects. James et al. (2004) collected over 3000 high speed video recordings of bowling deliveries at 15 English county grounds from 1999 to 2002. These video recordings were used to measure the ball speed immediately before and after bouncing on the wicket, thereby giving a means of assessing the amount of ball speed lost during a bounce, but not the effect of air resistance during pre and post bounce flight. They reported that on average 11.32% ± 1.61 of the ball speed was lost during the bounce of a delivery bowled at 36 m/s. However, this study did not account for variations in the length of the measured deliveries (e.g. short, good or full length) and as previously discussed aerodynamic effects were not investigated, as ball speed immediately before and after the bounce was calculated.

4.2.2. Ball-Tracking Data

Having been used by broadcasters since 2001 and approved by the International Cricket Council (ICC) since 2008, ball tracking systems are now used at almost all major Cricket grounds. The HawkEye system is one such example, which utilises six cameras recording at 340 Hz to capture data from every delivery in the game and reports an accuracy of 5 mm when considering ball position (HawkEye, 2019). Ball tracking data is typically used to report parameters including ball release speed, trajectory and bounce location, but also facilitates the measurement of the ball speed at any position in the flight and can therefore be used to determine the speed of the ball as it passes the batsman. However, given the volume of data

generated in a match, HawkEye operators typically only store the collected video for a short period to allow them to calculate the key parameters that are then televised. Unfortunately, this means that the ball speed when passing the batsman is not stored for every delivery and since the corresponding video is also not stored, post-event analysis is impossible. As such, this type of analysis must be negotiated with HawkEye.

Despite this, the data that is collected provides a rich source of in-situ data on elite level bowlers' release speeds from across the world. In this study, a database provided by HawkEye (containing data from 447 international bowlers, and from now on referred to as 'collective HawkEye data') was used to determine an appropriate impact speed. The collective HawkEye data was divided into bowling speed categories including variants on spin (n = 189) and medium to fast (n = 258) based on their reported bowling action. Within each category, bowlers were divided into 0.5 m/s windows, based on the measured maximum release speed. The number of bowlers in each of these windows was then determined as shown in Figure 36. The most common maximum release speed for the spin bowlers was 27.5 m/s (61.52 mph), with the maximum at 36.5 m/s, whereas the most common medium to fast paced bowlers release speed was 36 m/s (80.53 mph), with a maximum of 43 m/s (96 mph). As can be seen from Figure 36, most medium to fast pace bowlers achieved release speeds of 36 – 40 m/s, similar to the values reported by (Penrose et al., 1976 and Stockill and Bartlett, 1992).

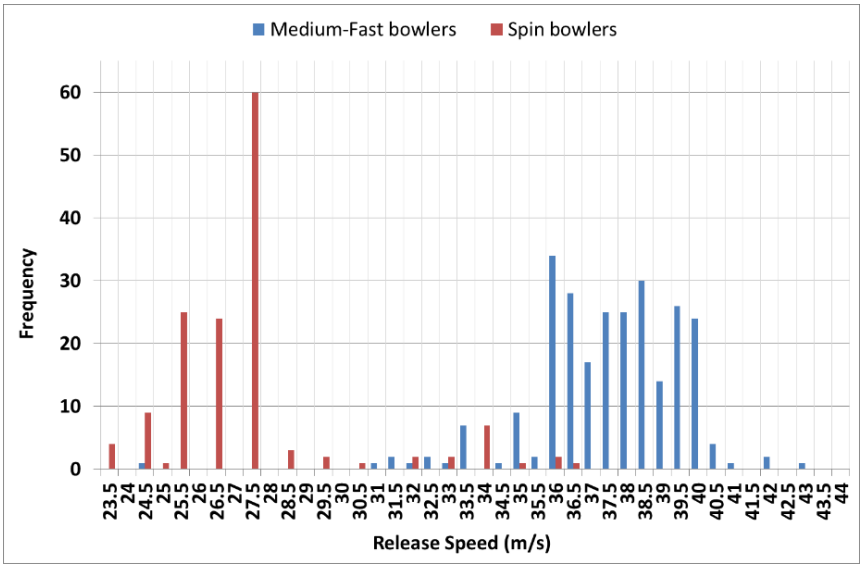

Figure 36. Histogram showing the frequency of release speeds in a 0.5 m/s bins for spin and medium to fast bowlers.

In terms of impact injury, a more important (though clearly related) parameter than release speed is the speed at which the ball is travelling as it reaches the batsman (inception speed). There will inevitably be a reduction from release to inception speed due to air

resistance during flight, and energy loss and frictional components during impact with the pitch. In order to assess the difference between release and inception speed, the HawkEye system was used to collect release and inception speed data from five full, good and short length deliveries from an International fast bowler in a competitive match. As can be seen in Figure 37, the short length deliveries tend to result in a lower inception speed than the good and full-length deliveries. This is likely due to the angle of impact with the ground – as the short deliveries have a greater angle of attack, the force normal to the ground will be greater, resulting in greater ground deformation and energy loss.

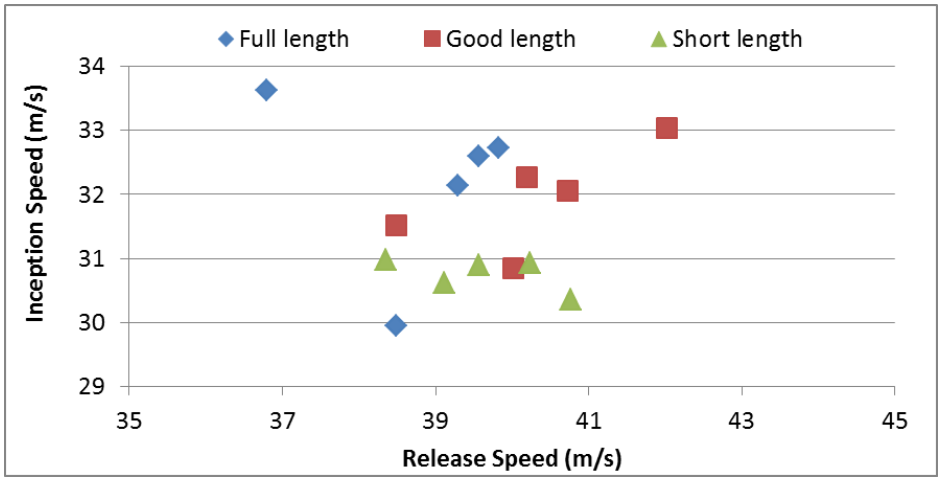

Figure 37. Measured release and inception speeds from 5 full, good and short length deliveries from an International bowler in a competitive match.

Although a number of factors (including variations in pitch construction, wear and environmental factors) will influence the speed loss from one delivery to another (Ball and Hrysomallis, 2012; Carré et al., 1999; James et al., 2004), if this data is assumed to be a representative sample of Cricket deliveries, then the previously discussed collective HawkEye data can be utilised to determine an appropriate laboratory impact speed representative of the inception speed measured in real-life scenarios.

4.2.3. Determining Appropriate Impact Speed

Two approaches can be taken to determine an appropriate impact speed from the data highlighted above. The first is to predict the most common inception speed, based on the collective HawkEye dataset and the relationship between release and inception speed. The second is to consider a worst-case scenario (i.e. the fastest recorded release speed combined with the lowest reduction in speed at inception).

When considering head impacts in Cricket, the fast paced, short deliveries are most relevant as these are more likely to bounce up around the batsman's head. Figure 38 shows

the relationship between release speed and percentage of release speed lost at inception for 5 short pitched deliveries. It is clear that as release speed increases, there is a greater percentage of release speed lost by the time the ball reaches the batsman. This is understandable, given that greater release speed would result in greater impact force, and therefore greater energy loss as a result of pitch deformation. Linear, logarithmic, exponential and power trendlines were fitted to the data, with the latter producing the greatest R^2 value (0.9515) (see Figure 38). Due to this strong relationship, the equation that defines this line can be used to predict the energy loss and therefore inception speeds of the maximum release speeds seen in the collective HawkEye data.

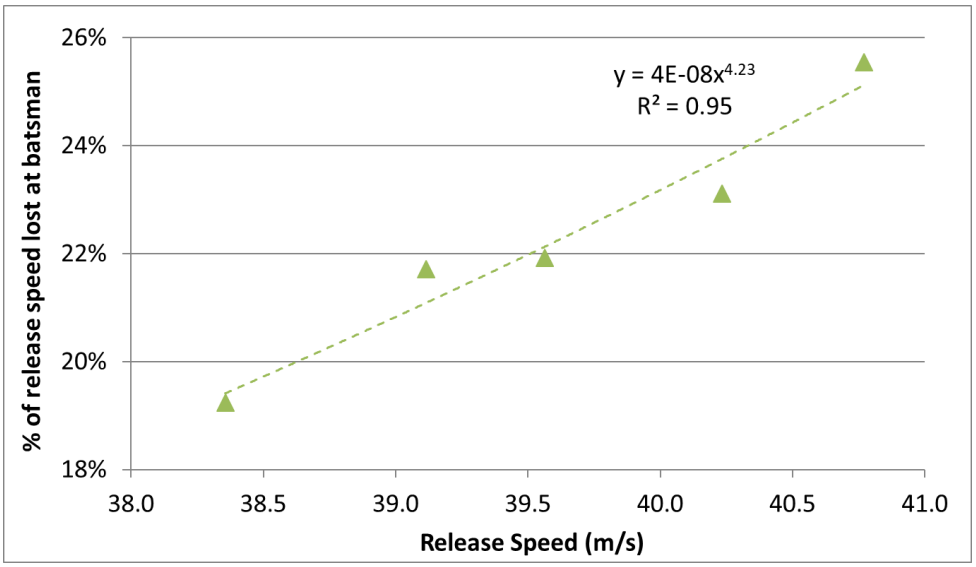

Figure 38. The relationship between release speed and percentage of release speed lost at inception for the short-pitched deliveries.

$$Vi \approx 4 \times 10^{-8} \times Vr^{4.23} \qquad \text{Eq. 15}$$

where: Vi *= Inceptions speed and* Vr *= Release speed*

Eq. 15, as shown in Figure 38, was applied to the measured maximum release speed of each bowler in the collective HawkEye data set, and the process used to produce histogram data was repeated for the predicted inception speed data. Figure 39 shows the histogram data for the release and inception speeds of medium to fast bowlers. Here it can be seen that, although the maximum release speeds are relatively evenly spread between 36 and 40 m/s, the vast majority of the predicted inception speeds lie between 30.5 and 31 m/s effectively (30.25 to 31.249 m/s). This is due to the increase in energy loss with release speed as seen in Figure 38, and suggests that in a given condition (including environmental, pitch wear/construction and ball degradation parameters) there is an optimal, and potentially sub-maximal, release speed that would produce the highest possible inception speed (for a

short length delivery a release speed of 38 m/s would achieve the greatest possible inception speed of 30.844 m/s).

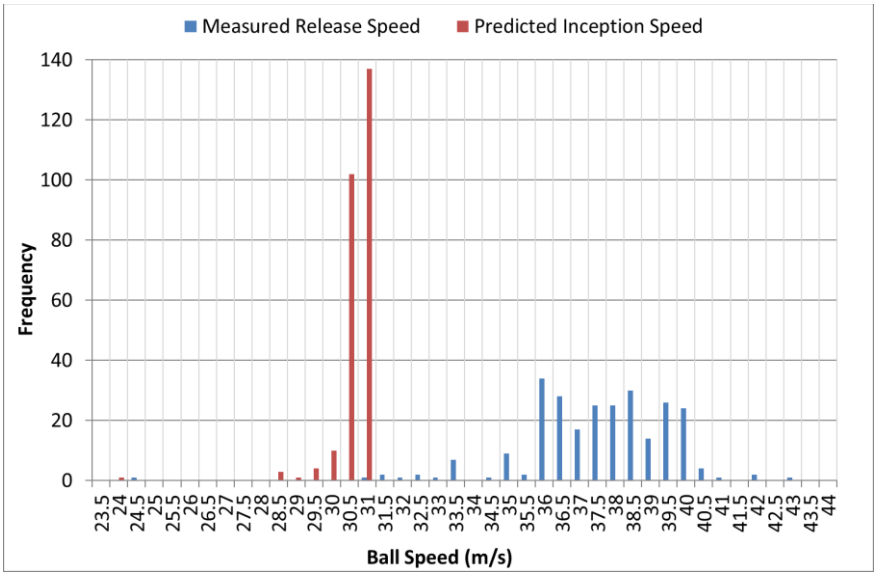

Figure 39. Histogram showing release and inception speeds for medium to fast paced bowlers.

An alternative approach to determine an appropriate impact speed is to consider that the number of factors influencing the change in ball speed from release to inception is so varied that this change is highly dependent on conditions on a given day. Therefore using data from five deliveries in one condition to build a model is limited. As such, the worst-case impact speed could be estimated by applying the lowest percentage speed loss observed, to the highest measured release speed. The appropriate parameters were extracted from the collective HawkEye data and the inception speed data to calculate the estimated worst-case impact speed of 34.7 m/s.

4.3. Impact Location and Angle

Impact location is an important parameter that will influence the dynamic response of the head during an impact. If the human head were considered a rigid body, a given impact force applied directly through the CoG would produce greatest linear acceleration. Alternatively, if the same impact force is applied to the head, but the line of force is a distance from the CoG, linear and angular acceleration will occur. As defined by the angular equivalent ($T = I\alpha$, where T = torque, I = MoI and α = angular acceleration) of Newton's second law, the magnitude of the observed angular acceleration will be proportional to the torque applied, and the MoI of the head about the axes of interest. As the MoI of the head about different axes varies (Albery and Whitestone, 2003; Becker, 1972; Beier et al., 1980;

Chandler et al., 1975), the impact location determines not only the line of force acting on the head, but also the axes about which the head rotates.

In addition to impact locations, impact angle also influences the line of force acting on the head. Direct impacts that occur perpendicular to the impact surface are likely to produce the greatest dynamic response of the head, since impacts that occur at an angle are more likely to be glancing blows, where less energy is transferred to the head (McIntosh and Janda, 2003). In real-life scenarios, the observed impact angle is a combination of the flight of the ball, the position of the batsman's head at impact and the local geometry of the head/helmet at the impact location.

It is important to note that these principles are based on the assumption that the human head responds as a rigid body response. Although this may be the case in impact scenarios where the striker is relatively compliant, and long contact times are observed (in for example American Football and Rugby), in Cricket, the stiffness and dimensions of the striker and the likely impact speeds are likely to result in short duration impacts that may result in local deformation and/or resonance frequency excitation (Hodgson et al., 1967; McElhaney et al., 1973; Thomas and Hodgson, 1969). Although the principles outlined above are still likely to hold, variations in some of these theoretical hypotheses may occur.

4.4. Definition of Impact Conditions for Laboratory Tests

As there are a multitude of impact speeds, locations and angles possible in Cricket (due to variations in ball bounce location, flight of the ball pre and post bounce, and the position and movement of the batsman himself), it would be impractical to assess every possible combination. A useful first step would be to understand the dynamic response of the head during ~worst-case scenario head impacts intended to generate linear and angular response about the x, y and z axes and how current PPE influences this response. This would provide important and novel data that improves the general understanding of the impact mechanics observed during head impacts in Cricket.

Based on ball tracking data, a nominal impact speed of 34.7 m/s was identified as representative of a ~worst-case scenario head impact. Direct impacts at three distinct locations were defined (described in Table 17 and Figure 40), with the intention that the dynamic response data derived from each would provide insight into each of the six DOF. In each impact location, the impact angle was defined as parallel to the Frankfort plane, as done by McIntosh and Janda (2003). As discussed in Chapter 3, the practical implications of using a more consistent ball with slower degradation meant that the Kookaburra ball,

orientated for impact with the Face orientation, was selected. Non-destructive drop tests conducted prior to, and after a defined number of impacts were identified as means of ensuring that the ball properties remained within a tolerable range. Overall, the data presented in this chapter and Chapter 3 has been used to determine appropriate and pragmatic impact conditions for the laboratory-based assessment of head impacts in Cricket.

Table 17. Description of the defined impact locations and ball flight paths.

Impact Location	Description
Frontal	Midway between the Frankfort plane and the Vertex, in the sagittal plane, with the ball flight perpendicular to the frontal plane.
Lateral	Midway between the Frankfort plane and the Vertex, in the frontal plane, with the ball flight perpendicular to the sagittal plane.
Oblique	Midway between the Frankfort plane and the Vertex, in a plane 45º between the frontal and sagittal planes, with the ball path perpendicular to the sagittal plane.

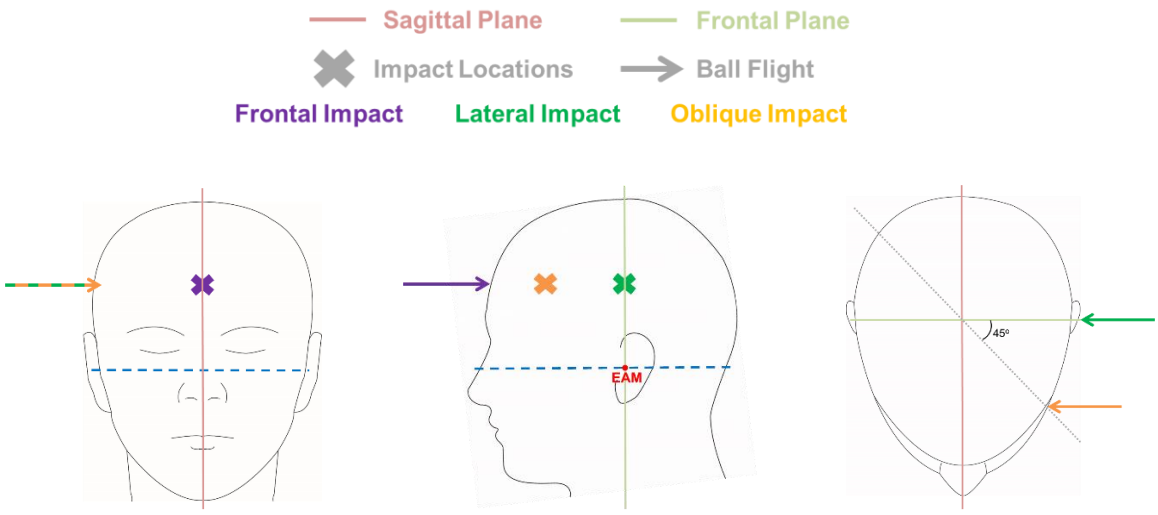

Figure 40. Definition of Impact locations and ball flight paths.

CHAPTER 5

Development of a Frangible Headform Suitable for the Assessment of Head Impacts in Cricket

5.1. Introduction

As discussed in Chapter 2, it is important that the parameters of the surrogate used to represent the human head are representative of those seen in real life. Although the Hybrid-III, NOCSAE and EN 960 headforms can be used to provide useful data in some circumstances (mainly the specific impact scenario for which they were developed), the limitations of the headforms should be considered before utilising them in other impact scenarios. Raymond (2008) reported that the dynamic response of the Hybrid-III headform is unrealistic in impacts that produce areas of high-pressure, due to the overly stiff steel skull component and as a result, the observed response during unprotected (and potentially protected) head impacts in Cricket is likely to be unrealistic. Logically, the same limitation can be expected when using the EN 960, since this headform is also overly stiff and does not include an external soft-tissue component. Although the NOCSAE headform has more realistic material properties and is therefore likely to produce a more biofidelic response in this impact scenario, the manufacturers advised that an unprotected Cricket ball impact may fracture the headform. Indeed , when using an unprotected NOCSAE headform, Clark et al. (2016a) used impact speeds below those observed in real-life scenarios in order to avoid permanent damage. Due to this, using this headform during unprotected impacts is likely to make this approach financially unviable, or require impact speeds unrepresentative of real-life scenarios. For these reasons, it was judged beneficial to develop a headform (LU headform) capable of producing realistic first order dynamic responses specifically for the assessment of protected and unprotected head impacts in Cricket.

In order to develop a headform capable of producing a suitable first order dynamic response during impact testing, certain design parameters were defined prior to the development process. The identified design parameters, and requirements thereof, are outlined in Table 18.

Table 18. Identified headform parameters and requirements.

Design Parameter	Requirement
Representative tissue components	Discreet components to represent bone, external soft tissue and the brain.
Geometry	Geometric properties (head length, breadth, depth and circumference) within one standard deviation of the average 50th percentile UK male. Skull thickness should be variable and representative of human data.
Mass	Mass within one standard deviation of the reported mean of previously reported values of the human head.
Moment of Inertia	Principal moments of inertia and moments of inertia about anatomical axes at the CoG within one standard deviation of the mean reported values for the human head.
Material Properties	Material properties of the components must be within the ranges of previous reported human tissue.
Instrumentation	Capability to mount a triaxial linear accelerometer and a triaxial angular rate sensor within the headform.
Modular components	The headform must be modular, so broken elements can be replaced, unless this compromises the impact mechanics.
Manufacturing costs	The time and financial cost of manufacturing the headform must be judged to be reasonable (<750 GBP).
Head neck complex	Compatible with the current Hybrid-III neck surrogate.

5.2. Design Methods

A CAD model of a human head was obtained from the Tokyo Institute of Technology. The model was derived from an MRI scan of a 25-year-old Japanese male (Height: 173 cm; Weight: 65 kg). The head model was segmented from the neck above the first cervical vertebrae, as described by Walker et al. (1973) and Yoganandan et al. (2009). The CAD model consisted of bone, external soft tissue and brain components which maintained the geometric properties of the scanned individual. The EAM and IMO were identified on the model and used to define the Frankfort plane (BSi, 2017). The headform model was positioned in the neutral position by aligning the Frankfort plane in the transverse plane, and a co-ordinate system was established (as shown in Figure 41), with the origin of the co-ordinate system midway between the left and right EAM. Abnormalities specific to the scanned individual were identified and removed from the CAD model. To minimise the directional effects of impacts, and account for the asymmetrical nature of the scanned human head, the headform model was split through the sagittal plane. One half of the bone, external soft tissue and brain components were removed, and the remaining halves were

mirrored about the sagittal plane. These components were then joined to create symmetrical components.

The bone elements of the model were divided into three distinct components – the cranium, face and mandible (see Figure 41). This was beneficial as it maintained the structural and mechanical integrity of the cranium component, but also meant that if any components were broken, the entire structure would not need to be replaced, thereby minimising financial cost. The soft tissue elements of the scan data were modelled as a single continuous component (see Figure 41).

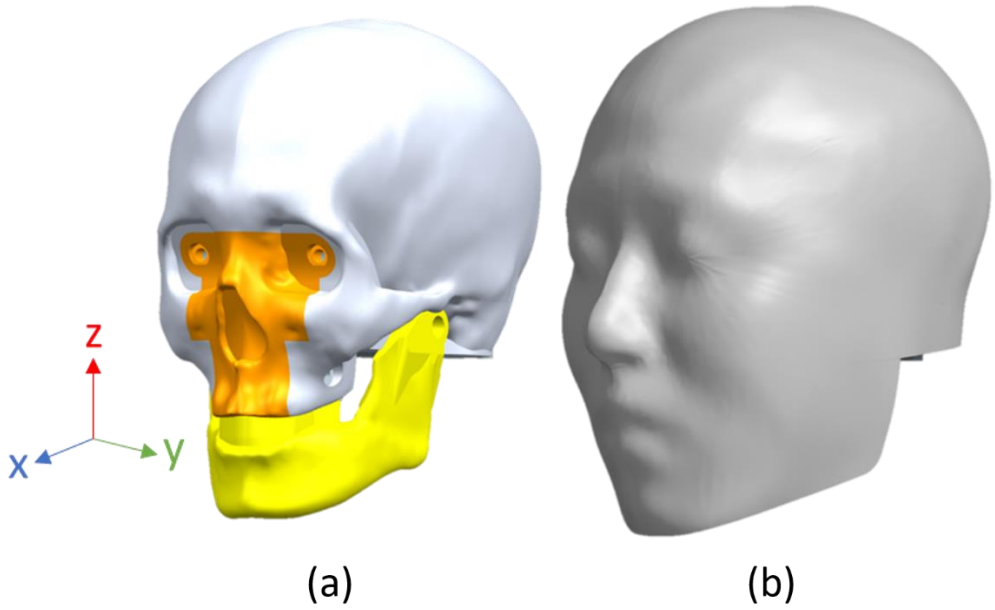

Figure 41. CAD assembley of the face, cranium and mandible bone components (a), and the soft tissue component (b) of the headform.

As discussed in Chapter 2, the falx cerebri and tentorium cerebelli structures of the dura mater separate sections of the brain and provide a mechanical barrier that helps to prevent excessive rotation of the brain (Glaister et al., 2017). As direct measurement of brain motion was not required in this application, incorporating geometrically accurate representations of the falx cerebri and tentorium cerebelli with appropriate material properties (as included in the model reported by Miyazaki et al.(2012)), was judged to be an over complication in this initial model, given the difficulty in accessing the inner surface of the skull component. Instead, the human scan data was used to determine the thickness and location of the base of both these structures, which were then modelled into the cranium component as shown in Figure 42, in an attempt to prevent over-rotation of the brain on impact. Although the effect of this structure is not directly measured, subsequent dynamic

validation tests would highlight if this causes divergence relative to that observed in human cadavers.

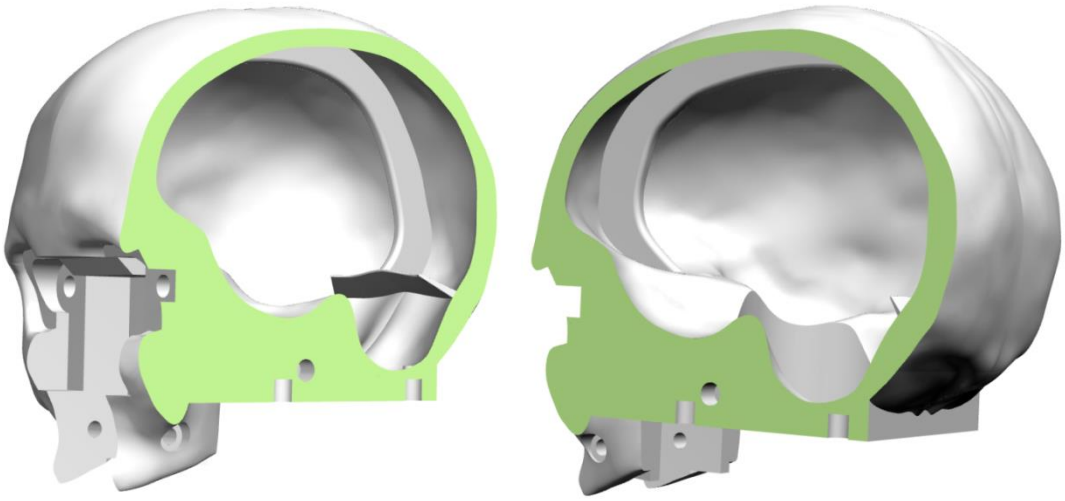

Figure 42. Cut-away of the cranium component showing the modelled base of the falx cerebri and tentorium cerreblli.

Anatomical landmarks were determined on the headform, including the EAM, IMO, glabella, vertex and occiput. Geometric measurements (specifically headform breadth (left EAM to right EAM), EAM to occiput, EAM to glabella, EAM to vertex and EAM to point of chin) were taken using these landmarks and compared to values reported for 50th percentile UK males by Peebles and Norris (1998) to produce scaling factors shown in Table 19.

Table 19. Scaling factors used to match the headform model dimensions to those reported by (Peebles and Norris, 1998).

Dimension	Scaling Factor
Head Breath	0.905
EAM to glabella	1.053
EAM to occiput	1.006
EAM to vertex	0.955
EAM to chin	1.059

These were applied independently to the respective axes, within the CAD environment. The CAD model was split through the transverse and frontal planes passing through the EAM. This allowed each section of the model to be scaled in the anterior, posterior, superior and inferior directions from the EAM. The geometric measurements were then repeated to ensure that the scaling factors had been applied correctly. Skull thickness measurements were taken from the scaled LU headform model at locations specified in

previous human cadaver studies (Hodgson et al., 1970; Lynnerup, 2001; McElhaney et al., 1970). External soft tissue thickness at the forehead and temporal regions, in addition to the occiput and vertex were also measured using the scaled LU headform model.

To secure the cranium, face and mandible components together, through holes for M6 screws and threaded pilot holes for M6 inserts were designed into the CAD model at specific locations as seen in Figure 43. This would allow two screws to connect the mandible to the cranium (highlighted in green in Figure 43), two screws to connect the mandible to the face (highlighted in red in Figure 43) and four screws to connect the face to the cranium (highlighted in pink in Figure 43).

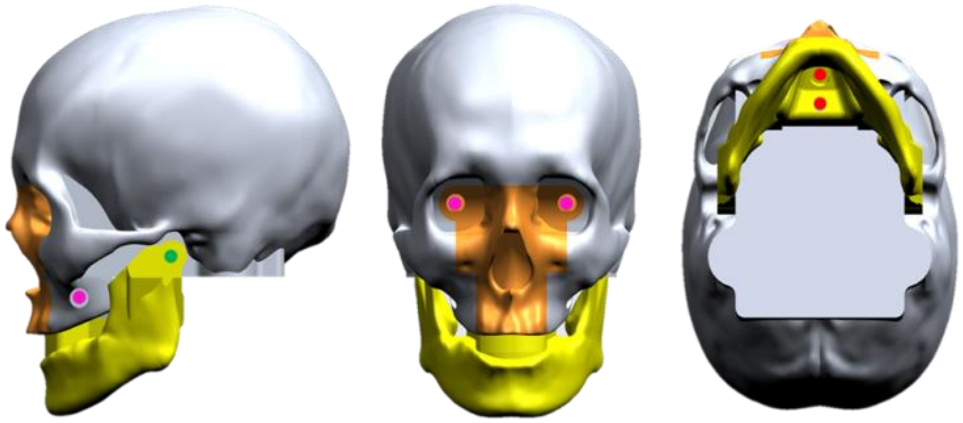

Figure 43. Locations of M6 screws to secure skull components.

To allow a brain simulant (gelatine filler) to be moulded into the skull, a 60mm diameter hole was removed from the inferior aspect of the cranium component (as shown in Figure 44). Four threaded M6 pilot holes were modelled around the hole into the same surface. These holes were positioned so that a component, similar to the Hybrid-III neck mount (part number 78051-383X-DN (Humanetics Innovations Solutions Inc., 2019)) could be accommodated, so that when attached to the Hybrid-III neck (part number 7085-297-DN), the location of pivot point (neck pin (part 1717)) was approximately at the occipital condyle in the sagittal plane (geometric offset from EAM reported by Chancey et al. (2007)). Alternatively, a custom plate could be used to seal the fill hole. This resulted in an enlarged base of the cranium, as seen in Figure 43 and Figure 44. Although this introduces some divergence from the human scan data, the inertial properties remained favourable (as discussed later). This enlargement should, however, be considered in the use of the LU headform, and as such, impacts around the base of the cranium are not recommended. The inside of the cranium was coated with a polyurethane based paint (Flexithane, Polymarine, UK), and polytetrafluoroethylene (PTFE) spray was applied prior to the moulding of the

gelatine filler to prevent the gelatine adhering to the inner skull and to provide an element of lubrication, similar to that observed in the human head and other headform models (Miyazaki et al., 2012; Petrone et al., 2018). Although not directly measured, this was assumed to allow brain motion in six DOF.

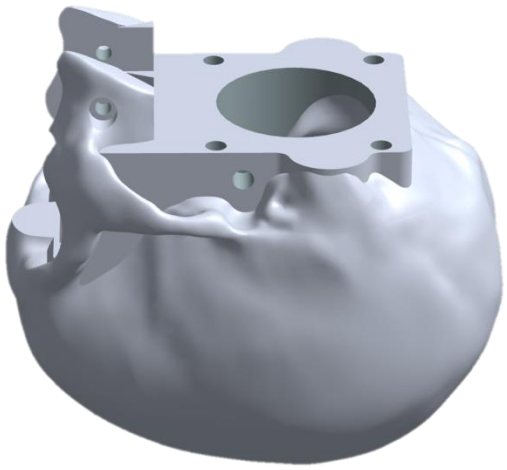

Figure 44. CAD image showing filling hole and location of M6 insert holes on the cranium component.

Sensors to measure the headforms dynamic response in six DOF were required to be mounted to the headform at appropriate locations. In this case, a 10 x 10 x 10 mm triaxial linear accelerometer and a 20.8 x 20.8 x 13 mm triaxial angular rate sensor would need to be accommodated. An appropriate mounting location was identified at the posterior aspect of the facial component where the centres of both sensors were positioned in the sagittal plane (neutral position on the y axis). Due to the dimensions of the two sensors and that of the cavity between the face and cranium components, the sensors were offset in the x axis to allow enough clearance for the cabling. A cavity was removed from the facial component to accommodate the angular rate sensor, and surfaces were extruded to mount the linear accelerometer superior and posterior to the angular rate sensor, as shown in Figure 45. Pilot holes were designed into the model at the required locations so that M2 threaded inserts could be fixed into these. A hole was removed from the linear accelerometer mounting surface so that an 8 mm M2.5 screw could be used to secure the linear accelerometer.

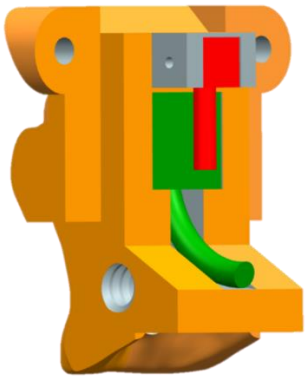

Figure 45. Posterior aspect of the face component showing linear accelerometer (red component) and angular rate sensor (green component) mounting locations.

When considering a suitable material to replicate the skull components, key material properties of density, tensile/flexural modulus and tensile/flexural strength were identified. Polyurethane has been used as a skull replicant by Thali et al. (2002), however this material would require moulding and would have to be moulded in two parts then adhered together to achieve the cranial cavity. This was judged to be inappropriate as the two-part construction and means of securing the two parts together may influence the mechanics of the impact. Epoxy resins mixed with glass fibre and urethane foams have also been used to produce material properties close to that of human bone (Merkle et al., 2010; Roberts et al., 2013). However, these materials have only been used to produce simple spheres or sheets and would therefore not be able to capture the geometric complexity of the cranium component of the LU headform. Falland-Cheung et al. (2017) assessed five skull simulant material – epoxy resin, fibre filled epoxy resin, polyethylene terephthalate glycol (PETG), polyactic acid (PLA) and self-cure dental acrylic denture base resin, where the PETG and PLA samples were 3D printed using an Ultimaker 2.0 (Ultimaker B.V., Geldermalsen, Netherlands). It was reported that, although epoxy resin showed the closest resemblance to the average tensile and flexural modulus reported by previous studies (Hubbard, 1971; McElhaney et al., 1970; Motherway et al., 2009; Robbins and Wood, 1969; Wood, 1971), all tested materials were within the reported range of values. It was also reported that due to the tensile and flexural strength of PLA (59.18 and 92.76 MPa respectively), this material would be best suited to high-speed, short duration, blunt force impacts. Although 3D printed PLA would be able to capture the complex geometry of the cranium and could be manufactured in-house at a relatively low financial cost, it was discounted due to an excessively long build time (c. 14 days continual build time for cranium component).

Other headform models have used 3D printed ABS-p430 as a skull simulant material (Mohotti et al., 2018; Petrone et al., 2018). This manufacturing approach allows the accurate

construction of the complex geometry of the components, facilitates the production of the cranial cavity, and can be manufactured in-house relatively rapidly (c. 90 hours for cranium component). As a result, 3D printed ABS-p430 was identified as a potentially viable material and manufacturing process.

In the LU headform, as in the Hybrid-III and NOCSAE headforms and those developed in research (Miyazaki et al., 2012; Petrone et al., 2018), the external soft tissue components of the head were modelled as a single, homogenous component. The external soft tissue component of the LU headform model was used to design two moulding structures, one for the face component, and one that covered the remaining parts (as shown in Figure 46). This allowed the face component and attached instrumentation to be removed easily, and without damage to other areas of silicone. Silicone rubbers have been used to replicate human external soft tissue in several studies (Behr et al., 2009; Delotte et al., 2008; Hyrsomallis, 2009; Payne et al., 2015a, 2015b, 2014) and have been found to produce more repeatable results than ethyl vinyl acetate foams after repeated impacts (Hyrsomallis, 2009). Silastic 3483 (Dow Corning Corporation, Michigan, USA) silicone was utilised by Hyrsomallis (2009) to represent human external soft tissues in the thigh region and has since been utilised in the sports PPE industry. The technical datasheet of Silastic 3483 reports that the cured density of the silicone is 1160 kg/m^3, with a tensile strength of 3.9 MPa which are within the ranges reported for human skin (CES EduPack, 2017).

As the aim of this chapter was to create a realistic first order dynamic response during an impact, the inertial effect of a brain simulant was identified as a greater priority than the exact material properties of the brain. Therefore, the key properties of the brain simulant were identified as density and bulk modulus. As the human brain consists of c. 80% water (Bell, 1989), a 20% gelatine solution (similar to that used in the NOCSAE headform) was deemed to be suitable as this would provide a density and bulk modulus close to that of the human brain. 250A gelatine powder (Defensible, England), which is used in legal cases and for firearms test standards in the USA and by NATO was selected due to its general acceptance and consistency.

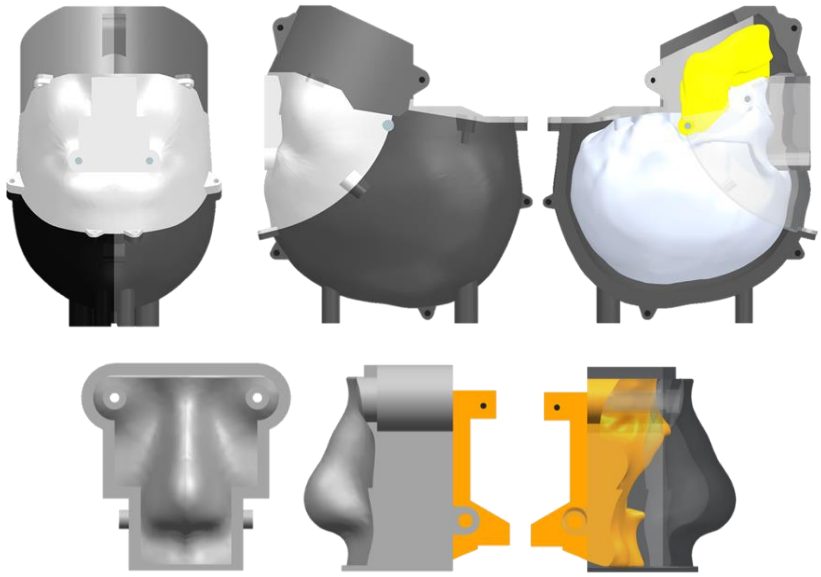

Figure 46. CAD images of the mould tooling with skull components in place.

5.3. Validation Methods

In order to incorporate inherent validity into the LU headform model, the material properties of each component were measured and compared to human cadaver data – with the aim of moving closer to human values than the currently available headforms that can be used in unprotected projectile impacts (Hybrid-III and EN 960). Following component validation tests, drop tests were completed and the dynamic response compared to previously reported values derived from human cadaver tests in order to provide a level of dynamic validation in line with that completed for currently available headforms.

To assess the material properties of the 3D printed ABS-p430, 15 tensile and 15 flexural test samples (dimensions as specified in BS EN ISO 178:2010+A1:2013 and BS EN ISO 527:2012 (BSi, 2013, 2012) respectively) were manufactured using fused deposition modelling (FDM) on a Dimension Elite machine (Stratasys, Minnesota, USA), set to solid build, with 0.254 mm resolution. Five of the tensile and flexural samples were built flat, five were built on the side, and five were built upright to assess the effect of build orientation on observed material properties. Following manufacture, the dimensions of the test samples were measured using a set of Vernier callipers (0.01 mm accuracy) and the mass of each sample was measured to 0.01 g accuracy.

A screw driven Instron 5569 universal test machine (Instron, Massachusetts, USA) was used to conduct tensile and three-point bend tests with a cross head speed of 500 mm/min, using a 0.1 kN load cell and linear variable differential transformer to measure displacement at 500 Hz. The tensile and three-point bend apparatus was set-up as per the

BS EN ISO 527:2012 and BS EN ISO 178:2010+A1:2013 specifications respectively. The load cell and displacement transducer were zeroed prior to testing, and a small (5 N) pre-load was applied to the sample followed by a constant velocity ramp protocol until the sample fractured. The force and displacement data obtained from the mechanical tests were used to calculate tensile strain, tensile stress, flexural strain and flexural stress using Equations 16, 17, 18 and 19. Tensile and flexural secant moduli were calculated between 0.01 and 0.02 strain ranges, and tensile and flexural strength were determined by identifying the strain at the fracture point.

$$\varepsilon_t = \frac{\Delta L_o}{L_o} \quad \text{Eq. 16}$$

where: ε_t *= tensile strain,* ΔL_o *= change in original gauge length,* L_o *= original gauge length.*

$$\sigma_t = \frac{F}{A} \quad \text{Eq. 17}$$

where: σ_t *= tensile stress,* F *= applied load (N),* A *= cross sectional area of sample*

$$\varepsilon_f = \frac{6\,sh}{L^2} \quad \text{Eq. 18}$$

where: ε_f *= flexural stress,* s *= deflection (mm),* h *= thickness of sample (mm),* L *= span (mm)*

$$\sigma_f = \frac{3\,FL}{2\,bh^2} \quad \text{Eq. 19}$$

where: σ_f *= flexural strain,* F *= applied load (N),* L *= span (mm,)* h *= thickness of sample (mm),* b *= width of sample (mm)*

To assess the Young's Modulus of Silastic 3483 (used to model the external soft tissue), compressive samples were manufactured and tested using the methodologies specified in BS ISO 7743:2017 (BSi, 2017). Five cylindrical test samples (diameter 29 mm, height 12.5 mm) were manufactured using a Silastic 3483 base and RTV-3083F curing agent (1:0.05 by weight). Following curing, the mass of each sample was measured to 0.01 g accuracy and the dimensions were measured using a set of Vernier callipers (±0.01 mm).

A screw driven Instron 5569 universal test machine (Instron, Massachusetts, USA) was used to conduct quasi-static compression tests at a strain rate of 0.4 s^{-1}, using a 0.1 kN load cell and linear variable differential transformer to measure displacement at 500 Hz. Each sample was placed between two flat, solid steel compressive platens. Petroleum jelly was used to lubricate the platens to reduce friction and limit the barrelling effect observed by Alaoui et al. (2008), which has been reported to cause up to 50% error in compressive stress

measurement (Wu et al., 2003). The load cell and displacement transducer were zeroed prior to testing, and a small (5 N) pre-load was applied to the sample. To maintain a constant strain rate, a triangular loading and unloading profile was programmed to apply five loading and unloading cycles to the specimen, up to 0.5 strain. For each test sample the force and displacement data from the fifth loading cycle was used to calculate engineering stress (σ) and engineering strain (ε), using Equations 20 and 21 as defined in BS ISO 7743:2017.

$$\varepsilon = \frac{\Delta l}{l_o} \qquad \text{Eq. 20}$$

where: l_o = original length and Δl = change in length.

$$\sigma = \frac{F}{A_o} \qquad \text{Eq. 21}$$

where: F = applied load and A_o = original cross-sectional area.

Following the selection of materials used in the manufacture of the headform, the material properties of the identified tissue simulants were applied to the relevant components of the CAD model using Siemens NX 10.0. The triaxial linear accelerometer and triaxial angular rate sensors were modelled into the identified locations and appropriate densities were applied based on the mass defined in the supplied datasheets. Threaded inserts and steel screws were also modelled into the CAD model at the appropriate locations. This allowed the inertial properties of the headform model to be calculated in the software. The inertial properties of the manufactured headform (mass, CoG offset and MoI about CoG) were then validated experimentally. Mass was measured using calibrated mettler Toledo scales (±0.1 g) and CoG was measured using a custom-built balance board using the same calibrated scales (estimated uncertainty ±0.5 mm). A custom-built torsional oscillation rig with an optical timing system (± 0.004 s) was used to measure the MoI about the CoG of the headform. Optical timing was completed with steel disks of known mass, which were positioned at known locations, to produce a calibration curve (as shown in Figure 47). Following this, multiple oscillations were measured with the headform positioned in the torsional rig. Four repeated trials were completed in three orientations (with the frontal, sagittal and transverse planes parallel to the ground and the measured CoG at the centre of the system). The measured oscillatory period was calculated and the equation presented in Figure 47 was used to determine the MoI about the CoG about each axis with uncertainty (±0.5 kg.cm^2) calculated based on the standard error of the calibration plus a 1 mm axial offset in the CoG location.

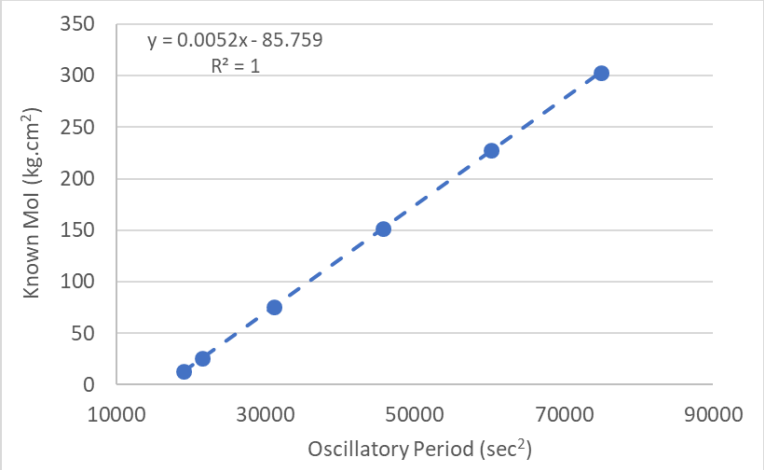

Figure 47. Calibration curve of MoI torsional rig.

Each stage of the manufacturing process is shown in Figure 48. The total time taken to manufacture the first version, and future iterations can be found in Table 20. As can be seen here, the financial cost of the initial version was 1588.08 GBP, with subsequent versions costing 628.02 GBP (includes FDM manufacture of cranium component, silicone base, curing agent, ballistic gelatine powder and extender).

Figure 48.Outline of the LU headform manufacture: (a) FDM of skull components, (b) FDM of mould tooling (shown in situ), (c) completed external soft tissue moulding, (d) Gelatine moulding.

Table 20. Breakdown of the financial costs and time demands to construct the LU headform.

Component	First headform		Subsequent headforms	
	Time (Days)	Cost (GBP)	Time (days)	Cost (GBP)
Cranium	3.8	£ 568.80	3.8	£ 568.80
Face and Jaw	4. 7	£ 141.60	-	-
External Soft tissue mould tooling	4. 7	£ 818.46	-	-
External Soft tissue	3.5	£ 44.92	3.5	£ 44.92
Gelatine filler	1.0	£ 14.30	1.0	£ 14.30
Total	17.7	£ 1,588.08	8.3	£ 628.02

At the time of purchase (December 2017), the Hybrid-III 50th percentile headform was quoted at 2765 GBP (Cellbond, UK), and the NOCSAE headform was quoted at 1953.58 GBP (Southern Impact Research Center LLC, TN, USA) (2455 USD at current exchange rate of 1 GBP to 1.26 USD). These costs were not inclusive of shipping and potential import duties which would vary based on location. As such, the initial version of the LU headform cost 55.3% and 78.2% of the Hybrid-III and NOCSAE headforms respectively, with future versions costing 22.7% and 32.1%. The price of 10 destructive impacts using the LU headform is 7,240.26 GBP, compared to 19,535.80 GBP using the NOCSAE headform (not including shipping).

Following the manufacture of each component (skull components manufactured using a Dimension Elite FDM machine (Stratasys, Minnesota, USA), set to a solid build with a resolution of 0.254 mm) and of the complete LU headform, a number of validation tests were completed. As skull deformation and resonance frequency excitation may be important aspects that influence the observed headform response in projectile sports impacts, the resonance frequency of the 3D printed skull component was determined. A calibrated triaxial linear accelerometer (DJB instruments, type AT/10-6) and force hammer (BrÜel & Kjaer, Type 8206-001) were used to collect data using Siemens LMS Test Lab 15.0. The skull component of the LU headform was suspended using bungee cords and data were collected at four combinations of response measurement and excitation locations. These were:

- Occipital measurement, frontal excitation
- Frontal measurement, occipital excitation
- Lateral measurement (Left side), Lateral Measurement (Right side)
- Frontal measurement, oblique excitation

Five trials were completed at each combination and used to determine the resonance frequencies of the skull. These were then compared to the results presented by Khalil et al. (1979), who collected data in a similar manner, at the same locations on dry human skulls.

With respect to the dynamic response, previous headforms have been validated by comparing the observed resultant linear acceleration at the headforms CoG with those reported by Hodgson and Thomas (1973), who instrumented 13 post mortem human subjects (PMHS) and the linear response of the CoG was estimated when subjected to drop tests onto a flat, rigid plate on the forehead region.

To validate the LU headform in this respect, a ±2000g triaxial linear accelerometer (IEPE Model 7131A) and ±6000 deg/s triaxial angular rate sensor (MEMS Model 603) were used to measure the dynamic response of the headform in 6 DOF. Five repeated drop tests

were conducted using the headform at impact speeds of 1, 1.5, 2 and 2.71 m/s. A linear drop tower was used to achieve the desired impact speed and location on the headform, which was dropped onto a flat rigid anvil, as defined by Hodgson and Thomas (1973). The triaxial linear accelerometer and triaxial angular rate sensors were connected to a DJB Instruments CV9-V and Endevco DC differential voltage amplifier (Model 136) respectively, and sampled at 1Ms/s using a Picoscope 5000 series digital oscilloscope. A pair of laser timing gates, separated by 10 mm, were used to measure impact speed and synchronously trigger the triaxial linear accelerometer and triaxial angular rate sensor. Drops were repeated at each impact speed until 5 suitable trials were collected at the nominal impact speed ±0.05 m/s. A custom MATLAB script was written to process the data. A 4th order low pass Butterworth filter was used to filter the measured linear acceleration at 1650 Hz and the angular velocity at 1000 Hz (as done by Hodgson and Thomas (1973)). The associated resultant linear acceleration at the CoG was calculated using known geometric offsets incorporated into Equation 22 (reported by Martin et al., 1998)). The contact period was defined as the time over which the resultant acceleration was above 2 g. Peak resultant linear accelerations were determined and compared to the data presented by Hodgson and Thomas (1973).

$$\begin{bmatrix} a_{CoGx} \\ a_{CoGy} \\ a_{CoGz} \end{bmatrix} = \begin{bmatrix} a_x + (\omega_y{}^2 + \omega_z{}^2)r_x + (\alpha_x - \omega_x\omega_y)r_y - (\alpha_y + \omega_z\omega_x)r_z \\ a_y - (\alpha_z + \omega_x\omega_y)r_x + (\omega_z{}^2 + \omega_x{}^2)r_y + (\alpha_x - \omega_y\omega_z)r_z \\ a_z + (\alpha_z - \omega_z\omega_x)r_x - (\alpha_x + \omega_y\omega_z)r_y + (\omega_x{}^2 + \omega_y{}^2)r_z \end{bmatrix} \quad \text{Eq. 22}$$

where: a_{CoG} = linear acceleration at the centre of gravity (g), a = measured linear acceleration (g), α = angular acceleration (rad/s/s), ω = angular velocity (rad/s) and r = geometric offset (m).

5.4. Results

The scaled CAD model was found to match the average 50th percentile UK male with respect to total head length, EAM to occiput, EAM to glabella, head breadth, total head height and EAM to vertex (Table 21). The circumference of the headform model was found to be lower than that reported by Peebles and Norris (1998), likely due to variations in head shape not captured by the reported dimensions. Despite this, the circumference of the CAD model was still within one standard deviation of the mean reported by Peebles and Norris (1998).

Table 21. Comparison of 50th percentile UK male head geometry (Peebles and Norris, 1998) with scaled LU headform, and commercially available headforms.

	UK 50th percentile male (mm) (mean (SD))	LU scaled (mm)	Hybrid III (mm)	NOCSAE (mm)	EN 960 (mm)
Head length	200.2 (7.6)	200.2	203.0	200.0	201.6
EAM to occiput	98.5 (7.6)	98.5	-	98.0	100.8
Head breadth	143.8 (6.3)	143.8	115.0	140.0	158.2
Head height	228.5 (11.3)	228.5	-	-	209.1
EAM to vertex	130.4 (8.5)	130.4	124.0	115.0	121.0
Head circumference	575.0 (16.8)	562.5	572.0	576.0	575.0

The measured thicknesses of the LU headform model at the frontal, lateral/temporal and occipital areas were found to be within one standard deviation of the mean reported in all previous reported values, other than at the lateral/temporal region reported by Mahinda and Murty (2009), as shown in Table 22. The thickness of the external soft tissue at the forehead and temporal regions, in addition to the occiput and vertex were within the range of 3 to 8 mm reported by Lin et al. (2008).

Table 22. Comparison of measured skull thickness of the LU headform and previously reported human data.

	Frontal (mean (SD))	Lateral (mean (SD))	Occipital (mean (SD))
LU	5.9	5.8	7.99
Hodgson et al. (1970)	5.99	-	-
McElhaney et al. (1970)	6.91 (1.19)	6.91 (1.19)	6.91 (1.19)
Lynnerup, (2001)	7.04 (1.27)	5.04 (1.25)	7.83 (1.66)
Mahinda and Murty (2009)	6.3 (1.27)	3.9 (0.93)	9.35 (1.42)

The tensile and flexural properties of the FDM ABS p-430 samples, and those reported for human skull bone (Blanton and Biggs, 1968; Hubbard, 1971; McElhaney et al., 1970; Motherway et al., 2009; Yeni et al., 1998) can be seen in Table 23. The orientation of the build material was found to have little effect on the observed density of the ABS-p430 samples. Although the tensile and flexural modulus and tensile and flexural strength were found to be similar in the flat and side builds, these parameters were lower in the samples built upright (as reported by Rodriguez-Panes et al. (2018), due to the inter-layer adhesion). However, as can be seen in Table 23, the material properties of the ABS-p430 flat and side build samples are comparable to those reported for human skull bone with respect to flexural and tensile strength and, although at the lower end, was within the range of reported tensile and flexural moduli. Although the material properties of the upright build samples were lower

than the human skull bone samples, the material properties of ABS-p430 are also more consistent with human tissue than the Hybrid-III and EN 960 headforms (see Table 23), and as such have been utilised in other research grade headforms (Mohotti et al., 2018; Petrone et al., 2018). It is important to note that the available equipment limited the strain rates that could be assessed here. Motherway et al. (2009) reported that strain rate has a significant effect on the measured human bone properties, and as such future tests should look to measure ABS p-430 properties at the higher strain rates that are likely to occur in high speed projectile impacts. The strain rates measured in this study do, however, allow comparisons with the previous studies. The density of ABS-p430 (988 ± 0.38 kg/m^3) was found to be similar to the values reported for cancellous bone (300 – 975 kg/m^3 but lower than that of the compact bone (1800 – 2000 kg/m^3) (CES EduPack, 2017).

Table 23. Comparison of measured material properties of FDM manufactured ABS-p430 with reported values for human skull bone (Blanton and Biggs, 1968; CES EduPack, 2017; Hubbard, 1971; McElhaney et al., 1970; Motherway et al., 2009; Yeni et al., 1998) and, materials used in the NOCSAE and Hybrid-III headforms (CES EduPack, 2017).

	Flexural Modulus (GPa) 0.01-0.02 strain mean (SD)	Tensile Modulus (GPa) 0.01-0.02 strain mean (SD)	Flexural Strength (MPa) mean (SD)	Tensile Strength (MPa) mean (SD)
ABS p430 flat build	2.46 (0.05)	2.08 (0.20)	76.74 (1.00)	51.56 (0.89)
ABS p430 side build	2.46 (0.07)	2.23 (0.02)	76.47 (1.14)	53.37 (0.65)
ABS p430 upright build	1.09 (0.04)	1.01 (0.03)	12.32 (0.80)	3.50 (0.32)
Hybrid-III skull simulant	71 - 75		200 - 221	
NOCSAE skull simulant	2.62 - 3.2		90 - 165	
Human skull bone	2.07 - 25.83	1.23 - 5.38	82.00 (25.50)	67.30 (17.80)

When calculating the inertial properties of the LU headform using the measured density of ABS-p430, the reported density of Silastic 3483, and the density of a 20% gelatine brain, the mass of the headform model (3.53 kg), principal moments (I1 = 163.3 kg/cm^2, I2 = 152.3 kg/cm^2 and I3 = 109.3 kg/cm^2) and moments of inertia about anatomical axes at the CoG (I_{xx} = 130.9 kg/cm^2, I_{yy} = 163.3 kg/cm^2 and I_{zz} = 130.65 kg/cm^2) were all found to be lower than the mean values reported for the human head (Albery and Whitestone, 2003; Becker, 1972; Hodgson et al., 1972). This was a result of the density of ABS-p430, which, as discussed previously, was found to be lower than that of human compact skull bone.

Introducing a metal filler to the silicone component of the headform provided a convenient method of increasing the inertial properties, given the density of the ABS-p430. This technique also provided an additional benefit of allowing the mass of the headform to be tuned to match other populations (e.g. 95th percentile) if necessary. The density of the

silicone component required to produce a headform mass of 4.14 kg (mean of the studies that reported head mass) was calculated to be 1810.9 kg/m^3.

Copper powder was identified as a filler that could be used with Silastic 3483, as its high density (4700 kg/m^3) meant that the required density could be reached by introducing the lowest possible volume. As the introduction of copper powder to the silicone would likely influence the material properties of the silicone, five test samples with the identified ratio of copper powder to silicone were manufactured using curing agents 3483R and 3483F and compared the virgin 3483F samples and tested as outlined previously. Silastic 3483R with copper powder was selected as the external soft tissue simulant that would be used in this headform as this was found to be more consistent with the virgin samples (secant moduli between 0.45 and 0.5 strain – virgin 3483F: 3.31 ±0.25 MPa; Copper 3483R: 3.14 ±0.19 MPa) (see Figure 49).

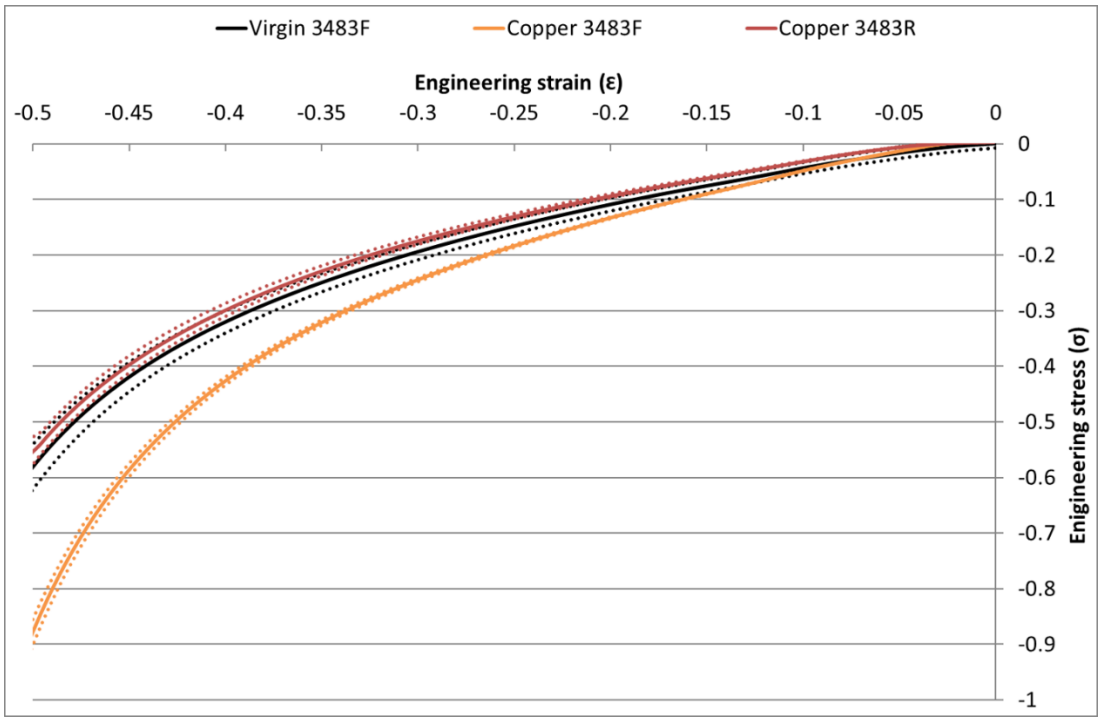

Figure 49.Average engineering stress-strain curves for virgin Silastic 3483 with RTV-3083F curing agent (Virgin 3483F), Silastic 3483 with RTV-3083F curing agent and copper (Copper 3483F) and Silastic 3483 with RTV-3083R curing agent and copper (Copper 3483R).

The adjusted density of the silicone component was then applied to the headform model and the inertial properties were re-calculated. Figure 50 shows the calculated mass of the LU headform compared to reported cadaver head masses and those of the Hybrid-III, NOCSAE and EN 960 headforms. As expected, the mass of the LU headform was calculated to be the exact value of the all study average, whereas all other headforms were at least one standard deviation above this mean. Although not desirable, a ~10% variation in

mass, due to manufacturing tolerances, would maintain a headform mass within one standard deviation of the all study average.

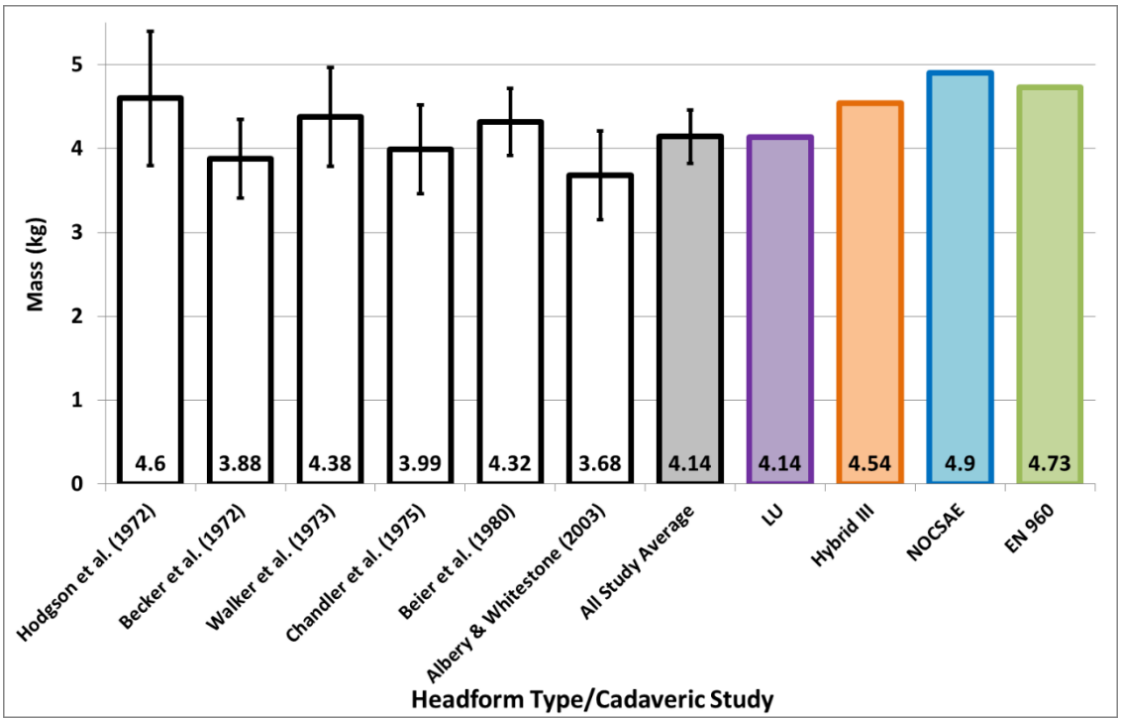

Figure 50.Comparison of calculated LU headform mass with cadaveric studies and commercially available headforms.

The CoG of the LU headform was calculated to be -5.56 and -4.26% different from the all study average in the x and z direction respectively (y axis offset was zero, due to the symmetry of the headform model), and was well within one standard deviation of the mean, as shown in Figure 51. The calculated first, second and third principal moments of the LU headform were found to be -6.93, -0.09 and -10.01% divergent from the average values reported in the literature respectively. Although the principal moments were lower than the all study average, they were still within one standard deviation of the mean, as shown in Figure 51.

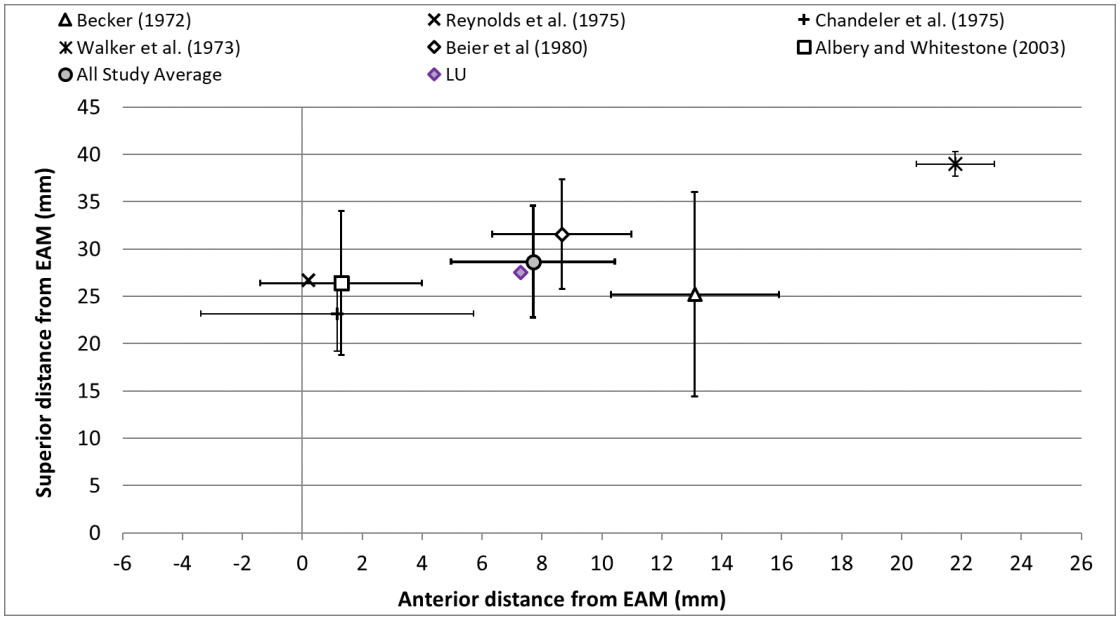

Figure 51. Comparison of calculated CoG location of LU headform and reported values from cadaveric studies.

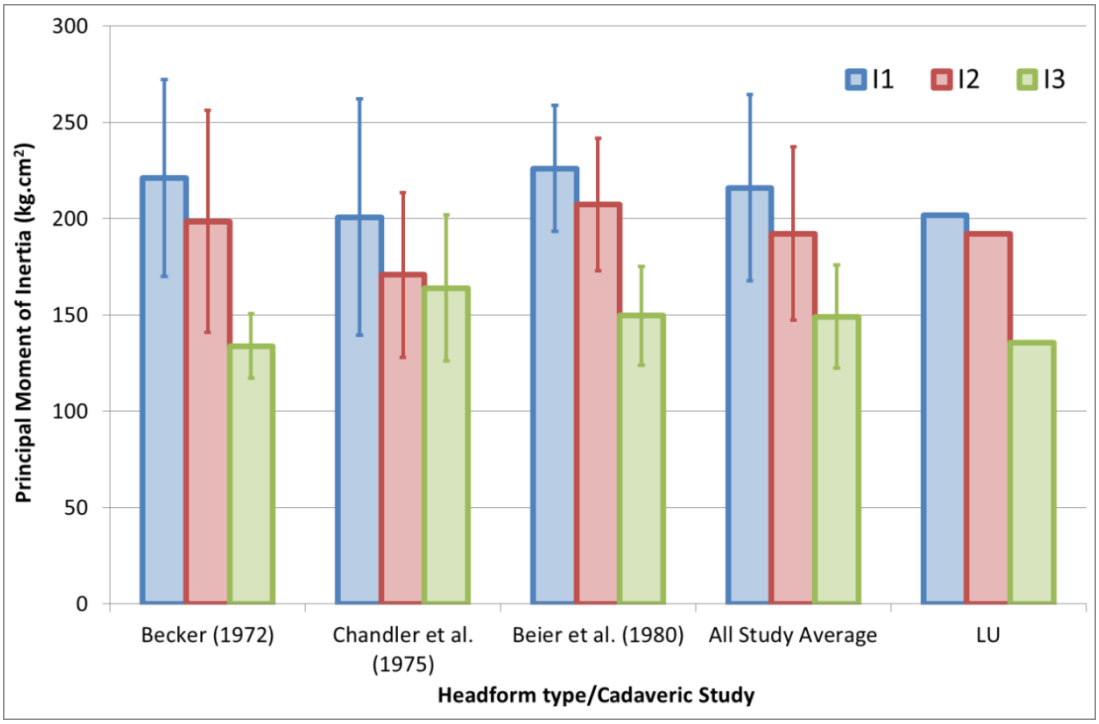

Figure 52.Comparison of calculated principal moments of the LU headform with values reported from literature.

The MoI about anatomical axes at the CoG of the LU headform were calculated to be close to the all study average in I_{xx}, I_{yy} and I_{zz}, showing divergences of -6.55 %, 2.71 % and 1.48 %, respectively. Relative to the Hybrid-III, NOCSAE and EN 960 headforms, the LU headform was found to better represent the average reported values in I_{yy} and I_{zz}, whereas in I_{xx}, the NOCSAE was slightly closer to the all study average (see Figure 52).

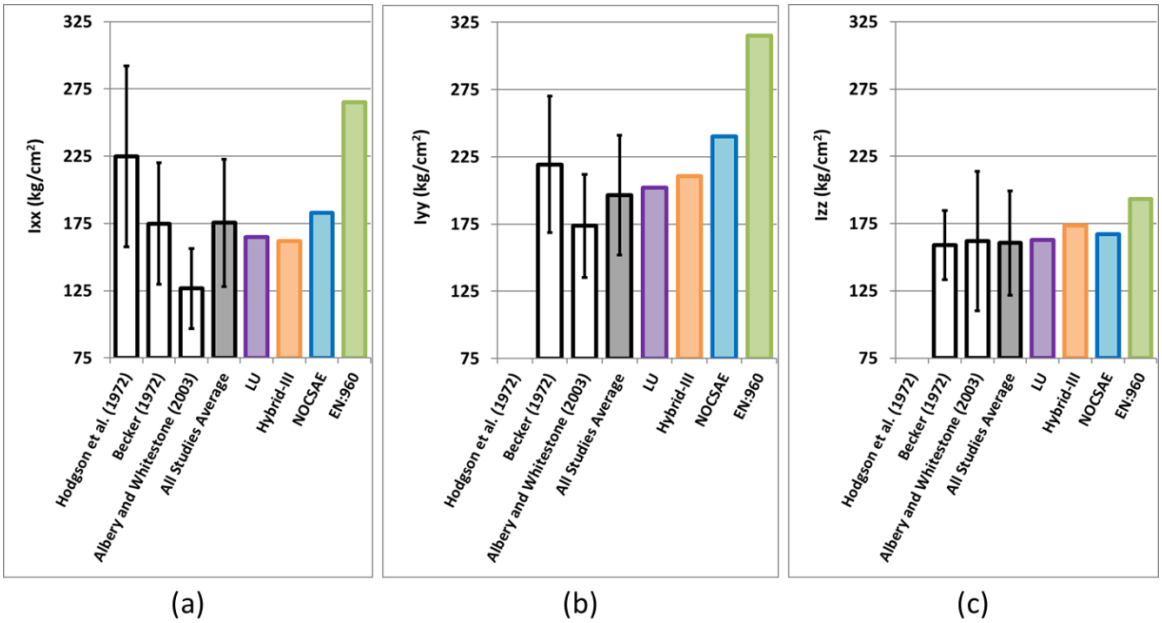

Figure 53. Comparison of calculated moments of inertia about the x (a), y (b) and z (c) axes at the CoG of the LU headform, cadaveric studies and commercially available headforms.

For completeness the moment of inertia about an imposed axis connecting the left and right EAM was calculated and compared to the same parameter reported by Walker et al. (1973). Here the calculated value for the LU headform (235.5 kg/cm^2) was just 0.97% greater than the mean value reported by Walker et al. (1973) (233.2 kg/cm^2).

A comparison of the calculated and measured inertial properties of the manufactured LU headform can be found in Table 24. Differences in the calculated and experimentally derived mass and moments of inertia about the CoG measurements were found to be maximally 3.9%. The differences observed in the CoG offset in the x and y axes were small and within the measurement uncertainty, whereas the offset in the z axis was larger, showing that the headform was slightly top heavy. This is potentially due to some of the copper powder sinking during the curing of the external soft tissue. This would also explain the slightly larger differences in I_{xx} (3.8%) and I_{yy} (2.7%) compared to I_{zz} (1.6%).

Table 24. Inertial properties of the LU headform calculated in Siemens NX 10.0 and experimentally derived measurements.

Inertial Property	Calculated	Measured(uncertainty)
Mass (kg)	4.14	4.30 (0.00)
CoG offset from EAM - x axis (mm)	7.30	7.79 (0.50)
CoG offset from EAM - y axis (mm)	0.00	0.33 (0.50)
CoG offset from EAM - z axis (mm)	27.50	42.00 (0.50)
I_{xx} (kg.cm^2)	164.70	170.90 (0.50)
I_{yy} (kg.cm^2)	201.95	207.40 (0.50)
I_{zz} (kg.cm^2)	162.92	165.60 (0.50)

The resonance frequencies observed in the 3D printed skull component and those of the human skull can be found in Table 25 and Table 26. A greater number of resonance frequencies were identified in the skull model for frequencies in the same region, and a systematic offset between the 3D printed skull and the human skull was observed with the former consistently showing slightly higher values. This is likely due to the material properties of the 3D printed components. As previously discussed, the stiffness of ABS-p430 was comparable to that of human skull bone, however, the density and therefore mass, was lower. Since the natural frequency is strongly influenced by the ratio of structural stiffness to its inertia, it follows that this was higher in the 3D printed skull model. Generally though, the resonance frequencies of the LU skull component showed good correlation with those observed in dried human skulls.

Table 25. Resonant frequencies of the 3D printed skull component of the LU headform.

Excitation/Measurement Locations	Frequency Associated with various mode numbers (Hz)										
	1	2	3	4	5	6	7	8	9	10	11
Frontal excitation - Occipital Measurement		1675				2570	2825		3315	3740	3840
Occipital Excitation - Frontal Measurement	1485	1695	2000			2600		3090	3315		4050
Temporal Excitation - Temporal Measurement	1415		1980	2225	2470	2640	2855	`	3550		3970
Oblique Excitation - Temporal Measurement	1415		2050	2210	2475		2835		3235		4115
Oblique Excitation - Frontal Measurement	1470		2010			2605			3310	3745	

Table 26. Resonant frequencies of dried human skull as reported by Khalil et al. (1979).

Excitation/Measurement Locations	Frequency Associated with various mode numbers (Hz)								
	1	2	3	4	5	6	7	8	9
Frontal excitation - Occipital Measurement	1385			2537	2810	3581			
Occipital Excitation - Frontal Measurement	1385			2547	2781	3572			
Temporal Excitation - Temporal Measurement	1385	1777		2449	2859	3289	3699		4157
Oblique Excitation - Temporal Measurement	1385	1747	1883	2440	2703	3289	3679		
Oblique Excitation - Frontal Measurement	1385	1786	1903	2449	2857	3386	3523	3845	4069

Figure 54 shows the peak resultant linear acceleration observed in the drop tests using the LU headform and those reported using human cadavers. When considering the impacts that resulted in skull fracture, the peak resultant linear acceleration values ranged from ~195 to ~370 g at ~2.5 m/s. There was also an impact at ~3.3 m/s that did not result in skull fracture and produced a peak resultant linear acceleration value of ~150 g. These differences are likely due to subtle individual variations in head mass, geometry, tissue thickness and stiffness in the tested cadavers. Given that Hodgson and Thomas (1973) estimated CoG acceleration and used a limited number of PMHS heads, the actual range of peak resultant linear accelerations may indeed be greater than that actually observed. As a result, the PMHS data should only be seen as a guide to establish a response corridor. Consequently, although the LU headform produced peak resultant linear accelerations towards the upper limit of those reported by Hodgson and Thomas, this was considered to produce a suitably biofidelic response.

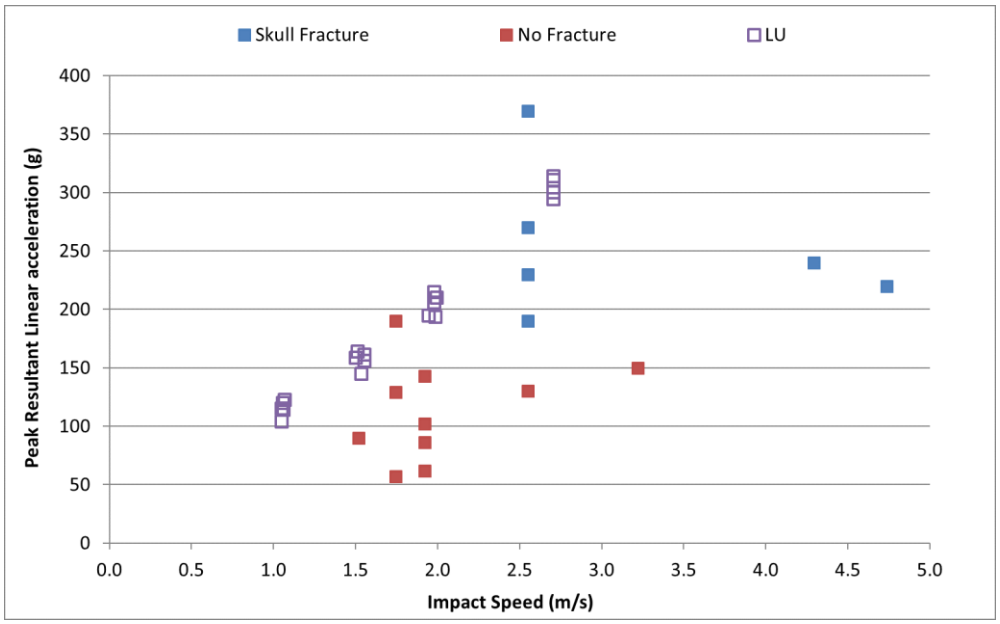

Figure 54. Peak resultant linear acceleration of the LU headform and PMHS as reported by Hodgson and Thomas (1973).

5.5. Conclusions

Overall, the research described in this chapter aimed to develop a novel headform (LU headform) that was representative of a 50th percentile UK male, capable of producing realistic first order dynamic responses, that could be used in the assessment of head impacts in protected and unprotected scenarios representative of those seen in Cricket, given the clear limitations of currently available approaches. Although the LU headform meets the design requirements set out prior to the developmental process (Table 18), it is

important to acknowledge the limitations of the LU headform in its current state. ABS-p430 was selected as the material used to represent the skull components due to the available manufacturing processes, and although this was found to have suitable material properties in two build orientations (flat and side), when built upright the material properties were lower and outside the range reported for human tissue. In future, it may be possible to manufacture the skull components using other materials, for example PLA, which have been shown to display favourable material properties (Falland-Cheung et al., 2017), and reduced effect of build orientation (Rodriguez-Panes et al., 2018). Currently, the brain is represented as a gelatine filler to contribute to the inertial properties of the headform. This is prevented from adhering to the inner surface of the skull through the application of PTFE spray prior to moulding. Although the exact motion of the human brain tissue under impact conditions, particularly in vivo, eludes the research community, it is apparent that the relative motion of brain tissue within the skull, and the influence it has on impact dynamics, is not well represented by the absence of a similar distribution of mass, stiffness and mobility within surrogate headforms. As the response of the headform during dynamic tests have been shown to be comparable to human cadaver responses, it may be assumed that the relative motion possible has a favourable effect on the observed response – this however, and the effect of the tentorium and falx cerebri modelled into the LU headform, has not been directly measured and should be an aim of future work. Unlike the models developed by Miyazaki et al. (2012) and Petrone et al. (2018), the LU headform does not permit direct measurement of brain motion. While such measurement might be included in future iterations, it is acknowledged that analysis of brain motion cannot be made directly from the LU headform. Although this is an intended outcome resulting from the targeted use of the headform in potentially destructive scenarios, the development and integration of instrumentation to directly measure the motion of the brain during impact would be a useful future advancement.

Despite these limitations, The LU headform was shown to represent a 50th percentile UK male in its geometry and mass, and each of these parameters has the potential to be tuned to accommodate a different population in future. With respect to the inertial properties of the LU headform, the location of the CoG of the LU headform has been calculated to be within 5.56 % of the average values reported in humans. The principal MoI and MoI at the CoG of the headform has been shown to accurately represent the average values presented in the literature to within 10.01 % and 6.55 % respectively, and is a better representation of the human head than the commercially available headforms discussed. The resonance frequency of the skull model was found to be comparable to that of the human skull, meaning that, unlike the Hybrid-III and EN 960 headforms, if resonance frequency excitation

occurs during an impact, this can also be observed and considered. The LU headform includes discreet elements to represent the bone and external soft tissue, which display material properties comparable to those previously reported for these tissues in humans and the skull cavity has been filled with gelatine solution contributing to the overall head mass and inertial properties. The headform was shown to display a dynamic response within the range presented for PMHS, when subjected to drop tests onto a flat, rigid anvil. Additionally, it has been shown that the headform could be manufactured quickly and at a cost that is not prohibitive. As each of the components of the LU headform have been shown to be closer to human tissues than those used in the Hybrid-III, the inherent biofidelity of the observed response is likely to be more biofidelic. Therefore, the LU headform is a suitable surrogate that, when used alongside commercially available headforms, may provide additional insight into the mechanics of protected and unprotected head impacts in Cricket.

CHAPTER 6

Development of a Projectile Test Methodology

Relative to impacts in other sports such as, for example, American Football, Rugby and Boxing, the mechanics of a head impact in Cricket can be broadly characterised as low mass – high velocity (as shown in Chapters 3 and 4). As a result, utilising methods such as drop tests or linear impactors, as used to simulate head impacts in American Football, Ice Hockey and Boxing (Carke et al., 2016; Pellman et al., 2003; Walilko et al., 2005), may be inappropriate and produce mechanical responses that are potentially erroneous when considering projectile impacts in Cricket. It is therefore important that, when assessing the mechanics of these types of impact using laboratory reconstructions, it is possible to create suitably representative impact conditions. As such, this chapter details the development of a projectile impact methodology suitable for the laboratory assessment of head impacts in Cricket, based on the findings of Chapters 3,4 and 5, and the framework defined in Figure 14.

6.1. Ball Propulsion

In the projectile impacts reported in this thesis, a pneumatic ram with carbon fibre rod was used to propel each ball at the desired nominal impact speed of 34.7 m/s identified as representative of a head impacts in Cricket (as presented in Chapter 4). The cannon used compressed air to drive a carbon fibre rod, which in turn propelled the test ball. An adjustable tee allowed the position of the stationary ball relative to the carbon fibre rod to be manipulated prior to propulsion, thereby permitting the appropriate orientation of the ball prior to impact. Initial impact tests showed that when set-up in this manner, the air cannon was capable of producing the desired impact speed (with ±0.5 m/s variation), while achieving the desired impact location (±10 mm) with negligible spin.

6.2. Headforms and Instrumentation

Four different types of headforms were used in the projectile tests. These were the EN 960 (size 575), Hybrid-III (50th percentile Male), NOCSAE (Medium) and LU (representative of a 50th percentile UK male). The impact locations defined in Chapter 4 were identified on each headform using Vernier calliper measurements from markings on the headform, identified anatomical landmarks, and dimensions supplied in the technical drawings where available. These locations were marked on each headform using a permanent marker.

Each headform was instrumented with a ±2000g triaxial linear accelerometer (IEPE Model 7131A), and a ±6000 deg/sec triaxial angular rate sensor (MEMS Model 603). The linear accelerometer was connected to a 9-channel charge Amplifier (Model CV9-V, DJB Instruments, UK) and the angular rate sensor was connected to an Endevco DC differential amplifier. The output from each of these was sampled at 1 MHz using a Picoscope 5000 series oscilloscope. In the EN 960 and Hybrid-III headforms, the linear accelerometer was screw mounted at the centre of gravity of the headform, with the sensitive axes aligned with that of the headform co-ordinate system (as shown in Figure 41). In the LU headform, the linear accelerometer was mounted a known distance from the CoG (x axis: 43.2 mm, y axis: 0 mm, z axis: 14.3 mm), with the sensitive axes aligned with those of the headform co-ordinate system, whereas in the NOCSAE headform, the linear accelerometer was mounted a known distance from the CoG at a known angle (x axis: 19.7 mm, y axis: -8.5 mm, z axis: -46.5 mm, angular offset: 23º), using a custom designed FDM manufactured mounting block (CAD image shown in Figure 55). This mounting block was screw mounted to the NOCSAE headform and FDM manufactured struts were used to engage the mass of the headform. The known geometric offsets meant that the measured acceleration at the sensor location when using the LU and NOCSAE headforms could be transformed to the CoG to provide a like for like comparison with the Hybrid-III and previously reported results.

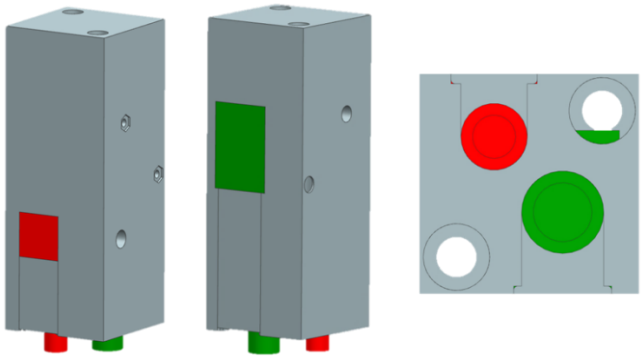

Figure 55. Side and bottom views of the mount block used to secure the linear accelerometer (red component) and angular rate sensor (green component).

Three Arri Pocket Par 400 lights were used to illuminate the impact area, and a Photron FastCam SA1 mono camera operating at 50 kHz was positioned perpendicular to the ball flight path, and in line with the impact location (as shown in Figure 56) to provide a qualitative assessment of impact location. A pair of laser timing gates, separated by 100 mm, were connected to a LeCroy WaveJet 324 digital oscilloscope sampling at 1MHz, and used to measure inbound ball speed. The output from the laser closest to the headform was

used to synchronously trigger data collection from the linear accelerometer, angular rate sensor and the HSV.

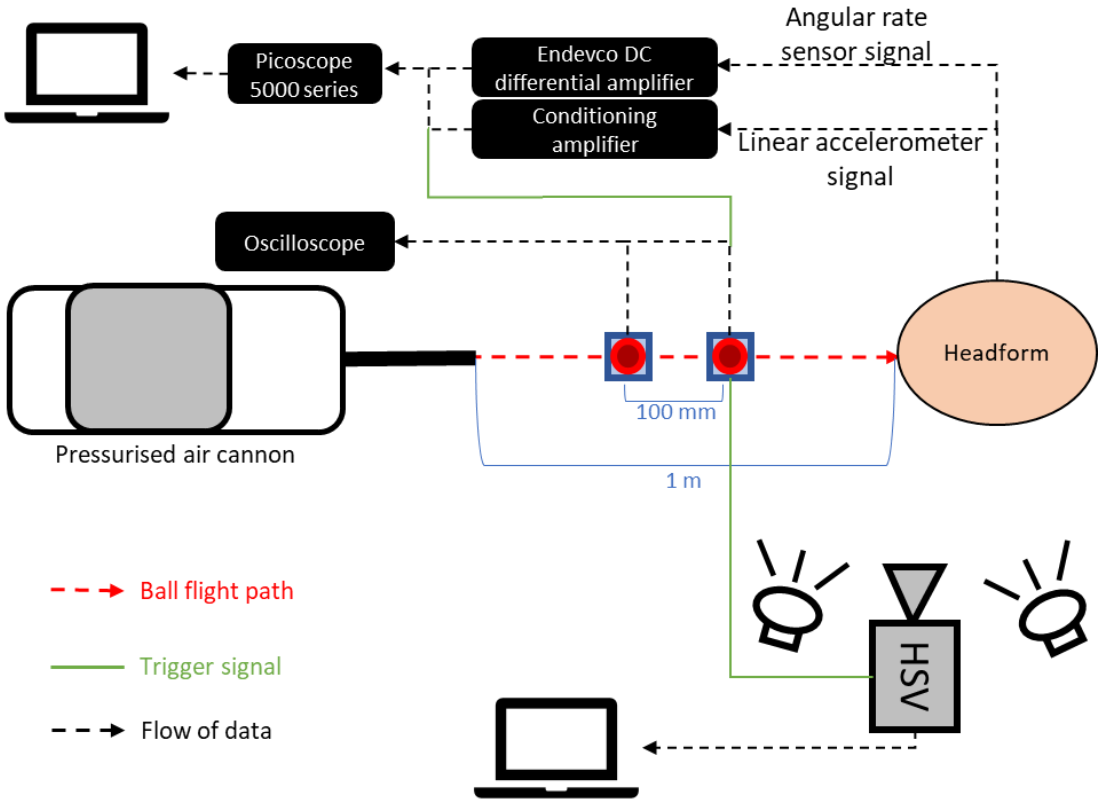

Figure 56. Schematic of the experimental setup.

6.3. Headform Suspension

To create a suitable impact response in a laboratory setting, any headform that is used must be suspended/mounted in an appropriate manner to represent the presence of the human neck. As discussed previously, a number of studies have used the Hybrid-III and/or NOCSAE headforms with the Hybrid-III neckform during laboratory assessments (Clark, 2015; Post et al., 2016; Walilko et al., 2005). However, as this neckform was developed for use in automotive crash testing, there are several factors that may limit the efficacy of this neckform during the assessment of some sports impacts. Firstly, the neckform was only validated for motion in the sagittal plane, meaning that the observed dynamic response observed in impacts that produce motion about the x or z axes defined in Chapter 5 (such as the lateral and oblique impact locations defined in Chapter 4) may be erroneous. Indeed, McElhaney et al. (1988) reported that, when in slight compression, the stiffness of the Hybrid-III neck was 18.6, 43.8 and 61.2 times that of the passive stiffness of the human cervical spine in flexion, extension and lateral loading respectively. When in slight tension,

the Hybrid-III neck stiffness was found to be 13.45, 13.5 and 17.4 times that of the passive stiffness of the human cervical spine in flexion, extension and lateral loading respectively. As such, although the Hybrid-III neckform has been shown to produce a suitably biofidelic response in frontal automotive crash tests (Foster et al., 1977), the biofidelity of lower energy impacts at varied locations, like those observed in Cricket) remains questionable.

Stone et al. (2017) assessed the effect of mounting technique on the observed response of an EN 960 headform when "~freely" suspended using bungee cords (comparable stiffness to a passive human neck) and a mounting technique that produced a stiffness ~28 times greater. It was found that when subjected to projectile impacts with a BOLA ball, there were minimal differences between the linear responses in both scenarios when considering the loading phase (time to maximum ball deformation), but significant differences during unloading (time from maximum ball deformation to final contact). Although it was suggested that these differences would have a negligible effect on the outcome of the penetration test specified in BS7928:2013, the subtle differences induced by such large variation in neck stiffness may have important ramifications when assessing the mechanics of impacts and potential injury mechanisms when considering mTBI and other brain injuries. Due to the previously discussed concerns around a ~fixed mounting scenario and the utilisation of the Hybrid-III neckform, the "~freely" suspended approach utilised by Stone et al. (2017), was used in these studies to produce a stiffness comparable to that of the passive stiffness of the human neck. Indeed, when considering the dynamic response of the headform, this approach is likely to represent a ~worst-case scenario since the motion of the headform is not restricted.

In order to suspend the headforms using bungee cords a custom-built rig was constructed using Rose and Krieger aluminium profile components (Rose+Krieger, Germany). This system allowed the manipulation of the vertical and lateral position of the headforms and thereby enabled each impact location to be arranged. Each headform was inverted and suspended using four bungee cords (10 mm diameter; 35 N pre-test tension), attached to the base of each headform using four small custom brackets and hook bungee ends. The custom brackets were adjusted so that the Frankfort plane of each headform was in line with the horizontal when at rest (measured using a digital spirit level positioned on the flat base of each headform). The distance between the suspended headform and the surrounding rig components was designed to allow uninterrupted motion of the headform during and after impact.

6.4. Helmet Information and Preparation

Helmets that were used at the professional level and available for commercial purchase at the time of testing (2018 season) were supplied directly from two prominent manufacturers. The components of the helmets were similar, with both helmet types displaying an outer shell (c. 2mm thick) of ABS plastic, and an expanded polystyrene layer (c. 10mm thick). The geometry of the helmets was also broadly similar, with the only noticeable difference occurring at the peak area. Here Helmet B displayed a sloped design, whereas Helmet A displayed a more traditional design (Figure 57 shows an example of a more traditional design). All helmets provided were defined and labelled for commercial sale as 'senior size medium' or equivalent, by the manufacturers. Agreements with the manufacturers meant that anonymised results, with only their product identifiable, would be made available to manufacturers for product development purposes, but not released publicly. As such, the helmet specific results are referred to as Helmet A and Helmet B.

All superfluous packaging and labels were removed, and all helmet samples were conditioned at 22^{o}C ± 2 and 15% ± 5 humidity for at least 24 hours prior to any measurements or impact tests. The mass of each helmet unit was measured to 0.1 g accuracy using Okaus EB series scales and labelled with a unique code (e.g. A_1, A_2, B_1, B_2 etc…) using a permanent marker to ensure that testing was conducted in the correct order and unwanted repeat impacts were prevented.

When fitting the helmets onto the required headforms, the front edge of the helmet was positioned a known distance above the Frankfort plane, based on the dimensions of the headform in use and the geometric offsets specified in BS 7928:2013 and BS EN 960:2006 (BSi, 2006). Each helmet was positioned on the headform and a 50 N force was applied to the crown to secure it. Small adjustments were made to the position of the helmet to ensure that the helmet position matched that defined in BS7928:2013, as shown in Figure 57. The chin strap was secured and positioned as recommended, and tightened to a force of 100 N, measured using an Omega LC103B-25 S type load cell. Once the fitted helmet was judged to be appropriate, the bungee cords were attached and the headform was positioned in the appropriate location in the impact rig.

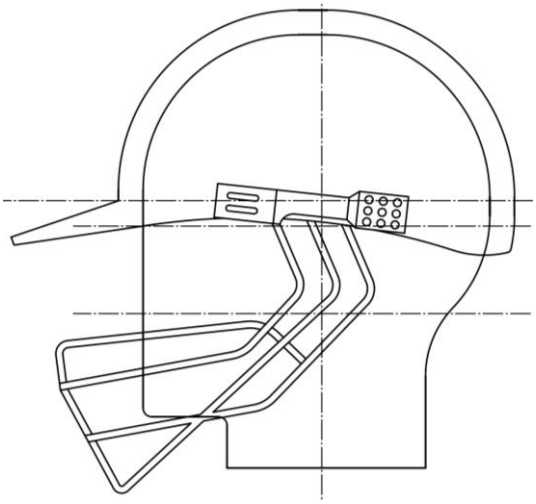

Figure 57. Helmet positioning defined in BS7928:2013.

6.5. Helmeted Impacts

When conducting the helmeted impacts, each helmet was subjected to a single impact at each location. The order of the locations that each helmet was impacted at was manipulated so that each location was tested with a fresh, unused helmet (eg Helmet A_1: frontal, lateral, oblique; Helmet A_2: lateral, oblique, frontal; Helmet A_3: oblique, frontal, lateral). A minimum of five-minutes was left between concurrent impacts on a given helmet. This impact order meant that the effect of any diffuse damage to the helmets following each impact could be assessed. Additionally, the effect of repeated impacts on helmet performance was assessed using five unused samples of each helmet type. On each of these helmet samples, five repeated impacts at the frontal location were completed using the LU headform.

6.6. Unprotected Impacts

As the manufacturer of the NOCSAE headforms suggested that an unprotected Cricket impact may cause permanent fracture to this headform, unprotected impacts were only conducted on the EN 960, Hybrid-III and LU headforms. When using the EN 960 and Hybrid-III impacts, five repeated impacts were completed at each impact location. Impact tests on the LU headform were conducted in the same manner, however after each impact, the headform was checked for fracture. When fracture was not evident, three validation drop tests were completed using the same protocol defined in Chapter 5. These results were then compared to the original, pre-projectile impact validation drops to ensure that the observed response remained within tolerable limits (± 1SD). For the LU headform, five repeated impacts were conducted at the frontal and lateral impact locations. In the oblique location,

three impacts were conducted that did not result in permanent damage, however the fourth impact did cause permanent skull fracture.

6.7. Protocol

Four testing phases were completed, with each phase consisting of all the impacts on one of the headforms. Once the helmet was fitted on the appropriate headform, the custom-built rig was manipulated to adjust the position of the headform based on the output from a laser pointer positioned down the centre of the carbon fibre rod that indicated ball flight path. When conducting helmeted impacts, the position of the suspended headform and helmet was adjusted so that, had the helmet not been present, the ball would have impacted the headform at the defined anatomical locations. Using this anatomically anchored approach meant that the dynamic response of the headform was always comparable, and differences in helmet design and geometry would influence the observed dynamic response of the headform. Once the headform position was confirmed, four points were marked on the headform(s) at visible locations. Four fixed lasers were arranged to point directly at the marked locations so that prior to the following impact, the position of the headform(s) could be adjusted to the same pre-impact position.

An unused Kookaburra Turf Cricket ball was assigned to each helmet type and headform combination (e.g. one ball for Hybrid-III – Helmet A). The helmet and headform assignment was marked on each ball, along with a running tally of the number of test impacts each had sustained. Prior to any impacts, the mass of each ball was measured and five repeated 1m drop tests were completed in the face orientation (as defined in Chapter 3) on each ball using the instrumentation and analysis methods described in Chapter 3. This methodology was repeated each time a ball had been used for three additional projectile impacts. Each set of post projectile impacts results were compared to the pre-impact results. As the projectile impacts were less severe than those seen in Chapter 3 (due to the movable headform and compliant helmet as opposed to the immovable concrete block), ball degradation was expected to be lower than that seen in Chapter 3 and as such, balls were used in their headform/helmet assignment if the calculated stiffness remained within one standard deviation of the pre-impact mean.

For each impact test, the assigned test ball was positioned on the tee, which was then adjusted so that it was in contact with the carbon fibre rod and the longitudinal axis of the rod was in line with the estimated centre of gravity of the ball (as shown in Figure 58). This ensured that the ball flight path was in line with the longitudinal axis of the carbon fire

rod, thereby achieving the desired impact location, with negligible spin imparted to the ball, resulting in impact in the desired orientation.

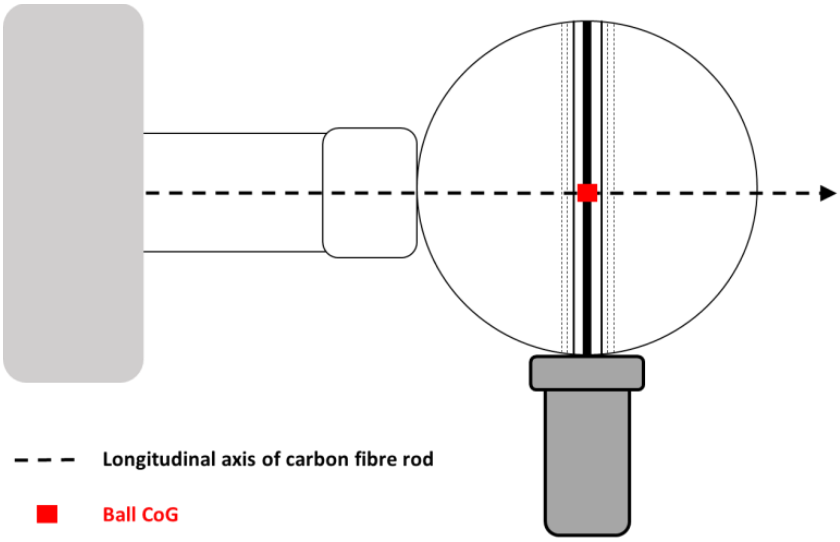

Figure 58. Schematic of the initial ball setup prior to impact tests.

6.8. Data Processing

Custom written MATLAB scripts were used to process all the collected data. Zero offset was removed from each signal channel by subtracting the mean of the first 5,000 data points from each channel prior to impact from the entire signal measured in the appropriate channel. Voltage outputs were then converted to SI units by applying the known sensitivity values to each channel output from the linear accelerometer and angular rate sensor.

Residual analysis (as described by Winter (1990)) was conducted using the measured responses using all four headforms. When using the EN 960 and Hybrid-III headforms, a low pass cut off frequency of 2 kHz was identified as a suitable compromise between noise reduction and signal distortion. This level of filtering was accepted, given that it is unlikely that any frequency components above this level would be representative of human-like response, as the materials used in the Hybrid-III and EN 960 headforms are dissimilar to organic tissues of the human head. When using the LU headforms, residual analysis suggested that a higher cut off frequency of 3 kHz would be suitable. Although higher than the level established for the EN 960 and Hybrid-III headforms, 3 kHz was considered an appropriate level, given that this would preserve potentially important biofidelic artefacts resulting from headform resonance (which has been shown to be comparable to that observed in humans, see Chapter 5). A comparable measure of the resonance frequency of the NOCSAE headform was unattainable, given that the skull component alone was not accessible and therefore could not be measured and compared

with the results of Khalil et al. (1979) who reported resonance frequencies of dried human skulls. However, given the residual analysis and knowledge of the construction and materials used in the NOCSAE headform, 3 kHz was selected as an appropriate cut off frequency that would preserve potentially important, biofidelic response artefacts. Therefore, the linear and angular data obtained using the EN 960 and Hybrid-III headforms were filtered using a 4th order low pass Butterworth filter set at 2 kHz, and the data obtained using the LU and NOCSAE headforms were filtered using a 4th order low pass Butterworth filter set at 3 kHz.

Following filtering, the linear accelerations measured in the LU and NOCSAE headforms were transformed to the CoG using the known geometric offsets and Equations 23, 24 and 25 as reported by Martin et al. (1998).

$$\begin{bmatrix} a_{CoGx} \\ a_{CoGy} \\ a_{CoGz} \end{bmatrix} = \begin{bmatrix} a_x + \left(\omega_y{}^2 + \omega_z{}^2\right)r_x + \left(\alpha_x - \omega_x\omega_y\right)r_y - \left(\alpha_y + \omega_z\omega_x\right)r_z \\ a_y - \left(\alpha_z + \omega_x\omega_y\right)r_x + \left(\omega_z{}^2 + \omega_x{}^2\right)r_y + \left(\alpha_x - \omega_y\omega_z\right)r_z \\ a_z + \left(\alpha_z - \omega_z\omega_x\right)r_x - \left(\alpha_x + \omega_y\omega_z\right)r_y + \left(\omega_x{}^2 + \omega_y{}^2\right)r_z \end{bmatrix} \quad \text{Eq. 23}$$

where: a_{CoG} = linear acceleration at the centre of gravity (g), a = measured linear acceleration (g), α = angular acceleration (rad/s/s), ω = angular velocity (rad/s) and r = geometric offset (m).

$$a_{rot} = a_m \times \begin{bmatrix} \cos(\theta) & 0 & \sin(\theta) \\ 0 & 1 & 0 \\ -\sin(\theta) & 0 & \cos(\theta) \end{bmatrix} \quad \text{Eq. 24}$$

$$\omega_{rot} = \omega_m \times \begin{bmatrix} \cos(\theta) & 0 & \sin(\theta) \\ 0 & 1 & 0 \\ -\sin(\theta) & 0 & \cos(\theta) \end{bmatrix} \quad \text{Eq. 25}$$

where: a_{rot} and ω_{rot} = rotated linear acceleration (g) and rotated angular velocity (rad/s) respectively, a_m and ω_m = measured linear acceleration (g) and angular velocity (rad/s) respectively and θ = angular offset (rad).

Resultant linear accelerations were calculated and used to identify the contact duration. This was defined as the time period when the resultant acceleration was greater than 2% of the peak value. Although the Hybrid-III was found to respond predominantly like a rigid body, the response measured with the EN 960 headform was found to contain additional artefacts that corrupted the expected ~rigid body response (see Figure 59). Further investigation identified the source of these artefacts to be the resonance frequency of the sensor mounting block used to mount the linear accelerometer and angular rate sensor. The lowest resonance frequency of this component was found to be around 1000 Hz. As the frequency of the linear and angular response pulse was similar to the resonance

frequency of the sensor mounting block, the observed responses were significantly influenced by this. Due to the similarity of the resonance and response frequencies, the removal of this artefact would result in significant distortion of the actual response signal. As the mounting block introduced frequency components that were not representative of a human response, and could not be removed, this headform was judged to be inappropriate for the assessment of projectile head impacts in Cricket and therefore excluded from further analyses.

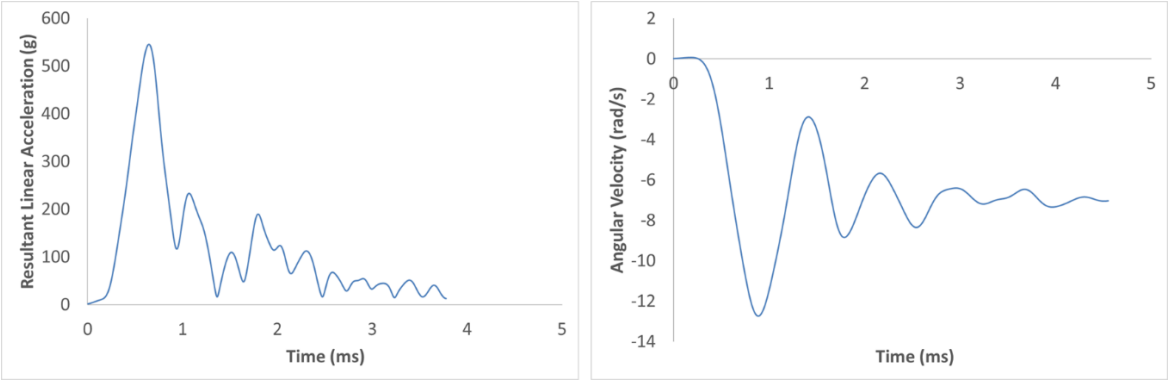

Figure 59. Examples of representative linear and angular response data using the EN 960 headform, filtered using a 4th order low pass Butterworth filter set at 2000 Hz.

When considering the angular response of the Hybrid-III, NOCSAE and LU headforms, it was found that angular acceleration (differentiated from the measured angular velocity) was extremely sensitive to cut off frequency whereas, the angular velocity was more robust to small changes to cut-off frequency (see Figure 60). Due to this, and previous findings that show angular velocity is better correlated with maximum principal strain and von Mises stress during short duration projectile impacts (Clark et al., 2016b), angular velocity was selected as the primary indicator of angular response.

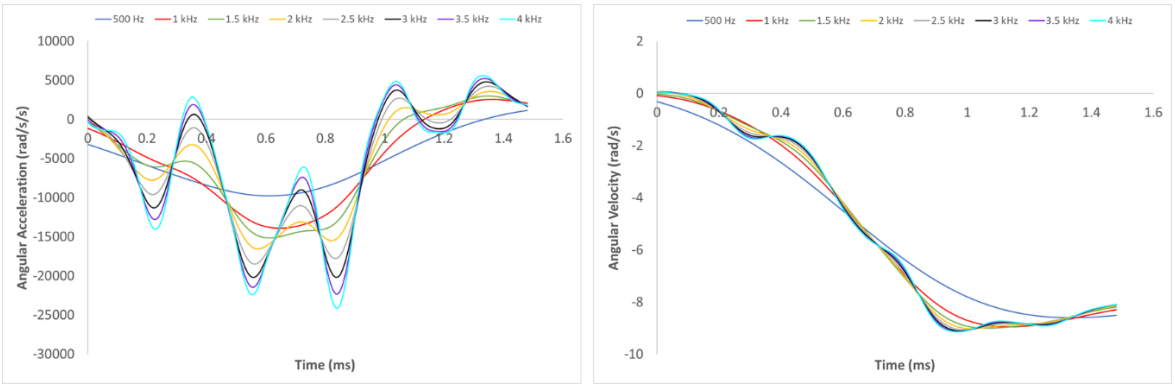

Figure 60. Examples of angular acceleration and velocity data using the Hybrid III-headform filtered at 0.5 kHz intervals.

At the frontal location, little angular velocity was generated about axes other than the y axis. Due to the defined impact locations in the lateral and oblique scenarios relative to the location of the CoG of the headforms, significant angular velocity was generated about the x and z axes at these locations. Examples of the angular velocity curves about each axis and in each headform type can be seen in Figure 61. In the interest of clarity, the parameters presented in relation to the angular response only reference these primary axes of rotation, though the calculated injury metrics take into account the response in all axes.

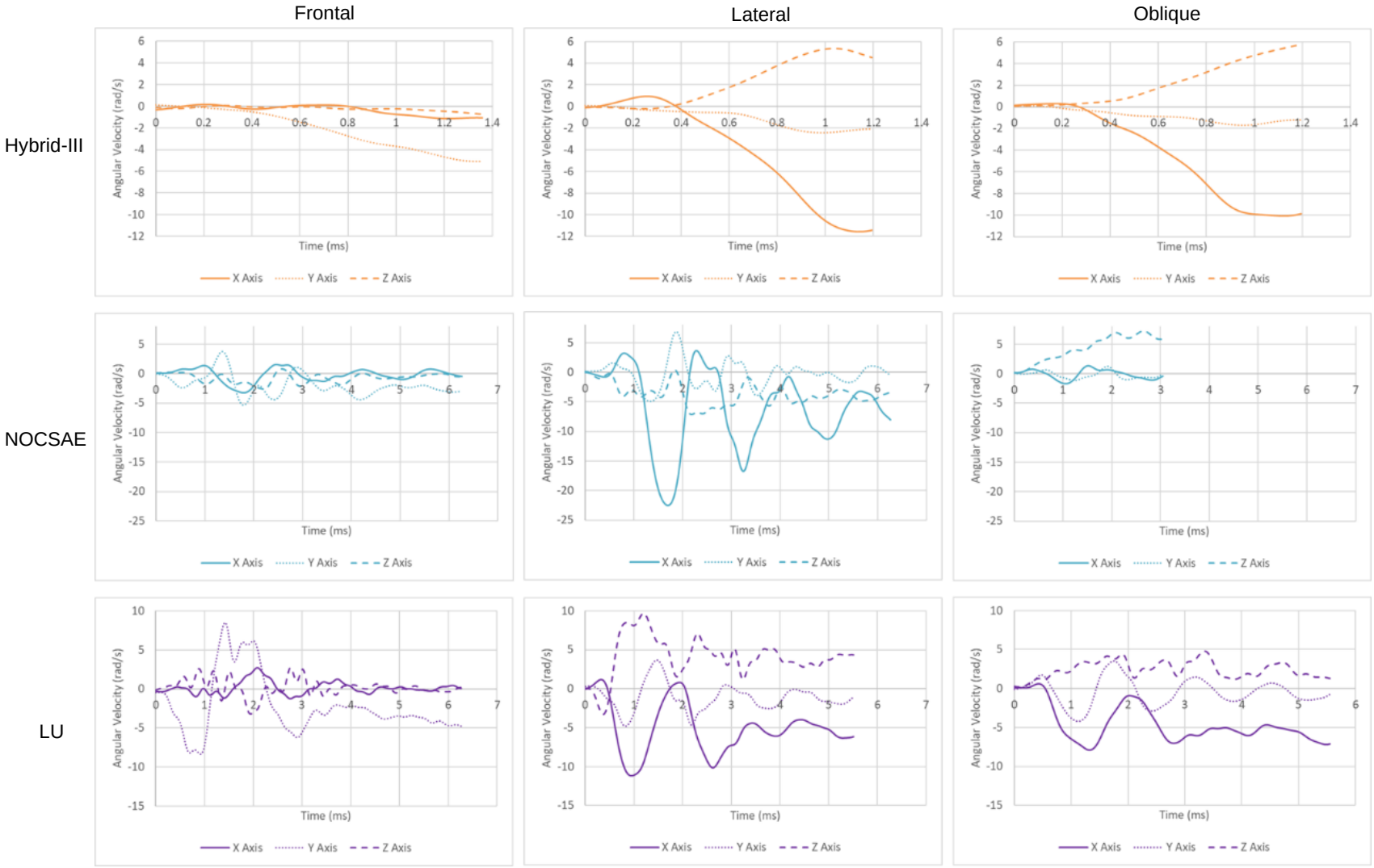

Figure 61. Examples of typical angular responses observed in each impact location using the Hybrid-III, NOCSAE and LU headforms.

All of the observed responses in a given impact scenario (for example, Hybrid-III-frontal location-Helmet A), were used to determine linear and angular response corridors by identifying the minimum and maximum values measured at each time point.

When using the Hybrid-III headform, key parameters (i.e. contact duration, peak resultant acceleration, time to peak resultant acceleration, peak angular velocity and time to peak angular velocity) were extracted from each trial, as identified using the technique shown in Figure 62. As the headform was found to respond predominantly as a rigid body, angular impulse was calculated using the peak angular velocity and MoI about the axes of interest. As the LU headform showed oscillations in the measured responses (see Figure 63) which were found to correspond with the measured natural frequencies (see Chapter 5), and similar oscillations were observed in the NOCSAE headform, a different approach was taken when analysing these signals. In the resultant linear acceleration signal, the peak acceleration and time to peak acceleration were identified. Any additional peaks that were greater than or equal to 75% of the absolute peak value were identified, and the magnitude and timing of these peaks were extracted. In addition, the magnitude and timing of the preceding troughs were also extracted (as shown in Figure 63). As can be seen in Figure 63 oscillations were also observed in the angular velocity signal. Here peak values, and time to these peaks were extracted, in addition to the magnitude and time to steady state angular velocity. Steady state was defined as the final time point where the magnitude of the angular velocity was outside of 5% of the mean of the final 5000 data points. In the LU and NOCSAE headforms, angular impulse was calculated using the steady state angular velocity and moment of inertia about the associated axes. As angular acceleration was found to be highly sensitive to cut off frequency, angular acceleration was estimated based on the magnitude and timing of the peaks identified in the angular velocity signal. Here the peak to peak angular acceleration was assumed to be represented by a half sine wave (Cross (1999) reported that force, and therefore acceleration, during a short duration tennis ball impact is represented as a half sine wave), with the maximum value estimated using Equation 26. This was then used to estimate the angular acceleration based on a half sine wave loading curve using Eq. 26.

$$\alpha_{sine} = \frac{\pi}{2 \times \left(\frac{\omega_n - \omega_{n-1}}{t_n - t_{n-1}}\right)} \qquad \text{Eq. 26}$$

where: α_{sine} = estimated maximum sinusoidal angular acceleration, ω_n = angular velocity at peak n, ω_{n-1} = angular velocity at peak n-1, t_n = time point of peak n and t_{n-1} = time point of peak n-1

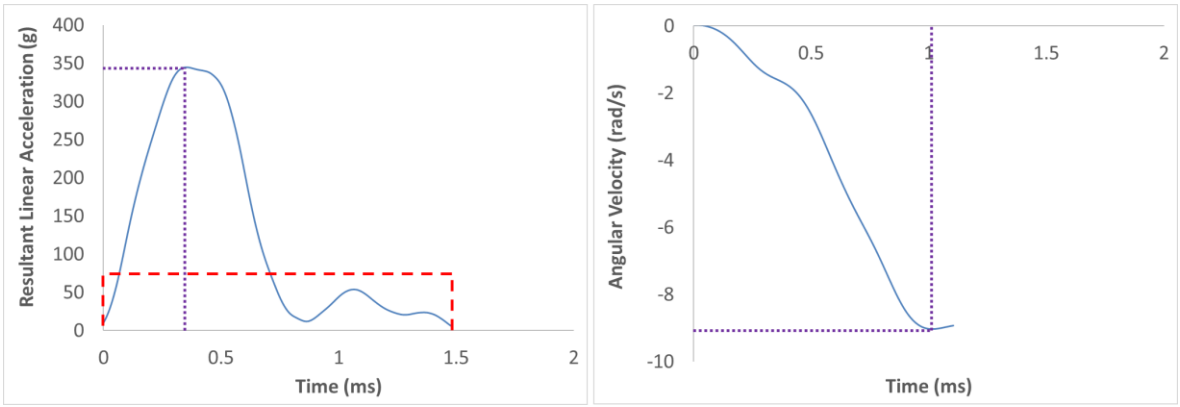

Figure 62. Representative linear acceleration curve using the Hybrid III headform and identified contact time (red), peak resultant linear acceleration/angular velocity and time to peak resultant linear acceleration/angular velocity (purple).

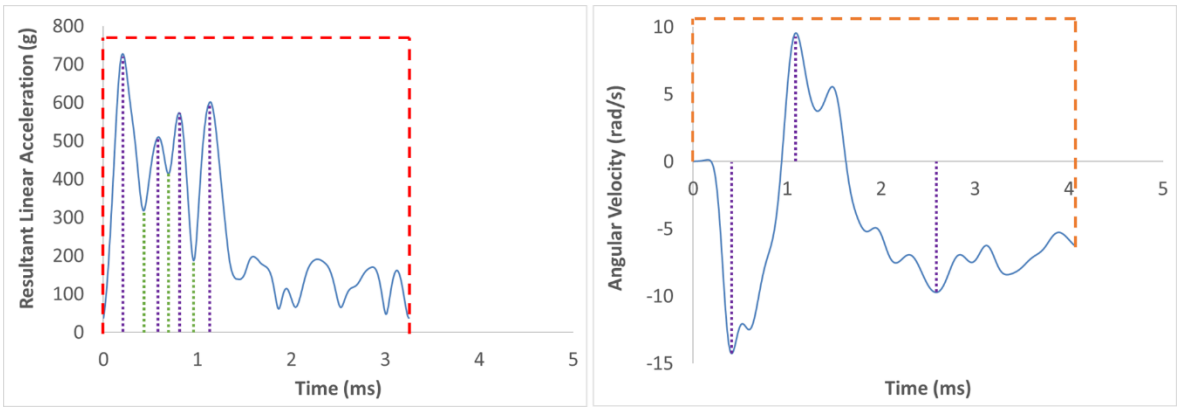

Figure 63. Representative linear and angular curves using the LU headform at the frontal location and the identification of contact time (red), peak values (purple), preceding troughs (green) and steady state (orange) values.

Although HIC and BrIC were developed in impact scenarios where the head would be expected to respond as a rigid body, which may not be the case when using the LU and/or NOCSAE headforms, these values were calculated using Equations 27 and 28, to provide a means of comparison with injury thresholds and results presented in other research. Two BrIC values were calculated for the LU and NOCSAE impacts, one based on the steady state angular velocities ($BrIC_{SS}$) and another based on the maximum angular velocities about each axis ($BrIC_{MAX}$). Calculated BrIC values were then used to predict the probability of sustaining AIS 1-4 injuries (PAIS) using equations 29 – 30 (Takhounts et al., 2013).

$$HIC = \left(\left[\frac{1}{t_2 - t_1} \int_{t_1}^{t_2} a(t)dt \right]^{2.5} (t_2 - t_1) \right)_{max} \quad \text{Eq. 27}$$

where: t_n = time point n and a = resultant linear acceleration

$$BrIC = \sqrt{\left(\frac{\omega_x}{\omega_{xC}}\right)^2 + \left(\frac{\omega_y}{\omega_{yC}}\right)^2 + \left(\frac{\omega_z}{\omega_{zC}}\right)^2} \quad \text{Eq.28}$$

where ω_{iC} are critical angular velocities (rad/s) and ω_i are maximum measured angular velocities (rad/s) in each direction. ω_{xC} = 66.25 rad/s, ω_{yC} = 56.45 rad/s and ω_{zC} = 42.87 rad/s

$$PAIS\ 1 = 1 - e^{-\left(\frac{BrIC}{0.120}\right)^{2.84}} \quad \text{Eq. 29}$$

$$PAIS\ 2 = 1 - e^{-\left(\frac{BrIC}{0.602}\right)^{2.84}} \quad \text{Eq. 30}$$

$$PAIS\ 3 = 1 - e^{-\left(\frac{BrIC}{0.987}\right)^{2.84}} \quad \text{Eq. 31}$$

$$PAIS\ 4 = 1 - e^{-\left(\frac{BrIC}{1.204}\right)^{2.84}} \quad \text{Eq. 32}$$

Where PAIS n are probabilities of sustaining AIS n injuries and BrIC is calculated using Eq. 28 on an impact by impact basis.

IBM SPSS version 15.0 was used to conduct statistical analyses on the extracted parameters. Following confirmation of normal distribution and homogeneity of variance, Independent T-Tests and repeated measures ANOVA followed by Bonferroni post hoc tests were completed when applicable to assess differences in parameters, with statistical significance set to a threshold of $p <= 0.05$. The results derived from this methodology are presented in the following chapters.

CHAPTER 7

Helmeted Projectile Impacts

7.1. Introduction

Previous chapters have addressed the individual components of the impact framework outlined in Figure 14. The findings from these chapters facilitated the development of a laboratory test method to assess the mechanics of head impacts in Cricket in a suitably representative scenario.

Previous research has used energy equivalent drop tests (Stretch, 2000) to assess the impact attenuation capabilities of Cricket helmets, however this work is limited by the different impact characteristics of a drop test compared to real-life projectile impacts. Indeed, McIntosh and Janda (2003) reported that the dynamic response of a 5th percentile, female Hybrid-III headform when subjected to drop tests was dissimilar to that observed during projectile impacts when protected by Cricket helmets. Although McIntosh and Janda (2003) utilised more realistic impact conditions, the measurements were limited to only linear acceleration and therefore could not provide insight into the angular motion of the headform during impact. The geometric, inertial and material differences between the average UK male and the 5th percentile Hybrid-III female headform used by McIntosh and Janda (2003) may also be considered a limitation. In addition, the results presented by McIntosh and Janda (2003) did not address differences produced from varied impact locations which may have important implications for the observed impact mechanics and did not account for the effect of repeated impacts at the same location.

Due to the limitations of previous work, further research into the mechanics of helmeted head impacts in Cricket is necessary for the improved understanding of injury mechanisms and the development of effective preventative strategies. This chapter aims to investigate the performance of currently available Cricket helmets in realistic impact scenarios through the improved physical test method defined in Chapter 6. Two types of commercially available helmets were assessed and analysed at three different impact locations, using three headforms (Hybrid-III 50th percentile male, NOCSAE and LU). Repeated impacts, conducted on a single impact site, were also completed using the LU headform, to investigate the effect of multiple strikes on helmet performance. The methodology outlined in Chapter 6 is utilised to measure the dynamic response of the headform(s) in six DOF.

The aims of this chapter were to:

1) Assess the effect of impact location on the observed headform dynamic response
2) Assess the effect of helmet type on the observed dynamic response of the headforms
3) Assess the effect of headform type on the observed dynamic response

7.2. Results

7.2.1. Linear Response

7.2.1.1. Hybrid-III Headform

Key parameters from the observed linear response, including peak resultant linear acceleration, contact time, time to peak resultant linear acceleration, impulse and HIC were calculated for each trial, as defined in Chapter 6. Mean and standard deviations for each helmet type using the Hybrid-III headform can be seen in Table 27, and response corridors with representative curves observed for the linear component of the helmeted impacts using the Hybrid-III headform can be found in Figure 64. The headform, as, expected, appears to respond predominantly as a rigid body during these impacts, with a relatively clear loading and unloading phase. In each helmet type and impact location, the responses corridors were found to be relatively tight, with good intra-helmet consistency, as reflected in the standard deviation values shown in Table 27.

Table 27. Mean and standard deviation values of key parameters calculated from the helmeted Hybrid-III trials.

Helmet Type	Impact Location	Contact Time (ms) (mean (SD))	Peak resultant linear acceleration (g) (mean (SD))	Time to Peak resultant linear acc. (ms) (mean (SD))	Impulse (N.s) (mean (SD))	HIC (mean (SD))
A	Frontal	1.72 (0.07)	201.91 (5.57)	0.76 (0.03)	5.84 (0.48)	142.00 (14.92)
	Lateral	1.70 (0.31)	214.17 (18.47)	0.72 (0.01)	6.59 (0.82)	204.17 (40.51)
	Oblique	1.88 (0.01)	202.02 (7.91)	0.68 (0.02)	5.47 (0.13)	134.75 (5.63)
B	Frontal	3.23 (0.29)	98.05 (5.23)	0.66 (0.03)	5.44 (0.44)	44.63 (2.06)
	Lateral	1.92 (0.01)	260.74 (16.86)	0.70 (0.02)	7.44 (0.12)	257.65 (12.56)
	Oblique	1.89 (0.03)	198.80 (1.55)	0.71 (0.00)	5.28 (0.04)	110.71 (3.12)

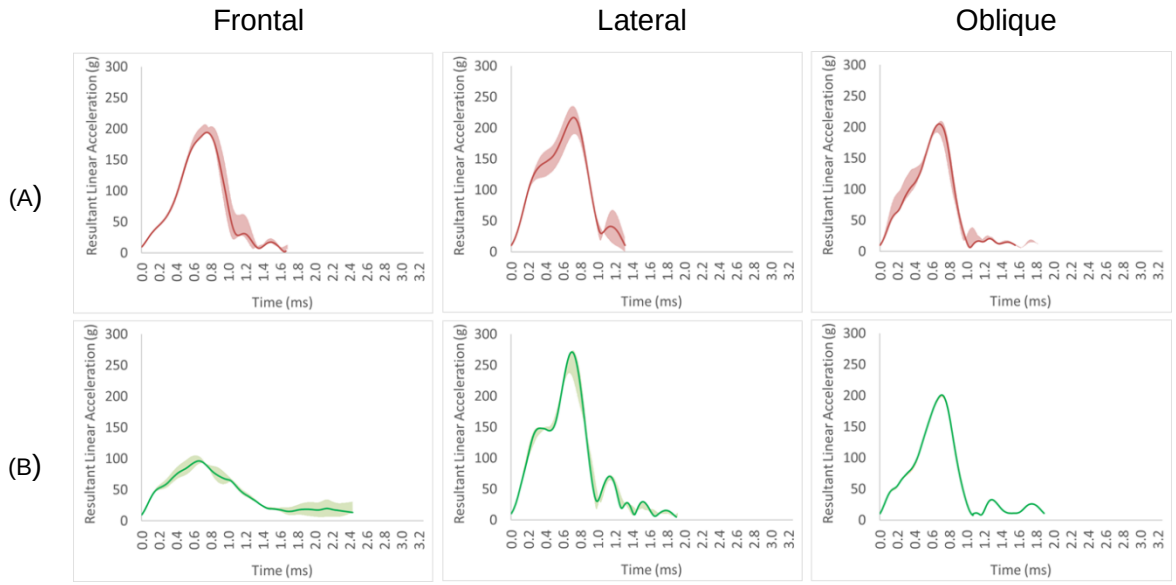

Figure 64. Response corridors and representative curves for the linear response of helmeted impacts using the Hybrid-III.

As can be seen in Table 27 and Figure 64, the observed dynamic response varies based on impact location and helmet type. In both helmet types the highest peak resultant linear acceleration, impulse and HIC value was observed in the lateral impact location. The lowest peak resultant linear acceleration was observed in the frontal impact location for both helmet types.

Helmet A showed no statistically significant differences in contact time (p = 0.582), peak resultant linear acceleration (p = 0.539), impulse (p = 0.201) or HIC (p = 0.062) when comparing impact locations. The latter of these is surprising, given the apparent differences in mean HIC between the frontal/oblique and lateral results (see Table 27) – but may be a result of the greater variation at the lateral location, leading to wider 95% confidence intervals (80.9 – 327.43). The only parameter that showed statistically significant differences based on impact location was time to peak resultant linear acceleration (p = 0.024), where the oblique impact was found to be significantly lower than the frontal location (p = 0.026). In Helmet B, the frontal location was found to produce significantly lower peak resultant linear acceleration and HIC in addition to longer contact times (p < 0.047) when compared to the other impact locations. The lateral location produced higher peak resultant linear acceleration, impulse and HIC, which were found to be statistically significant (p > 0.003).

Figure 65 shows the representative resultant linear acceleration curves for each helmet type at the frontal, lateral and oblique location when using the Hybrid III headform. At the frontal location, Helmet B was found to have significantly longer contact time, lower peak

resultant linear acceleration and lower HIC than Helmet A ($p < 0.001$). There was no statistically significant difference between the helmet types when considering time to peak resultant linear acceleration or impulse ($p >= 0.096$). No statistically significant differences between helmet types were observed between the helmet types in any of the parameters identified in Table 27 in either the lateral or oblique locations ($p > 0.093$)

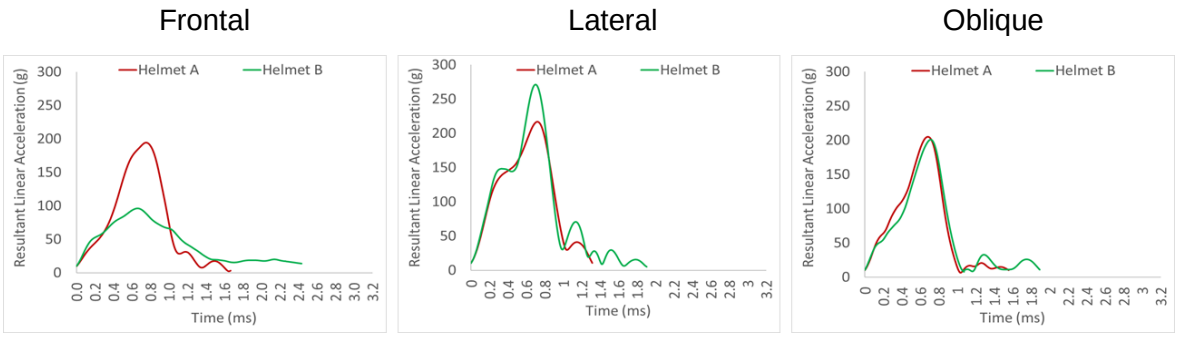

Figure 65. Representative resultant linear acceleration curves from each helmet type at each location using the Hybrid III headform.

7.2.1.2. NOCSAE Headform

Figure 66 shows the resultant linear acceleration response corridors and representative trials for the helmeted impacts using the NOCSAE headform. It is clear from these results that greater oscillations are present in the linear response compared to the results observed when using the Hybrid-III. Given the materials used in the NOCSAE headform, and as the frequency of these oscillations is comparable to the resonance frequencies observed in the human head (Khalil et al., 1979), these oscillations may be considered legitimate response artefacts when considering these types of head impact. This suggests that unlike the response observed when using the Hybrid-III headform (see Figure 64), the NOCSAE headform does not respond as a rigid body during helmeted impacts in Cricket. As can been seen from Figure 66, this results in multiple peaks in the linear response during impact. Parameters extracted over the entire contact period can be found in Table 28. Table 29 shows additional analysis where the magnitude and timing of any peak above 75% of the maximum in the same trial was identified (as described in Chapter 6).

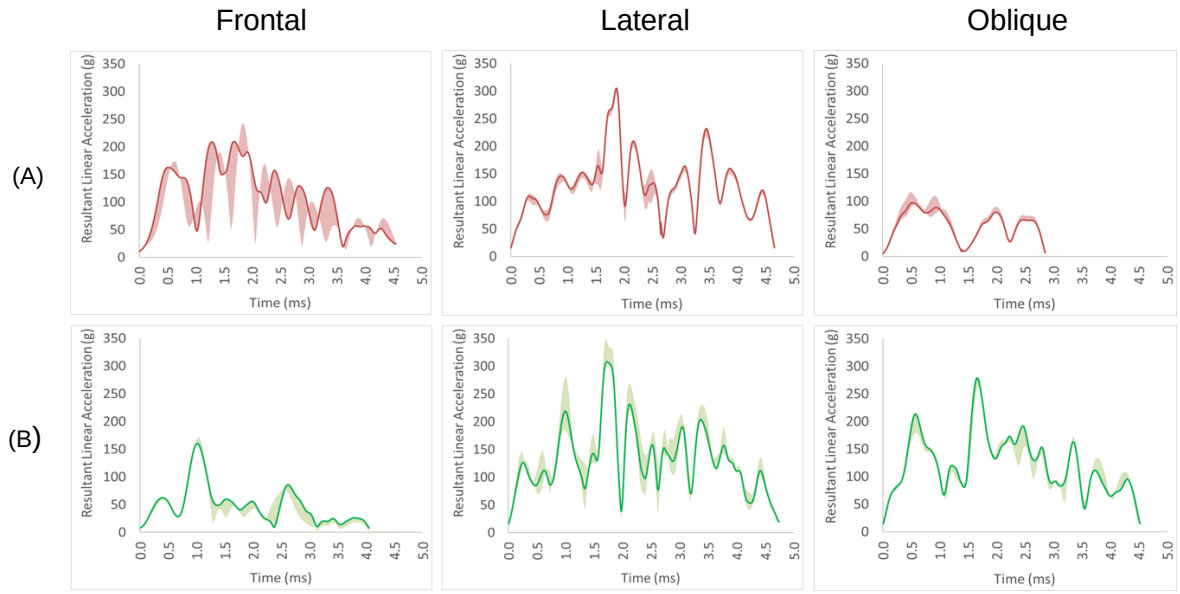

Figure 66. Response corridors and representative curves for the linear response of helmeted impacts using the NOCSAE headform.

Table 28. Mean and standard deviation values of key parameters calculated from the helmeted NOCSAE trials.

Helmet Type	Impact Location	Contact Time (ms) (mean (SD))	Peak resultant linear acceleration (g) (mean (SD))	Time to peak resultant linear acc. (ms) (mean(SD))	Impulse (N.s) (mean (SD))	HIC (mean (SD))
A	Frontal	4.59 (0.08)	222.57 (14.04)	1.79 (0.07)	21.35 (1.65)	484.18 (103.47)
	Lateral	4.63 (0.03)	302.08 (3.43)	1.87 (0.01)	28.51 (0.82)	869.60 (61.27)
	Oblique	2.82 (0.02)	102.78 (9.70)	0.54 (0.05)	8.12 (0.48)	79.53 (12.08)
B	Frontal	4.01 (0.05)	166.91 (4.76)	1.02 (0.01)	8.97 (0.41)	70.32 (6.53)
	Lateral	5.89 (0.01)	322.50 (17.95)	1.73 (0.02)	34.38 (1.64)	1082.15 (128.74)
	Oblique	5.71 (0.02)	273.59 (8.25)	1.67 (0.01)	28.96 (0.91)	755.49 (50.23)

As observed in the Hybrid-III impacts, when using the NOCSAE headform there are measurable differences in the linear response when considering helmet type and impact location. In Helmet A, the oblique location showed shorter contact time and time to peak resultant linear acceleration, but lower peak resultant linear acceleration, impulse and HIC in than the frontal and lateral locations, all of which were found to be statistically significant ($p < 0.001$). The lateral location was also found to produce significantly higher peak resultant linear acceleration, impulse and HIC than the frontal and oblique locations ($p < 0.011$). In Helmet B, the frontal location displayed shorter contact time and time to peak resultant linear acceleration, and lower peak resultant linear acceleration, impulse and HIC than the lateral and oblique locations, all of which were statistically significant ($p < 0.019$). Similar to the

results observed when using Helmet A, in Helmet B, the lateral location produced the highest peak resultant linear acceleration, impulse and HIC, all of which were statistically significant ($p < 0.011$).

Figure 67 shows the representative linear response curves obtained from both helmets at each impact location when using the NOCSAE headform. In the frontal location, Helmet B produced a shorter contact time and time to peak resultant linear acceleration than Helmet A, both of which were statistically significant ($p < 0.001$). Helmet B also produced significantly lower peak resultant linear acceleration, impulse and HIC values than Helmet A at the frontal location ($p < 0.013$). At the lateral location, there were no statistically significant differences between Helmets A and B when considering peak resultant linear acceleration or HIC ($p > 0.069$). Helmet B was however found to produce longer contact times, but shorter time to peak resultant linear acceleration, in addition to higher impulse values than Helmet A, all of which were found to be statistically significant. At the oblique location, Helmet A produced shorter contact time and time to peak resultant linear acceleration, along with lower peak resultant linear acceleration, impulse and HIC values, all of which were statistically significant ($p < 0.026$).

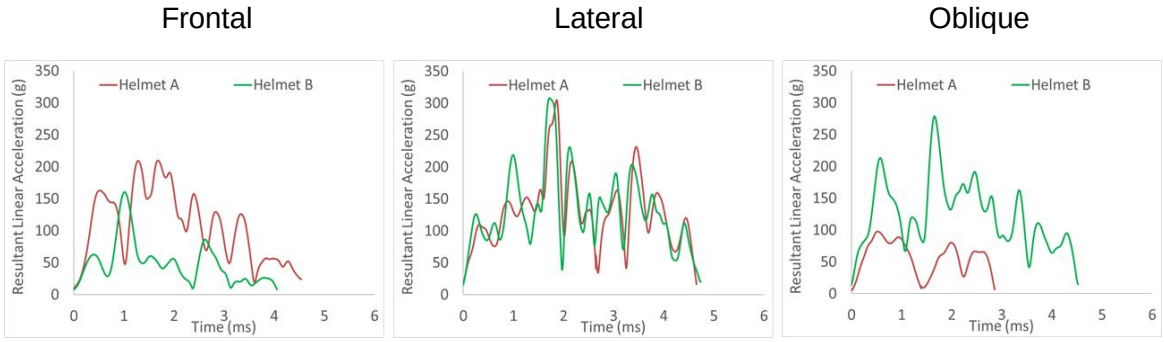

Figure 67. Representative resultant linear acceleration curves from each helmet type at each location using the NOCSAE headform.

Table 29. Mean and standard deviations of the peak analysis for the linear response when using the NOCSAE headform.

Helmet Type	Impact Location	Peak 1 time to peak (ms) (mean (SD))	Peak 1 Magnitude (g) (mean(SD))	Peak 1 Jerk (g/s ($x10^5$)) (mean (SD))	Peak 2 time to peak (ms) (mean (SD))	Peak 2 magnitude (g) (mean (SD))	Peak 2 Jerk (g/s ($x10^5$)) (mean (SD))	Peak 3 time to peak (ms) (mean (SD))	Peak 3 magnitude (g) (mean (SD))	Peak 3 Jerk (g/s ($x10^5$)) (mean (SD))
A	Frontal	0.58 (0.05)	168.20 (4.45)	2.74 (0.18)	1.36 (0.06)	194.80 (10.31)	6.06 (1.73)	1.77 (0.07)	222.57 (14.04)	5.59 (2.60)
	Lateral	1.87 (0.01)	302.07 (3.44)	1.54 (0.12)	-	-	-	-	-	-
	Oblique	0.54 (0.05)	102.78 (9.70)	1.84 (0.32)	0.97 (0.05)	95.06 (10.75)	8.58 (0.32)	1.99 (0.00)	82.99 (4.90)	1.31 (8.48)
B	Frontal	1.03 (0.01)	166.92 (4.77)	1.55 (0.32)	-	-	-	-	-	-
	Lateral	1.73 (0.02)	322.50 (17.95)	1.77 (0.11)	-	-	-	-	-	-
	Oblique	0.58 (0.00)	198.93 (14.32)	3.22 (0.25)	1.67 (0.01)	273.60 (8.26)	3.60 (0.06)	-	-	-

As can be seen in Table 29 and Figure 67, multiple peaks were observed when assessing the linear response of the NOCSAE headform, particularly in Helmet A. As discussed previously, these peaks were defined and identified if the magnitude observed was at least 75% of the maximum linear acceleration observed during impact.

The number of peaks observed in the linear response varied based on helmet type and impact location – suggesting varied excitation of the resonance frequency of the headform during impacts. Helmet A produced three peaks at the frontal and oblique location, but only one at the lateral. At the frontal location, the third of these peaks was of the highest magnitude, however, the second peak showed the greatest jerk. At the oblique location, the first peak showed the greatest magnitude, but the second peak resulted in a much greater jerk value, as the duration from the preceding trough was much shorter. In helmet B single peaks were observed at the frontal and lateral location, with lower peak resultant linear acceleration and jerk magnitudes. Two peaks were observed at the oblique location, with higher peak resultant linear acceleration and jerk values observed in the second peak.

7.2.1.3. LU Headform

Similar to the response observed when using the NOCSAE headform, measurable oscillations were observed in the helmeted responses using the LU headform. These oscillations were in line with the resonance frequencies of the skull component of the LU headform (presented in Chapter 5) and resulted in the multiple peaks observed in Figure 68. As a result of this, the analysis extracted parameters from the contact duration as a whole and a peak analysis. These parameters can be found in Table 30 and Table 31.

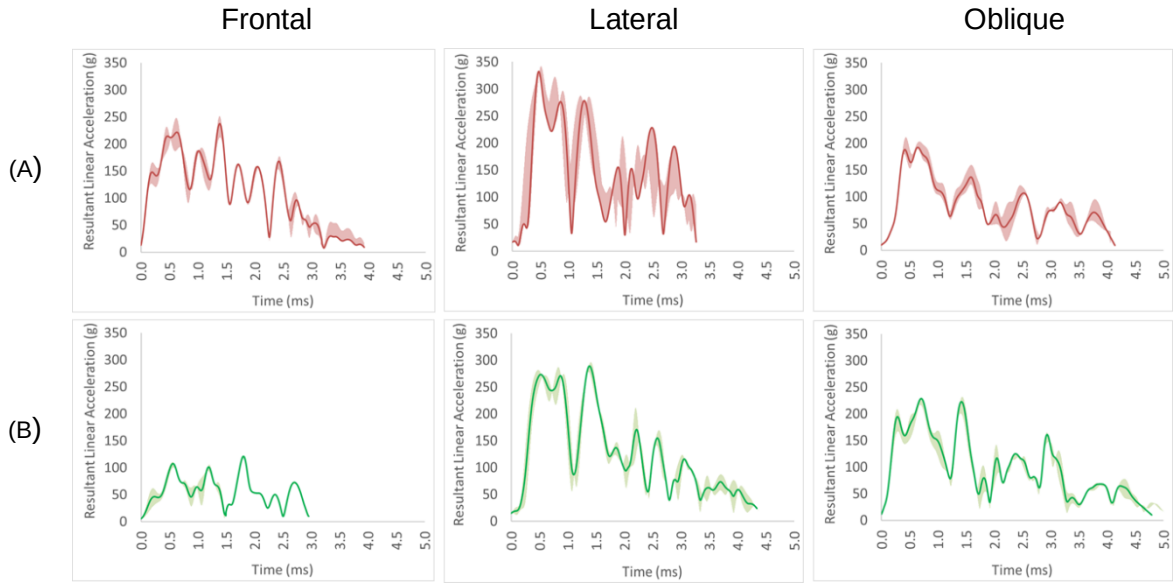

Figure 68. Response corridors and representative curves for the linear response of helmeted impacts using the LU headform.

Table 30. Mean and standard deviations of linear response parameters extracted from the entire contact period when using the LU headform.

Helmet Type	Impact Location	Contact Time (ms) (mean (SD))	Peak resultant linear acceleration (g) (mean (SD))	Time to peak resultant linear acc. (ms) (mean (SD))	Impulse (N.s) (mean (SD))	HIC (mean (SD))
A	Frontal	3.68 (0.36)	245.87 (6.03)	1.13 (0.36)	17.46 (0.66)	653.15 (24.60)
	Lateral	4.78 (0.06)	332.34 (7.96)	0.48 (0.02)	23.74 (0.69)	991.69 (108.84)
	Oblique	4.10 (0.07)	198.42 (9.13)	0.57 (0.10)	14.64 (1.50)	303.96 (77.98)
B	Frontal	3.16 (0.04)	119.11 (1.84)	1.81 (0.00)	7.01 (0.15)	70.31 (3.77)
	Lateral	4.36 (0.01)	290.89 (3.95)	1.21 (0.27)	22.21 (0.83)	899.11 (100.59)
	Oblique	5.65 (0.46)	225.85 (6.55)	0.94 (0.35)	20.08 (0.24)	535.36 (43.02)

In Helmet A, the oblique location produced lower peak resultant linear acceleration, impulse and HIC values than the frontal and lateral locations, all of which were statistically significant ($p < 0.036$). In Helmet B, the frontal location produced shorter contact durations but longer time to peak resultant linear acceleration, in addition to lower peak resultant linear acceleration, impulse and HIC values than the lateral and oblique locations, all of which were statistically significant ($p < 0.013$). The lateral location showed the highest peak resultant linear acceleration, impulse and HIC in both Helmets, all of which were statistically significant ($p < 0.027$).

Figure 69 shows the representative linear response curves obtained from each helmet at each impact location when using the LU headform. At the frontal location, Helmet A produced higher peak resultant linear acceleration, impulse and HIC values, in addition to shorter time to peak resultant linear acceleration than Helmet B. All of these differences were found to be statistically significant ($p < 0.033$). At the lateral location there were no statistically significant differences between Helmets A and B when considering impulse or HIC ($p > 0.053$). Helmet A did however produce higher peak resultant linear acceleration, shorter time to peak resultant linear acceleration and longer contact time than Helmet B, all of which were found to be statistically significant ($p < 0.022$). At the oblique location, there were no statistically significant differences between Helmets A and B when comparing contact time, time to peak resultant linear acceleration or peak resultant linear acceleration ($p > 0.063$). Helmet B did however show impulse and HIC values that were significantly higher than Helmet A ($p < 0.028$). As previously discussed, the multiple peaks observed when using the LU headform concur with the observations made when using the NOCSAE headform, and suggest that the headform does not respond as a rigid body when subjected impacts representative of those seen in Cricket, even when protected using currently available Cricket helmets.

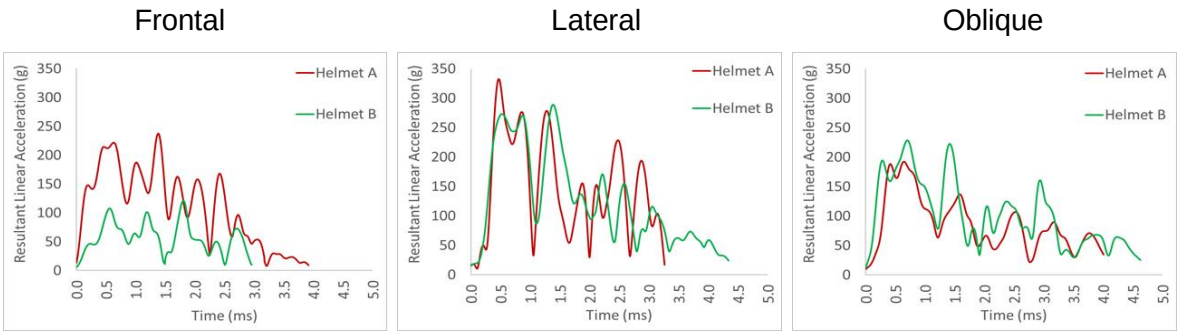

Figure 69. Representative resultant linear acceleration curves from each helmet type at each location using the LU headform.

In Helmets A, two peaks were observed at the frontal and oblique locations, whereas three peaks were observed at the lateral location. The peaks observed at the frontal and lateral locations were of similar magnitude, but produced significantly different jerk values, due to the time differences between the preceding troughs. At the oblique location, although the magnitude of the third peak was lower than that of the preceding two peaks, the jerk was significantly greater. In Helmet B, all three impact locations produced three linear acceleration peaks. At the frontal location, the magnitude of the resultant linear acceleration and jerk values were all comparable. At the lateral location, the magnitude of the resultant linear acceleration was consistent across the peaks, but the jerk values varied, with the greatest values occurring in the third peak. Although the second peak produced the highest resultant linear acceleration values at the oblique location, this peak also produced the lowest jerk value – the highest of which occurred at the third peak.

Table 31. Mean and standard deviations extracted from the linear response peak analysis when using the LU headform.

Helmet Type	Impact Location	Peak 1			Peak 2			Peak 3		
		Time to peak (ms) (mean (SD))	Magnitude (g) (mean (SD))	Jerk (g/s ($x10^5$)) (mean (SD))	Time to peak (ms) (mean (SD))	Magnitude (g) (mean (SD))	Jerk (g/s ($x10^5$)) (mean (SD))	Time to peak (ms) (mean (SD))	Magnitude (g) (mean (SD))	Jerk (g/s ($x10^5$)) (mean (SD))
A	Frontal	0.57 (0.08)	234.08 (10.97)	3.98 (0.66)	1.38 (0.00)	233.68 (16.44)	6.01 (0.81)	-	-	-
	Lateral	0.48 (0.02)	332.36 (7.97)	6.56 (0.14)	0.84 (0.06)	298.48 (18.84)	4.01 (0.38)	1.32 (0.04)	282.10 (3.70)	9.18 (1.68)
	Oblique	0.41 (0.02)	192.97 (13.43)	4.44 (0.13)	0.66 (0.02)	195.70 (5.31)	2.37 (0.52)	-	-	-
B	Frontal	0.56 (0.01)	106.12 (4.36)	1.79 (0.09)	1.19 (0.01)	100.38 (4.93)	2.38 (0.52)	1.81 (0.00)	119.10 (1.85)	2.55 (1.33)
	Lateral	0.53 (0.05)	275.78 (4.31)	4.95 (0.54)	0.88 (0.04)	277.52 (6.96)	3.27 (1.07)	1.39 (0.02)	287.82 (7.55)	7.95 (0.77)
	Oblique	0.28 (0.00)	190.02 (17.56)	6.31 (0.65)	0.70 (0.02)	224.19 (5.29)	2.40 (0.35)	1.42 (0.01)	218.48 (13.21)	7.07 (0.95)

7.2.1.4. Headform Comparison

Representative resultant linear acceleration magnitude curves of each helmet and impact location using the Hybrid-III, NOCSAE and LU headforms can be found in Figure 70. It is clear from Figure 70, and the results presented previously, that headform surrogate selection influences the observed response and the key parameters extracted from the contact duration. As can be seen in Figure 70 there are a number of impact conditions where the linear responses of the headforms were similar during the initial loading phase of the impacts. However, as discussed previously, excitation of the resonance frequencies of the NOCSAE and LU headforms influenced the mid to later stages of the impact response, and resulted in longer contact times and multiple peaks. In the impact scenarios that showed dissimilar initial loading responses (for example, Helmet A – lateral location), this was likely due to resonance frequency excitation when using the NOCSAE and LU headforms.

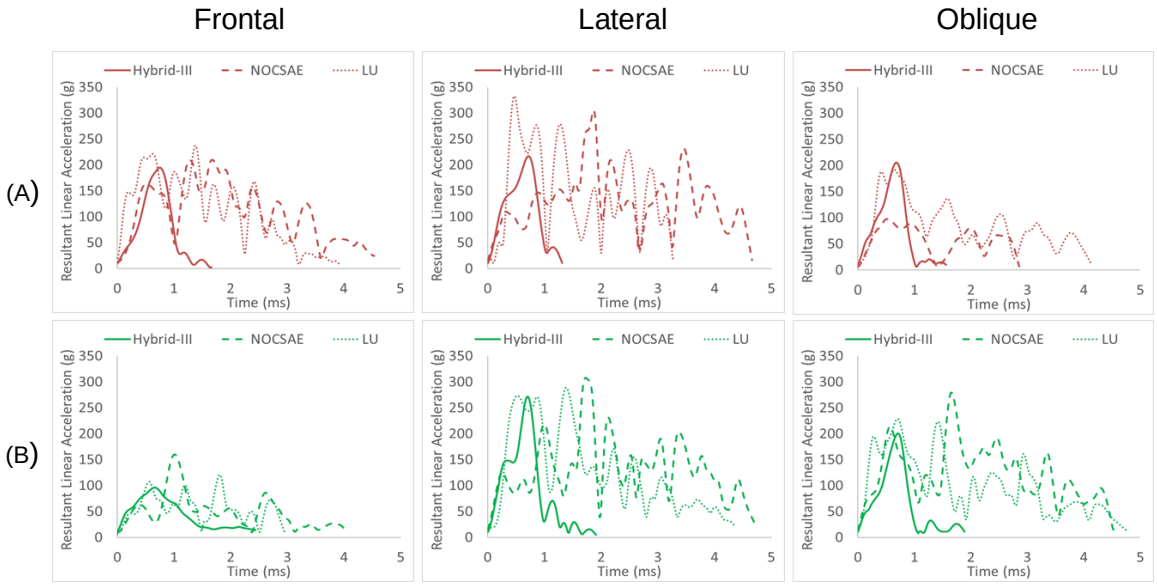

Figure 70. Representative linear response curves for each helmet type and impact location on the Hybrid-III, NOCSAE and LU headforms.

7.2.1.5. Repeated Impacts

Five repeated impacts at the frontal location were conducted on five previously unused helmets of each type, using the LU headform. Representative resultant linear acceleration curves from the repeated impacts in both helmets can be seen in Figure 71. Key parameters extracted from the observed linear response over the entire impact duration can be seen in Figure 72, with the percentage change from impact 1 to 5 shown in Table 33.

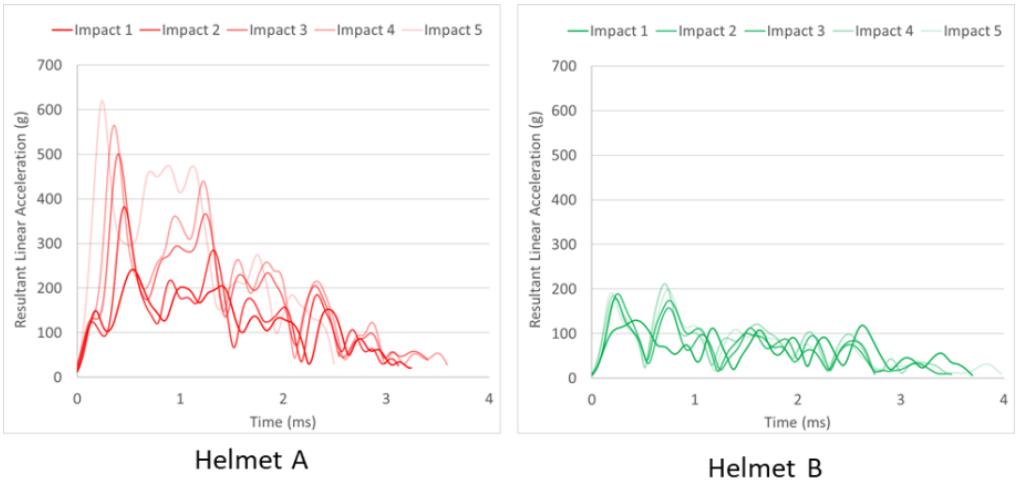

Figure 71. Representative resultant linear acceleration curves from the repeated impacts using Helmet A and B.

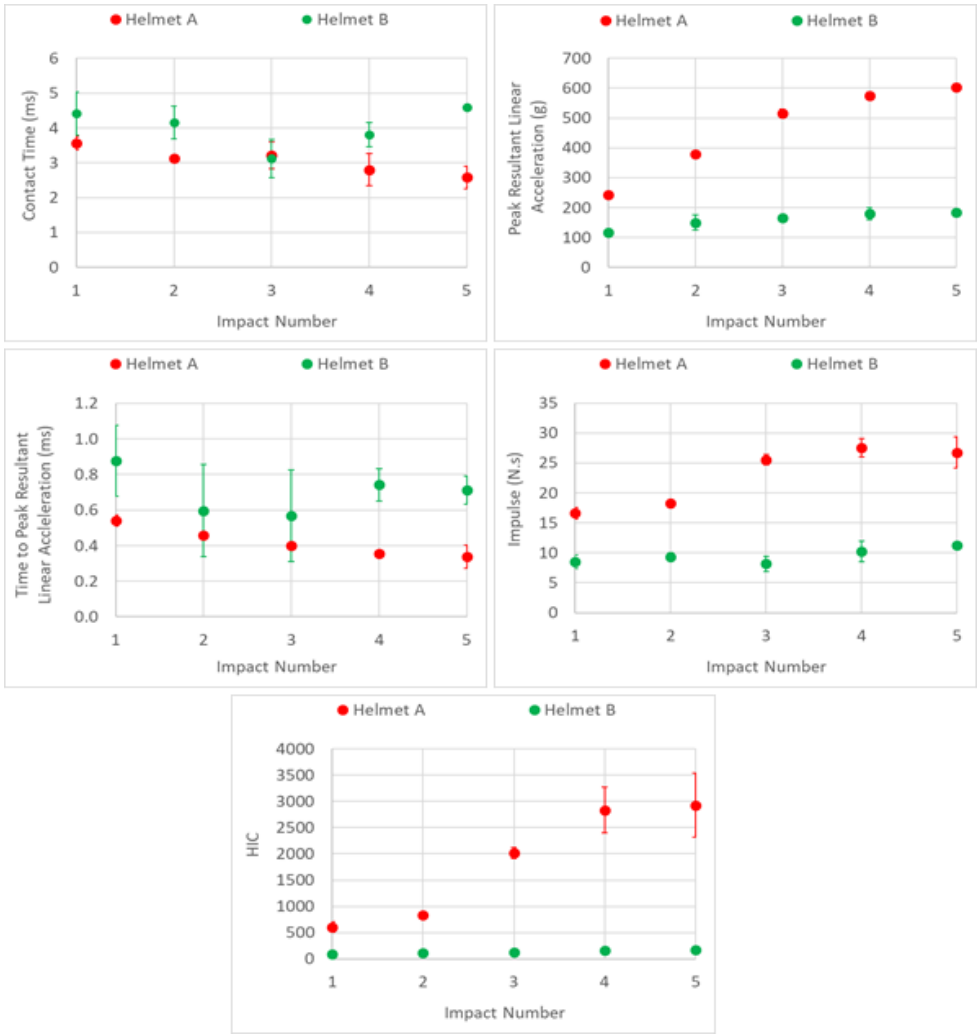

Figure 72. Change in selected linear response parameters extracted from the entire impact duration.

Table 32. Percentage change from impact 1 to impact 5 in selected parameters extracted from the linear response throughout the entire contact duration.

Helmet Type	Contact Time	Peak Resultant Linear Acceleration	Time to Peak Resultant Linear Acceleration	Impulse	HIC
A	-27.59	148.95	-69.57	61.01	385.10
B	43.35	57.29	-60.24	57.47	128.04

With respect to contact time, repeated impacts at the same location resulted in reduced contact times in Helmet A (27.59% shorter), but elongated contact times in Helmet B (43.35% increase). Helmet A and B showed decreased time to peak resultant linear acceleration (69.57 and 60.24% decrease respectively) however this decrease was predominately observed between impacts 1 and 2 with all subsequent impacts having little effect. Peak resultant acceleration increased in both helmet types, however Helmet A (148.95% increase) showed a much larger increase than Helmet B (57.47% increase), and resulted in a value of 602.08 ±12.19 g during the fifth impact. Helmet A also showed a larger increase in HIC (385.1% increase) than Helmet B (128.04% increase), resulting an average HIC value of 2926.57 ±610.94 in the fifth impact using Helmet A. Despite a 128.04% increase from impact one to five when using Helmet B, the value observed in the fifth impact 165.91 ±28.77, remained lower than that of the first impact on Helmet A.

7.2.2. Angular Response

7.2.2.1. Hybrid-III headform

As discussed previously (Chapter 6), due to the defined impact locations relative to the CoG of the headforms, the frontal location produced non-negligible angular velocity about a single axis, while the lateral and oblique locations produced non-negligible angular velocity about two axes. Figure 73 shows the angular velocity response corridors and representative trials about the primary axes of rotation for a given impact location (e.g. y axis for frontal, x and z axes for lateral and oblique).

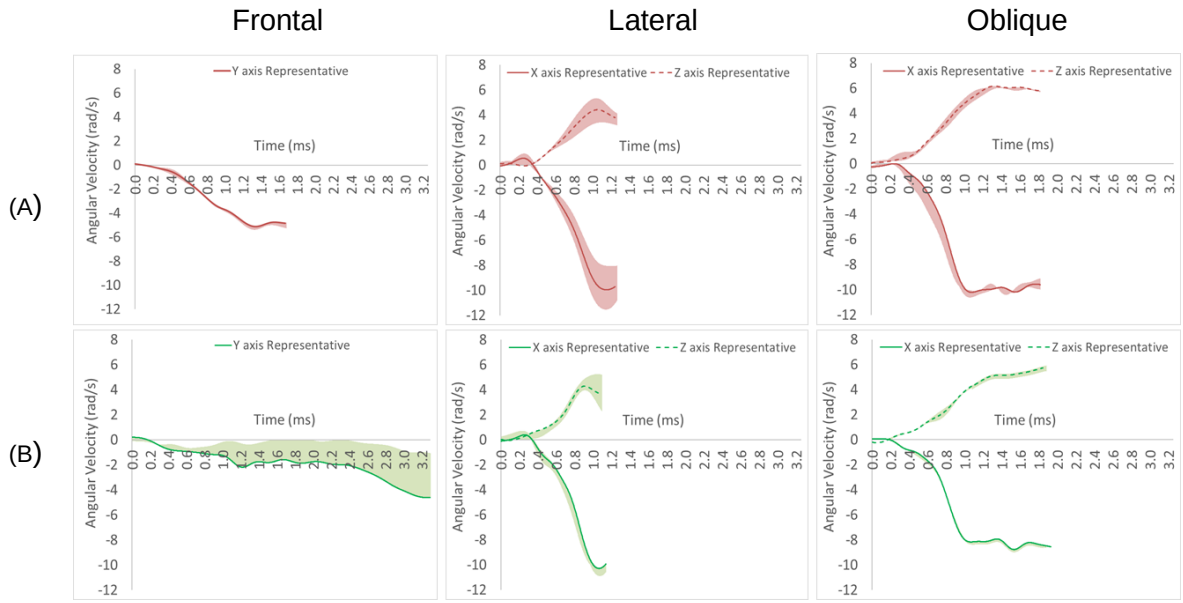

Figure 73. Response corridors and representative curves for the angular component of helmeted impacts using the Hybrid-III headform.

As can be seen in Figure 73, there does appear to be greater intra-helmet variability, compared to the linear response observed in Figure 64, particularly in Helmet A at the lateral impact location, and Helmet B in the frontal location. Differences in the angular response when using both helmet types can be observed in the mean and standard deviations values for key parameters, including maximum angular velocity, time to maximum angular velocity and estimated maximum sinusoidal acceleration values, as shown in Table 33. BrIC values were calculated for each impact condition and used to predict the probability of sustaining AIS injuries 1-4, as shown in Table 34.

Table 33. Mean and standard deviation values of measured and calculated angular response parameters when using the Hybrid-III.

Helmet Type	Impact Location	Maximum angular velocity about axes of interest (rad/s) (mean (SD)	Time to maximum angular velocity (ms) (mean(SD)	Maximum estimated α_{sine} (krad/s/s) (mean (SD)	Impulse (kg m^2 s^{-1}) (mean (SD))
A	Frontal	Y: -5.29 (0.12)	Y: 1.50 (0.23)	Y: -5.67 (0.75)	X: -0.11 (0.00)
	Lateral	X: -9.85 (1.42)	X: 1.17 (0.03)	X: -13.30 (2.21)	Y: -0.16 (0.02)
		Z: 4.39 (0.79)	Z: 1.06 (0.03)	Z: 6.51 (1.31)	Z: 0.06 (0.01)
	Oblique	X: -10.41 (0.17)	X: 1.20 (0.18)	X: -13.94 (1.92)	X: -0.17 (0.00)
		Z: 6.08 (0.06)	Z: 1.35 (0.02)	Z: 7.09 (0.18)	Z: -0.10 (0.00)
B	Frontal	Y: -2.33 (1.64)	Y: 3.12 (0.38)	Y: -1.14 (0.77)	X: -0.05 (0.00)
	Lateral	X: -10.53 (0.26)	X: 1.07 (0.01)	X: -5.80 (0.33)	X: -0.11 (0.01)
		Z: 4.50 (0.35)	Z: 0.95 (0.07)	Z: 1.37 (0.19)	Z: -0.03 (0.01)
	Oblique	X: -8.55 (0.18)	X: 1.38 (0.22)	X: -9.98 (1.55)	X: -0.14 (0.00)
		Z: 5.73 (0.21)	Z: 1.89 (0.03)	Z: 4.77 (0.14)	Z: -0.09 (0.00)

In both helmet types, the frontal location produced lower maximum angular velocity and maximum estimated sinusoidal angular acceleration than the lateral and oblique locations, which were found to be statistically significant differences ($p < 0.014$). In Helmet A the oblique location produced higher maximum angular velocity and maximum estimated sinusoidal angular acceleration about the x and z axes than that observed in the lateral impacts, these however were not found to be statistically significant ($p > 0.11$). No statistically significant differences were found between impact locations when comparing time to maximum angular velocity ($p > 0.3$). In Helmet B, the lateral location produced higher maximum angular velocity about the x axis which was statistically significant ($p = 0.013$), whereas no statistically significant differences were found about the z axis ($p = 0.83$). Statistically significant differences were also found between the lateral and oblique locations when comparing the time to maximum angular velocity about the z axis ($p = 0.027$). The lateral location also showed higher maximum estimated sinusoidal angular acceleration than the oblique location in both axes ($p < 0.009$).

Figure 74 shows the representative angular response curves for both helmet types for each impact location. At the frontal location, Helmet A produced shorter contact time and time to maximum angular velocity, higher maximum angular velocity, maximum estimated sinusoidal angular acceleration and impulse, all of which were found to be statistically significant ($p < 0.023$). At the lateral location, the only statistically significant differences between helmet types was found when comparing time to maximum angular velocity, where Helmet A produced a longer time than Helmet B in both axes ($p < 0.015$). At the oblique location, Helmet A produced higher maximum angular velocity in the x and z axes than Helmet B, but statistically significant differences were only found when comparing the x axis ($p = 0.026$). Similarly, Helmet A produced lower time to maximum angular velocity than the Helmet B in the x and z axes, however statistically significant differences were only found when comparing the z axis ($p = 0.006$). Statistically significant differences were also found between Helmets A and B when comparing maximum estimated sinusoidal angular acceleration in both the x and z axes, where Helmet A produced greater values than Helmet B ($p < 0.003$).

Frontal Lateral Oblique

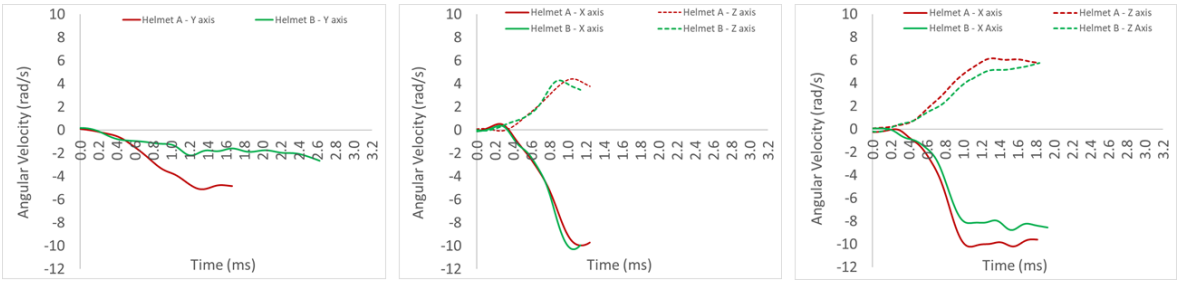

Figure 74. Representative angular velocity curves from each helmet type at each location using the Hybrid III headform.

Table 34 shows the calculated BrIC and PAIS 1-4 values based on the observed angular velocities about all three axes during impact. As angular velocities about axes other than those outlined in Table 33 were minimal, the BrIC and PAIS values reflect the maximum angular velocity values shown in Table 33. Helmet A produced higher PAIS 1-4 values at the frontal and oblique locations than Helmet B, all of which were found to be statistically significant ($p < 0.001$). At the lateral location, Helmet B produced higher PAIS 1-4 values, but none of these were found to be statistically significant ($p > 0.809$).

Table 34. Mean and standard deviation values for calculated BrIC and PAIS1-4.

Helmet Type	Impact Location	BrIC Value	PAIS1 (%) (mean (SD))	PAIS2 (%) (mean (SD))	PAIS3 (%) (mean (SD))	PAIS4 (%) (mean (SD))
A	Frontal	0.11 (0.01)	54.27 (0.15)	0.80 (0.00)	0.20 (0.00)	0.11 (0.00)
	Lateral	0.18 (0.03)	96.54 (1.79)	3.39 (0.02)	0.84 (0.00)	0.48 (0.00)
	Oblique	0.22 (0.00)	99.45 (0.00)	5.20 (0.00)	1.30 (0.00)	0.74 (0.00)
B	Frontal	0.05 (0.02)	9.90 (1.09)	0.11 (0.00)	0.03 (0.00)	0.01 (0.00)
	Lateral	0.19 (0.01)	97.87 (0.02)	3.87 (0.00)	0.96 (0.00)	0.55 (0.00)
	Oblique	0.19 (0.01)	97.13 (0.02)	3.58 (0.00)	0.89 (0.00)	0.51 (0.00)

7.2.2.2. NOCSAE headform

Angular response corridors and representative trials for helmeted impacts using the NOCSAE headform can be seen in Figure 75. As observed in the linear response, there are clearly response artefacts in the measured signal that are not present in the Hybrid-III responses. These responses may be due to resonance frequency excitation of the NOCSAE headform.

As discussed in Chapter 6, multiple parameters were extracted from each angular response curve during the contact time. These included the maximum angular velocity about the axes of interest, time to maximum velocity, steady state angular velocity and impulse, and peak analysis was completed to assess maximum peak to peak estimated sinusoidal angular acceleration (see Table 36).

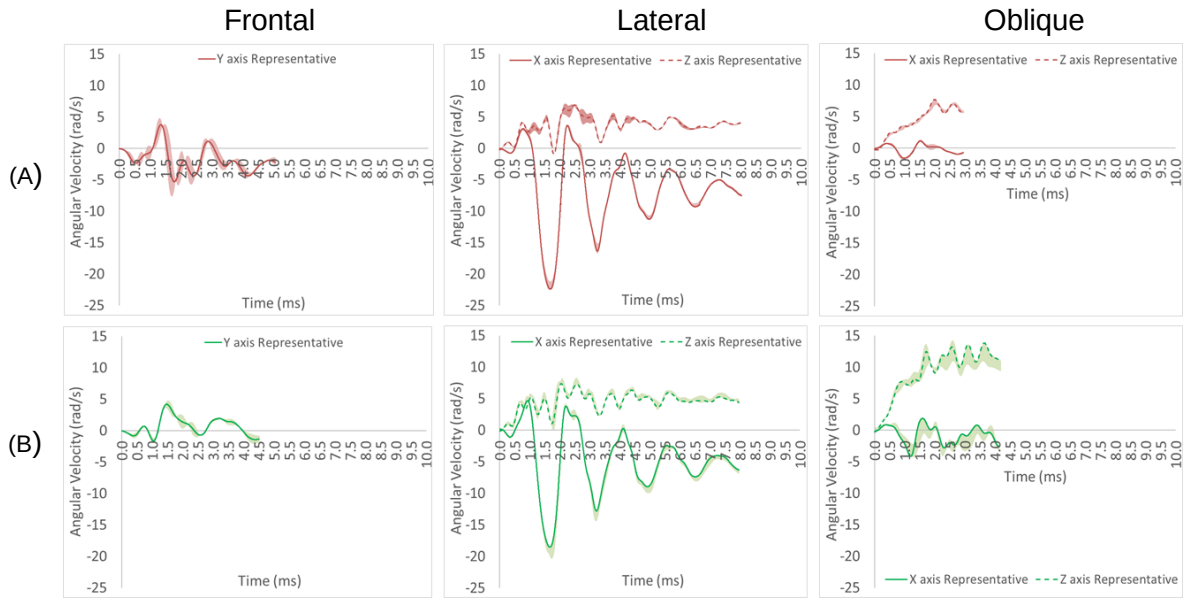

Figure 75. Response corridors and representative curves for the angular response of helmeted impacts using the NOCSAE headform.

Table 35. Mean and standard deviations of parameters from the angular response when using the NOCSAE headform.

Helmet Type	Impact Location	Maximum Angular Velocity about axes of interest (rad/s) (mean (SD))	Time to Maximum Angular Velocity (ms) (mean (SD))	Maximum peak to peak α_{sine} (krad/s/s) (mean (SD))	Steady State Angular Velocity (rad/s) (mean (SD))	Impulse (kg m^2 s^{-1}) (mean (SD))
A	Frontal	Y: -6.27 (0.98)	Y: 1.80 (0.08)	Y: - 38.94 (5.22)	Y: -2.86 (0.59)	Y: -0.07 (0.01)
	Lateral	X: -22.03 (0.59) Z: 7.00 (0.08)	X: 1.69 (0.00) Z: 2.47 (0.07)	X: 64.56 (1.62) Z: 34.27 (1.86)	X: -5.81 (0.24) Z: 4.04 (0.11)	X: -0.11 (0.00) Z: 0.07 (-0.01)
	Oblique	X: -1.70 (0.12) Z: 7.19 (0.36)	X: 1.00 (0.04) Z: 2.04 (0.03)	X: - 2.70 (0.29) Z: 5.54 (0.35)	X: -0.59 (0.14) Z: 5.77 (0.17)	X: -0.01 (0.00) Z: 0.10 (0.00)
B	Frontal	Y: 4.19 (0.48)	Y: 1.48 (0.03)	Y: 21.03 (0.86)	Y: -0.48 (0.41)	Y: -0.01 (0.01)
	Lateral	X: -19.45 (0.75) Z: 7.93 (0.41)	X: 1.67 (0.04) Z: 2.10 (0.05)	X: 51.77 (2.55) Z: 39.14 (3.36)	X: -5.65 (0.25) Z: 4.43 (0.36)	X: -0.10 (0.00) Z: 0.07 (0.01)
	Oblique	X: -4.02 (0.32) Z: 12.25 (1.28)	X: 2.27 (0.01) Z: 1.75 (0.06)	X: -9.12 (1.12) Z: 11.03 (1.29)	X: -0.65 (1.55) Z: 11.22 (1.27)	X: -0.01 (0.03) Z: 0.19 (0.02)

As can be seen in Figure 76 and Table 35, the lateral location produced the highest maximum angular velocity, and was found to be significantly greater than the frontal and oblique locations in both helmet types ($p < 0.003$). In Helmet B, the frontal location produced significantly lower maximum angular velocity than the oblique location ($p = 0.015$), whereas in Helmet A, this comparison was not statistically significant ($p = 0.565$). In both helmet types, the frontal location produced significantly lower steady state angular velocity than the lateral and oblique locations ($p < 0.001$). Although the differences in steady state angular velocity between the lateral and oblique locations were not statistically significant in Helmet

A (p > 0.27), statistically significant differences were found when using Helmet B, with the oblique location producing higher values than the lateral.

Figure 76 shows the representative angular response curves for both helmet types for each impact location. At the frontal location, Helmet A was found to produce longer time to maximum angular velocity, and higher maximum peak to peak estimated sinusoidal angular acceleration, steady state angular velocity and impulse than Helmet B (p < 0.017). The direction of the maximum angular velocity observed in Helmets A and B differed, likely as a result of the resonance frequency excitation, however when comparing absolute values, no statistically significant differences were observed (p = 0.115). At the lateral location, no statistically significant differences were observed in any of the parameters identified in Table 35 (p > 0.07). Contrary to the observations made when using the Hybrid-III headform, minimal angular velocity was observed about the x axis when using the NOCSAE headform (see Figure 76). Helmet A was found to produce higher maximum angular velocity, maximum peak to peak estimated sinusoidal angular acceleration, steady state angular velocity and impulse than Helmet B, all of which were found to be statistically significant (p < 0.017).

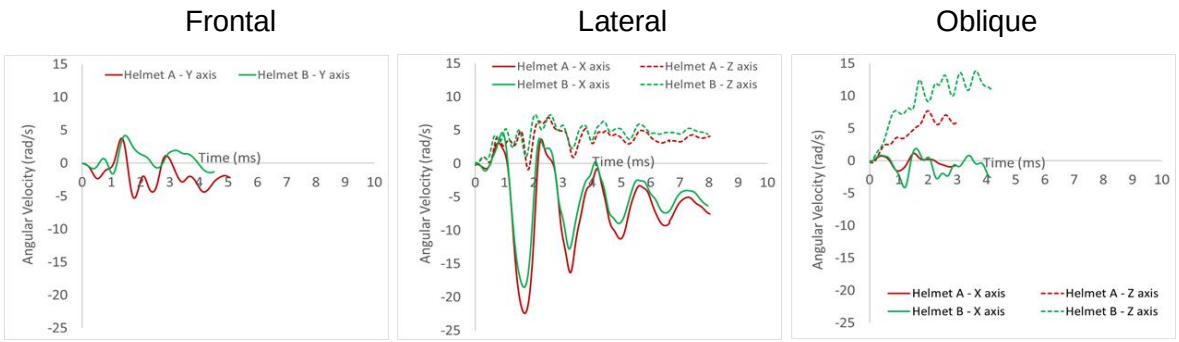

Figure 76. Representative angular velocity curves from each helmet type at each location using the NOCSAE headform.

The BrIC values and probability of sustaining AIS injuries 1-4 were calculated based on maximum and steady state angular velocity values, as shown in Table 36 and Table 37 respectively. As can be seen here, the BrIC and PAIS values varied based on whether these parameters were calculated using the steady state or maximum angular velocity values, due to the oscillations observed in Figure 76. In both helmet types the frontal location produced statistically significant lower $BrIC_{SS}$ and $PAIS_{SS}$, and $BrIC_{MAX}$ and $PAIS_{MAX}$ values than the lateral and oblique locations (p < 0.001). There were no differences between the lateral and oblique locations when considering Helmet A (p = 0.894), whereas in Helmet B the oblique location produced statistically significant greater $BrIC_{SS}$ and $PAIS_{SS}$, values than the oblique (p <0.001). In both helmet types, the lateral location was found to produce higher $BrIC_{MAX}$

and $PAIS_{MAX}$ values than the oblique location, differences which were found to be statistically significant ($p < 0.032$).

When comparing both the $BrIC_{SS}$ and $PAIS_{SS}$, and $BrIC_{MAX}$ and $PAIS_{MAX}$ values, there were no statistically significant differences between Helmets A and B at the lateral location ($p > 0.755$). At the frontal location, Helmet A produced higher values than Helmet B but lower values at the oblique location, both of which were found to be statistically significant ($p < 0.017$).

Table 36. Mean and standard deviations of BrIC and PAIS 1-4 values based on the steady state angular velocity when using the NOCSAE headform.

Helmet Type	Impact Location	$BrIC_{SS}$ Value (mean (SD))	$PAIS1_{SS}$ (%) (mean (SD))	$PAIS2_{SS}$ (%) (mean(SD))	$PAIS3_{SS}$ (%) (mean (SD))	$PAIS4_{SS}$ (%) (mean (SD))
A	Frontal	0.06 (0.02)	9.90 (0.17)	0.11 (0.00)	0.03 (0.00)	0.01 (0.00)
	Lateral	0.13 (0.00)	70.50 (0.01)	1.24 (0.00)	0.31 (0.00)	0.17 (0.00)
	Oblique	0.13 (0.01)	74.90 (0.01)	1.41 (0.00)	0.35 (0.00)	0.20 (0.00)
B	Frontal	0.01 (0.01)	0.12 (0.04)	0.00 (0.00)	0.00 (0.00)	0.00 (0.00)
	Lateral	0.13 (0.01)	74.47 (0.11)	1.39 (0.00)	0.34 (0.00)	0.20 (0.00)
	Oblique	0.26 (0.04)	99.99 (4.43)	8.92 (0.05)	2.27 (0.01)	1.30 (0.01)

Table 37. Mean and standard deviations of BrIC and PAIS 1-4 values based on maximum angular velocity values when using the NOCSAE headform.

Helmet Type	Impact Location	$BrIC_{MAX}$ Value (mean (SD))	$PAIS1_{MAX}$ (%) (mean (SD))	$PAIS2_{MAX}$ (%) (mean (SD))	$PAIS3_{MAX}$ (%) (mean (SD))	$PAIS4_{MAX}$ (%) (mean (SD))
A	Frontal	0.14 (0.02)	81.04 (0.64)	1.69 (0.01)	0.42 (0.00)	0.24 (0.00)
	Lateral	0.39 (0.01)	100.00 (0.10)	25.01 (0.00)	6.83 (0.00)	3.94 (0.00)
	Oblique	0.17 (0.01)	93.76 (0.07)	2.80 (0.00)	0.70 (0.00)	0.40 (0.00)
B	Frontal	0.08 (0.01)	28.17 (0.06)	0.34 (0.00)	0.08 (0.00)	0.05 (0.00)
	Lateral	0.38 (0.01)	100.00 (0.23)	24.31 (0.00)	6.61 (0.00)	3.81 (0.00)
	Oblique	0.30 (0.03)	100.00 (1.98)	13.00 (0.02)	3.36 (0.01)	1.93 0.00)

7.2.2.3. LU headform

Angular response corridors and representative trials for helmeted impacts using the LU headform can be seen in Figure 77, with extracted parameters found in Table 38. As observed previously, the angular response contains signal artefacts at frequencies similar to the resonance frequency of the LU headform. As previously mentioned, these artefacts are not observed when using the Hybrid-III headform.

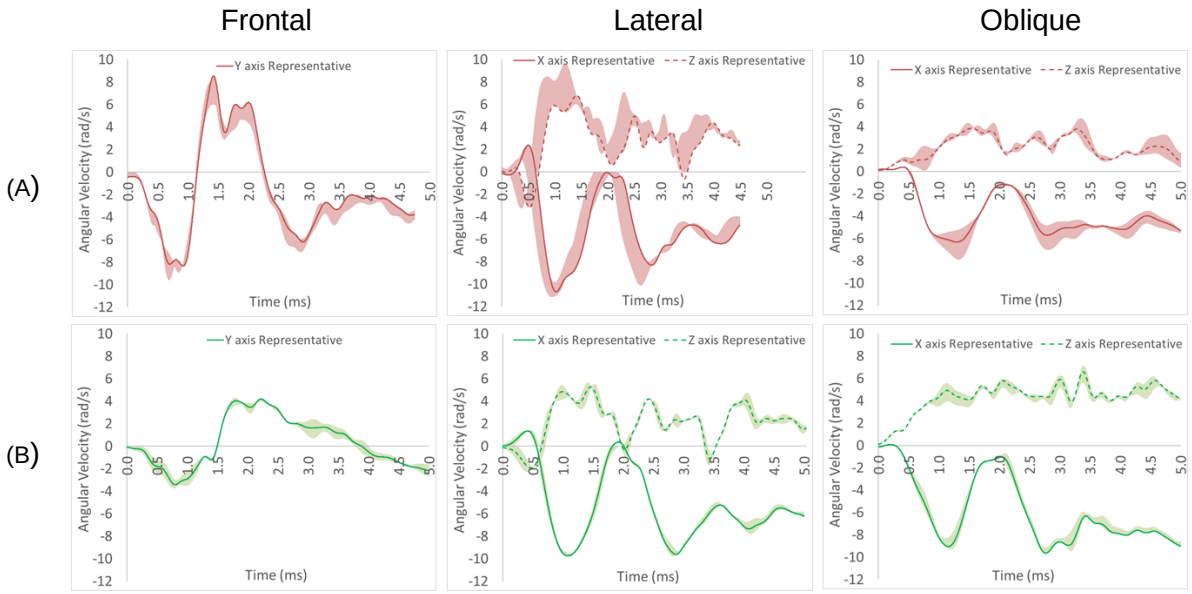

Figure 77. Response corridors and representative curves for the angular response of helmeted impacts using the LU headform.

Table 38. Mean and standard deviation values of the angular response when using the LU headform.

Helmet Type	Impact Location	Maximum Angular Velocity about axes of interest (rad/s) (mean (SD))	Time to Maximum Angular Velocity (ms) (mean(SD))	Maximum peak to peak α_{sine} (krad/s/s) (mean (SD))	Steady State Angular Velocity (rad/s) (mean (SD))	Impulse (kg m^2 s^{-1}) (mean (SD))
A	Frontal	Y: -8.89 (0.58)	Y: 0.74 (0.07)	Y: 39.30 (2.17)	Y: -5.64 (0.35)	Y: -0.11 (0.01)
	Lateral	X: -10.55 (0.55) Z: 7.54 (0.58)	X: 0.99 (0.03) Z: 1.06 (0.03)	X: -16.78 (1.29) Z: 16.98 (1.43)	X: -5.95 (0.18) Z: 3.69 (0.60)	X: -0.10 (0.00) Z: 0.06 (0.01)
	Oblique	X: -6.62 (0.93) Z: -4.18 (0.23)	X: 1.20 (0.17) Z: 1.64 (0.18)	X: 10.72 (3.27) Z: 4.04 (0.41)	X: -6.12 (0.54) Z: -0.74 (0.49)	X: -0.10 (0.01) Z: -0.01 (0.01)
B	Frontal	Y: 4.07 (0.18)	Y: 1.86 (0.08)	Y: 11.10 (1.36)	Y: -2.53 (0.12)	Y: -0.05 (0.00)
	Lateral	X: -9.64 (0.09) Z: 5.50 (0.16)	X: 1.09 (0.02) Z: 0.96 (0.07)	X: -18.94 (0.94) Z: 7.62 (0.89)	X: -7.43 (0.75) Z: 2.58 (0.62)	X: -0.12 (0.01) Z: 0.04 (0.01)
	Oblique	X: -9.41 (0.21) Z: -6.68 (0.36)	X: 2.77 (0.01) Z: 3.26 (0.18)	X: -18.13 (1.63) Z: 6.42 (1.18)	X: -8.02 (0.31) Z: -2.80 (0.13)	X: -0.13 (0.01) Z: -0.05 (0.00)

In Helmet A, the lateral location produced the highest maximum angular velocity values, followed by the frontal and oblique locations – with statistically significant differences observed between the oblique and lateral locations (p = 0.004). The frontal location did however show the highest maximum peak to peak estimated sinusoidal angular acceleration with statistically significant differences between the lateral and oblique locations (p < 0.001). The oblique location produced the longest time to maximum angular velocity, and highest steady state angular velocity and impulse values, followed by the lateral and frontal locations

respectively. However, the only statistically significant differences were found between the lateral and oblique locations (p = 0.015).

In Helmet B, the frontal location produced lower maximum angular velocity values and maximum estimated sinusoidal angular acceleration than the lateral and oblique locations, with statistically significant differences observed in these comparisons (p < 0.001). The lateral and oblique locations did not show statistically significant differences with respect to maximum angular velocity (p = 0.743). The oblique location produced the longest time to maximum angular velocity, steady state angular velocity and impulse values, followed by the frontal and lateral locations. However, no statistically significant differences were found between the impact locations (p > 0.309).

Figure 78 shows a comparison of the representative curves observed in Helmets A and B at each impact location. At the frontal location, Helmet A produced shorter time to maximum angular velocity, and higher maximum angular velocity, maximum peak to peak estimated sinusoidal angular acceleration, steady state angular velocity and impulse than Helmet B – all of which were found to be statistically significant (p < 0.003). At the lateral location, there were no statistically significant differences between helmet types in any of the parameters identified in Table 38. At the oblique location, statistically significant differences were observed in all the parameters identified in Table 38. At this location, Helmet B was found to produce higher maximum angular velocity, maximum peak to peak estimated sinusoidal angular acceleration, steady state angular velocity and impulse than Helmet A – all of which were statistically significant (p < 0.016).

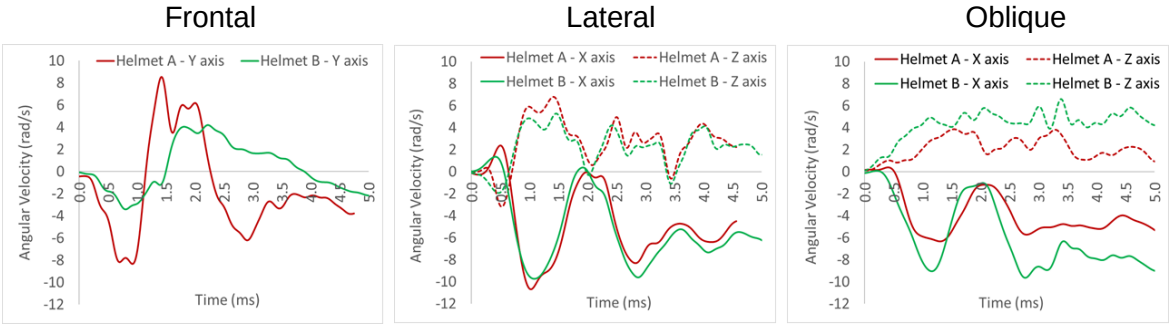

Figure 78. Representative angular velocity curves from each helmet type at each location using the LU headform.

Table 39 and Table 40 show the calculated $BrIC_{SS}$ and $PAIS_{SS}$, and $BrIC_{MAX}$ and $PAIS_{MAX}$ values. In Helmet A, the lowest $BrIC_{SS}$ and $PAIS_{SS}$, and $BrIC_{MAX}$ and $PAIS_{MAX}$ values were found at the oblique location followed by the frontal and lateral locations respectively. When comparing $BrIC_{SS}$ and $PAIS_{SS}$ the only statistically significant differences were found between the lateral and oblique locations (p = 0.048). The lateral location

produced significantly higher $BrIC_{MAX}$ and $PAIS_{MAX}$ values than both the frontal and oblique locations ($p < 0.032$).

In Helmet B, the frontal location produced the lowest $BrIC_{SS}$ and $PAIS_{SS}$, and $BrIC_{MAX}$ and $PAIS_{MAX}$ values. Statistically significant differences were found when comparing the frontal to the lateral and oblique locations ($p < 0.003$), but not when comparing the lateral to the oblique location ($p > 0.842$).

Table 39. Mean and standard deviations for BrIC and PAIS values based on steady state angular velocity when using the LU headform.

Helmet Type	Impact Location	$BrIC_{SS}$ Value (mean (SD))	$PAIS1_{SS}$ (%) (mean (SD))	$PAIS2_{SS}$ (%) (mean (SD))	$PAIS3_{SS}$ (%) (mean (SD))	$PAIS4_{SS}$ (%) (mean (SD))
A	Frontal	0.11 (0.01)	50.56 (0.07)	0.72 (0.00)	0.18 (0.00)	0.10 (0.00)
	Lateral	0.12 (0.02)	67.43 (0.29)	1.14 (0.00)	0.28 (0.00)	0.16 (0.00)
	Oblique	0.10 (0.02)	42.34 (0.31)	0.56 (0.00)	0.14 (0.00)	0.08 (0.00)
B	Frontal	0.05 (0.01)	6.99 (0.04)	0.07 (0.00)	0.02 (0.00)	0.01 (0.00)
	Lateral	0.13 (0.02)	69.36 (0.49)	1.21 (0.01)	0.30 (0.00)	0.17 (0.00)
	Oblique	0.14 (0.01)	77.20 (0.03)	1.50 (0.00)	0.37 (0.00)	0.21 (0.00)

Table 40. Mean and standard deviation for BrIC and PAIS values based on maximum observed angular velocity when using the LU headform.

Helmet Type	Impact Location	$BrIC_{MAX}$ Value (mean (SD))	$PAIS1_{MAX}$ (%) (mean (SD))	$PAIS2_{MAX}$ (%) (mean(SD))	$PAIS3_{MAX}$ (%) (mean (SD))	$PAIS4_{MAX}$ (%) (mean (SD))
A	Frontal	0.20 (0.02)	98.42 (0.35)	4.16 (0.00)	1.04 (0.00)	0.59 (0.00)
	Lateral	0.25 (0.03)	99.98 (1.81)	8.32 (0.02)	2.11 (0.00)	1.21 (0.00)
	Oblique	0.16 (0.01)	88.19 (0.19)	2.17 (0.00)	0.54 (0.00)	0.31 (0.00)
B	Frontal	0.08 (0.01)	28.91 (0.03)	0.35 (0.00)	0.09 (0.00)	0.05 (0.00)
	Lateral	0.22 (0.01)	99.55 (0.04)	5.39 (0.00)	1.35 (0.00)	0.77 (0.00)
	Oblique	0.23 (0.01)	99.78 (0.04)	6.06 (0.00)	1.52 (0.00)	0.87 (0.00)

When comparing the helmet types, Helmet B produced significantly lower $BrIC_{SS}$ and $PAIS_{SS}$, and $BrIC_{MAX}$ and $PAIS_{MAX}$ values than Helmet A at the frontal location ($p < 0.024$). Although Helmet A produced lower $BrIC_{SS}$ and $PAIS_{SS}$ than Helmet B at the lateral location, these differences were not found to be statistically significant ($p > 0.433$). Helmet B produced higher $BrIC_{MAX}$ and $PAIS_{MAX}$ values than Helmet A, but again, these were not found to be statistically significant ($p > 0.277$). At the oblique location, Helmet B produced higher $BrIC_{SS}$ and $PAIS_{SS}$ and $BrIC_{MAX}$ and $PAIS_{MAX}$ values than Helmet A, with statistically significant differences observed in all these comparisons ($p < 0.027$).

7.2.2.4. Headform Comparison

As can be seen in Figure 79, there are also clear differences between the angular responses observed when using the Hybrid-III, NOCSAE and LU headforms. As observed in the linear response, the Hybrid-III was found to respond as a rigid body, while the NOCSAE and LU headforms displayed additional frequency artefacts. At the frontal location the LU and NOCSAE headforms displayed a higher maximum angular velocity than the Hybrid-III headform during initial loading, followed by an oscillatory response which was not present in the response curves observed when using the Hybrid-III. At the lateral location the initial loading phase of the angular response was similar when comparing the LU and Hybrid-III headforms, whereas the NOCSAE headform produced a greater angular velocity during initial loading, followed by a response similar to a classic spring dampener response in both helmet types. When considering the initial loading phases at the oblique location, the LU and Hybrid-III headforms showed a comparable response about the x and z axes in Helmet B. In Helmet A, the Hybrid-III headform produced a higher magnitude than the LU headform.

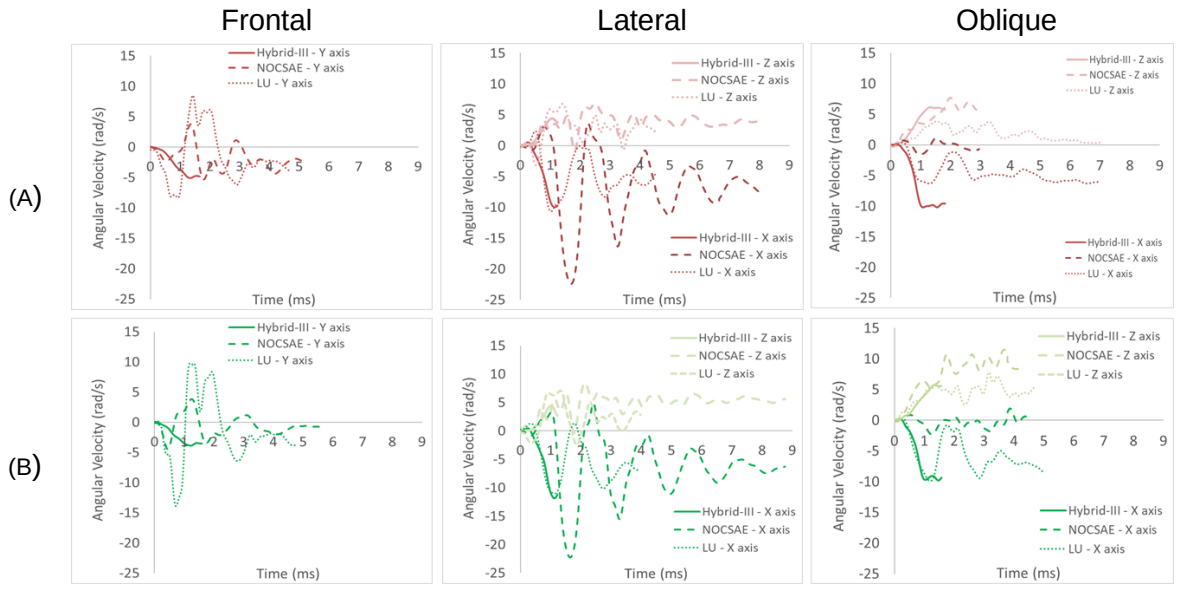

Figure 79. Representative angular response curves for each helmet type and impact location on the Hybrid-III, NOCSAE and LU headforms.

7.2.2.5. Repeated Impacts

Representative angular response curves from the repeated impacts using Helmet A and B can be found in Figure 80, with the mean and standard deviation values of the extracted parameters found in Figure 81. Helmet B showed a slight (6.91%) increase in steady state angular velocity, whereas Helmet A showed a slight decrease in this parameter (-2.84%) (see Table 41). Since the impulse was calculated as the steady state angular velocity multiplied by the MoI, the percentage changes in the Impulse parameter were the same as

those observed in the steady state angular velocity. Although minimal changes in steady state angular velocity were observed, both helmets showed a shorter time to maximum angular velocity with repeated impacts. There were much greater differences observed in the maximum angular velocity, with Helmet A producing the greatest increase (108.23%). Helmet A also showed a large increase in maximum peak to peak estimated sinusoidal angular acceleration (247.3% increase.) As can be seen in Figure 81 and Table 41, Helmet B showed lower percentage increase in maximum angular velocity (39.89 %) and maximum peak to peak estimated sinusoidal angular acceleration (165.16%). The maximum angular velocity and maximum peak to peak estimated sinusoidal angular acceleration observed in the fifth impact on Helmet B remained lower than that measured in the first impact on Helmet A.

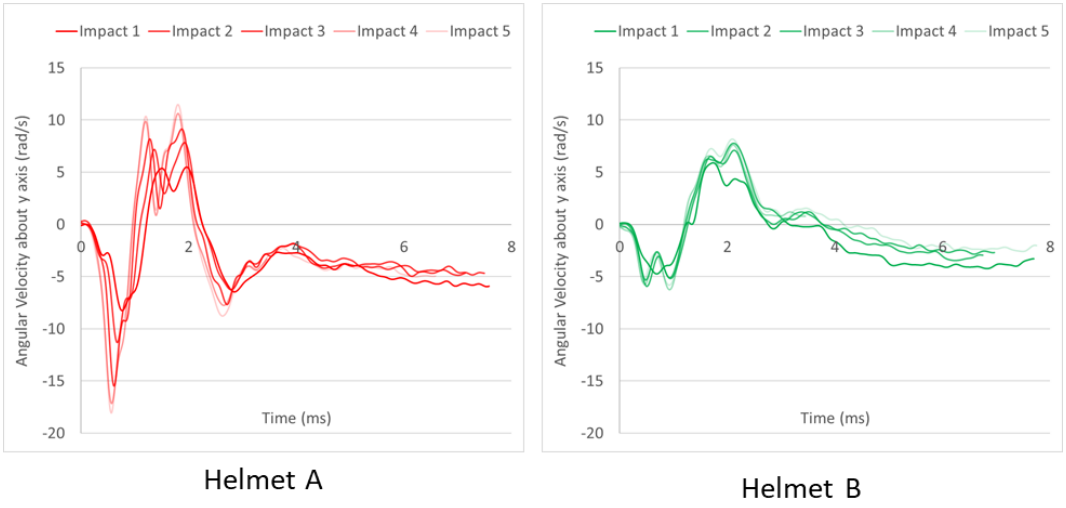

Figure 80. Representative angular response curves for the repeated impacts using Helmets A and B.

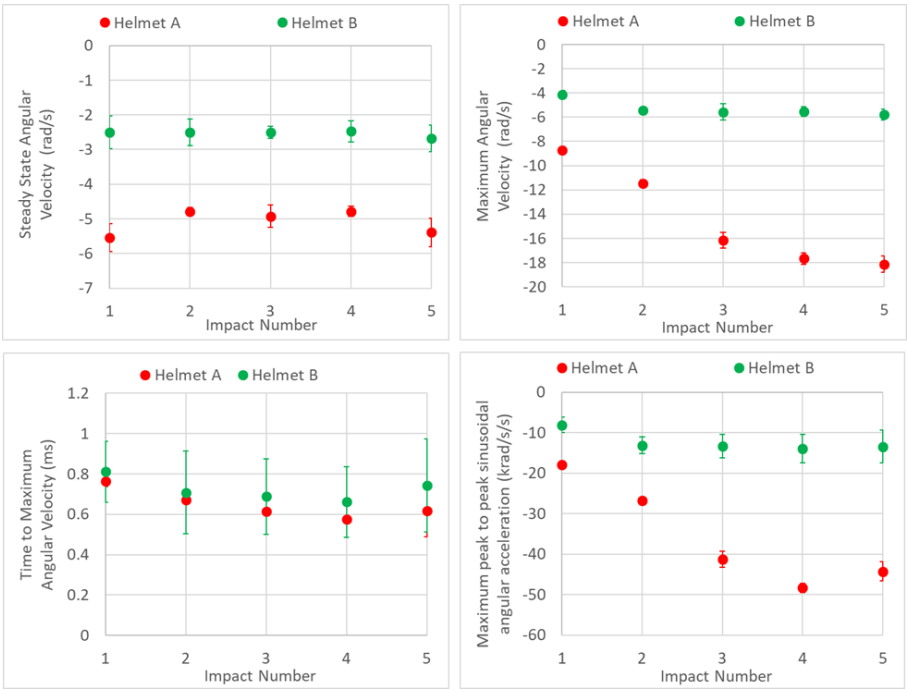

Figure 81.Change in selected angular response parameters extracted from the entire impact duration.

Table 41. Percentage change in angular response parameters from impact 1 to impact 5.

	% Change from Impact 1 to 5			
Helmet Type	Steady State Angular Velocity	Maximum Angular Velocity	Time to Maximum Angular Velocity	Maximum peak to peak sinusoidal angular acceleration
A	-2.84	108.23	`-19.51	247.33
B	6.91	39.89	-8.39	165.16

As the $BrIC_{SS}$ values (see Figure 82) are calculated based on the steady state angular velocity, these followed a similar trend to that observed in Figure 81, with Helmet A, showing a small percentage decrease in the observed $BrIC_{SS}$ (maximally -6.89%), and Helmet B showing a small increase in $BrIC_{SS}$ (5.89%). As a result of this, the calculated $PAIS1\text{-}4_{SS}$ values remained fairly constant across the repeated impacts. As can also be seen in Figure 82, Helmet A showed the highest increase in $BrIC_{MAX}$ values, with a 97.71 increase. Helmets B also showed an increase in $BrIC_{MAX}$ from impacts 1 to 5, however this was lower at 65.01%. As can be seen in Table 43, this increase in $BrIC_{MAX}$ results in an increase in $PAIS1\text{-}4_{MAX}$ values. In Helmet A, $PAIS1_{MAX}$ values were found to be greater than 95% in all impacts. The $PAIS2_{MAX}$ values were found to increase by 516.21%, from impact 1 (3.96% ±0.47) to impact 5 (24.42% ±2.95). Although Helmet B showed a 156.88 increase in $PAIS2_{MAX}$ from impact 1 to 5 respectively, the value calculated in the fifth impact remained below 4%. The observed $PAIS3_{MAX}$ values were found to increase to greater than 5% in

Helmet A in impacts 3 to 5. Calculated $PAIS4_{MAX}$ values remained below 5% in all of the repeated impacts across both helmet types.

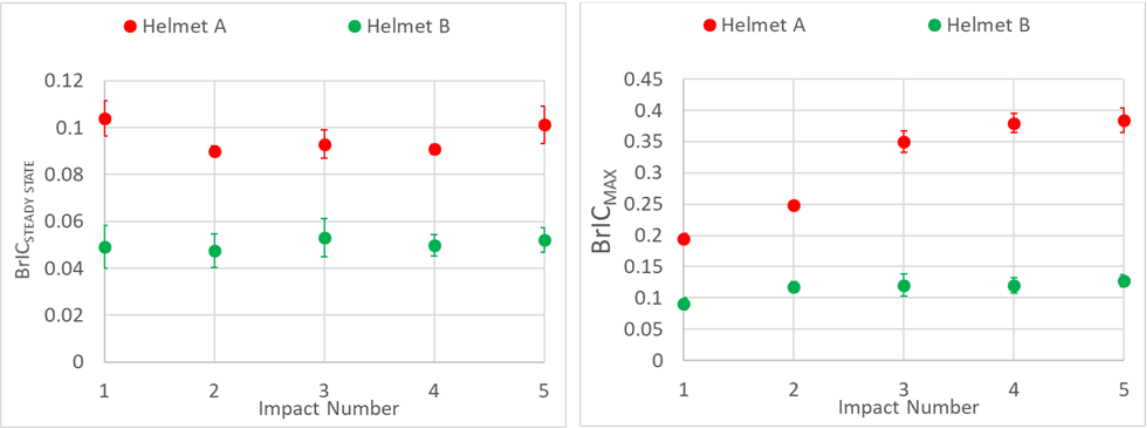

Figure 82.Change in BrIC values calculated using the steady state and maximum angular velocity values.

Table 42. $PAIS_{MAX}$ parameters from impact 1 to impact 5.

Helmet Type	Impact Number	$PAIS1_{MAX}$ (%) (mean (SD))	$PAIS2_{MAX}$ (%) (mean (SD))	$PAIS3_{MAX}$ (%) (mean (SD))	$PAIS4_{MAX}$ (%) (mean (SD))
A	1	97.84 (0.99)	3.96 (0.47)	0.99 (0.12)	0.56 (0.07)
	2	99.96 (0.02)	7.79 (0.55)	1.97 (0.15)	1.13 (0.08)
	3	100.00 (0.00)	19.29 (2.49)	5.14 (0.73)	2.95 (0.42)
	4	100.00 (0.00)	23.67 (2.33)	6.43 (0.70)	3.71 (0.41)
	5	100.00 (0.00)	24.42 (2.95)	6.66 (0.89)	3.84 (0.52)
B	1	36.58 (8.65)	0.47 (0.13)	0.12 (0.03)	0.07 (0.02)
	2	60.36 (7.71)	0.96 (0.20)	0.24 (0.05)	0.14 (0.03)
	3	62.28 (15.18)	1.08 (0.42)	0.27 (0.10)	0.15 (0.06)
	4	62.93 (10.28)	1.05 (0.30)	0.26 (0.07)	0.15 (0.04)
	5	68.68 (7.80)	1.22 (0.26)	0.30 (0.07)	0.17 (0.04)

7.3. Discussion

When assessing the linear and angular response of the Hybrid-III, NOCSAE and LU headforms in helmeted impacts, it is clear that the type of headform used during these impacts influenced the observed responses, due to the construction, material and inertial properties of each. Although the Hybrid-III headform responded predominantly as a rigid body, the NOCSAE and LU headforms showed significant additional frequency components in the measured response. This concurs with previous research by Hodgson et al.(1967), McElhaney et al. (1973) and Thomas and Hodgson (1969) who reported that impacts shorter than 6 ms tend to excite the bending modes in the skull, and Raymond et al. (2008) who reported similar responses to those observed in this study, when subjecting human cadaver skulls to projectile impacts with metal pucks. As the resonance frequency of the LU

headform was found to be representative of human skull resonance frequency (See Chapter 5), the oscillations introduced through resonance frequency excitation should be considered relevant artefacts. Although the resonance frequency of the NOCSAE headform was not directly measured, it could be considered comparable to that seen in the LU headform due to the materials and construction. Due to previous research (Hodgson et al., 1967; McElhaney et al., 1973; Raymond et al., 2008; Thomas and Hodgson, 1969), and the measured resonance frequency of the LU headform, the response observed when using the LU headform should be considered a closer representation to that of a human than the Hybrid-III in short duration, projectile head impacts representative of those seen in Cricket. However, the Hybrid-III headform may provide a more consistent measure of the underlying rigid body response during impact and provide a means of comparing the response observed here with that measured in other sports.

There were also clear differences between the LU and NOCSAE headforms when considering the oscillations observed. These differences were particularly evident at the lateral impact location where the angular velocity response of the NOCSAE headform was found to be similar to a classical spring dampener response (Hibbeler, 2015). Although it is possible that the response observed here is a result of the resonance frequency of the headform, the sensor mounting technique shown in Chapter 6 should also be considered as a potential source of this frequency component. Although every precaution was taken to engage the mass of the headform with the sensor mounting block, the shape and securing technique may contribute to the response observed in Figure 55 – leading to potentially erroneous results. Although the designed mounting technique used in the NOCSAE headform was necessary to accommodate the linear accelerometer and angular rate sensor, the mounting technique used here should be investigated and, if necessary, alternative solutions should be considered in future studies.

The excitation of the resonance frequency of the NOCSAE and LU headforms resulted in the multiple peaks presented here – producing higher peak resultant linear accelerations than that seen in the Hybrid-III, and extremely large levels of jerk. In some sporting impact scenarios, a ~rigid body response may be expected, however, in other impact scenarios, such as short duration projectile impacts, excitation and local deformation of the headform may be an important injury mechanism that has yet to be explored. Previous research that has assessed head impacts in Cricket and other projectile sports have failed to report this, either due to the utilisation of rigid headforms such as the Hybrid-III or EN 960 (McIntosh and Janda, 2003; Post et al., 2016; Yang et al., 2014), excessive filtering due to the application of SAE J211 filtering conventions (SAE, 1995) developed for alternative scenarios (Clark, 2015), or the attribution of the oscillations as ‘noise’ rather than genuine

artefact worthy of further analysis (Kendall et al., 2012b). The different responses observed in the Hybrid-III and LU headforms outlined in this study highlights the need to consider resonance frequency excitation when investigating short duration head impacts typical of those observed in projectile sports, through laboratory reconstructions and FE modelling.

When considering the effect of impact location on the observed dynamic response, the lateral location was found to produce the highest peak resultant linear acceleration in both helmet types and all headforms. In the Hybrid-III impacts, the lateral location generally produced the highest maximum angular velocity value about the x axis, however the oblique location produced higher angular velocity about the z axis. When using the NOCSAE and LU headforms, although the lateral location often produced greater maximum angular velocity, the oblique location often produced the greatest steady state angular velocity. This resulted in greater $BrIC_{MAX}$ and PAIS1-4_{MAX} values in the lateral location, but greater $BrIC_{SS}$ and PAIS1-4_{SS} values in the oblique location. It is important to note however, that BrIC was developed using rigid body motion of the head, and therefore may not be applicable when assessing impacts where local deformation and resonance frequency excitation occur. The results relating to impact location observed in this study generally correspond to those reported by Liao et al. (2016) who reported that in American Football, impacts to the side of the head were more commonly associated with diagnoses of mTBI.

Along with the inertial properties of the headforms, variations in helmet design may also influence the observed differences in impact location. Indeed, the clear differences observed between helmet types at the frontal location may be explained by the more prominent slope of the peak of Helmet B, which diverted the path of the ball and resulted in a more glancing blow than that observed in Helmet A. This is also likely to have influenced the repeated impact results (discussed later).

McIntosh and Janda (2003), conducted projectile impacts using an undefined Cricket ball type at 36 m/s (comparable to the 34.7 m/s used in this study) and a 5th percentile female Hybrid-III headform. Higher resultant linear acceleration values (316 g ±86) were reported by McIntosh and Janda (2003) which may suggest that the performance of Cricket helmets has improved since the study. However, a direct comparison is difficult as the presented results were averaged across three impact locations (frontal, lateral and rear), and included repeated impacts at the same site, which as shown in this study, can influence the observed peak resultant linear acceleration measured in some helmet types. Additionally, the reduced mass of the 5th percentile female headform (3.73 kg) compared to the 50th percentile male (4.54 kg) has been found to produce higher responses during drop tests (Oeur et al., 2019a) and therefore is also likely to have influenced these results. Although

Stretch (2000) assessed the performance of Cricket helmets using a drop test methodology, the variations observed based on helmet type and impact locations concur with the results presented in this study.

Although this study shows the dynamic response of the Hybrid-III to be dissimilar to that of the NOCSAE and LU headform, the Hybrid-III results observed in this study can be compared to other studies that have used this headform to investigate projectile head impacts in sport. Coulson et al. (2009) reported similar contact times to those observed in this study when impacting a Hybrid-III headform with an Ice Hockey puck, as did Post et al. (2016) who assessed helmeted Baseball impacts. Post et al. (2016) also reported similar mean peak resultant linear acceleration (77.6 g to 240.6 g) but higher peak angular acceleration (7.3 krad/s^2 to 14.9 krad/s^2) than the Cricket helmets tested in this study, at a location comparable to the frontal location used here. The peak resultant linear acceleration and maximum angular acceleration values observed at the lateral location used in this study were comparable to the range reported by Post et al. (2016) at a similar location (130.6 to 278.8 g and 11.4 krad/s^2 to 30.1 krad/s^2). Clark et al. (2018) also assessed the dynamic response of a 50th percentile Hybrid-III headform when subjected to projectile impacts at 40 m/s using an Ice Hockey puck. Clark et al. (2018) reported higher peak resultant linear acceleration at locations similar to the lateral and oblique locations used in this study (c. 350 and 250 g respectively). In a different study, Clark et al. (2019) also reported higher angular acceleration values of around 43 krad/s^2 and around 31 krad/s^2 at the lateral and oblique locations respectively.

The results observed in this study when using the Hybrid-III headform can also be compared to those observed in contact and combat sports such as American Football (Greenwald et al., 2008; Pellman et al., 2003; Walsh et al., 2011; Zanetti et al., 2013; Zhang et al., 2004), Rugby (McIntosh et al., 2000) and Boxing (Walilko et al., 2005) where the same headform was utilised. The contact times observed in the Cricket impacts (1.18 to 3.46 ms) were found to be shorter than those observed in American Football and Boxing (5.5 to 13.7 ms and 11.4 ±1.4 ms) (Greenwald et al., 2008; Walilko et al., 2005). Peak resultant linear acceleration was also found to be higher than those reported in American Football, Rugby and Boxing impacts (Frechede and McIntosh, 2009; Pellman et al., 2003; Walilko et al., 2005; Zanetti et al., 2013; Zhang et al., 2004) in all but one impact scenario (Helmet B, frontal location). When considering the angular response, the maximum estimated angular acceleration values observed in a number of the impact scenarios were within the range reported in American Football, Rugby and Boxing, however the values observed at the lateral location in this study were again much greater than those reported in these sports

(Frechede and McIntosh, 2009; Pellman et al., 2003; Walilko et al., 2005; Zanetti et al., 2013; Zhang et al., 2004).

When assessing the response of the NOCSAE headform, the peak resultant linear acceleration values observed in this study were considerably higher than those reported by Clark et al. (2018b) when assessing puck impacts to Ice Hockey goaltender helmets using the same headform. Although the maximum angular velocity values observed here were greater than those observed by Clark et al. (2018b), the steady state angular velocity values were comparable. This however may be due to the filtering technique applied by Clark et al. (2018b), which removed any resonance frequency artefacts and essentially reduced the response to that of a rigid body. Unfortunately, these studies did not report additional parameters such as contact time, time to peak resultant linear acceleration, impulse, HIC or maximum angular velocity.

When using the Hybrid-III headform, the lateral location produced the highest HIC values in both helmet types. In Helmet B, the HIC value was above 235 at the lateral location, which King et al. (2003) equated to a 50% probability of sustaining mTBI. Indeed, only Helmet B at the frontal location produced a HIC value significantly lower than 136, which was reported by King et al. (2003) as corresponding to 25% probability of sustaining mTBI. The elongated contact time and oscillations present in the NOCSAE and LU headforms meant that all impact scenarios (other than Helmet B – frontal location) produced HIC values above 333, which King et al. (2003) reported as corresponding to 75% probability of sustaining mTBI.

All of the impact scenarios tested here produced angular velocity values below the 25 rad/s threshold for ‘mild cerebral concussion’ defined by Gennarelli et al. (2003). Despite this, when calculating BrIC values and predicting the probability of AIS1-4 injuries using the technique described by Takhounts et al. (2013), the probability of sustaining AIS1 injury was found to be high, particularly at the lateral and oblique impact locations when using all headforms. However even when calculated using the maximum angular velocity values observed when using the NOCSAE and LU headforms, the PAIS 2-4 values were below 10% in all impact locations and headforms (other than PAIS 2_{MAX} values at the lateral location using the NOCSAE headform).

It is important to note that the HIC and BrIC injury metrics were not developed for use in projectile based impacts. As such, the results presented here are simply included for comparison with other impact scenarios, and further work should look to develop appropriate injury metrics based on the observed response during high-velocity, low-mass projectile impacts, like those seen in many projectile sports.

The repeated impacts conducted on the LU headform resulted in a change in the observed parameters in both helmet types tested. Larger increases were observed in Helmet A, where peak resultant linear acceleration, HIC and impulse increased to 602 g, 2927 and 26.75 N.s respectively, compared to 184 g, 166 and 11.26 N.s in Helmet B. In both helmets, the maximum angular velocity increased with repeated impacts, whereas the steady state angular velocity showed little change. This suggests that although the excitation of the resonance frequency of the headform increased (thereby resulting in higher peak resultant linear acceleration and maximum angular velocity), the total amount of angular energy transferred to the headform remained relatively consistent. Due to the closed cell structure of expanded polystyrene (EPS), permanent deformation occurs during impacts of sufficient magnitude, thereby reducing the materials ability to absorb energy in subsequent impacts. Given that both helmets use EPS as their primary energy absorbing component, the decrease in helmet performance is unsurprising. As previously discussed, the geometry of Helmet B at the frontal location diverted the path of the ball, resulting in non-direct blows and potentially less EPS deformation, which in turn likely explains the less pronounced reduction in performance of this helmet relative to Helmet A. However, despite clear differences in the linear and angular responses, with repeated impacts, there was minimal superficial damage to the helmets themselves. Although helmet manufacturers and BS 7928:2013 state that helmets should be replaced after one severe impact, medical staff, players and officials may judge a helmets integrity based on external appearance. This may lead to the continued use of helmets despite the reduced capability of the helmet to attenuate force.

The research presented in this chapter is the first of its kind to report the linear and angular response of multiple, helmeted headform types, when subjected to impacts representative of those seen in Cricket, and the effect of repeated impacts on helmet performance. However, it is important to note the limitations of this study. The headform suspension technique used in this study was selected based on previous research and the expected duration of the projectile impacts. Future work should investigate potential variations in observed dynamic response resulting from varied mounting conditions (including a ~Fixed condition, Hybrid-III neckform, and a neckform with improved biofidelity). Additionally, further investigations into the observed response of the NOCSAE headform at the lateral location should be conducted in order to determine the source of the apparent additional frequency artefact.

Considering the limitations of the study, the following conclusions can be drawn from this study:

- Impact location and headform type influences the observed response. While the Hybrid-III responded predominantly as a rigid body, the NOCSAE and LU headforms shown a potentially more biofidelic response, with additional frequency responses that were in line with the expected resonance frequency.
- Geometric variations in helmet design may be an effective means of influencing dynamic response characteristics.
- The dynamic response of a headform during impacts representative of those seen in cricket are dissimilar to those observed previously in contact and combat sports.
- Traditional injury metrics that have been developed in alternative impact scenarios may not be suitable for the assessment of head impacts in short duration projectile impacts.

CHAPTER 8

Unprotected Projectile Impacts

8.1. Introduction

Chapter 7 investigated the dynamic response of three headforms during projectile impacts representative of those seen in Cricket, when protected by currently available Cricket helmets. However, in order to facilitate a thorough assessment of the performance of currently available PPE, an understanding of the dynamic response observed during unprotected impacts is necessary. This approach has been utilised to assess the efficacy of head protectors used in Lacrosse (Clark et al., 2018b), Ice Hockey (Clark, 2015), and simulated falls in sport (Nishizaki et al., 2014; Oeur et al., 2019).

In this study, two unprotected headforms were subjected to projectile impacts at three impact locations, utilising the methodology outlined in Chapter 6. The two headforms used in this study were the Hybrid-III 50th percentile male and the LU headform. Although the NOCSAE headform has been used for unprotected impacts in other sporting scenarios (Clark, 2015) and may produce a response closer that of a human head during unprotected head impacts in Cricket than the Hybrid-III, correspondence with the manufacturer suggested that permanent damage may be caused from an impact of this nature and as such this headform was not assessed as it was judged to be financially prohibitive. As the measured response when using the EN 960 headform was found to contain non-biofidelic frequency artefacts that could not be removed without inducing significant signal distortion (see Chapter 6), this headform was also omitted from the unprotected impacts.

Impacts were arranged to occur at the frontal, lateral and oblique Locations as described in Chapter 6. An unused Kookaburra Turf Cricket ball was used at each location. When using the Hybrid-III headform, five impacts were completed at each location. When using the LU headform, five locations were completed at the frontal and lateral locations, and 3 impacts were completed at the oblique location – the fourth impact at the oblique location resulted in fracture. Following each unprotected impact using the LU headform, three drop tests were completed as described in Chapter 5. This approach ensured that the response of the headform remained within a tolerable limit (± 1SD), relative to that of the observed pre-impact response.

The aim of this study was to investigate the dynamic response of the Hybrid-III and LU headforms when subjected to unprotected impacts representative of those seen in

Cricket and compare these to the results presented in Chapter 7, to evaluate the efficacy of currently available Cricket helmets.

8.2. Results

8.2.1. Linear Response

8.2.1.1. Hybrid-III headform

Representative linear response curves and response corridors at each impact location during unprotected Hybrid-III headform impacts can be seen in Figure 83. As in Chapter 7, the Hybrid-III headform was found to respond predominantly as a rigid body, and as such key parameters were extracted from the entire contact phase of the linear response (see Table 43). As can be seen here, the lateral location produced the highest peak resultant linear acceleration, impulse and HIC values and the shortest contact time. Statistically significant differences were found between the lateral location and the frontal and oblique locations when comparing contact time, peak resultant linear acceleration and HIC ($p < 0.022$).

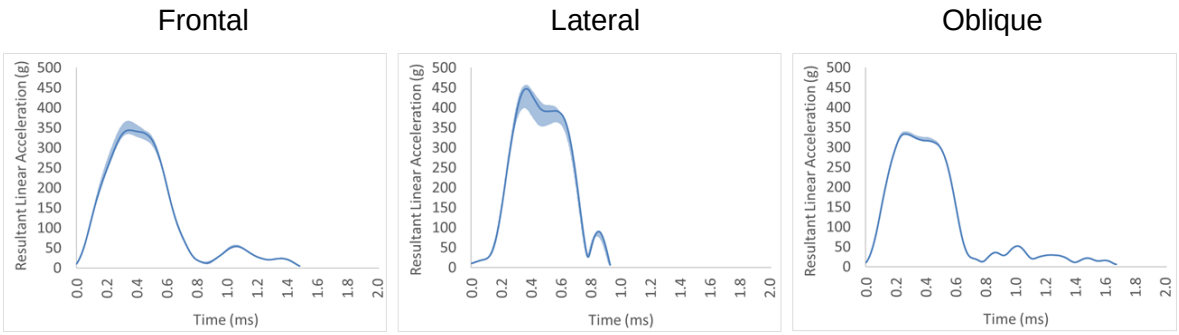

Figure 83. Representative linear response curves for each impact location on the Hybrid-III headform.

Table 43. Mean and standard deviation values of key parameters calculated from the linear response of the unprotected Hybrid-III headform.

Impact Location	Contact Time (ms) (mean (SD))	Peak resultant linear acceleration (g) (mean (SD))	Time to Peak resultant linear acc. (ms) (mean (SD))	Impulse (N.s) (mean (SD))	HIC (mean (SD))
Frontal	1.48 (0.00)	346.29 (11.25)	0.37 (0.03)	8.32 (0.19)	598.43 (37.97)
Lateral	0.93 (0.01)	440.19 (21.18)	0.37 (0.00)	9.19 (0.33)	848.38 (71.18)
Oblique	1.74 (0.14)	335.95 (2.69)	0.27 (0.01)	8.09 (0.06)	599.299.20)

8.2.1.2. LU headform

Representative linear response curves and response corridors for the impacts that did not result in fracture during unprotected impacts using the LU headform are shown in Figure 84. Similar to the helmeted results presented in Chapter 7, resonance frequency excitation of the LU headform can be clearly seen to influence the unprotected impacts. Key parameters extracted from the linear response over the entire contact duration can be found in Table 45. The frontal location produced the shortest time to peak resultant linear acceleration, and the highest peak resultant linear acceleration, and HIC values, all of which were found to be statistically significant when compared to the lateral and oblique locations ($p < 0.036$). The frontal location also produced the shortest contact time and highest impulse, but no statistically significant differences were found when comparing these parameters ($p > 0.255$).

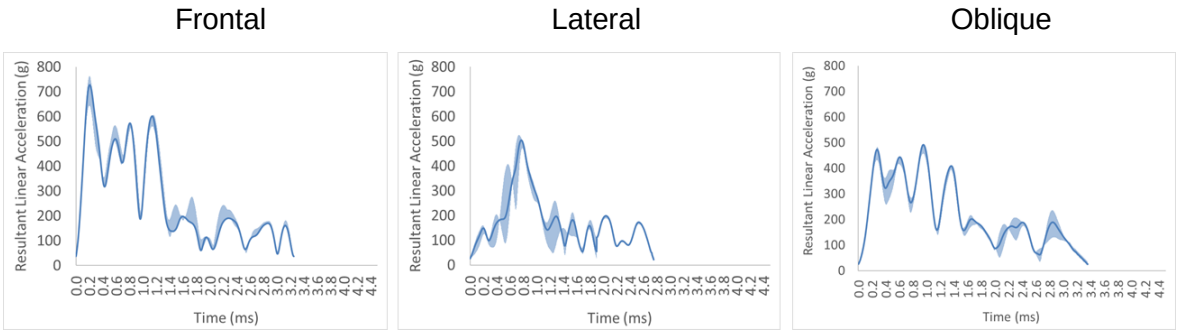

Figure 84. Representative linear response curves for each impact location on the LU headform.

Table 44. Mean and standard deviation values of key parameters extracted from the linear response of the unprotected LU headform impacts.

Impact Location	Contact Time (ms) (mean (SD))	Peak resultant linear acceleration (g) (mean (SD))	Time toPeak resultant linear acc. (ms) (mean (SD))	Impulse (N.s) (mean (SD))	HIC (mean (SD))
Frontal	3.24 (0.01)	710.79 (38.97)	0.20 (0.00)	36.14 (0.70)	5635.06 (83.12)
Lateral	3.58 (0.17)	495.30 (18.26)	0.77 (0.02)	23.06 (0.70)	1166.77 (96.16)
Oblique	3.75 (0.07)	489.03 (4.78)	0.73 (0.32)	31.02 (0.77)	2763.25 (177.40)

The fourth impact at the oblique location resulted in the fracture of the LU headform (as shown in Figure 85a). As can be seen from Figure 85b and Figure 85c, the depressed comminuted skull fracture observed when using the LU headform is comparable to that observed in projectile impacts to human heads. The linear and angular response observed during this impact, relative to the non-fracture impacts can be seen in Figure 86.

Figure 85. Photograph of the fracture sustained to (a) the LU headform at the oblique impact location, (b) a scan of a comminuted skull fracture resulting from a baseball impact (News, 2019), and (c) a photograph of the skull fracture sustained to a human cadaver (Raymond et al., 2008).

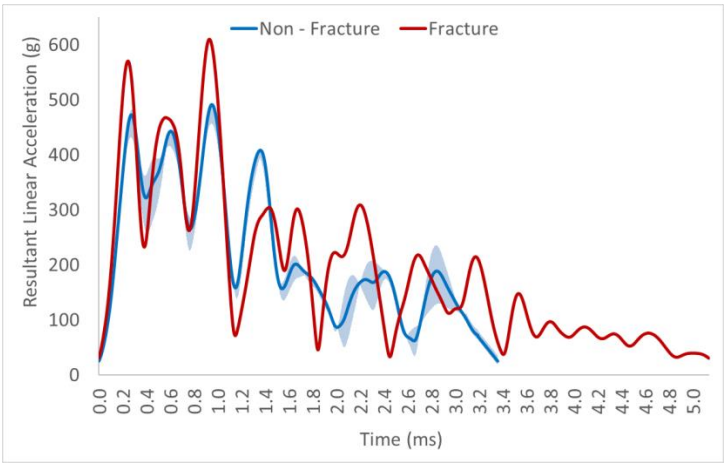

Figure 86. Linear response curves for the impacts that did and did not result in fracture when impacting the LU headform at the oblique location.

The impact resulting in fracture produced longer contact time (5.14 ms vs 3.75 ±0.07 ms), higher resultant linear acceleration peaks and lower resultant linear acceleration troughs (and therefore higher jerk). The peak resultant linear acceleration was found to be 610.05 g, compared to the mean of 489.03 g ±4.78 observed during the non-fracture impacts. The mean HIC value calculated in the non-fracture impacts was found to be 2763.25 ±177.4, whereas in the fracture impact this value was 3505.06. The difference in fracture and non-fracture response observed here concurs with that reported by Raymond et al. (2008) who observed similar findings when impacting human cadaver heads with metal pucks of comparable diameter to a Cricket ball, at similar impact speeds to those used in this study.

8.2.1.3. Headform and Cadaver comparison

Raymond et al. (2008) published resultant linear acceleration curves of human cadavers when subjected to projectile impacts with similar conditions to those seen in the lateral impacts conducted in this study in this study (metal puck with 38 mm diameter and 103g mass, travelling at 33.6 m/s). The responses observed by Raymond et al. (2008) and those observed when using the Hybrid-III and LU headforms in this study can be found in Figure 87. The results of Raymond et al. (2008) showed variable responses, with two trials reaching peak values of 970 g and 788 g, and all other trials ranging between ~400 and ~600g. This is likely due to variations in the human cadavers tested. The results observed when using the LU headform were comparable to those reported by Raymond et al. (2008) with respect to peak resultant linear acceleration, time to peak resultant linear acceleration and contact time and the multiple peaks observed. Of the seven impacts conducted by Raymond et al. (2008), five resulted in depressed comminuted skull fracture, whereas when using the LU headform no fractures occurred at the lateral location. This, along with the drop tests results presented in Chapter 5 suggest that, although the material properties of the LU headform are closer to human tissue than the Hybrid-III, the LU headform is less likely to fracture than human cadavers. Although the Hybrid-III produced a similar peak resultant linear acceleration, the time to this peak, and the total contact time were generally shorter than those presented by Raymond et al. (2008).

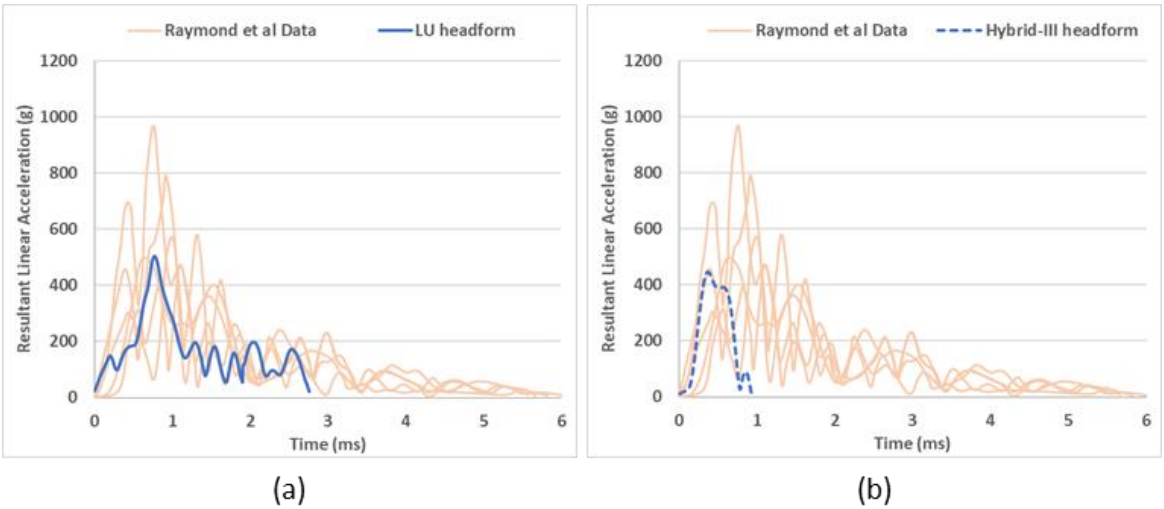

Figure 87. Comparison of resultant linear acceleration reported by Raymond et al. (2008), with representative response curves observed when using the LU headform (a) and Hybrid-III (b).

As can be seen in Figure 88, The resonance frequency excitation observed when using the LU headform resulted in mean contact times that were 2.15 to 3.86 times longer and mean peak resultant linear accelerations that were 1.13 to 2.05 times higher than the

unprotected Hybrid-III headform. Larger relative differences were seen in the Impulse and HIC values which were up to 4.35 and 9.42 times greater than the Hybrid-III values respectively (due to the longer contact time and higher resultant linear acceleration).

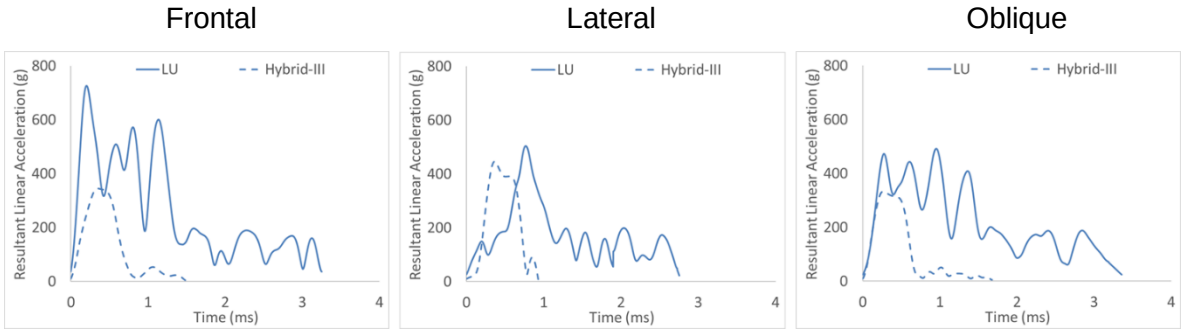

Figure 88.Comparison of representative resultant linear response curves observed when using the Hybrid-III and LU headforms in unprotected impacts.

These findings are in line with the suggestion by Hodgson et al. (1967), McElhaney et al. (1973) and Thomas and Hodgson (1969), that impacts shorter than 6 ms would likely result in skull resonance frequency excitation and result in this type of response – a factor clearly overlooked when using the Hybrid-III.

8.2.2. Angular Response

8.2.2.1. Hybrid-III headform

Representative angular response curves and response corridors observed in the unprotected Hybrid-III impacts can be seen in Figure 89, with extracted parameters presented in Table 45. When considering the angular response about a single axis, the lateral location produced the highest maximum angular velocity, shortest time to maximum velocity, and highest maximum estimated angular acceleration and Impulse than the frontal and oblique locations. Of these comparisons, time to maximum angular velocity, maximum estimated angular acceleration and impulse were found to be statistically significant ($p < 0.024$). In the z axis, the oblique location produced higher maximum angular velocity, longer time to maximum angular velocity, and higher maximum estimated angular acceleration and impulse – with statistically significant differences observed when comparing maximum angular velocity, time to maximum angular velocity and impulse ($p < 0.017$).

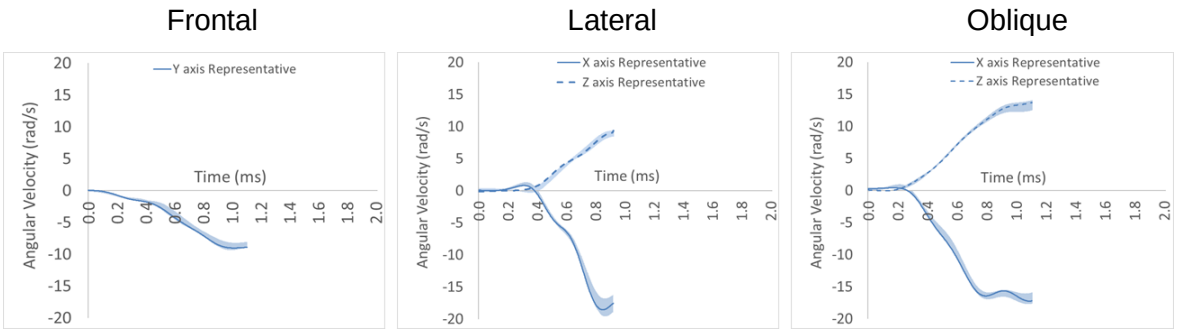

Figure 89. Representative angular response curves for each impact location on the Hybrid-III headform.

Table 45. Mean and standard deviation values of measured and calculated angular response parameters during the unprotected Hybrid-III impacts.

Impact Location	Maximum Angular Velocity about axes of interest (rad/s) (mean (SD))	Time to Maximum Angular Velocity (ms) (mean (SD))	Maximum estimated α_{sine} (krad/s/s) (mean (SD))	Impulse (kg m^2 s^{-1}) (mean (SD))
Frontal	Y: -8.61 (0.48)	Y: 1.07 (0.11)	Y: -12.80 (1.61)	Y: 0.17 (0.01)
Lateral	X: -18.64 (0.97) Z: 8.86 (0.31)	X: 0.86 (0.01) Z: 0.92 (0.01)	X: -33.86 (1.72) Z: 15.13 (0.62)	X: 0.29 (0.02) Z: 0.15 (0.01)
Oblique	X: -17.07 (0.54) Z: 13.73 (0.47)	X: 1.08 (0.01) Z: 1.22 (0.02)	X: -24.93 (0.65) Z: 17.74 (0.81)	X: 0.25 (0.01) Z: 0.22 (0.01)

The calculated BrIC and PAIS values can be found in Table 46. Although the probability of sustaining AIS1 injury was found to be greater than 90% in all the impact locations, the oblique location produced greater angular velocity about the z axis than that observed in the lateral impacts – leading the higher BrIC and PAIS1-4 values. Statistically significant differences in the BrIC and PAIS 1-4 values were observed between the frontal location and the lateral and oblique locations, and between the lateral and oblique locations when comparing BrIC and PAIS 2-4 values.

Table 46.Mean and standard deviation values for calculated BrIC and PAIS1-4 calculated from the unprotected Hybrid-III headform response.

Impact Location	BrICValue	PAIS1 (%) (mean (SD))	PAIS2 (%) (mean (SD))	PAIS3 (%) (mean (SD))	PAIS4 (%) (mean (SD))
Frontal	0.16 (0.01)	90.67 (0.05)	2.40 (0.00)	0.60 (0.00)	0.34 (0.00)
Lateral	0.35 (0.01)	100.00 (0.11)	19.38 (0.00)	5.15 (0.00)	2.96 (0.00)
Oblique	0.41 (0.01)	100.00 (0.02)	29.10 (0.00)	8.10 (0.00)	4.69 (0.00)

8.2.2.2. LU headform

Representative angular response curves and response corridors observed in the unprotected LU impacts can be seen in Figure 90, with extracted parameters presented in Table 47. As observed in the Hybrid-III impacts, the lateral impact location produced the highest maximum angular velocity about a single axis (x axis), with statistically significant

differences observed between this and the frontal and oblique locations ($p < 0.039$). However, as in the Hybrid-III impacts, the oblique location produced a higher angular velocity about the z axis, along with higher steady state angular velocity and impulse with statistically significant differences observed relative to the other impact locations ($p < 0.022$). The frontal location produced the lowest maximum angular velocity, steady state angular velocity and impulse, but the highest estimated peak to peak sinusoidal angular acceleration, with statistically significant differences relative to the other impact locations ($p < 0.01$).

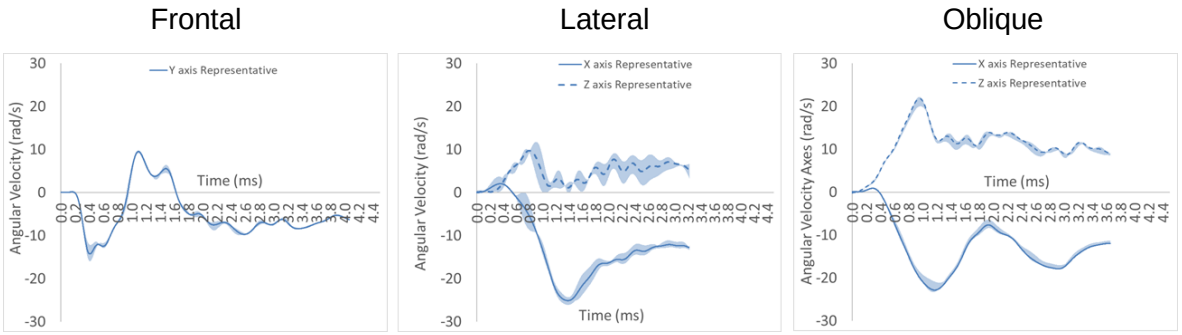

Figure 90. Representative angular response curves for each impact location on the LU headform.

Table 47. Mean and standard deviation values of the angular response during an unprotected impact using the LU headform.

Impact Location	Maximum Angular Velocity about axes of interest (rad/s) (mean(SD))	Time to Maximum Angular Velocity (ms) (mean (SD))	Maximum peak to peak α_{sine} (krad/s/s) (mean (SD))	Steady State Angular Velocity (rad/s) (mean (SD))	Impulse (kg m^2 s^{-1}) (mean (SD))
Frontal	Y: -14.46 (1.32)	Y: 0.41 (0.00)	Y: 55.16 (5.26)	Y: -6.55 (0.54)	Y: -0.13 (0.01)
Lateral	X: -25.31 (0.62) Z: 10.15 (0.83)	X: 1.37 (0.01) Z: 0.80 (0.02)	X: -28.93 (0.76) Z: 19.39 (1.08)	X: -12.31 (0.62) Z: 2.16 (0.72)	X: -0.20 (0.01) Z: 0.03 (0.01)
Oblique	X: -22.42(0.94) Z: 21.35 (0.96)	X: 1.19 (0.04) Z: 0.96 (0.01)	X: -31.45 (2.23) Z: 36.93 (3.61)	X: -11.96(0.25) Z: 9.54 (0.28)	X: -0.20 (0.00) Z: -0.16 (0.00)

As in the Hybrid-III impacts, the higher maximum and steady state angular velocity generated about the z axis resulted in higher $BrIC_{SS}$, $BrIC_{MAX}$, $PAIS1\text{-}4_{SS}$ and $PAIS1\text{-}4_{MAX}$ values at the Oblique location (as seen in Table 48 and Table 49). Statistically significant differences were found between all impact locations when comparing $BrIC_{MAX}$ and $PAIS2\text{-}4_{MAX}$ values ($p < 0.01$). When comparing values calculated using steady state angular velocity, statistically significant differences were observed between the frontal location and the lateral and oblique locations in $BrIC_{SS}$ and $PAIS1\text{-}4_{SS}$ and between the oblique and lateral locations in $BrIC_{SS}$ and $PAIS2\text{-}4_{SS}$ ($p < 0.036$).

Table 48. Mean and standard deviations for BrIC and PAIS values based on steady state angular velocity during the unprotected LU headform impacts.

Impact Location	$BrIC_{SS}$ Value (mean (SD))	$PAIS1_{SS}$(%) (mean (SD))	$PAIS2_{SS}$(%) (mean (SD))	$PAIS3_{SS}$(%) (mean (SD))	$PAIS4_{SS}$(%) (mean (SD))
Frontal	0.12 (0.01)	65.91 (0.27)	1.10 (0.00)	0.27 (0.00)	0.15 (0.00)
Lateral	0.19 (0.03)	97.84 (1.67)	3.86 (0.02)	0.96 (0.00)	0.55 (0.00)
Oblique	0.29 (0.01)	100.00 (0.05)	11.48 (0.00)	2.95 (0.00)	1.69 (0.00)

Table 49. Mean and standard deviation for BrIC and PAIS values based on maximum observed angular velocity during the unprotected LU headform impacts.

Impact Location	$BrIC_{MAX}$ Value (mean (SD))	$PAIS1_{MAX}$ (%) (mean (SD))	$PAIS2_{MAX}$ (%) (mean (SD))	$PAIS3_{MAX}$ (%) (mean (SD))	$PAIS4_{MAX}$ (%) (mean (SD))
Frontal	0.29 (0.03)	100.00 (1.57)	11.97 (0.02)	3.08 (0.00)	1.76 (0.00)
Lateral	0.46 (0.01)	100.00 (0.04)	37.21 (0.00)	10.80 (0.00)	6.29 (0.00)
Oblique	0.61 (0.03)	100.00 (1.23)	64.42 (0.01)	22.42 (0.00)	13.44 (0.00)

The angular response observed during the oblique impact that resulted in fracture can be found in Figure 91. As can be seen here, higher maximum and steady state angular velocity about the x and z axes were observed in the impact that resulted in fracture. In the x axis, the maximum angular velocity was found to be -26.91 rad/s in the fracture impact compared to -22.42 rad/s ±0.94 in the non-fracture impacts. The maximum peak to peak estimated sinusoidal acceleration about the x axis was also greater in the fracture impact (-34.43 krad/s/s) compared to the non-fracture impact (-31.45 krad/s/s ±2.23). This was also the case when comparing steady state angular velocity (-16.55 rad/s in the fracture impact compared to -11.97 rad/s ±0.25 in the non-fracture impacts). The same results were observed in the z axis, with higher maximum angular velocity (25.36 rad/s in the fracture impact compared to 21.35 rad/s ±0.96 in the non-fracture impacts), maximum peak to peak estimated sinusoidal acceleration (42.56 krad/s/s in the fracture impact compared to 36.93 krad/s/s ±3.61 in the non-fracture impacts) and steady state angular velocity (14.81 rad/s in the fracture impact compared to 9.53 rad/s ±0.28 in the non-fracture impacts) observed in the impact that resulted in fracture.

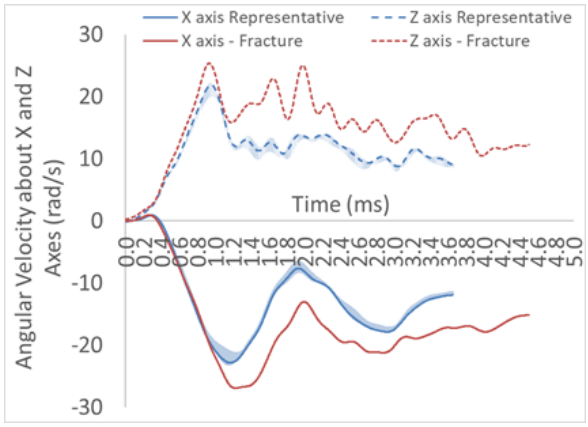

Figure 91. Angular response curves for the impacts that did and did not result in fracture when impacting the LU headform at the oblique location.

Representative angular responses observed in the unprotected impacts using the LU and Hybrid-III headforms can be found in Figure 92. It is clear from these and the results presented in Table 45 and Table 47, that the angular response observed when using the LU headform is different to the Hybrid-III response, particularly with respect to the maximum angular velocity values, which are again a result of the resonance frequency excitation of the LU headform. The steady state angular velocity values observed in the LU headform were however generally lower than those seen in the Hybrid-III. This led to $BrIC_{SS}$ and $PAIS_{SS}$ that were lower than that seen with the Hybrid-III, but higher $BrIC_{MAX}$ and $PAIS_{MAX}$.

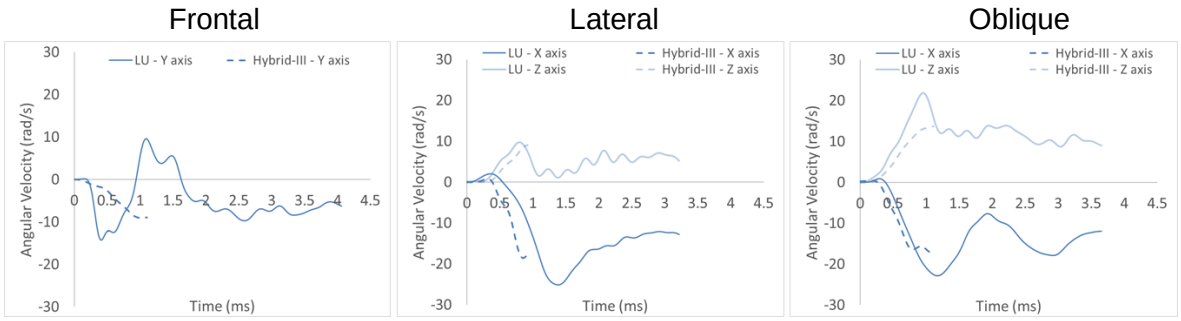

Figure 92.Comparison of representative angular response curves observed when using the Hybrid-III and LU headforms in unprotected impacts.

8.2.3. Helmeted Comparison

Representative linear and angular response curves from the unprotected and helmeted trials at each impact location using the Hybrid-III headform can be found in Figure 93. The percentage reduction in linear and angular parameters in each helmet type and at each location can be found in Table 50 and Table 51 respectively.

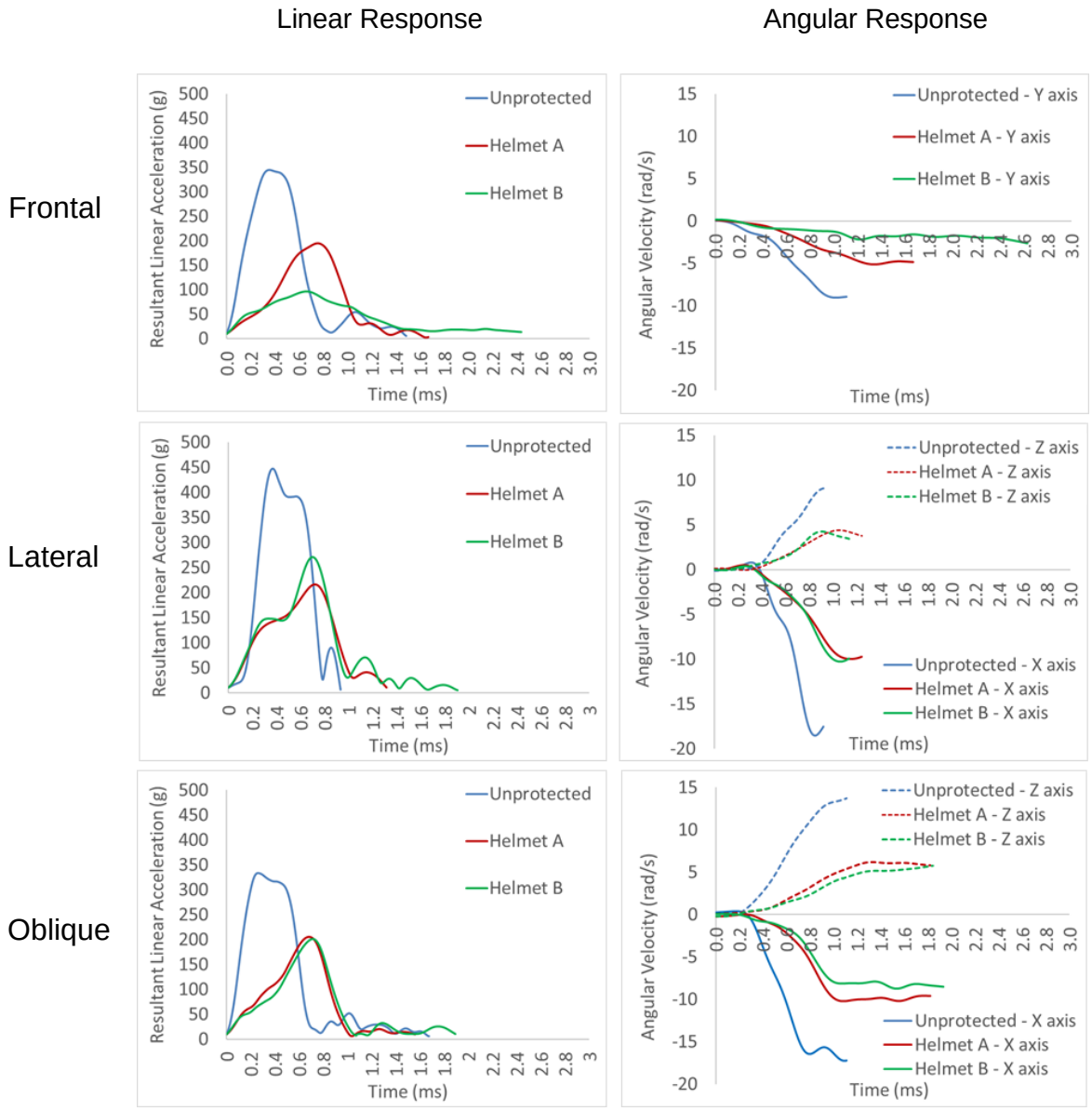

Figure 93. Representative linear and angular response curves from the unprotected and helmeted Hybrid-III impacts.

Table 50. Percentage change in mean linear parameters from the unprotected to the helmeted impacts using the Hybrid-III headform.

Helmet Type	Impact Locaton	Contact Time	Peak resultant linear acceleration	Time to Peak resultant linear acc.	Impulse	HIC
A	Frontal	16.50	-41.69	108.74	-29.74	-76.27
	Lateral	82.65	-51.35	96.76	-28.28	-75.93
	Oblique	8.38	-39.87	155.45	-32.43	-77.52
B	Frontal	118.21	-71.69	80.15	-34.54	-92.54
	Lateral	107.26	-40.77	89.49	-19.06	-69.63
	Oblique	8.55	-40.82	168.34	-34.78	-81.53

As can be seen here, both helmet types reduced the peak resultant linear acceleration, impulse and HIC while lengthening the contact time and time to peak resultant linear acceleration. At the frontal location, Helmet B reduced the peak resultant linear

acceleration, impulse and HIC and elongated the contact time more than Helmet A, whereas at the lateral location Helmet A reduced the peak resultant linear acceleration, impulse and HIC to a greater extent than Helmet B. At the oblique location, both helmet types produced similar changes in the linear response parameters outlined in Table 50.

Both helmets reduced the maximum angular velocity/impulse and maximum estimated angular acceleration while elongating the time to maximum angular velocity. Similar to the results observed in the linear response, at the frontal location, Helmet B showed greater reduction in these parameters than Helmet A. Although Helmet A showed greater reduction in linear parameters at the lateral location, both helmets produced similar reductions in angular parameters. At the oblique location, Helmet B showed greater reduction in angular parameters than Helmet A.

Table 51. Percentage changes in mean angular parameters from the unprotected to the helmeted impacts using the Hybrid-III headform.

Helmet Type	Impact Location	Maximum Angular Velocity/impulse about axes of interest	Time to Maximum Angular Velocity	Maximum Angular acceleration
A	Frontal	Y: -38.63	Y: 39.86	Y: -55.75
	Lateral	X: -47.14 Z: - 50.45	X: 35.06 Z: 15.22	X: -60.71 Z: -56.97
	Oblique	X: -39.03 Z: -55.70	X: 11.33 Z: 10.80	X: -44.09 Z: -60.03
B	Frontal	Y: -72.91	Y: 192.03	Y: -91.09
	Lateral	X: -43.51 Z: - 37.92	X: 24.15 Z: 3.26	X: -54.49 Z: -51.22
	Oblique	X: -49.90 Z: -58.26	X: 28.31 Z: 54.99	X: -59.98 Z: -73.08

The reductions in maximum angular velocity observed in Table 51 are reflected in the BrIC and PAIS values shown in Table 52. Here Helmet B shows greater reductions in BrIC and PAIS1-4 values in the frontal and oblique locations, whereas at the lateral location both helmets show similar reductions.

Table 52. Mean percentage change in calculated BrIC and PAIS1-4 when comparing unprotected to helmeted impacts using the Hybrid-III headform.

Helmet Type	Impact Location	BrIC Value	PAIS1 (%) (mean (SD))	PAIS2 (%) (mean (SD))	PAIS3 (%) (mean (SD))	PAIS4 (%) (mean (SD))
A	Frontal	-32.32	-40.14	-66.74	-66.94	-66.97
	Lateral	-47.54	-3.46	-82.51	-83.64	-83.79
	Oblique	-48.11	-0.55	-82.14	-83.92	-84.16
B	Frontal	-66.72	-89.08	-95.55	-95.59	-95.60
	Lateral	-44.98	-2.13	-80.03	-81.28	-81.45
	Oblique	-54.65	-2.87	-87.71	-89.01	-89.18

Figure 94 shows the representative linear and angular response curves observed in the unprotected and helmeted impacts at each impact location, using the LU headform. As can be seen here, the frequency response that was observed in the helmeted impacts remained present in the unprotected impacts, however the magnitude of the observed oscillations was greater in the unprotected impacts – suggesting increased resonance frequency excitation. The percentage change in the observed linear and angular parameters of each helmet type when compared to the unprotected values can be found in Table 53 and 54.

Table 53. Mean percentage change in mean linear parameters from the unprotected to the helmeted impacts using the LU headform.

Helmet Type	Impact Location	Contact Time	Peak resultant linear acceleration	Time to Peak resultant linear acc.	Impulse	HIC
A	Frontal	13.49	-65.41	456.71	-51.70	-88.41
	Lateral	33.35	-32.90	-37.30	2.96	-15.01
	Oblique	9.25	-59.43	-21.33	-52.79	-89.00
B	Frontal	-2.58	-83.24	790.20	-80.60	-98.75
	Lateral	21.84	-41.27	57.38	-3.68	-22.94
	Oblique	50.54	-53.82	28.87	-35.26	-80.63

Table 54. Mean percentage change in mean angular parameters from the unprotected to the helmeted impacts using the LU headform.

Helmet Type	Impact Location	Maximum Angular Velocity about axes of interest	Time to Maximum Angular Velocity	Maximum peak to peak sinusoidal angular acceleration	Steady State Angular Velocity/Impulse
A	Frontal	Y: -38.49	Y: 79.94	Y: -28.75	Y: -13.80
	Lateral	X: -58.32 Z: -25.71	X: -28.02 Z: 32.50	X: -42.00 Z: -12.43	X: -51.64 Z: -70.83
	Oblique	X: -70.48 Z: -80.40	X: 1.32 Z: 71.72	X: -65.91 Z: -89.06	X: -48.88 Z: -92.21
B	Frontal	Y: -76.62	Y: 93.04	Y: -79.88	Y: -61.33
	Lateral	X: -61.93 Z: -45.81	X: -20.84 Z: 20.00	X: -165.47 Z: -60.70	X: -39.65 Z: -19.44
	Oblique	X: -58.04 Z: -68.72	X: 133.23 Z: `241.14	X: -157.65 Z: -82.62	X: -33.00 Z: -70.63

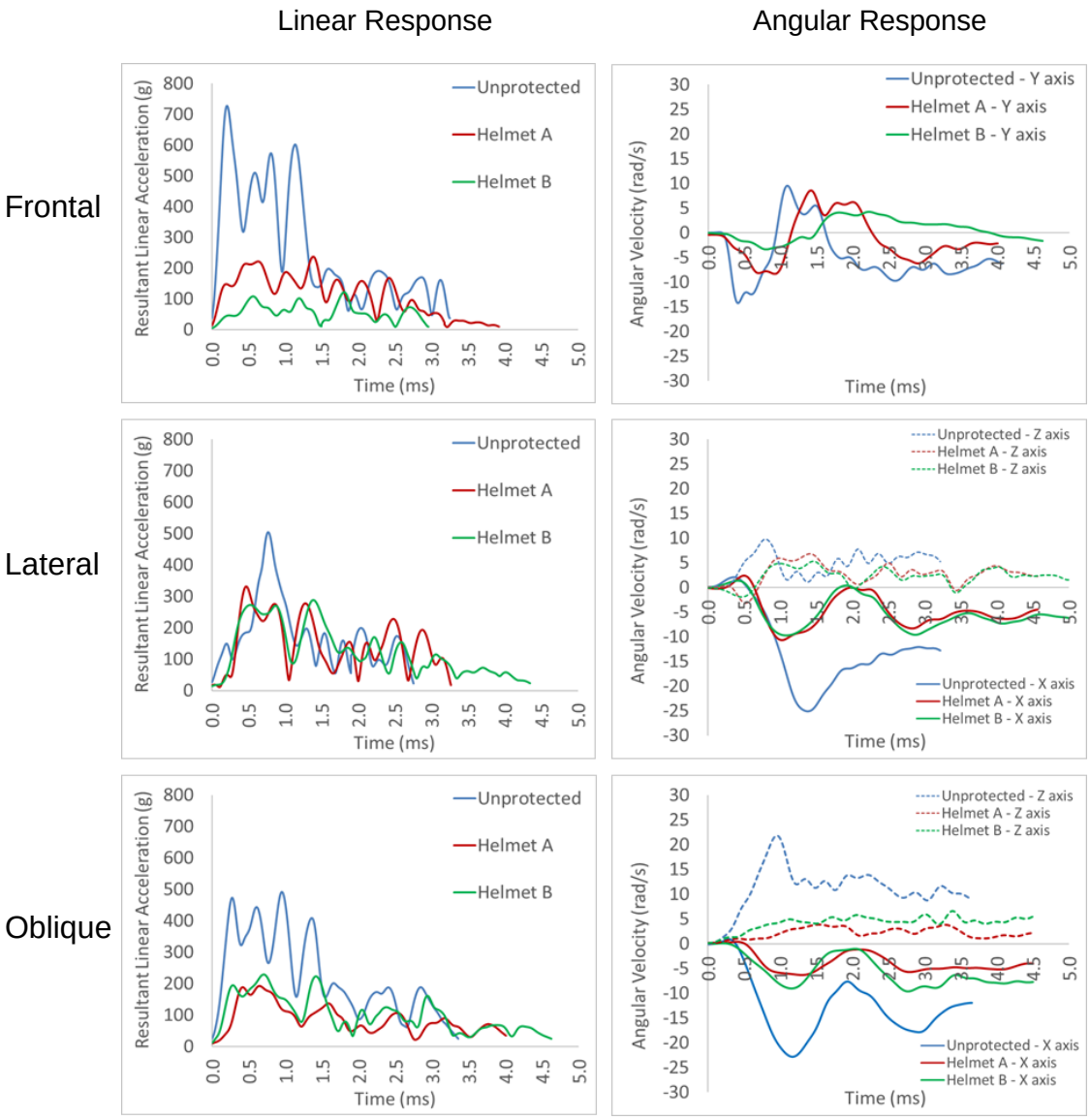

Figure 94. Representative linear and angular response curves from the unprotected and helmeted LU headform impacts.

Figure 94 and Table 53, both helmet types reduced the peak resultant linear acceleration and HIC values observed at each impact location. Contact time was elongated in all impact scenarios other than at the frontal location when using Helmet B. As observed in the Hybrid-III impacts, Helmet B produced greater reduction in peak resultant linear acceleration, impulse, HIC, maximum angular velocity, maximum peak to peak estimated sinusoidal angular acceleration and steady state angular velocity than Helmet A at the frontal location. At the lateral location Helmet B also showed a greater reduction in peak resultant linear acceleration, impulse and HIC than Helmet A, in addition to greater reduction in maximum angular velocity and maximum peak to peak estimated sinusoidal angular acceleration. At this location, Helmet A did however, show greater reduction in steady state angular velocity.

At the oblique location, Helmet A showed greater reductions in peak resultant linear acceleration, impulse, HIC, maximum angular velocity, and steady state angular velocity, but lower reduction in maximum peak to peak estimated sinusoidal angular acceleration than Helmet B.

The reduction in maximum and steady state angular velocity resulted in the reduction in $BrIC_{MAX}$, $BrIC_{SS}$, $PAIS1\text{-}4_{MAX}$ and $PAIS1\text{-}4_{SS}$ values, as shown in Table 55 and Table 56. Helmet A showed greater reductions in $BrIC_{SS}$, $BrIC_{MAX}$, $PAIS1\text{-}4_{SS}$ and $PAIS1\text{-}4_{MAX}$ at the oblique location, but lower reductions at the frontal location. At the lateral location, reductions in $BrIC_{SS}$ and $PAIS1\text{-}4_{SS}$ were similar in both helmet types.

Table 55. Mean percentage change in calculated $BrIC_{SS}$ and $PAIS1\text{-}4_{SS}$ when comparing unprotected and helmeted impacts using the LU headform.

Helmet Type	Impact Location	$BrIC_{SS}$	$PAIS1_{SS}$	$PAIS2_{SS}$	$PAIS3_{SS}$	$PAIS4_{SS}$
A	Frontal	-13.86	-23.29	-34.42	-34.51	-34.53
	Lateral	-35.15	-31.09	-70.36	-70.67	-70.71
	Oblique	-66.11	-57.66	-95.10	-95.31	-95.33
B	Frontal	-61.33	-89.40	-93.23	-93.26	-93.26
	Lateral	-33.92	-29.11	-68.75	-69.07	-69.11
	Oblique	-52.01	-22.80	-86.90	-87.41	-87.48

Table 56. Mean percentage change in calculated $BrIC_{MAX}$ and $PAIS1\text{-}4_{MAX}$ when comparing unprotected and helmeted impacts using the LU headform.

Helmet Type	Impact Location	$BrIC_{MAX}$	$PAIS1_{MAX}$	$PAIS2_{MAX}$	$PAIS3_{MAX}$	$PAIS4_{MAX}$
A	Frontal	-32.05	-1.58	-65.02	-66.28	-66.43
	Lateral	-44.61	-0.02	-77.63	-80.45	-80.83
	Oblique	-74.26	-11.81	-96.64	-97.61	-97.73
B	Frontal	-71.81	-71.09	-97.08	-97.21	-97.23
	Lateral	-52.73	-0.45	-85.51	-87.48	-87.75
	Oblique	-62.76	-0.22	-90.59	-93.20	-93.53

8.3. Discussion

The study presented in this chapter is the first research of its kind to assess unprotected head impacts representative of those see in Cricket using two headforms – the Hybrid-III and a sport specific headform (LU). Although the results presented here should be considered in the context of the limitations outlined in Chapter 7, it is clear from the results presented in this study, that the resonance frequency of the LU headform plays a significant role in the observed response. As discussed previously, the resonance frequency artefacts observed when using the LU headform should be considered legitimate response phenomenon given that the resonance frequency of the LU headform was representative of human skull (see Chapter 5), and the response observed in the LU headform was comparable to that

observed by Raymond et al. (2008) in similar impact conditions. As a result of the resonance frequency excitation, the LU headform showed longer contact times, and higher peak resultant acceleration, Impulse, and HIC values at all impact locations than those seen in the Hybrid-III headform. The frontal location showed the greatest difference in peak resultant linear acceleration, Impulse and HIC, where the LU headform produced values 2.05, 4.34 and 9.42 times greater than those observed in the Hybrid-III respectively. This may be due to the positioning of the linear accelerometer and angular rate sensors relative to the impact location and the bending modes of the headform, however further research should be done to confirm this. The LU headform also displayed greater maximum angular velocity about the principal axes of interest relative to that observed in the Hybrid-III. Whereas, the steady state angular velocity was higher than in the Hybrid-III impacts. This may be due to the increased compliance of the LU skull which, like the human skull, is likely to offer some energy absorbing capacity (van Lierde et al., 2003) but also leads to a higher response during initial loading.

The results observed in this study when using the Hybrid-III headform can be compared to previous studies that have utilised similar methodologies, using a comparable headform surrogate. McIntosh and Janda (2003) reported that when subjecting an unprotected 5th percentile female Hybrid-III headform to impacts with a Cricket ball travelling at 27 m/s, mean peak resultant linear acceleration was reported as 347 g – similar to that observed at the frontal and oblique location in this study (346.29 g ±11.25 and 335.95 g ±2.69 respectively), but lower than that observed at the lateral location (440.19 g ±2.18). However, as the values reported by McIntosh and Janda (2003) were averaged over three impact locations (frontal, lateral and rear), the variation in these results were overlooked. Additionally, the impact velocity of 27 m/s was lower than the 34.7 m/s used in this study, and the inertial properties of the 5th percentile female Hybrid-III headform are dissimilar to the 50th percentile male headform, which has been shown to influence the observed dynamic response (Oeur et al., 2019). Indeed, the discrepancy in the inertial properties of the headforms likely explains the similar peak resultant linear acceleration values observed by McIntosh and Janda (2003), despite the lower impact velocity. Finally, the Cricket ball type used in these impacts was not specified, and measurements of ball to ball variations in characteristics and degradation are not reported.

Yang et al. (2014) assessed the response of a 50th percentile male Hybrid-III headform mounted on a Hybrid-III neckform in helmeted and unprotected impacts representative of Baseball impacts. Yang et al. (2014), used impact locations similar to the frontal and oblique location defined in this study, along with a comparable impact speed of 34 m/s. At the frontal and oblique locations, Yang et al. (2014) reported peak resultant linear accelerations that

were 20.3 to 24.4% and 18.7 to 27.2% lower than the mean values observed in the Cricket impacts respectively. Yang et al. (2014) also reported HIC values that were 32.3 to 40% and 26.4 to 29.2% lower than those observed in this study at the frontal and oblique locations respectively. At the frontal location the peak angular acceleration values observed by Yang et al (25.2 to 26.8 krad/s/s) were larger than the estimated maximum angular accelerations (12.8 ±1.61 krad/s/s) observed in the Cricket impacts. The differences in the observed response of the Baseball and Cricket impacts may be due to the varied properties of the Baseball and Cricket balls (discussed in Chapter 3), but may also be influenced by the mounting technique used (Hybrid-III neckform vs ~Freely suspended)

The linear response of the unprotected Hybrid-III headform observed in this study was also greater than that previously reported by Walsh et al. (2011), who assessed the response of an unprotected Hybrid-III headform when subjected to impacts representative of those seen in American Football. At locations comparable to the frontal and lateral locations assessed in this study, Walsh et al. (2011) reported peak resultant linear acceleration values that were 64.97% and 59.83% lower than those observed in Cricket impacts investigated in this study. The angular acceleration reported at these locations were also just 30% and 27.7% of the estimated maximum sinusoidal angular acceleration in the Cricket impacts at the frontal and lateral locations respectively. Importantly though, the impact locations used by Walsh et al, were arranged to be slightly closer to the Frankfort plane than those used in this study. This would reduce the moment arm and therefore torque applied to the headform which would likely have contributed somewhat to the reduced angular response, but may have also increased the observed linear response. The peak linear resultant acceleration observed in the unprotected Hybrid-III impacts in this study was also found to be at least two times greater than values reported in American Football (Newman et al., 2000a; Pellman et al., 2003; Wilberger, 1993; Zanetti et al., 2013; Zhang et al., 2004), three times greater than that observed during concussive impacts in Rugby (McIntosh et al., 2000) and at least four times greater than that observed in Boxing (Walilko et al., 2005). The contact durations were much shorter in the Cricket impacts than in all of these impact scenarios.

Clark et al. (2017) assessed unprotected and helmeted scenarios observed to occur in Ice Hockey goaltenders, that were representative of puck impacts at 29.3 m/s. In this study, impact velocities were based on the minimum observed from video analysis, in an attempt to prevent damage to the unprotected NOCSAE headform. Therefore, the responses presented here are not a true representation of the worst-case scenario for this type of impact. In addition to this, the measured signals were filtered with a low pass filter set at 30Hz, thereby removing any legitimate resonance frequency artefacts that may have influenced the observed response and likely reduced the response to the rigid body motion. Regardless,

the peak resultant linear acceleration reported by Clark et al. (2017) during the unprotected puck impacts were maximally around 90g – 73% lower than the values observed in the unprotected Hybrid-III Cricket impacts and 82% lower than those observed in the unprotected LU headform impacts. The maximum angular velocity reported by Clark et al. (2017), was around 14.5 rad/s – comparable to the maximum angular velocity, and steady state angular velocity observed at the lateral and oblique locations in the Cricket impacts when using the Hybrid-III and LU headforms respectively, but lower than the maximum angular velocity values observed at the lateral and oblique locations when using the LU headform. These differences may be due to a number of factors, including the properties of the striker, impact speed, variations in impact location and filtering technique.

The responses observed, and injury metrics calculated during unprotected Hybrid-III and LU headform impacts were significantly higher than previously reported injury thresholds for mTBI. The peak resultant linear acceleration values observed at each impact location when using the Hybrid-III and LU headforms were all above the value corresponding to 95% probability of mTBI according to Newman et al. (2000a) and above the value corresponding to 50% probability of sustaining AIS6 injury, according to Newman (1986). When using the Hybrid-III headform, the calculated HIC values were above the level corresponding to 95% probability of mTBI (according to Zhang et al. (2004)), and close to the value corresponding to 'Severe but not life threatening' as reported by Shuaeib et al. (2002). The resonance frequency artefact observed when using the LU headform resulted in longer, and higher linear response curves, which resulted in higher HIC values. According to Hopes and Chinn (1989) and Horgan (2005), the HIC values observed in the frontal and oblique locations corresponded to 65% and 31% probability of death, while the lateral location corresponded to 16% probability of life-threatening injury. Although the angular velocity observed in the Hybrid-III headform was below that related to mTBI, the maximum angular accelerations ranged from mild to severe diffuse axonal injury, as reported by Gennarelli et al. (2003). The steady state angular velocity values observed at each impact location when using the LU headform were also below the threshold for mTBI reported by Gennarelli et al. (2003). The frontal and oblique locations produced maximum angular velocity values below the 25 rad/s threshold suggested by Gennarelli et al. (2003), whereas the lateral location was just above this. This variation in the injury metrics associated with angular acceleration and angular velocity was also observed by Clark et al. (2016b) when assessing puck impacts in ice hockey. In both the Hybrid-III and LU headforms, the lateral and oblique locations produced the highest BrIC and therefore PAIS1-4 values. At these locations the probability of sustaining PAIS2 injury was 19.28 and 29.10% respectively when using the Hybrid-III headform. When using the LU headform, these values were found to be 3.86 and 11.48%

when calculated using the steady state angular velocity, and 37.21 and 64.42% when calculated using the maximum angular velocity.

Importantly though, as discussed in Chapter 7, the direct application of these thresholds should be used with caution as the impact conditions and dynamic response observed in impacts representative of those seen in Cricket has been shown to be dissimilar to those used to develop the injury thresholds. This is particularly evident in the angular response of the Hybrid-III, where the angular acceleration value was related to potentially severe diffuse axonal injury, whereas the angular velocity was, for all but one impact scenario, below the level expected to produce mTBI. As a result of this, further work should look to elucidate injury thresholds in short duration, projectile impacts.

Raymond et al. (2008) subjected human cadaver heads to projectile impacts at 33.6 m/s using a metal puck 38 mm in diameter. In these impacts, a number of human cadavers presented depressed comminuted fractures. This type of fracture was also found in the LU headform during the impact that resulted in fracture (as shown in Figure 85). Similar to the results presented in this chapter, Raymond et al. (2008) reported that impacts resulting in fractures tended to produce higher resultant linear acceleration at the centre of gravity than those that did not.

McIntosh and Janda (2003) compared the response of an unprotected 5th percentile female Hybrid-III headform, to that observed in helmeted scenarios. Although helmeted results were reported at 19, 27, 36 and 45 m/s, unprotected results were only reported at 19 and 27 m/s. At 27 m/s, the peak resultant linear acceleration observed during helmeted impacts was reduced on average by 62.4% relative to the unprotected impacts. This reduction was greater than all the helmeted impact scenarios, other than Helmet B at the frontal location observed in the Hybrid-III Cricket impacts conducted in this study. This may be due to the lower impact speed of 27 m/s used by McIntosh and Janda (2003), compared to the 34.7 m/s utilised in this study. Indeed, McIntosh and Janda (2003) reported that the ability of Cricket helmets to attenuate impact force decreased as impact speed increased. Yang et al. (2014) reported that Baseball helmets reduced the peak linear acceleration and peak angular acceleration by around 62% and 75% respectively, when using the Hybrid-III headform at an impact speed of c.33 m/s. Clark et al. (2016a), utilised the NOCSAE headform and reported that during puck impacts, Ice Hockey goal tender helmets reduced peak resultant linear acceleration values by around 55 to 73% and angular velocity by around 50 to 62%, dependent on the impact location. The reductions in peak resultant linear acceleration and angular acceleration reported by Clark et al. (2016a) and Yang et al. (2014) were greater than all of the values observed in this study, other than Helmet B at the frontal

location, when using the Hybrid-III headform. When using the LU headform, both helmets produced reductions in peak resultant linear acceleration that were similar to those reported by Clark et al. (2016a) and Yang et al. (2014) at the frontal and oblique locations, whereas at the lateral location, lower reductions were observed in the Cricket impacts. Both helmets also produced reductions in maximum angular velocity that were similar to that reported by Clark et al. (2016a), and Helmet B produced reductions in estimated peak to peak maximum acceleration that were greater than that reported by Yang et al. (2014).

However, as the excitation of the resonance frequency of the headform has been shown to be a factor that has considerable effect on the observed dynamic response in these types of impact, comparing helmet performance based on the rigid body motion observed when using the Hybrid-III headform may be misleading. This is particularly important given that the reduction in linear and angular parameters when using the helmets varied when using either the Hybrid-III or LU headforms and based on impact location. As discussed in Chapter 7, further research should look to establish whether resonance frequency excitation is a potentially important mechanism for injury when considering mTBI in short duration projectile impacts, and if so, suitable headform surrogates should be used in the assessment of Cricket helmet performance.

In summary, the following conclusions can be drawn from this study:

- The unprotected dynamic response observed using the Hybrid-III is dissimilar to that observed when using the LU headform.
- The response observed when using the LU headform compares favourably with results previously reported using human cadavers with similar impact conditions. This increases the confidence in the biofidelity of the LU headform.
- Although the tested cricket helmets reduced the dynamic response of the headform in a number of parameters (ie peak linear acceleration, peak angular velocity), other parameters (ie steady state angular velocity) remained comparable to the unprotected scenarios.
- Although not a direct aim when developing the LU headform, the fracture observed when using this headform was similar to fractures observed in comparable real-life impact scenarios. Further work should look to validate this aspect of the response.

CHAPTER 9

Assessment of the Impact Attenuation Test Specified in the Current British Standard (BS 7928:2013)

9.1. Introduction

As discussed in Chapter 2, standards tests exist in order to ensure that products meet a suitable level of performance. Since manufacturers develop products to pass the relevant standard, it is imperative that the methods used and measurements taken when conducting standards tests are a suitable means of assessing product performance. Therefore, the impact characteristics of the standard tests must be representative of real-life impact scenarios, as a failure to ensure this may lead to ineffective PPE. It is important to note however, that this process is a compromise, as standards tests must also be affordable and practically convenient, to avoid additional costs being passed onto the consumer.

The current British Standard for Head Protectors for Cricketers (BS 7928:2013) is based around two principal tests. The penetration test is designed to ensure that a helmet and faceguard can prevent the occurrence of facial contact during projectile testing. In this test, an adult BOLA ball (as described in Chapter 3) is projected onto the helmet, mounted onto an EN 960 headform, at a number of locations and angles, with an impact speed of 28 ±3 m/s. If any part of the ball or helmet makes contact with the headform, the product is deemed to have failed. Although in Chapter 3, the dynamic properties of the BOLA ball were found to be unrepresentative of elite level Cricket balls, this ball was selected due to the better consistency and reduced degradation, and the subsequent reduction in incurred cost. Despite the unrepresentative properties of the BOLA ball, injury surveillance from the ECB suggests that, since the introduction of the penetration test to BS 7928:2013, the number of facial injuries in First-Class Cricket has drastically reduced (0 reported in 2018). This suggests that although the penetration test assesses the capability of a product to prevent facial contact during an impact with a BOLA ball, this has proved to be sufficient to also prevent facial contact when considering a Cricket ball.

The impact attenuation test is designed to ensure that the shell of the helmet can provide sufficient protection and prevent/limit the occurrence of skull fractures and brain injury. In this test, the test product is mounted onto an EN 960 headform, with a triaxial linear accelerometer mounted at the centre of gravity of the headform. This is dropped onto a rigid hemispherical anvil (diameter 73 mm) at 2.53 +0.01,-0 m/s, at four defined regions (though

specific impact locations are not defined). In this test, the peak resultant linear acceleration is used as the pass-fail criteria, with the maximal permittable value of 250 g. However, the mechanical characteristics of the defined test are dissimilar to those observed in real life projectile impacts and as such the external validity of this test may be questionable.

Ankrah and Mills (2003) stated the importance of accurately reflecting impact speed (due to strain rate dependencies of materials incorporated into the PPE), effective impact energy and momentum when developing standard tests that reflect real life scenarios. Table 57 shows a comparison of these parameters when considering the currently specified drop test using a 4.7 kg headform and average helmet mass of 0.938 kg, and a projectile impact using the same headform and helmet masses, with a 0.156 kg ball travelling at 34.7 m/s. It can be seen that there are clear differences between impact speed, effective impact energy and momentum between the two types of impact. As a result, observations made when using the standard drop test may not reflect those seen in real-life Cricket impacts. Indeed, Clark et al. (2018a) reported that, when assessing ice hockey goaltender masks, drop tests cannot be used to adequately describe projectile impacts.

Table 57. Comparison of impact characteristics of the BS7928:2013 impact attenuation test and the projectile tests outlined in Chapter 6.

	BS 7928:2013 Impact Attenuation Drop Test	Projectile Test
Impact Speed (m/s)	2.53	34.7
Effective Impact Energy (J)	18.04	93.92
Impact Momentum (kg.m/s)	14.26	5.41
Impactor Stiffness (kN/mm)	c.∞	0.79 – 2.44

Due to the clear differences in the mechanics of the currently specified drop tests and projectile tests, the external validity of the impact attenuation test currently specified in BS7928:2013 should be investigated. Therefore, the aim of this study is to assess the suitability of the currently specified impact attenuation test by comparing the observed dynamic response of a headform when subjected to the currently specified impact attenuation test to the previously presented projectile tests that are more representative of those seen in Cricket.

9.2. Methodology

Drop tests were conducted in line with the currently specified impact attenuation tests outlined in BS7928:2013, with some changes to the defined methodology. As the impact locations are vaguely defined in the current test standard, the frontal, lateral and oblique impact locations defined in Chapter 4 were used in this testing to allow the direct comparison

with the projectile tests. BS7928:2013 also specifies the sole use of a linear accelerometer to assess the severity of the impact. To provide a more thorough investigation of the current drop tests and provide a like-for-like comparison with the projectile tests, the headform used in the drop tests were instrumented with the same instrumentation (±2000g triaxial linear accelerometer and ±6000 triaxial angular rate sensor) described in Chapter 6.

A linear drop tower was used to drop the helmet and headform system on to a hemispherical (73 mm diameter) anvil, at the required impact speed defined in BS 7928:2013 (2.53 (+0.1/-0.0) m/s). A pair of lasers separated by a 10 mm distance were used to measure the velocity of the headform immediately prior to impact with the hemispherical anvil. Lubrication fluid was applied to the drop tower prior to each drop test to minimise friction. However as some degree of friction remained, testing was conducted to establish a suitable drop height to achieve the desired impact speed of 2.53 (+0.1/-0.0) m/s (schematic of experimental setup shown in Figure 95. Once the suitable drop height was established, a pin locking system was used to ensure that all drops were conducted from the defined height. Impact velocity was measured for each trial to ensure that this remained within the acceptable range.

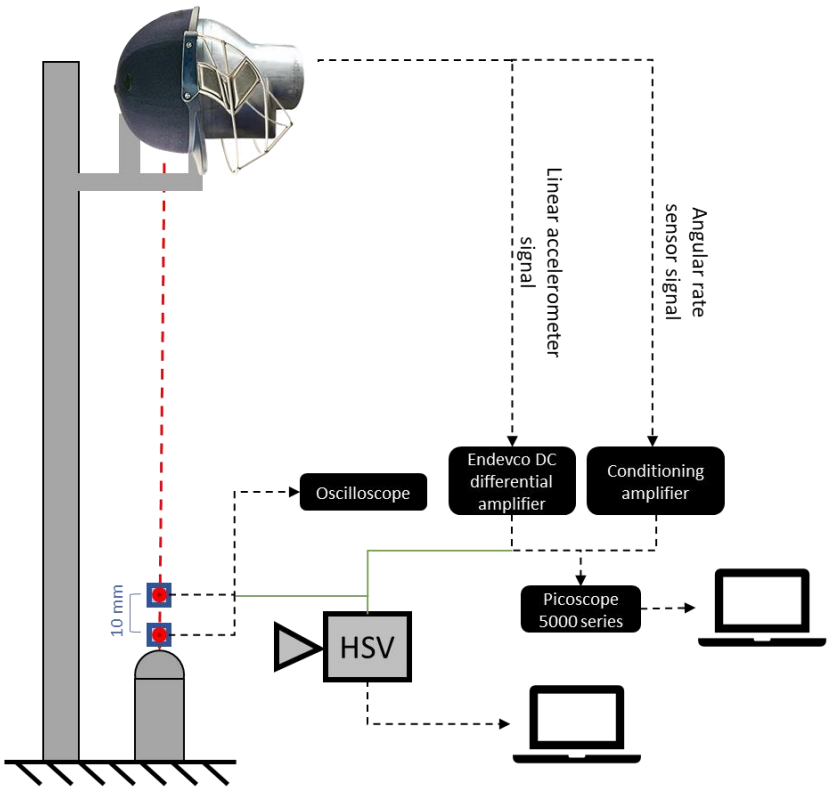

Figure 95. Schematic of experimental setup used to measure the dynamic response of the EN 960 headform during standard drop tests. The position of the helmeted headform can be adjusted to test alternative impact locations defined previously.

The triaxial linear accelerometer was screw mounted at the centre of gravity of the headform using the manufacturer supplied mounting block. Two threaded holes were positioned on the mounting block to allow the angular rate sensor to be screw mounted onto the same mounting block 25 mm below the linear accelerometer. As in the projectile impacts, the linear accelerometer was connected to a 9-channel charge Amplifier (Model CV9-V, DJB Instruments, UK) and the angular rate sensor was connected to an Endevco DC differential amplifier. The output from each of these was sampled at 1 MHz using a Picoscope 5000 series oscilloscope.

Three unused samples of each helmet type defined in Chapter 6 were used in this battery of drop tests. Each helmet was fitted on the headform as outlined in BS7928:2013, with the front edge of the helmet midway between the 'AA' line and the reference plane. A 50 N vertical force was applied to the crown of the helmet, and the chin strap was secured and positioned as recommended and tightened to a force of 100 N, measured using an Omega LC103B-25 S type load cell. Once the helmet was judged to be fitted appropriately, the helmet and headform system were positioned on the drop rig to achieve the desired impact location. Each helmet was impacted once at frontal location, followed by the lateral location, then the oblique location, with a minimum of five minutes between impacts.

A custom MATLAB script was written to process the linear and angular outputs. As described in Chapter 6, zero offset was removed from each axis of each sensor by subtracting the average of the first 5,000 data points of the signal, which was always prior to the initiation of impact. Sensitivity values were then applied to convert the voltage output to SI units. As conducted in the projectile test methods, cut off frequencies were defined based on residual analysis (as used in Chapter 6 and defined by Winter (1990)) and confirmed through visual assessment of the filtered and non-filtered curves. This process resulted in the linear acceleration and angular rate data being filtered using a fourth order low pass Butterworth filter set at 1.5 kHz. Resultant linear acceleration was calculated and used to identify the start and end of contact using a threshold defined as 2% of the peak resultant linear acceleration observed during the impact. The full resultant linear acceleration and angular velocity data was then truncated to just the period identified as contact. The resultant linear acceleration data was then used to identify contact time, peak resultant linear acceleration, time to peak resultant linear acceleration and calculate impulse and HIC. Angular velocity data was used to identify maximum angular velocity and time to maximum angular velocity, in addition to the estimation of angular acceleration and calculation of BrIC and PAIS1-4 values.

9.3. Results

9.3.1. Linear Response

Representative linear response curves and response corridors for both helmet types and impact locations can be found in Figure 96. As can be seen here (and as expected), the headform responded as a rigid body with minimal noise introduced from the excitation of the unrepresentative resonance frequency of the headform, which was observed in the projectile impacts using the same headform. As in Chapter 6, linear parameters were extracted from the entire contact period and can be found in Table 58. Unsurprisingly, both helmets tested would comfortably pass the impact attenuation component of the current British Standard test (BS7928:2013), which specifies threshold peak resultant linear acceleration value of 250g.

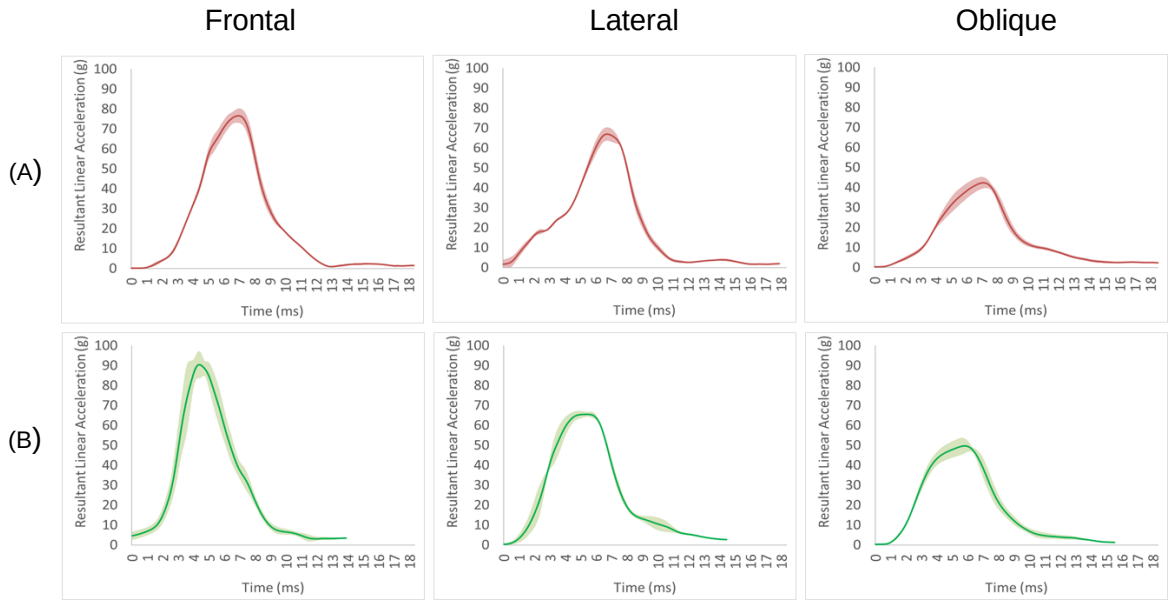

Figure 96. Response corridors and representative curves for the angular response of helmeted impacts using the EN 960 headform during impact attenuation tests specified in BS7928:2013.

Table 58. Mean and standard deviation values of key parameters extracted from the standard drop tests.

Helmet Type	Impact Location	Contact Time (ms) (mean (SD))	Peak resultant linear acceleration (g) (mean (SD))	Time to Peak resultant linear acc. (ms) (mean (SD))	Impulse (N.s) (mean (SD))	HIC (mean (SD))
A	Frontal	11.24 (0.26)	77.11 (3.53)	5.53 (0.44)	15.86 (0.27)	128.44 (9.74)
	Lateral	17.08 (1.22)	66.96 (3.35)	6.36 (0.26)	14.59 (0.37)	81.67 (3.96)
	Oblique	17.75 (0.16)	42.61 (2.76)	6.30 (0.37)	10.63 (0.15)	32.97 (3.74)
B	Frontal	13.13 (1.27)	93.67 (4.84)	4.51 (0.35)	16.60 (0.24)	105.63 (9.54)
	Lateral	14.11 (0.86)	66.43 (1.85)	4.62 (0.78)	15.03 (0.29)	106.62 (10.31)
	Oblique	14.64 (0.23)	50.39 (3.35)	5.08 (0.42)	11.83 (0.21)	57.79 (5.32)

As can be seen in Figure 96 and Table 58, unlike in the projectile impacts, the frontal location produced the highest peak resultant linear acceleration in both helmet types, with the shortest contact time and time to peak resultant linear acceleration values. In Helmet A statistically significant differences were found between the frontal and other locations when comparing contact time and HIC ($p < 0.015$), and the oblique location when comparing peak resultant linear acceleration, impulse and HIC ($p < 0.034$). In Helmet B, statistically significant differences were found between the oblique location and other locations when comparing peak resultant linear acceleration, impulse and HIC ($p < 0.02$). Statistically significant differences were also found when comparing the peak resultant linear acceleration observed at the frontal location to that observed at the lateral and oblique locations ($p < 0.001$).

Unlike in the projectile impacts, at the frontal location the only statistically significant difference between the two helmet types was found when comparing peak resultant linear acceleration ($p < 0.019$), with Helmet B producing higher values than Helmet A. No statistically significant differences were found at the lateral location in any of the parameters in Table 58. At the oblique location, Helmet B produced shorter contact time and time to peak resultant linear acceleration along with higher peak resultant linear acceleration, impulse and HIC all of which were found to be statistically significant ($p < 0.031$).

9.3.2. Angular Response

Figure 97 shows the representative curves and response corridors for the angular responses observed in both helmet types, across all impact locations for the contact duration as identified from the linear response curve. Table 59 shows parameters extracted from the contact phase and estimated angular accelerations. In both helmet types, statistically significant differences were found when comparing the maximum angular velocity observed at the frontal location, compared to the highest value observed in the other impact locations ($p < 0.034$). In Helmet B, statistically significant differences were also found when comparing

the maximum angular acceleration observed at the frontal location, compared to the highest value observed in the other impact locations ($p < 0.004$). No statistically significant differences were found when comparing the maximum angular velocity about the x axis in the lateral and oblique locations ($p > 0.55$). There were however statistically significant differences between the maximum angular velocity, maximum angular acceleration and impulse about the z axis ($p < 0.001$).

At the frontal location, statistically significant differences were found between Helmets A and B with the former producing greater maximum angular velocity, maximum angular acceleration and impulse ($p < 0.02$). At the lateral location there were no statistically significant differences between the helmets in any of the parameters in Table 59 ($p > 0.212$). There were also no statistically significant differences between the lateral and oblique locations when comparing the response about the x axis ($p > 0.155$). Statistically significant differences were, however, found when comparing the maximum angular velocity, maximum angular acceleration and impulse about the z axis ($p > 0.031$), with the oblique location producing greater values than the lateral.

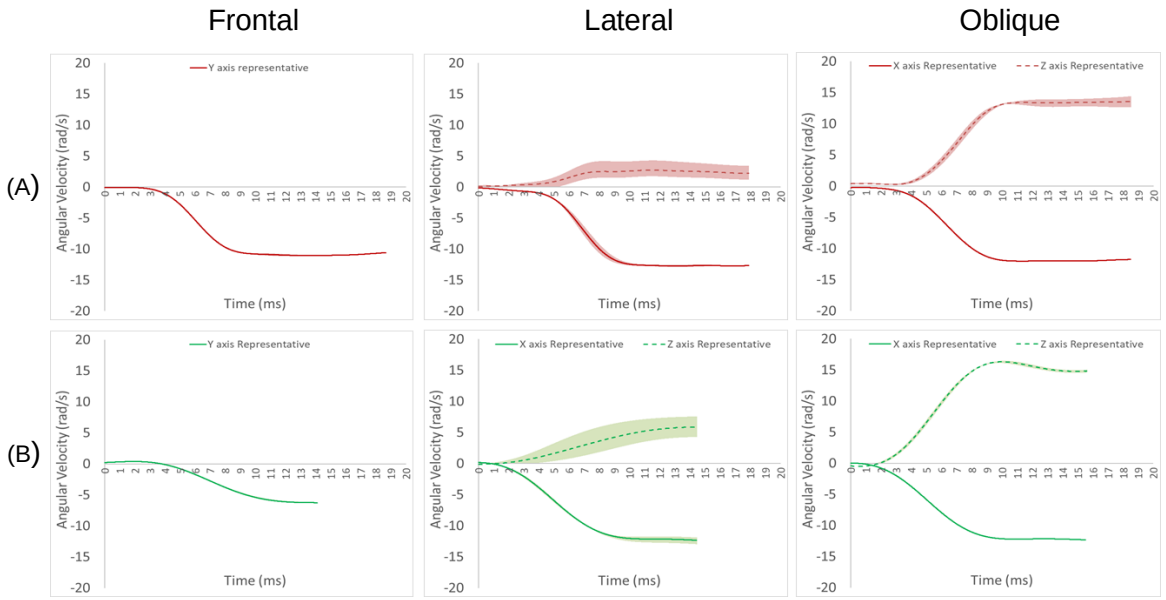

Figure 97. Response corridors and representative curves for the angular response of helmeted impacts using the EN 960 headform during impact attenuation tests specified in BS7928:2013.

Table 59. Mean and standard deviation values of measured and calculated angular response parameters during the standard drop tests

Helmet Type	Impact Location	Maximum Angular Velocity about axes of interest (rad/s) (mean (SD))	Time to Maximum Angular Velocity (ms) (mean (SD))	Maximum Angular acceleration (krad/s/s) (mean (SD))	Impulse (kg m^2 s^{-1}) (mean (SD))
A	Frontal	Y: -11.04 (0.09)	Y: 11.25 (0.25)	Y: -1.54 (0.03)	Y: -0.35 (0.00)
	Lateral	X: -12.74 (0.13) Z: 3.95 (0.34)	X: 13.06 (0.08) Z: 11.33 (0.23)	X: -1.53 (0.01) Z: 1.05 (0.16)	X: -0.34 (0.00) Z: 0.08 (0.01)
	Oblique	X: -12.03 (0.05) Z: 13.75 (0.51)	X: 11.34 (1.40) Z: 13.00 (3.72)	X: -1.69 (0.20) Z: 1.83 (0.60)	X: -0.32 (0.00) Z: 0.27 (0.01)
B	Frontal	Y: -6.24 (0.08)	Y: 11.68 (0.42)	Y: -0.84 (0.04)	Y: -0.20 (0.00)
	Lateral	X: -12.31 (0.36) Z: 5.87 (1.36)	X: 14.12 (0.86) Z: 14.66 (0.31)	X: -1.38 (0.12) Z: 0.78 (0.19)	X: -0.33 (0.01) Z: 0.12 (0.02)
	Oblique	X: -12.29 (0.28) Z: 16.32 (0.16)	X: 12.11 (1.79) Z: 9.46 (0.14)	X: -1.62 (0.19) Z: 2.71 (0.02)	X: -0.33 (0.00) Z: 0.32 (0.01)

Table 60 shows the calculated BrIC and PAIS1-4 values for each helmet type and impact location, based on the measured maximum angular velocities. As observed in the projectile impacts, the oblique location produced greater BrIC and PAIS 2-4 values than the frontal and lateral locations, that were statistically significant ($p < 0.001$) in both helmet types, due to the previously discussed higher angular velocity about the z axis. In Helmet B, statistically significant differences were also found between the frontal location and other impact locations when comparing BrIC and PAIS 1-4 values ($p < 0.001$).

Table 60. Mean and standard deviation values for calculated BrIC and PAIS1-4 during the standard drop tests.

Helmet Type	Impact Location	BrIC Value	PAIS1 (%) (mean (SD))	PAIS2 (%) (mean (SD))	PAIS3 (%) (mean (SD))	PAIS4 (%) (mean (SD))
A	Frontal	0.20 (0.00)	98.37 (0.11)	4.13 (0.07)	1.03 (0.02)	0.59 (0.01)
	Lateral	0.21 (0.01)	99.01 (0.62)	4.81 (0.61)	0.84 (0.15)	0.48 (0.09)
	Oblique	0.37 (0.01)	100.00 (0.00)	22.02 (1.61)	5.93 (0.48)	3.42 (0.28)
B	Frontal	0.12 (0.01)	59.40 (0.69)	0.94 (0.18)	0.23 (0.05)	0.13 (0.03)
	Lateral	0.23 (0.02)	99.71 (0.33)	6.71 (1.38)	1.69 (0.36)	0.97 (0.20)
	Oblique	0.42 (0.00)	100.00 (0.00)	30.90 (0.20)	8.68 (0.07)	5.03 0.04)

9.3.3. Comparison with Projectile Tests

The representative linear response curves measured during the projectile tests (as shown previously in Figure 70) are compared to representative curves measured during the standard drop tests in Figure 98 and extracted parameters compared in Table 61. It is clear from the representative curves and extracted parameters that the standard drop tests produced a different linear response to that observed in the projectile tests. Statistically significant differences in contact time and time to peak resultant acceleration were observed between the standard drops and the projectile impacts in both helmet types, in all impact locations ($p < 0.001$). Statistically significant differences were also observed between the standard drops and projectile impacts when considering peak resultant linear acceleration in all impact scenarios ($p < 0.001$), other than when comparing to Helmet B at the lateral location when using the Hybrid-III headform. Impulse and HIC values were found to vary based on headform type, impact location and test method.

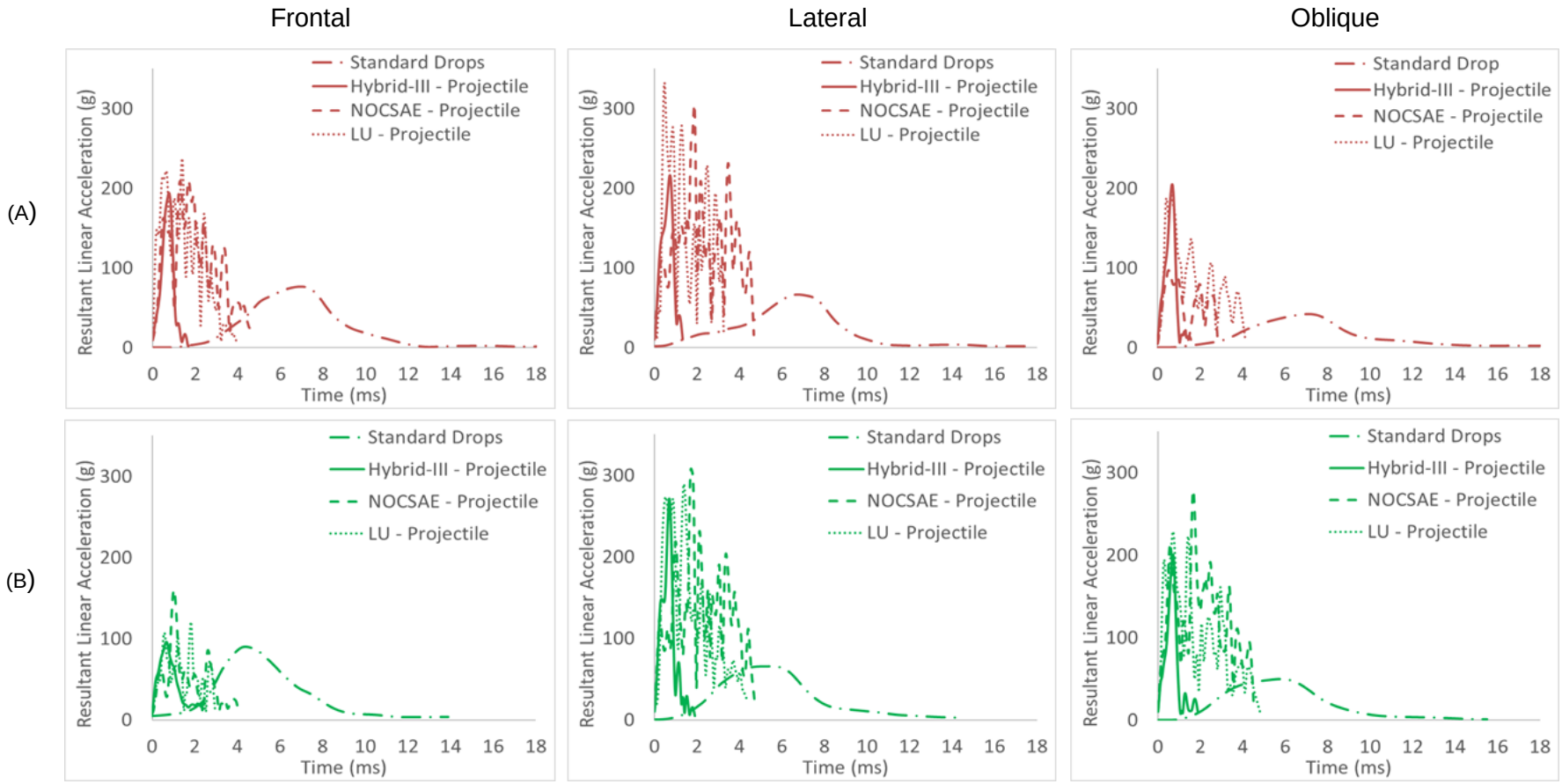

Figure 98. Representative linear response curves observed in the standard drop tests and those observed during the more realistic projectile impacts (as shown previously in Figure 70).

Table 61. Comparison of linear parameters extracted from standard drop tests and projectile tests using the Hybrid-III, NOCSAE and LU headforms.

Impact Location	Helmet Type	Headform /Method	Contact Time (ms) (mean (SD))	Peak resultant linear acceleration(g) (mean(SD))	Time to peak resultant linear acc. (ms) (mean (SD))	Impulse (N.s) (mean (SD))	HIC (mean (SD))
Frontal	A	Hybrid-III	1.72 (0.07)	201.91 (5.57)	0.76 (0.03)	5.84 (0.48)	142.00 (14.92)
		NOCSAE	4.59 (0.08)	222.57 (14.04)	1.79 (0.07)	21.35 (1.65)	484.18 (103.47)
		LU	3.68 (0.36)	245.87 (6.03)	1.13 (0.36)	17.46 (0.66)	653.15 (24.60)
		Standard Drop	11.24 (0.26)	77.11 (3.53)	5.53 (0.44)	15.86 (0.27)	128.44 (9.74)
	B	Hybrid-III	3.23 (0.29)	98.05 (5.23)	0.66 (0.03)	5.44 (0.44)	44.63 (2.06)
		NOCSAE	4.01 (0.05)	166.91 (4.76)	1.02 (0.01)	8.97 (0.41)	70.32 (6.53)
		LU	3.16 (0.04)	119.11 (1.84)	1.81 (0.00)	7.01 (0.15)	70.31 (3.77)
		Standard Drop	13.13 (1.27)	93.67 (4.84)	4.51 (0.35)	16.60 (0.24)	105.63 (9.54)
Lateral	A	Hybrid-III	1.70 (0.31)	214.17 (18.47)	0.72 (0.01)	6.59 (0.82)	204.17 (40.51)
		NOCSAE	4.63 (0.03)	302.08 (3.43)	1.87 (0.01)	28.51 (0.82)	869.60 (61.27)
		LU	4.78 (0.06)	332.34 (7.96)	0.48 (0.02)	23.74 (0.69)	991.69 (108.84)
		Standard Drop	17.08 (1.22)	66.96 (3.35)	6.36 (0.26)	14.59 (0.37)	81.67 (3.96)
	B	Hybrid-III	1.92 (0.01)	260.74 (16.86)	0.69 (0.02)	7.44 (0.12)	257.65 (12.56)
		NOCSAE	5.89 (0.01)	322.50 (17.95)	1.73 (0.02)	34.38 (1.64)	1082.15 (128.74)
		LU	4.36 (0.01)	290.89 (3.95)	1.21 (0.27)	22.21 (0.83)	899.11 (100.59)
		Standard Drop	14.11 (0.86)	66.43 (1.85)	4.62 (0.78)	15.03 (0.29)	106.62 (10.31)
Oblique	A	Hybrid-III	1.88 (0.01)	202.02 (7.91)	0.68 (0.02)	5.47 (0.13)	134.75 (5.63)
		NOCSAE	2.82 (0.02)	102.78 (9.70)	0.54 (0.05)	8.12 (0.48)	79.53 (12.08)
		LU	4.10 (0.07)	198.42 (9.13)	0.57 (0.10)	14.64 (1.50)	303.96 (77.98)
		Standard Drop	17.75 (0.16)	42.61 (2.76)	6.30 (0.37)	10.63 (0.15)	32.97 (3.74)
	B	Hybrid-III	1.89 (0.03)	198.80 (1.55)	0.71 (0.00)	5.28 (0.04)	110.71 (3.12)
		NOCSAE	5.71 (0.02)	273.59 (8.25)	1.67 (0.01)	28.96 (0.91)	755.49 (50.23)
		LU	5.65 (0.38)	225.85 (28.46)	0.94 (0.02)	20.08 (0.26)	535.36 (78.54)
		Standard Drop	14.64 (0.23)	50.39 (3.35)	5.08 (0.42)	11.83 (0.21)	57.79 (5.32)

Figure 99 shows the representative angular response curves measured in the projectile tests (as shown in Figure 79) with those observed in the standard drops tests, with extracted parameters shown in Table 62. As in the linear responses, it is clear that the standard drops produce an angular response that is dissimilar to that observed in the more realistic projectile tests. At the frontal and oblique impact locations, the maximum angular velocity and maximum peak to peak estimated sinusoidal angular acceleration observed in the standard drops was greater than that seen in the projectile tests when using any headform. At the lateral location, the NOCSAE headform produced higher maximum angular velocity about the x axis than the standard drops in both helmet types, but lower maximum angular velocity about the z axis in Helmet A.

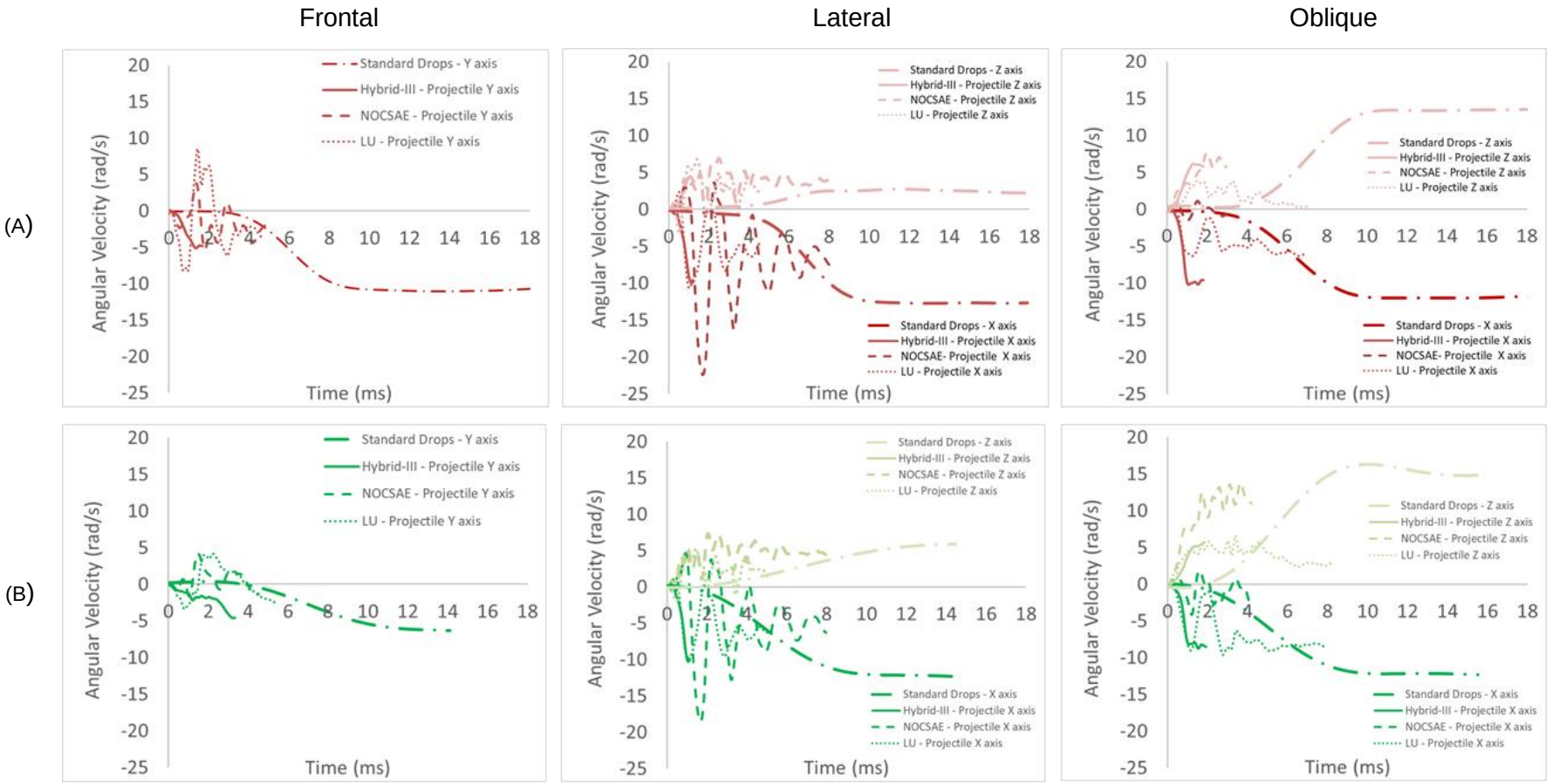

Figure 99. Representative angular response curves observed in the standard drop tests and those observed during the more realistic projectile impacts (as shown previously in Figure 79).

Table 62. Comparison of angular parameters extracted from standard drop tests and projectile tests using the Hybrid-III, NOCSAE and LU headforms.

Impact Location	Helmet Type	Headform /Method	Maximum Angular Velocity (rad/s) (mean (SD))	Time to max Angular velocity (ms) (mean (SD))	Maximum peak to peak sinusoidal Angular acceleration (krad/s/s) (mean (SD))	Steady State Angular velocity (rad/s) (mean (SD))	Impulse (Ns) (mean (SD))
Frontal	A	Hybrid-III	Y: -5.29 (0.12)	Y: 1.50 (0.23)	Y: -5.67 (0.75)	Y: -5.29 (0.12)	Y: -0.11 (0.00)
		NOCSAE	Y: -6.27 (0.98)	Y: 1.80 (0.08)	Y: -38.94 (5.22)	Y: -2.86 (0.59)	Y: -0.07 (0.01)
		LU	Y: -8.89 (0.58)	Y: 0.74 (0.07)	Y: 39.30 (2.17)	Y: -5.64 (0.35)	Y: -0.11 (0.01)
		Standard Drop	Y: -11.04 (0.09)	Y: 11.25 (0.25)	Y: -1.54 (0.03)	Y: -11.04 (0.09)	Y: -0.35 (0.00)
	B	Hybrid-III	Y: -2.33 (1.64)	Y: 3.12 (0.38)	Y: -1.14 (0.77)	Y: -2.33 (1.64)	Y: -0.05 (0.03)
		NOCSAE	Y: 4.19 (0.48)	Y: 1.48 (0.03)	Y: 21.03 (0.86)	Y: -0.48 (0.41)	Y: -0.01 (0.01)
		LU	Y: -3.38 (0.31)	Y: 0.80 (0.02)	Y: 11.10 (1.36)	Y: -2.53 (0.12)	Y: -0.05 (0.00)
		Standard Drop	Y: -6.24 (0.08)	Y: 11.68 (0.42)	Y: -0.84(0.04)	Y: -6.24 (0.08)	Y: -0.20 (0.00)
Lateral	A	Hybrid-III	X: -9.85 (1.42)	X: 1.17 (0.03)	X: -13.30 (2.21)	X: -9.85 (1.42)	X: -0.16 (0.02)
			Z: 4.39 (0.79)	Z: 1.06 (0.03)	Z: 6.51 (1.31)	Z: 4.39 (0.79)	Z: 0.06 (0.01)
		NOCSAE	X: -22.03 (0.59)	X: 1.69 (0.00)	X: 64.56 (1.62)	X: -5.81 (0.24)	X: -0.11 (0.00)
			Z: 7.00 (0.08)	Z: 2.47 (0.07)	Z: 34.27 (1.86)	Z: 4.04 (0.11)	Z: 0.07 (0.01)
		LU	X: -10.55 (0.55)	X: 0.99 (0.03)	X: -16.78 (1.29)	X: -5.95 (0.18)	X: -0.10 (0.00)
			Z: 7.54 (0.58)	Z: 1.06 (0.03)	Z: 16.98 (1.43)	Z: 3.69 (0.60)	Z: 0.06 (0.01)
		Standard Drop	X: -12.74 (0.13)	X: 13.06 (0.08)	X: -1.53 (0.01)	X: -12.74 (0.13)	X: -0.34 (0.00)
			Z: 3.95 (0.34)	Z: 11.33 (0.23)	Z: 1.05 (0.16)	Z: 3.95 (0.34)	Z: 0.08 (0.01)
	B	Hybrid-III	X: -10.53 (0.26)	X: 1.07 (0.01)	X: -15.41 (0.41)	X: -10.53 (0.26)	X: -0.17 (0.00)
			Z: 5.50 (0.55)	Z: 0.95 (0.07)	Z: 7.38 (0.42)	Z: 5.50 (0.55)	Z: 0.03 (0.01)
		NOCSAE	X: -19.45 (0.75)	X: 1.67 (0.04)	X: 51.77 (2.55)	X: -5.65 (0.25)	X: -0.10 (0.00)
			Z: 7.93 (0.41)	Z: 2.10 (0.05)	Z: 39.14 (3.36)	Z: 4.43 (0.36)	Z: 0.07 (0.01)
		LU	X: -9.64 (0.09)	X: 1.09 (0.02)	X: -18.94 (0.94)	X: -7.43 (0.75)	X: -0.12 (0.01)
			Z: 5.50 (0.16)	Z: 0.96 (0.07)	Z: 7.62 (0.89)	Z: 2.58 (0.62)	Z: 0.04 (0.01)
		Standard Drop	X: -12.31 (0.36)	X: 14.12 (0.86)	X: -1.38 (0.12)	X: -12.31 (0.36)	X: -0.33 (0.01)
			Z: 5.87 (1.36)	Z: 14.66 (0.31)	Z: 0.78 (0.19)	Z: 5.87 (1.36)	Z: 0.12 (0.02)
Oblique	A	Hybrid-III	X: -10.41 (0.17)	X: 1.20 (0.18)	X: -13.94 (1.92)	X: -10.41 (0.17)	X: -0.17 (0.00)
			Z: 6.08 (0.06)	Z: 1.35 (0.02)	Z: 7.09 (0.18)	Z: 6.08 (0.06)	Z: 0.11 (0.00)
		NOCSAE	X: -1.70 (0.12)	X: 1.00 (0.04)	X: -2.70 (0.29)	X: -0.59 (0.14)	X: -0.01 (0.01)
			Z: 7.19 (0.36)	Z: 2.04 (0.03)	Z: 5.54 (0.35)	Z: 5.77 (0.17)	Z: 0.10 (0.00)
		LU	X: -6.62 (0.93)	X: 1.20 (0.17)	X: 10.72 (3.27)	X: -6.12 (0.54)	X: -0.10 (0.01)
			Z: 4.18 (0.23)	Z: 1.64 (0.18)	Z: 4.04 (0.41)	Z: 0.74 (0.49)	Z: 0.01 (0.01)
		Standard Drop	X: -13.75 (0.51)	X:13.00 (3.72)	X: -1.69 (0.20)	X:-13.75 (0.51)	X: -0.27 (0.01)
			Z: 12.03 (0.05)	Z: 11.34 (1.40)	Z: 2.71 (0.02)	Z: 12.03 (0.05)	Z: 0.32 (0.00)
	B	Hybrid-III	X: -8.55 (0.18)	X: 1.38 (0.22)	X: -9.98 (1.55)	X: -8.55 (0.18)	X: -0.14 (0.00)
			Z: 5.73 (0.21)	Z: 1.89 (0.03)	Z: 4.77 (0.14)	Z: 5.73 (0.21)	Z: 0.10 (0.00)
		NOCSAE	X: -4.02 (0.32)	X: 2.27 (0.01)	X: -9.12 (1.12)	X: -0.65 (1.55)	X: -0.01 (0.03)
			Z: 12.25 (1.28)	Z: 1.75 (0.06)	Z: 11.03 (1.29)	Z: 11.22 (1.27)	Z: 0.19 (0.02)
		LU	X: -9.41 (0.21)	X: 2.77 (0.01)	X: -18.94 (0.94)	X: -8.02 (0.31)	X: -0.13 (0.01)
			Z: 6.68 (0.36)	Z: 3.26 (0.18)	Z: 7.62 (0.89)	Z: 2.80 (0.13)	Z: 0.05 (0.00)
		Standard Drop	X: -16.32 (0.16)	X: 9.46 (0.14)	X: -1.62 (0.19)	X: -16.32 (0.16)	X: -0.32 (0.00)
			Z: 12.29 (0.28)	Z: 12.11 (1.79)	Z: 2.71 (0.02)	Z: 12.29 (0.28)	Z: 0.33 (0.01)

Table 63 and Table 64 show the calculated $BrIC_{MAX}$, PAIS 1-4_{MAX}, $BrIC_{SS}$ and PAIS 1-4_{SS} values observed during the projectile and standard drop tests. As expected, these results tend to mirror those observed in the maximum and steady state angular velocity. Statistically significant differences were observed between BrIC and PAIS1-4 values when comparing the standard drop tests to the projectile impacts when using the Hybrid-III in the frontal and oblique locations ($p < 0.005$) but not the lateral location ($p > 0.555$). The standard drops also produced significantly higher $BrIC_{SS}$ and PAIS 1-4_{SS} than the NOCSAE and LU headforms at all impact locations ($p < 0.001$). Statistically significant differences were observed between standard drops and projectile impacts using the NOCSAE and LU

headforms when comparing the $BrIC_{MAX}$ and PAIS 1-4_{MAX} values at the oblique location ($p < 0.001$), with the standard drops producing higher values. The NOCSAE headform did however produced significantly lower $BrIC_{MAX}$ and PAIS 1-4_{MAX} values than the standard drops.

Table 63. BrIC and PAIS1-4 values calculated based on maximum angular velocity.

Impact Location	Helmet Type	Headform /Method	$BrIC_{MAX}$	$PAIS1_{MAX}$	$PAIS2_{MAX}$	$PAIS3_{MAX}$	$PAIS4_{MAX}$
Frontal	A	Hybrid-III	0.11 (0.01)	54.27(0.00)	0.80 (0.00)	0.20 (0.00)	0.11 (0.00)
		NOCSAE	0.14 (0.02)	81.04 (0.01)	1.69 (0.00)	0.42 (0.00)	0.24 (0.00)
		LU	0.20 (0.02)	98.42 (0.00)	4.16 (0.00)	1.04 (0.00)	0.59 (0.00)
		Standard Drop	0.20 (0.00)	98.4 (0.00)	4.10 (0.00)	1.00 (0.00)	0.60 (0.00)
	B	Hybrid-III	0.05 (0.02)	9.90 (0.01)	0.11 (0.00)	0.03 (0.00)	0.01 (0.00)
		NOCSAE	0.08 (0.01)	28.17 (0.00)	0.34 (0.00)	0.08 (0.00)	0.05 (0.00)
		LU	0.08 (0.01)	28.91 (0.00)	0.35 (0.00)	0.09 (0.00)	0.05 (0.00)
		Standard Drop	0.10 (0.01)	59.4 (0.07)	0.90 (0.00)	0.20 (0.00)	0.1 (0.00)
Lateral	A	Hybrid-III	0.18 (0.03)	96.54 (0.02)	3.39 (0.00)	0.84 (0.00)	0.48 (0.00)
		NOCSAE	0.39 (0.01)	100 (0.00)	25.01 (0.00)	6.83 (0.00)	3.94 (0.00)
		LU	0.25 (0.03)	99.98 (0.02)	8.32 (0.00)	2.11 (0.00)	1.21 (0.00)
		Standard Drop	0.20 (0.01)	99.01 (0.01)	4.81 (0.01)	1.20 (0.00)	0.69 (0.00)
	B	Hybrid-III	0.19 (0.01)	97.87 (0.00)	3.87 (0.00)	0.96 (0.00)	0.55 (0.00)
		NOCSAE	0.38 (0.01)	100 (0.00)	24.31 (0.00)	6.61 (0.00)	3.81 (0.00)
		LU	0.22 (0.01)	99.55 (0.00)	5.39 (0.00)	1.35 (0.00)	0.77 (0.00)
		Standard Drop	0.20 (0.00)	99.71 (0.01)	6.71 (0.01)	1.69 (0.00)	0.97 (0.00)
Oblique	A	Hybrid-III	0.22 (0.00)	99.45 (0.00)	5.20 (0.00)	1.30 (0.00)	0.74 (0.00)
		NOCSAE	0.17 (0.01)	93.76 (0.00)	2.80 (0.00)	0.70 (0.00)	0.40 (0.00)
		LU	0.16 (0.01)	88.19 (0.00)	2.17 (0.00)	0.54 (0.00)	0.31 (0.00)
		Standard Drop	0.40 (0.01)	100 (0.02)	22.02 (0.02)	5.93 (0.00)	3.42 (0.00)
	B	Hybrid-III	0.19 (0.01)	97.13 (0.00)	3.58 (0.00)	0.89 (0.00)	0.51 (0.00)
		NOCSAE	0.30 (0.03)	100 (0.02)	13.00 (0.00)	3.36 (0.00)	1.93 (0.00)
		LU	0.23 (0.01)	99.78 (0.00)	6.06 (0.00)	1.52 (0.00)	0.87 (0.00)
		Standard Drop	0.40 (0.00)	100 (0.00)	30.90 (0.00)	8.68 (0.00)	5.03 (0.00)

Table 64. BrIC and PAIS1-4 values calculated based on steady state angular velocity.

Impact Location	Helmet Type	Headform /Method	$BrIC_{SS}$	$PAIS1_{SS}$	$PAIS2_{SS}$	$PAIS3_{SS}$	$PAIS4_{SS}$
Frontal	A	Hybrid-III	0.11 (0.01)	54.27 (0.00)	0.80 (0.00)	0.20 (0.00)	0.11 (0.00)
		NOCSAE	0.05 (0.01)	9.90 (0.00)	0.11 (0.00)	0.03 (0.00)	0.01 (0.00)
		LU	0.11 (0.01)	50.56 (0.00)	0.72 (0.00)	0.18 (0.00)	0.10 (0.00)
		Standard Drop	0.20 (0.00)	98.40 (0.00)	4.10 (0.00)	1.00 (0.00)	0.60 (0.00)
	B	Hybrid-III	0.05 (0.02)	9.90 (0.01)	0.11 (0.00)	0.03 (0.00)	0.01 (0.00)
		NOCSAE	0.01 (0.01)	0.12 (0.00)	0.00 (0.00)	0.00 (0.00)	0.00 (0.00)
		LU	0.05 (0.01)	6.99 (0.00)	0.07 (0.00)	0.02 (0.00)	0.01 (0.00)
		Standard Drop	0.10 (0.01)	59.40 (0.07)	0.9 (0.00)	0.20 (0.00)	0.10 (0.00)
Lateral	A	Hybrid-III	0.18 (0.03)	96.54 (0.02)	3.39 (0.00)	0.84 (0.00)	0.48 (0.00)
		NOCSAE	0.13 (0.00)	70.50 (0.0)	1.24 (0.00)	0.31 (0.00)	0.17 (0.00)
		LU	0.12 (0.02)	67.43 (0.00)	1.14 (0.00)	0.28 (0.00)	0.16 (0.00)
		Standard Drop	0.20 (0.01)	99.01 (0.01)	4.81 (0.01)	1.20 (0.00)	0.69 (0.00)
	B	Hybrid-III	0.19 (0.01)	97.87 (0.00)	3.87 (0.00)	0.96 (0.00)	0.55 (0.00)
		NOCSAE	0.13 (0.01)	74.47 (0.00)	1.39 (0.00)	0.34 (0.00)	0.20 (0.00)
		LU	0.13 (0.02)	69.36 (0.00)	1.21 (0.00)	0.30 (0.00)	0.17 (0.00)
		Standard Drop	0.20 (0.00)	99.71 (0.01)	6.71 (0.01)	1.69 (0.00)	0.97 (0.00)
Oblique	A	Hybrid-III	0.22 (0.00)	99.45 (0.00)	5.20 (0.00)	1.30 (0.00)	0.74 (0.00)
		NOCSAE	0.13 (0.01)	74.90 (0.00)	1.41 (0.00)	0.35 (0.00)	0.20 (0.00)
		LU	0.10 (0.02)	42.34 (0.00)	0.56 (0.00)	0.14 (0.00)	0.08 (0.00)
		Standard Drop	0.40 (0.01)	100 (0.02)	22.02 (0.02)	5.93 (0.00)	3.42 (0.00)
	B	Hybrid-III	0.19 (0.01)	97.13 (0.00)	3.58 (0.00)	0.89 (0.00)	0.51 (0.00)
		NOCSAE	0.26 (0.04)	99.99 (0.04)	8.92 (0.00)	2.27 (0.00)	1.30 (0.00)
		LU	0.14 (0.01)	77.20 (0.00)	1.50 (0.00)	0.37 (0.00)	0.21 (0.00)
		Standard Drop	0.40 (0.00)	100 (0.00)	30.90 (0.00)	8.68 (0.00)	5.03 (0.00)

9.4. Discussion

The standard drop test results presented in this study showed that the frontal location produced the greatest peak resultant linear acceleration and shortest time to peak resultant linear acceleration in both helmet types. This was not the case in the helmeted projectile tests, where the lateral location was found to produce the greatest peak resultant linear acceleration in both helmet types. When considering the angular response, Helmet A was found to produce relatively consistent maximum angular velocity at each impact location. However, Helmet B showed higher angular velocity at the oblique location.

The contact time, time to peak resultant linear acceleration, and time to maximum angular velocity observed in the standard drop tests were all found to be significantly longer than that observed in the projectile impacts. These results are in line with those presented by Clark et al. (2018a), who found that when assessing ice hockey goaltender masks using drop and projectile tests, the former produced significantly longer impact durations. The differences in contact time and time to peak resultant linear acceleration observed in this study indicate differences in the loading rate during impact. In the projectile tests, the rapid loading will likely produce an increased strain rate relative to that observed in the standard drop tests, which is likely to influence the stiffness and damping properties of the materials incorporated into the PPE (Ling et al., 2018), and therefore influence the protective capacity of the equipment.

Contrary to the results presented by Clark et al. (2018a), the results presented in this study show the peak resultant linear acceleration to be significantly lower in the drop tests than that observed in the projectile tests. These differences in the peak resultant linear acceleration results are likely due to the variations in helmet design and construction, and potentially influenced by variations in impact characteristics such as impact location, speed and projectile properties, in addition to the filtering process used by Clark et al. (2018a). However, as also reported by Clark et al. (2018a), typically the maximum and steady state angular velocity values were also greater in the drop tests.

During the drop tests, the HIC values observed in the standard drop tests were lower than the 136 threshold value suggested by King et al. (2003) in all impact scenarios. This is in contrast to the results observed in the projectile impacts, where most impact scenarios produced significantly higher HIC values, particularly when using the NOCSAE and LU headforms, due to the previously discussed effect of the resonance frequency of these headforms. The Hybrid-III produced HIC values that were more similar to those observed in the standard drop tests, but remained higher in all but one impact scenario (frontal location,

Helmet B). The calculated BrIC and PAIS1-4 values were greater in the standard drop tests than during the projectile impacts when using the Hybrid-III headform, particularly at the frontal location. The BrIC and PASI1-4 values derived from the standard drop tests were comparable to those observed when using the LU headform during projectile tests when calculated using the maximum angular velocity value observed in the projectile tests at the frontal and lateral locations. However, the BrIC and PAIS1-4 values calculated using the steady state angular velocity observed during the projectile impacts using the LU headform were lower than that observed during the standard drop tests. This was also the case when considering the projectile tests using the NOCSAE headform at the frontal and oblique locations. At the lateral location, the NOCSAE headform produced higher BrIC and PAIS1-4 values when calculated using the maximum angular velocity value, however this is potentially due to a potentially erroneous noise component, as discussed previously.

Therefore, the results of this study and those previously observed in projectile impacts suggest that the dynamic response of the EN 960 headform during the impact attenuation test currently specified in BS7928:2013 is dissimilar to that observed in more realistic projectile impact scenarios. This is unsurprising given the differences in impact conditions outlined in Table 57. This conclusion is consistent with that of McIntosh and Janda (2003), who reported that when testing Cricket helmets, projectile and drop tests produced differing results, and those of Clark et al. (2018a) who reported that drop tests were an inadequate means of assessing ice hockey goaltender masks.

The differences in the mechanics observed between the standard drop tests and projectile tests may have important implications for the assessment of PPE. The shorter contact duration will subject the materials incorporated into the PPE to higher strain rates than those observed in the standard drop tests and as such, may influence the ability of the materials to absorb/attenuate the impact energy. Variations in the impact conditions shown in Table 57 may also influence the effect of the geometric design off a helmet on the observed dynamic response of the headform. The potential effect of this can be seen in Helmet B at the frontal location. This helmet produced significantly lower peak resultant linear acceleration than Helmet A in the projectile impacts and significantly higher values in the standard drop tests. As previously mentioned, the sloped peak of Helmet B results in a slight deviation of the ball path during projectile impacts, which in turn is likely to produce a reduced peak resultant linear acceleration. Although the impact location remained consistent in the standard drop tests, the increased mass of the headform and anvil resulted in a minimal diversion of the impact path and therefore a more direct impact.

As stated in previous chapters, further work is required to develop the understanding of the injury mechanisms associated with the development of mTBI in projectile impacts in Cricket. Although we cannot yet compare the probable injury mechanisms in projectile and standard drop tests, these are likely to vary given the differences in the observed mechanical response outlined here. As such, it may be prudent to initiate a shift in the standard test methodology away from the currently specified drop tests to a more realistic projectile test method.

However, this is not a simple task, and does pose additional challenges that require further consideration. Firstly, a shift towards a projectile test would require the implementation of a different headform, as the currently specified EN 960 headform was found to produce dynamic response results that were corrupted by non-biofidelic resonance frequency artefacts. The Hybrid-III headform may be considered a repeatable, and relatively biofidelic alternative when considering rigid body motion, but does not account for the excitation of the resonance frequency of the skull, which as discussed in Chapters 7 and 8, may be an important factor related to the development of injury. Secondly, a suitably realistic test ball would also be required in a projectile based impact attenuation test. The approach used in this study (to utilise elite level Cricket balls and conduct repeat testing to ensure representative properties) would likely be financially unviable for test houses and so an alternative solution would be required to prevent additional cost being passed to the consumer. Finally, although the ability to propel the specified test balls at representative ball speeds should not be a problem, given the penetration test currently specified in BS7928:2013, variations in accuracy and speed would need to be checked to ensure that suitable repeatability of the desired impact characteristics could be achieved.

In summary:

- Significant differences were observed between the standard drop tests and more realistic projectile impacts.
- The varied impact mechanics may have a significant influence on the performance of PPE during standard testing, relative to impacts that are likely to be seen in real-life.
- A shift towards a more representative standard test is recommended, although the challenges associated with doing so are significant.

CHAPTER 10

Conclusions and Recommendations for Future Work

10.1 Conclusions

The research presented in this thesis addressed a number of the short comings evident in the current literature to improve the understanding of the mechanics of head impacts in Cricket. This was achieved through a systematic investigation of each component of the framework outlined in Figure 14 which led to a number of novel and important findings.

It can be concluded that Cricket balls exhibit different characteristics based on the construction and materials used, the orientation of the ball at impact and the level of wear. Indeed, the Dukes balls were found to be at least 15% stiffer than the Kookaburra balls and the Kookaburra balls were found to be 30.6, 13.1 and 9.0% more compliant in the seam orientation than in the face at the low, medium and high-speed impacts respectively. In addition, after 20 repeated high-speed impacts, the Dukes and Kookaburra balls were found to be at least 36.3 and 20.5% more compliant respectively. Additionally, it can be concluded that Cricket balls differ in characteristics to Cricket training balls since both Cricket balls were found to be at least three times stiffer than the Cricket training ball, but also showed greater ball to ball variation. This study highlighted the need to use a representative impact ball during laboratory-based tests and to monitor changes in ball properties throughout. The research presented here led to the selection of the Kookaburra ball (impacting in the face orientation) as a suitable test ball as this was a good representation of real-life impacts while showing better ball to ball consistency and slower degradation relative to the Dukes. In addition to this, the importance of the assessment of ball properties throughout the impact tests was established and non-destructive methods were identified as a means of ensuring suitable consistency.

Based on the materials and construction of the Hybrid-III, EN 960 and NOCSAE headforms, the development of a headform that was capable of producing realistic first order dynamic responses during projectile impacts was deemed necessary. From the research presented in this thesis it has been demonstrated that it is possible to produce a headform (LU headform) consisting of a skull, external soft tissue and brain components with improved geometric, inertial and material properties within the required time and financial constraints for use in protected and unprotected head impacts in Cricket. The headform geometry was manipulated to match that reported for a 50th percentile UK male (as reported by Peebles and Norris (1998)), with skull and external soft tissue thicknesses within previously reported

ranges (Hodgson et al., 1970; Lin et al., 2008; Lynnerup, 2001; Mahinda and Murty, 2009; McElhaney et al., 1970). The principal MoI and MoI at the CoG of the headform has been shown to accurately represent the average values presented in the literature to within 10.01% and 6.55% respectively. Furthermore, empirical evidence found the inertial properties of the manufactured headform to be within 3.8% of the calculated values. The inherent validity of the LU headform was established through material tests which showed each component to be comparable to values reported for human tissue. In addition, the resonance frequency of the skull component of the LU headform was found to be comparable to that reported for dry human skulls. The response of the LU headform during drop test and projectile impact tests was found to be within the range reported in human cadaver responses with similar impact conditions.

The research concerning ball characteristics and novel headform development coupled with ball tracking data collected during elite match-play facilitated the development of a test methodology that was a better representation of head impacts observed in Cricket than that achieved in previous research. This was used to derive, for the first time, dynamic response data at three impact locations, in helmeted and unprotected scenarios. A number of important conclusions can be drawn from the projectile impact tests presented in this thesis.

Firstly, it was determined that the dynamic response observed during the helmeted and unprotected projectile impacts was influenced by the headform that was used. The sensor mounting block used in the EN 960 headform was found to introduce non-biofidelic frequency artefacts at a similar frequency to the underlying response frequency. As these could not be removed without significant signal distortion, it was determined that this headform is unsuitable for the assessment of projectile head impacts in Cricket. Although the Hybrid-III responded predominantly as a rigid body, the response observed in the NOCSAE and LU headforms was found to contain additional frequency components, which were present even in the helmeted impacts. In the LU headform, these artefacts were in-line with the measured resonance frequencies of the skull component. This resulted in longer contact times when using the LU and NOCSAE headforms (excluding Helmet B at the frontal location, the Hybrid-III impacts were at least 33.3% shorter), despite comparable initial loading phases in a number of impact scenarios. These findings concurred with Hodgson et al. (1967), McElhaney et al. (1973) and Thomas and Hodgson (1969), who suggested that impacts of a duration shorter than 6 ms would result in resonance frequency excitation. Indeed, Raymond et al. (2008) showed that the resonance frequency excitation occurred when subjecting human cadaver heads to projectile impacts with similar conditions to those seen in the lateral location in this study. As such, the observed frequency artefacts

measured when using the LU headform should be considered a legitimate impact phenomenon that warrants further research. Although the materials and construction of the NOCSAE headform suggest this should respond with biofidelic resonance frequencies, and therefore be a better representation of the human head than the Hybrid-III, the response observed at the lateral location warrants further research, given that this is similar to a classical spring-dampener system. As this could have been introduced from an alternative source (such as the sensor mounting block), it therefore may be unrepresentative of a human head. Overall the results presented in this thesis highlight the importance of using suitably biofidelic surrogates (such as the LU headform) when assessing head impacts in Cricket, and other short duration impacts typical of those observed in projectile impacts, even in protected scenarios.

As reported in head impacts in other sports, it can also be concluded that impact location influences the observed dynamic response of the headforms during helmeted and unprotected impacts. When using the Hybrid-III, Helmet A was found to produce similar peak resultant linear acceleration values across all three impact locations (maximal differences of 5.7%). Whereas, when using Helmet B, and in the unprotected impacts, the lateral location produced the highest peak resultant linear acceleration (at least 50.7% greater than other locations). In the unprotected impacts and when using either helmet type, the lateral location generally produced the highest maximum angular velocity value about an individual orthogonal axis (in this instance the x axis). However, in addition to comparable angular velocity about the x axis, the oblique location produced higher angular velocity about the z axis, resulting in higher BrIC and PAIS1-4 values at this location. When using the LU headform, the frontal location produced the highest peak resultant linear acceleration in the unprotected impacts (at least 30.3% higher than other locations), and the lateral location produced the highest peak resultant linear acceleration when using either helmet (at least 22.4% higher than other locations). In the unprotected impacts, the lateral location produced the highest maximum angular velocity and steady state velocity about a single axis, but as in the Hybrid-III impacts, the oblique location produced significant motion about the x and z axes leading the higher $BrIC_{MAX}$ and $BrIC_{SS}$ values (at least 24.6 and 34.5% greater than other locations respectively). When using Helmet A, the lateral location produced the highest maximum and steady state angular velocities and therefore higher $BrIC_{MAX}$ and $BrIC_{SS}$ values (at least 36 and 8.3% greater than other locations respectively). In Helmet B, the maximum and steady state angular velocities, and $BrIC_{MAX}$ and $BrIC_{SS}$ were comparable in the lateral and oblique locations (maximal differences of 7%).

It can also be concluded that, relative to unprotected impacts, currently available helmets reduce the linear and angular response observed during head impacts in Cricket.

Additionally, as skull fracture resulting from helmeted impacts is a rare (or non-existent) occurrence in match-play, and that fracture was observed in the unprotected impacts but not the helmeted impacts when using the LU headform, it may also be concluded that helmets reduce the likelihood of this type of injury. Typically, when using both headforms, the helmeted responses reported in this thesis produced shorter contact times and higher peak linear and angular parameters than those previously reported in American Football, Rugby and Boxing, but within the range of values reported in baseball and ice hockey. When using the Hybrid-III headform, the peak resultant linear acceleration, maximum angular velocity, HIC and BrIC values were reduced by at least 39.9, 37.9, 69.6 and 32.3% respectively when helmeted. When using the LU headform, peak resultant linear acceleration, maximum angular velocity, HIC, $BrIC_{MAX}$ and $BrIC_{SS}$ were reduced by at least 32.9, 25.7, 15.0, 32.05 and 13.86% respectively when helmeted. Helmets A and B showed comparable responses at the lateral and oblique locations, whereas Helmet B produced a greater reduction in the linear and angular response at the frontal location – potentially due to the geometric design of Helmet B. When using the LU headform, all but one helmeted impact scenario produced HIC values above 333, which King et al. (2003) reported as corresponding to 75% probability of sustaining mTBI. In the unprotected impacts using the LU headform, the HIC values observed in the frontal and oblique locations corresponded to 65% and 31% probability of death, while the lateral location corresponded to 16% probability of life-threatening injury. However, as the HIC was not developed for short duration impacts where resonance frequency excitation is likely to occur, this should be used with caution. This is also the case for all of the injury thresholds discussed in this thesis, and as such it can be concluded that the development of injury thresholds for these types of impact should be a focus of future work.

The research presented in this thesis is also the first of its kind to assess the effect of repeated impacts on the performance of Cricket helmets. From this it can be concluded that repeated impacts reduce a helmets ability to attenuate the linear and angular response during an impact despite minimal external damage. In Helmet A, peak resultant linear acceleration, impulse and HIC were found to increase by 149, 61 and 385% respectively after five impacts at the frontal location. The same parameters increased by 43, 57.5 and 128% in Helmet B. Maximum angular velocity was found to increase by 108 and 40 % from the first to fifth impact in helmets A and B respectively, whereas the steady state angular velocity remained more consistent (change of -3% and 7% in Helmets A and B respectively). The effect of the repeated impacts varied between helmets A and B – a factor which may also be attributed to the geometric differences between the helmets at this location.

Through a comparison of the dynamic response observed during the projectile impacts with those derived from drop tests (conducted as specified in the current British Standard), it can be concluded that these test methods produce different dynamic responses. The drop tests were found to produce contact time and time to peak resultant linear acceleration at least 61.4 and 59.9% longer than the projectile tests respectively. With the exception of Helmet B in the frontal location, peak resultant linear acceleration was at least 161.8% lower in the standard drop tests. Generally, the steady state angular velocity was greater in the standard drop tests, and although the maximum angular velocity observed when using the LU and NOCSAE headforms was comparable to that of the standard drops in a number of impact scenarios, the time to maximum angular velocity was at least 65.5% shorter in the projectile tests.

Although the standard test appears to have achieved what it aimed to do when introduced (i.e. ensure PPE can prevent skull fracture), the drop test currently specified in BS7928:2013 should be considered unrepresentative of projectile impacts observed in real-life scenarios and as such may be inappropriate in the prevention of mTBI. These differences in impact characteristics and observed dynamic response likely induce varied PPE performance due to differing material properties as a result of the altered strain rates experienced by materials incorporated in the PPE. Due to differences between the standard drop tests and projectile tests observed in this chapter, a move towards a more realistic projectile test in the standard is recommended.

10.2 Recommendations for Future Work

The work presented in this thesis provides an important step in the understanding of the mechanics of head impacts in Cricket. There are a number of avenues that could utilise the work presented in this thesis to continue to develop the knowledge and understanding in this area. Future work should look to elaborate on the following points.

- Á Although the work concerned with ball characteristics presented here assessed two elite level cricket balls and a cricket training ball, the methodology presented here should be utilised to assess other ball types. This should include white and pink balls (used in elite one-day and day/night matches respectively), and balls used at sub-elite levels.
- Á In this thesis, ball tracking data was used to determine impact speed, using a database of release speeds, and the application of a model based on a limited number of observations made on release and ‘at batsman’ speed. As this is likely sensitive to a number of factors (including, but not limited to, pitch construction,

atmospheric/environmental conditions and ball type/degradation), future work should look to derive more data of this type to complete a more thorough investigation using observations made at multiple time points, and on multiple pitches. Additionally, the raw high-speed video collected by HawkEye (though currently only stored for a couple of minutes) could be used to determine additional impact characteristics such as location, angle and head position.

- The design of the LU headform presented in this thesis was based on data reported for a 50th percentile UK male. However, future work may look to tune the geometry, tissue thicknesses and inertial properties of the headform to match other populations (for instance, 5th or 95th percentile, female or child). Importantly though, sufficient attention should be directed to the material selection, as these populations may display organic tissue properties dissimilar to those observed in typical adult males (Koncan et al., 2019 and Mirzaali et al., 2016).
- The material properties and manufacturing techniques described here were constrained by those currently available and the associated financial implications. However, developments in manufacturing techniques may facilitate the production of components with improved material properties, or indeed model both the cortical and cancellous bone structures, which would in turn move the LU headform closer to the human form. In its current form, the LU headform does not permit the direct measurement of brain motion (as done by Miyazaki et al. (2012) Petrone et al. (2018)). As such, future iterations should look to include more detailed representations of the Falx Cerebri, Tentorium cerebelli and brain tissue, and permit the direct measurement of brain motion. Future work should also look to investigate the further development of measurement technologies such as fibre optic or hall effect sensors (Paun et al., 2013) that may be incorporated into the model to measure parameters such as strain or impact pressure.
- In the projectile tests presented in this thesis, three impact locations were defined and tested at a nominal impact speed of 34.7 m/s, at an impact angle parallel to the Frankfort plane. As a multitude of impact locations, angles and speeds are possible in Cricket, future work should look to establish the effect of varied impact conditions on the observed dynamic response of the headforms. Indeed, laboratory reconstructions of impacts observed in match play that did and did not result in mTBI may provide useful information into the development of projectile specific injury thresholds
- Future work may also look to assess the effect of varied mounting conditions (for instance a ~Fixed condition, Hybrid-III neckform, and a neckform with improved biofidelity) on the dynamic response observed in head impacts in Cricket. In addition, although the work presented in this thesis showed measurable inter- and intra-ball

variations in properties, which may influence the observed dynamic response of the headform during impacts, this was not directly measured and may be a focus of future work.

Á As discussed in chapters 7 and 8, the responses observed when using the LU headform produced large linear accelerations at the CoG of the headform, due to a combination of the global acceleration and the local deformation/resonance frequency excitation of the LU headform. Although the results presented in this thesis achieved the defined aims by illustrating the differences between headforms on a like-for-like basis, an alternative processing pathway may provide additional insight in future research. A potentially useful method for evaluating the response of the LU headform in future may be to filter the measured signals at two different frequencies. Initially, a 4th order low pass Butterworth filter with a cut off frequency of 1 kHz would facilitate the assessment of the global acceleration of the headforms CoG, while a bandpass filter between 1 and 3 kHz would provide insight into the resonance components. Initial assessments using this technique were conducted on the representative trials observed at the frontal location during unprotected impacts and when using Helmet A (see Figure 100). From this it is clear that Helmet A reduces both the global acceleration and the resonance frequency excitation of the headform during impact.

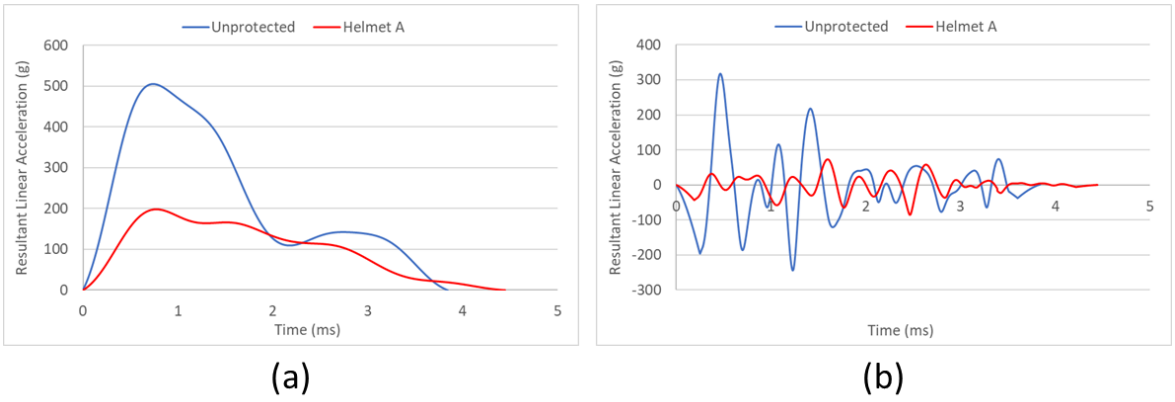

Figure 100. Representative linear response curves overserved at the frontal location during unprotected impacts and when using Helmet A, filtered at (a) lowpass filter at 1kHz and (b) bandpass filter between 1 and 3 kHz.

Á This approach may also be used to good effect when assessing the effect of repeated head impacts on helmet performance. Representative linear response curves observed when using Helmet A and processed in this manner can be seen in Figure 101. It can be clearly seen here that repeated impacts at the frontal location reduce the ability of Helmet A to reduce global acceleration and resonance frequency excitation of the headform. This approach to processing the data obtained usin g the LU headform

may be particularly useful in the development of PPE as it highlights the components of a dynamic response that the protective equipment may or may not be effective at mitigating, without the need to test using multiple headforms (i.e. using the Hybrid-III for the assessment of global acceleration and LU headform for resonance frequency excitation).

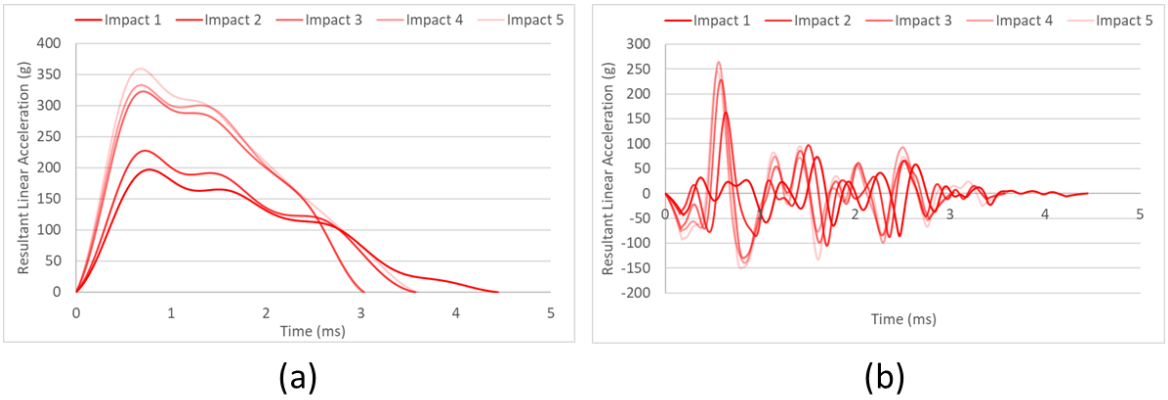

Figure 101. Representative linear response curves observed during the repeated impacts using Helmet A, filtered at (a) lowpass filter at 1kHz and (b) bandpass filter between 1 and 3 kHz.

- The likely mechanisms of injury and associated injury thresholds in short duration, projectile impacts like those seen in Cricket are also areas for future research. FE models have been used in this regard in other sports (Carke et al., 2016; Ghajari et al., 2017; Oeur et al., 2019; Post et al., 2016, 2013; Viano et al., 2005b; Zhang et al., 2006, 2001), and as such, the research presented in this thesis (i,e, ball properties, CAD headform model and material properties, and dynamic response data) facilitates the development and validation of FE models specifically for the assessment of injury mechanisms and injury thresholds for head impacts in Cricket. This would provide useful information that could be practically applied in PPE design, development and manufacture, in addition to the development of more appropriate standard certifications.
- Based on the research presented in this thesis, a move towards a projectile based standard test is recommended. To facilitate this, future work should look to develop a ball that has dynamic properties comparable to those observed in Cricket balls in Chapter 3, but is more resistant to degradation. This would prevent the need for multiple, elite level Cricket balls and therefore prevent the increased cost of standards testing being passed to the consumer.

References

Alaoui, A., Woignier, T., Scherer, G., Phalippou, J., 2008. Comparison between flexural and uniaxial compression testst to measure the elastic modulus of silica aerogel. J. Non. Cryst. Solids 354, pp. 4556–4561.

Albery, C., Whitestone, J., 2003. Comparison of caderveric human head mass properties: Mechanical measurement vs calculation from medical imaging, in: Injury Biomechanics Research.

Al-Bsharat, A., Hardy, W.N., Yang, K.H., Khalil, T.B., Tashman, S., King, A.I., 1999. Brain/skull relative displacement magnitude due to blunt head impact: New experimental data and model, in: 43rd Stapp Car Crash Conference.

Allsop, D.L., Warner, C.Y., Wille, M.G., Schneider, D.., Nahum, A.M., 1988a. Facial impact response - A Comparison of the Hybrid III Dummy and Human Cadaver. J. Passeng. Cars 97, pp. 1224–1240.

Allsop, D.L., Warner, C.Y., Wille, M.G., Schneider, D.., Nahum, A.M., 1988b. Facial impact response - a comparison of the hybrid III dummy and human cadaver. Proc. 32nd Stapp Car Crash Conf.

Ankerson, J., Birkbeck, A., Thomson, R., Vanezis, P., 1999. Puncture resistance and tensile strength of skin simulants, in: Proceedings of the Institute of Mechanical Engineers, Part H: Journal of Engineering in Medicine. pp. 493–501.

Ankrah, S., Mills, N.J., 2003. Performance of football shin guards for direct stud impacts. Sport. Eng. 6, 207. doi:10.1007/BF02844024

Atha, J., Yeadon, M., Sandover, J., Parsons, K., 1985. The damaging punch. Br. Med. J. 291, pp. 1756-1757.

Athiviraham, A., Bartsch, A., Mageswaran, P., Benzel, E.C., Perse, B., Jones, M.H., Schickendantz, M., 2012. Analysis of baseball-to-helmet impacts in major league baseball. Am. J. Sports Med. 40, pp. 2808–2814. doi:10.1177/0363546512461754

Balaraman, K., Mukherjee, S., Chawla, A., Malhotra, R., 2012. Dynamic Compressive Response of Human passive Muscle using Split Hopkinson Pressure Bar. Indian J. Biomech. 1, pp. 20-28.

Ball, K., Hrysomallis, C., 2012. Synthetic grass cricket pitches and ball bounce characteristics. J. Sci. Med. Sport 15, pp. 272–276.

Becker, E., 1972. Measurement of mass distribution parameters of anatomical segments, in: Proceedings of the Stapp Casr Crash Conference. pp. 525–538.

Behr, M., Thollon, L., Delotte, J., Brunet, C., 2009. Investigating the possible role of placenta position in road accident consecutive foetal loss. Int. J. Crashworthiness 14, pp. 447–482.

Beier, G., Schuller, E., Schuck, M., Ewing, C.L., Becker, E.D., Thomas, D.J., 1980. Center of gravity and moments of inertia of human heads, in: IRCOBI conference 1. pp. 218–228.

Bell, B., 1989. Measurement of changes in brain water in man by resonance imaging. Ann. R. Coll. Surg. Engl. 71, pp. 375–380.

Beyer, J.A., Rowson, S., Duma, S.M., 2012. Concussions experienced by major league baseball catchers and umpires: field data and experimental baseball impacts. Ann. Biomed. Eng. 40, pp. 150–159. doi:10.1007/s10439-011-0412-4

Biesen, E., Smith, L. V., 2007. Describing the plastic deformation of aluminium softball bats. Sport. Eng. 10, pp. 185–193.

Blanton, P., Biggs, N., 1968. Density of fresh and embalmed human compact and cancellous bone. Am. J. Phys. Anthropol. 29, pp. 39–44.

Blausen, 2014. Wikiversity Journal of Medicine. URL https://en.wikiversity.org/wiki/WikiJournal_of_Medicine/Medical_gallery_of_Blausen_Medical_2014

Bledsoe, G., Li, G., Levy, F., 2005. Injury risk in professional boxing. South Med. J. 98, pp. 994–998.

Bradshaw, D., Ivarsson, J., Morfey, C., Viano, D., 2001. Simulation of acute subdural hematoma and diffuse

axonal injury in coronal head impact. J. Biomech. 34, pp. 85–94.

Bridge, N.J., 1998. The way balls bounce. Phys. Educ. 33, pp. 174–181. doi:10.1088/0031-9120/33/3/018

British Standards Institute, 2017. BS EN ISO 7250-1:2017. Basic human body measurements for technological design. Body measurement definitions and landmarks.

British Standards Institute, 2013. BS EN ISO 178:2010+A1:2013. Plastics - Determination of flexural properties.

British Standards Institute, 2012. BS EN ISO 527-1:2012. Plastics - Determination of tensile properties. General principles.

British Standards Institute, 2013. BS 7928:2013 Specification for head protectors for cricketers.

British Standards Institute, 2006. BS EN 960:2006 Headforms for use in the testing of protective helmets, British Standards Institution, London.

Brooks, J.H.M., Fuller, C.W., Kemp, S.P.T., Reddin, D.B., 2005. Epidemiology of injuries in English professional rugby union: part 1 match injuries. Br. J. Sports Med. 39, pp. 757–66. doi:10.1136/bjsm.2005.018135

Brukner, P., Gara, T., Fortington, L., 2018. Traumatic cricket-related fatalities in Australia: a historical review of media reports. Med. J. Aust. 208, pp. 261–264.

Carke, J., Post, A., Hoshizaki, T.B., Gilchrist, M.D., 2016. Protective Capacity of Ice Hockey Helmets against Different Impact Events. Ann. Bioeng. pp. 1–12. doi:10.1007/s10439-016-1686-3

Carré, M.J., Baker, S.W., Newell, A.J., Haake, S.J., 1999. The dynamic behaviour of cricket balls during impact and variations due to grass and soil type. Sport. Eng. 2, pp. 145–160.

Carré, M.J., James, D.M., Haake, S.J., 2004. Impact of a non-homogeneous sphere on a rigid surface. Proc. Inst. Mech. Eng. Part C J. Mech. Eng. Sci. 218, pp. 273–281. doi:10.1243/095440604322900408

Casson, I.R., Viano, D.C., Powell, J.W., Pellman, E.J., 2010. Twelve years of National Football League concussion data. Sports Health 2, pp. 471–483. doi:10.1177/1941738110383963

CES EduPack, 2017. Granta Design Limited.

Chancey, V., Ottaviano, D., Myers, B., Nightingale, R., 2007. A kinematic and anthropometric study of the upper cervical spine and the occipital condyles. J. Biomech. 40, pp. 1953–1959.

Chandler, R.M., Clauser, C.E., McConville, J.T., Reynolds, H.M., Young, J.W., 1975. Investigation of the inertial properties of the human body.

Cheng, N., Subic, A., Takla, M., 2008. Development of a fast solving numerical model for the structural analysis of cricket balls. Sport. Technol. 1, pp. 132–144.

Clark, J.M., 2015. Evaluation of the protective capacity of Ice Hockey Goaltender masks for three accident events using dynamic response and brain stress and strain. University of Ottawa.

Clark, J.M., Connor, T.A., Post, A., Hoshizaki, T.B., Gilchrist, M.D., 2019. The influence of impact surface on head kinematics and brain tissue response during impacts with equestrian helmets. Sport. Biomech. 24, pp. 1–14.

Clark, J.M., Hoshizaki, T.B., Gilchrist, M.D., 2018a. Event-specific impact test protocol for ice hockey goaltender masks. Sport. Biomech. 2, pp. 1–22.

Clark, J.M., Hoshizaki, T.B., Gilchrist, M.D., 2018b. Assessing women's Lacrosse head impacts using finite element modelling. J. Mech. Behav. Biomed. Mater. 80, pp. 20–26.

Clark, J.M., Hoshizaki, T.B., Gilchrist, M.D., 2017. Protective capacity of an ice hockey goaltender helmet for three events associated with concussion. Comput. Methods Biomech. Biomed. Engin. 12, pp. 1–13.

Clark, J.M., Post, A., Hoshizaki, T.B., Gilchrist, M.D., 2016a. Protective capacity of Ice Hockey helmets against different impact events. Ann. Biomed. Eng. 44, pp. 3693–3704.

Clark, J.M., Post, A., Hoshizaki, T.B., Gilchrist, M.D., 2016b. The association among injury metrics for different events in ice hockey goaltender impacts, in: IRCOBI Conference. Malaga.

Clark, J.M., Taylor, K., Post, A., Hoshizaki, T.B., Gilchrist, M.D., 2018c. Comparison of Ice Hockey goaltender helmets for concussion type impacts. Ann. Biomed. Eng. 46, pp. 986–1000.

Collins, F., Brabazon, D., Moran, K., 2010. The dynamic viscoelastic characterisation of the impact behaviour of the GAA sliotar. Procedia Eng. 2, pp. 2991–2997. doi:10.1016/j.proeng.2010.04.100

Collins, F.C., 2011. Parametric Impact Characterisation of a Solid Sports Ball , With a View To Developing a Standard Core for the GAA Sliotar.

Corrigan, A., 1984. Cricket injuries. Aust. Fam. Physician 13, pp. 559–562.

Coulson, N., Foreman, S., Hoshizaki, T.B., 2009. Translational and rotational accelerations generated during reconstructed Ice Hockey impacts on a Hybrid III headform. J. ASTM Int. 6, pp. 1–8.

Crandall, J., Bose, D., Forman, J., Untaroiu, C., Arregui-Dalmases, C., Shaw, C., Kerrigan, J., 2011. Human surrogates for injury biomechanics research. Clin. Anat. 24, pp. 362–371.

Crisco, J.J., Hendee, S.P., Greenwald, R.M., 1997. The influence of baseball modulus and mass on head and chest impacts: a theoreical study. Med. Sci. Sports Exerc. 29, pp. 26–36.

Crisp, T., 1990. Cricket injuries. Sport. Ther. 1, pp. 22–23.

Cross, R., 1999. Dynamic properties of tennis balls. Sport. Eng. 2, pp. 23–33.

Curtain, D., 2016. Independent Review into the Death of Phillip Joel Hughes. Avaliable through Cricket Australia

Davis, K., Blanksby, B., 1976. The segmental components of fast bowling in cricket. Aust. J. Heal. Phys. Educ. Recreat. 71, pp. 9–15.

Delille, R., Lesueur, D., Potier, P., Drazetic, P., Markiewicz, E., 2007. Experimental study of the bone behaviourof them human skull bone for the development of a physical head model. Int. Journal of Crashworthiness 12, pp. 101–108.

Delotte, J., Behr, M., Thollon, L., Arnoux, P., Baquw, P., Bongain, A., 2008. Pregnant women and road safety: experimental crash test with post mortem human subject. Surg. Radiol. Anat. 30, pp. 185–189.

Donnelly, B., Medige, J., 1997. Shear properties of human brain tissue. J. Biomech. Eng. 119, pp. 127–138.

Duris, J.G., Smith, L. V., 2004. Evaluating test methods used to charaterize softballs, in: The Engineering of Sport International Conference. Davis, CA, pp. 80–86.

ECB, 2015. Head injury and concussion guidelines.URL: https://www.wtchc.co.uk/wp-content/uploads/2016/08/ECB_Head_Injury_Concussion_Guidelines_2018.pdf. Accessed 10/03/2019

Elliot, B., Davis, J., Khanqure, M., Hardcastle, P., Foster, D., 1993. Disc degeneration and the young fast bowler in cricket. Clin. Biomech. 8, pp. 227–234.

Elliot, B., Hardcastle, P., Burnett, A., Foster, D., 1992. The influence of fast bowling and physical factors on radiologic features in high performance young fast bowlers. Sport. Med. Train. Rehabil. 3, pp. 113–130.

Falland-Cheung, L., Scholze, M., Lozano, P., Ondruschka, B., Tong, D., Brunton, P., Waddell, J., Hammer, N., 2018. Mechanical properties of the human scalp in tension. J. Mech. Behav. Biomed. Mater. 84, pp. 188–197.

Falland-Cheung, L., Waddell, J., Li, K., Tong, D., Brunton, P., 2017. Investigation of the elastic modulus, tensile and flexural strength of five skull simulant materials for impact testing of a forensic skin/skull/brain model. J. Mech. Behav. Biomed. Mater. 68, pp. 303–307.

Fallenstein, G.T., Hulce, V.D., Melvin, J.W., 1969. Dynamic mechanical properties of human brain tissue. J. Biomech. 2, pp. 217–226.

Feng, Y., Abney, T.M., Okamoto, R.J., Pless, R.B., Genin, G.M., Bayly, P.V., 2010. Relative brain displacement and deformation during constrained mild frontal head impact. J. R. Soc. Interface 7, pp. 1677–1688.

Fenner, H., Thomas, D., Gennarelli, T., Pintar, F.A., Becker, E., Newman, J.A., Yoganandan, N., 2005. Final Report of Workshop on Criteria for Head Injury and Helmet Standards.

Fernandes, F.A.O., Sousa, R.J.A.D., 2015. Head injury predictors in sports trauma - A state-of-the-art review.

Proc. Inst. Mech. Eng. Part H J. Eng. Med. 229, pp. 592–608. doi:10.1177/0954411915592906

Fijalkowski, R., Yoganandan, N., Zhang, J., Pintar, F.A., 2009. A finite element model of region-specific response for mild diffuse brain injury. Stapp Car Crash Journal2 53, pp. 193–213.

Foster, J., Kortge, J. and Wolanin, M., 1977. Hybrid III - a biomechanically based crash test dummy. SAE Technical Paper 770938. doi: 10.4271/770938

Franceschini, G., Bigoni, D., Regitnig, P., Holzapfel, G.A., 2006. Brain tissue deforms similarly to filled elastomers and follows consolidation theory. J. Mech. Phys. Solids 54, pp. 2592–2620.

Frechede, B., McIntosh, A.S., 2009. Numerical reconstruction of real-life concussive football impacts. Med. Sci. Sports Exerc. 41, pp. 390–398.

Friswell, M.I., Mottershead, J.E., 1995. Finite Element Model Updating in Structural Dynamics. Springer, Dordrecht. doi: 10.1007/978-94-015-8508-8

Frost, W., Chalmers, D., 2014. Injury in elite New Zealand cricketers 2002-2008: descriptive epidemiology. Br. J. Sports Med. 48, pp. 1002–1007.

Fuss, F.K., 2008. Cricket balls: construction, non-linear visco-elastic properties, quality control and implications for the game. Sport. Technol. 1, pp. 41–55. doi:10.1002/jst.8

Gallagher, A., Ni Annaidh, A., Bruyere, K., 2012. Dynamic tensile properties of human skin, in: IRCOBI 20122. Dublin, pp. 494–502.

Gefen, A., Marguiles, S.S., 2004. Are in vivo and in situ brain tissues mechanically similar? J. Biomech. 37, pp. 1339–1352.

Gennarelli, T.A., Pintar, F.A., Yoganandan, N., 2003. Biomechanical tolerances for diffuse brain injury and a hypothesis for genotypic variability in response to trauma. Annu. Proceedings/Association Adv. Automot. Med. 47, pp. 624–628.

Gennarelli, T.A., Thibault, L.E., Adams, J.H., Graham, D.I., Thompson, C.J., Marcincin, R.P., 1983. Diffuse axonal injury and traumatic coma in primate. Ann. Neurol. 12, pp. 564–574.

Gennarelli, T.A., Thibault, L.E., Ommaya, A., 1972. Pathophysiological responses to rotational and translational accelerations of the head. SAE TEchnical Paper 720970. 16th Stapp Car Crash Conf. doi: 10.4271/720970

Gennarelli, T.A., Thibault, L.E., Ommaya, A., 1971. Comparison of translational and rotational accelerations in experimental cerebral concussion. 15th Stapp Car Crash Conf.

Gennarelli, T., Wodzin, E., 2008. The Abbreviated Injury Scale 2005. Updated 2008. American Association for Automotive Medicine.

Ghajari, M., Hellyer, P.J., Sharp, D.J., 2017. Computational modelling of traumatic brain injury predicts the location of chronic traumatic encephalopathy pathology. Brain 140, pp. 333–343. doi:10.1093/brain/aww317

Gilchrist, A., Mills, N.J., 1996. Protection of the side of the head. Accid. Anal. Reconstr. 28, pp. 525–535.

Gilchrist, M.D., 2003. Modelling and accident reconstruction of head impact injuries. Key Eng. Mater. pp. 245–246.

Glaister, J., Carass, A., Pham, D., Butman, J., Prince, J., 2017. Automatic falx cerebri and tentorium cerebelli segmentation from Magnetic Resonance Images. Proc. SPIE 10137, Medical Imaging 2017: Biomedical Applications in Molecular, Structural, and Functional Imaging. doi: 10.1117/12.2255640.

Goldsmith, W., 1981. Current Controversies in the Stipulation of Head Injury Criteria. J. Biomech. 14, pp. 883–884. doi:10.1080/13518040701205365

Goldsmith, W., 1960. Impact: the theory and physical behaviour of colliding solids. Richard Clay and Company.

Greenwald, R.M., Gwin, J.T., Chu, J.J., Crisco, J.J., 2008. Head impact severity measures for evaluating mild traumatic brain injury risk exposure. Neurosurgery2 62, pp. 789–798.

Greenwald, R.M., Penna, L.H., Crisco, J.J., 2001. Difference in batted ball speed with wood and aluminium baseball bats: A batting cage study. J. Appl. Biomech. 17, pp. 241–252.

Gurdjian, E., Gurdjian, E., 1980. Acute head injury: A review. Ann. Trauma 12, pp. 223–241.

Gurdjian, E.S., Gurdjian, E.S., 1975. Re-evaluation of the biomechanics of blunt impact injury to the head. Gynecol. Obstet. 140, pp. 845–850.

Gurdjian, E.S., Lissner, H.R., Evans, F.G., 1961. Intracranial Pressure and Acceleration Accompanying Head Impacts in Human Cadavers. Surgery, Gynecol. Obstet. 112, pp. 185–190.

Gurdjian, E.S., Lissner, H.R., Patrick, L.M., 1963. Concussion-mechanism and pathology. Proc. 7th Stapp Car Crash Conf. pp. 470–482.

Gurdjian, E.S., Lissner, H.R., Webster, J.E., 1947. The mechanism of production of linear skull fracture; further studies on deformation of the skull by the stresscoat technique. Surgery, Gynecol. Obstet. 85, pp. 195–210.

Gurdjian, E.S., Webster, J.E., 1945. Linear acceleration causing shear in the brain stem in trauma of the central nervous system. Ment. Adv. Dis. pp. 24–28.

Gurdjian, E.S., Webster, J.E., Lissner, H.R., 1955. Observations on the mechanism of brain concussion, contusion and laceration. Surgery, Gynecol. Obstet. 101, pp. 680–690.

Gurdjian, E.S., Webster, J.E., Lissner, H.R., 1950. The mechanism of skull fracture. J. Neurosurg. 7, pp. 106–114.

Gurdjian, E.S., Webster, J.E., Lissner, H.R., 1949. Studies on skull fracture with particular reference to engineering factors. Am. J. Surg. 78, pp. 736–742.

Hammond, D., Davies, D., Su, Z., 2015. Do we forget to treat concussion? Fac. Dent. J. 6. doi: 10.1308/204268515X14174408396046

Hardy, W.N., Foster, C.D., Mason, M.J., Yang, K.H., King, A.I., Tasman, S., 2001. Investigation of head injury mechanisms using neutral density technology and high-speed biplanar x-ray. Stapp Car Crash J. 45, pp. 337–368.

Hardy, W.N., Mason, M.J., Foster, C.D., Shah, C.S., Kopacz, J.M., Yang, H., King, A.I., Bishop, J., Bey, M., 2008. A study of the response of the human cadaver head to impact. Stapp Car Crash J 51, pp. 17–80. doi:10.1016/j.bbi.2008.05.010

HawkEye, 2019. Paul Hawkins response to ESPN CricInfo Blog - “Why ball-tracking can”t be trusted’. URL https://platform-static-files.s3.amazonaws.com/test/HawkEye/document/2015/08/27/76ee8967-f365-4b0a-9d29-13b4dab6232c/CricInfo_Hawkins_Responds.pdf (accessed 11.23.19).

Hendee, S.P., Greenwald, R.M., Crisco, J.J., 1998. Static and Dynamic Properties of Various Baseballs. J. Appl. Biomech. 14, pp. 390–400.

Hernandez, F., Wu, L.C., Yip, M.C., Laksari, K., Hoffman, A.R., Lopez, J.R., Grant, G.A., Kleiven, S., Camarillo, D.B., 2015. Six degree-of-freedom measurements of human mild traumatic brain injury. Ann. Biomed. Eng. 43, pp. 1918–1934.

Hibbeler, R.C., 2015. Engineering Mechanics Dynamics, 14th Edition. ed. Pearson.

Hodgson, V.R., Brinn, J., Thomas, L., Greenberg, S., 1970. Fracture Behavior of the Skull Frontal Bone Against Cylindrical Surfaces. 14th Stapp Car Crash Conf.

Hodgson, V.R., Gurdjian, E.S., Thomas, L., 1967. Determination of response characteristics of the head when impacting another body, with emphasis on mechanical impedance techniques. Proc. 11th Stapp Car Crash Conf.

Hodgson, V.R., Mason, M., Thomas, L., 1972. Head model for impact, in: Proceedings of the Stapp Car Crash Conference. pp. 1–13.

Hodgson, V.R., Thomas, L.M., 1973. Breaking strength of the human skull vs impact surface curvature. Wayne State University School of Medicine, Detroit.

Holbourn, A., 1943. Mechanics of head injuries. Lancet 242, pp. 438–441.

Hopes, P., Chinn, B., 1989. Helmets: A new look at design and possible protection. Proc. 1989 Int. IRCOBI Conf. Biomech. impact.

Horgan, T., 2005. A finite element model of the human head for use in the study of pedestrian accidents. University College Dublin.

Horgan, T.J., Gilchrist, M.D., 2003. The creation of three-dimensional finite element models for simulating head impact biomechanics The creation of three-dimensional finite element models for simulating head impact biomechanics. Int. J. Crashworthiness 8, pp. 353–366. doi:10.1533/ijcr.2003.0243

Hoshizaki, T.B., Brien, S.E., 2004. The science and design of head protection in sport. J. Neurosurgery2 55, pp. 956–967.

Hoshizaki, T.B., Post, A., Oeur, R.A., Brien, S.E., 2014. Current and future concepts in helmet and sports injury prevention. Neurosurgery 75, pp. 136–148. doi:10.1227/NEU.0000000000000496

Hubbard, R., 1971. Flexure of layered cranial bone. J. Biomech. 4, pp. 251–263.

Humanetics Innovations Solutions Inc., 2019. Hybrid-III 50th Male Dummy - Brand Harmonized Parts Catalog.

Hyrsomallis, C., 2009. Surrogate thigh model for assessing impact force attenuation of protective pads. J. Sci. Med. Sport 12, pp. 35–41.

Hyrsomallis, C., 2004. Impact energy attenuation of protective football headgear against a yielding surface. J. Sci. Med. Sport 7, pp. 156–164.

International Organization for Standardization, 2017. ISO 7743:2017. Rubber, vulcanized or thermoplastic -- Determination of compressive stress-strain properties.

James, D.M., Carré, M.J., Haake, S.J., 2004. The playing performance of county cricket pitches. Sport. Eng. 7, pp. 1–14.

Karton, C., 2012. The effect of inbound mass on the dynamic response of a hybrid III headform and brain tissue deformation. University of Ottawa.

Keep, R., Hua, Y., Guohua, X., 2012. Brain water content. A misunderstood measurement? Transl. Stroke Res. 3, pp. 263–265.

Kendall, M., Walsh, E.S., Hoshizaki, T.B., 2012a. A comparison of the dynamic impact response and brain deformation metrics of head impact reconstructions for three mechanisms of head injury in ice hockey, in: IRCOBI 2012.

Kendall, M., Walsh, E.S., Hoshizaki, T.B., 2012b. Comparison between Hybrid III and Hodgson – WSU headforms by linear and angular dynamic impact response. Proc IMechE Part P J. Sport. Eng. Technol., pp. 1–6. doi:10.1177/1754337112436901

Kennedy, J.C., Hawkins, R.J., Willis, R B, Danylchuck, K.D., 1976. Tension studies of human knee ligaments. Yield point, ultimate failure, and disruption of the cruciate and tibial collateral ligaments. J. Bone Jt. Surg.

Khalil, T.B., Viano, D.C., Smith, D.L., 1979. Experimental Analysis of the Vibrational Characteristics of the Human Skull. J. Sound Vib. 63, pp. 352–376.

King, A., Yang, K., Zhang, L., 2003. Is head injury caused by linear or angular acceleration, in: IRCOBI Conference. pp. 1–12.

King, D., Hume, P.A., Brughelli, M., Gissane, C., 2014. Instrumented mouthguard acceleration analyses for head impacts in amateur Rugby Union players over a season of matches. Am. J. Sport. Med.

Kleiven, S., 2013. Why Most Traumatic Brain Injuries are Not Caused by Linear Acceleration but Skull Fractures are. Front. Bioeng. Biotechnol. 1, pp. 1–5. doi:10.3389/fbioe.2013.00015

Kleiven, S., 2007. Predictors for traumatic brain injuries evaluated through accident reconstructions. Stapp Car Crash J. 51, pp. 81–114. doi:2007-22-0003 [pii]

Kleiven, S., 2002. Finite element modelling of the human head. Royal Institute of Technology Stockholm.

Koncan, D., Gilchrist, M.D., Vassilyadi, M., Hoshizaki, T.B., 2019. A three-dimensional finite element model of a 6-year-old child for simulating brain response from physical reconstructions of head impacts. Proc IMechE Part P J. Sport. Eng. Technol. 233, pp. 277–291.

Leung, L.Y., Zhang, L., Yang, K.H., King, A.I., Jin, X., Lee, J.B., 2006. Biomechanical response of the bovine pia-

arachnoid complex to tensile loading. Stapp Car Crash J. 50, pp. 637–649.

Li, S., Demirci, E., Silberschmidt, V., 2013. Variability and anisotropy of mechanical behavior of cortical bone in tension and compression. J. Mech. Behav. Biomed. Mater. 21, pp. 109–120.

Liao, S., Lynall, R., Mihalik, J., 2016. The effect of head impact location on day of diagnosed concussion in college football. Med. Sci. Sport. Exerc. 48, pp. 1239–43.

Lim, J., Hong, J., Chen, W., Weerasooriya, T., 2011. Mechanical response of pig skin under dynamic tensile loading. Int. J. Impact Eng. 38, pp. 130–135.

Lin, S.J., Hanasono, M.M., Skoracki, R.J., 2008. Scalp and calverial reconstruction. Semin. Plast. Surg. 22, pp. 281–293.

Ling, C., Ivens, J., Cardiff, P., Gilchrist, M.D., 2018. Deformation response of EPS foam under combined compression-shear loading. Part II: High strain dynamci tests. Int. J. Mech. Sci. 145, pp. 9–23.

Lippert, S.A., Grimm, M.J., 2003. Estimating material properties of brain tissue at impact frequencies: A curve-fitting solution., in: Summer Bioengineering Conference. Key Biscayne.

Lubock, P., Goldsmith, W., 1980. Experimental cavitation studies in a model head-neck system. 1Journal Biomech. 13, pp. 1041–1052.

Lynnerup, N., 2001. Cranial thickness in relation to age, sex and general bdy build in a Danish forensic sample. Forensic Sci. Int. 1, pp. 45–51.

MacManus, D.B., Murphy, J., Gilchrist, M.D., 2018. Mechanical characterisation of brain tissue to 35% strain at 1, 10, and 100/s using a custom built micro-indentation apparatus. J. Mech. Behav. Biomed. Mater. 87, pp. 256–266.

MacManus, D.B., Pierrat, B., Murphy, J., Gilchrist, M.D., 2017. Region and species dependent mechanical properties of adolescent and young adult brain tissue. Sci. Rep. 7.

Mahinda, H., Murty, O., 2009. Variability in Thickness of Human Skull Bone and Sternum - An Autopsy Experience. Indian J. Forensic Med. Toxicol. 126, pp. 26–31.

Martin, P.G., Hall, G.W., Crandall, J., Pilkey, W.D., 1998. Measuring the acceleration of a rigid body. Shock Vib. 5, pp. 211–224.

MCC, Laws of Cricket. URL https://www.lords.org/mcc/laws-of-cricket/laws/law-4-the-ball/ (accessed 5.3.18).

McCroy, P., Feddermann-Demont, N., Dvorak, J., Cassidy, J., McIntosh, A., Vos, P., Echemendia, R., Meeuwisse, W., Tarnutzer, A., 2017. What is the definiton of sports-related concussion: A systematic review. Br. J. Sports Med. 51, pp. 877–887.

McElhaney, J.H., Doherty, B., Paver, J., Myers, B., 1988. Combined bending and axial loading responses of the human cervical spine, in: 32nd Stapp Car Crash Conference. pp. 21–28.

McElhaney, J.H., Fogle, J.L., Melvin, J.W., Haynes, R.R., Roberts, V.L., Alem, N.M., 1970. Mechanical properties of cranial bone. J. Biomechancis 3, pp. 495–511.

McElhaney, J.H., Stalnaker, R.L., Roberts, V.L., 1973. Biomechanical aspects of head injury, in: King, W.F., Mertz, H. (Eds.), Human Impact Response: Measurement and Simulation. pp. 85–112.

McIntosh, A.S., Andersen, T.E., Bahr, R., Greenwald, R., Kleiven, S., Turner, M., Varese, M., Mccrory, P., 2011. Sports helmets now and in the future. Br. J. Sports Med. 45, pp. 1258–1265. doi:10.1136/bjsports-2011-090509

McIntosh, A.S., Janda, D., 2003. Evaluation of cricket helmet performance and comparison with baseball and ice hockey helmets. Br. J. Sports Med. 37, pp. 325–330. doi:10.1136/bjsm.37.4.325

McIntosh, A.S., McCrory, P., 2005. Preventing head and neck injury. Br. J. Sports Med. 39, pp. 314–319. doi:10.1136/bjsm.2005.018200

McIntosh, A.S., McCrory, P., Comerford, J., 2000. The dynamics of concussive head impacts in rugby and Australian rules football. Med Sci Sport. Exerc 32, 1980–1984. doi:10.1097/00005768-200012000-00002

Meaney, D.F., Smith, D.H., 2011. Biomechanics of Concussion. Clin. Sport. Med. 30, pp. 19–31.

doi:10.1016/j.csm.2010.08.009

Merkle, A.C., Wing, I.D., Roberts, J.C., 2010. Human surrogate head response to dynamic overpressure loading in protected and unprotected conditions, in: 26th Southern Biomedical Engineering Conference. pp. 22–25.

Mez, J., Daneshvar, D.H., Kiernan, P.T., Abdolmohammadi, B., Alvarez, V.E., Huber, B.R., Alosco, M.L., Solomon, T.M., Nowinski, C.J., McHale, L., Cormier, K.A., Kubilus, C.A., Martin, B.M., Murphy, L., Baugh, C.M., Montenigro, P.H., Chaisson, C.E., Tripodis, Y., Kowall, N.W., Weuve, J., McClean, M.D., Cantu, R.C., Goldstein, L.E., Katz, D.I., Stern, R.A., Stein, T.D., McKee, A.C., 2017. Clincopathological evaluation of chronic traumatic encephalopathy in players of American football. JAMA 318, pp. 360–370.

Miller, K., Chinzei, K., 2002. Mechanical properties of brain tissue in tension. J. Biomech. 35, pp. 483–490.

Miller, K., Chinzei, K., Orssengo, G., Bednarz, P., 2000. Mechanical properties of brain tissue in-vivo: experimental and computer simulation. J. Biomech. 33, pp. 1369–1376.

Mirzaali, M., Schwiedrzik, J., Thaiwichai, S., Best, P., Michler, J., Zysset, P., Wolfram, U., 2016. Mechanical properties of cortical bone and their relationship with age, gender, composition and microidentation properties in the elderly. Bone 93, pp. 196–211.

Miyazaki, Y., Tachiya, H., Hojo, A., Sakamoto, Y., 2012. Visualization of relative displacement between skull and brain under occipital impact using a 3D transparent physical head model. Trans. Japan Soc. Mech. Eng. Ser. A 78, pp. 106–115.

MLB, 2016. Official Baseball Rules: 2016 Edition.

Mohotti, D., Fernando, P., Zaghloul, A., 2018. Evaluation of possible head injuries ensuing a cricket ball impact. Comput. Methods Programs Biomed, 158. pp. 193-205.

Moonda, F., 2012. Eye injury ends Boucher's career. ESPN Cricinfo. URL http://www.espncricinfo.com/england-v-south-africa-2012/content/story/571732.html (accessed 7.18.16).

Motherway, J.A., Verschueren, P., Van der Perre, G., Sloten, J. V, Gilchrist, M.D., 2009. The mechanical properties of cranial bone: the effect of loading rate and cranial sampling position. J. Biomechancis 42. pp. 2129-2135.

Mullins, L., 1969. Softening of Rubber by Deformation. Rubber Chem Technol. 42, pp. 339–362.

Murtaugh, K., 2001. Injury patterns among female field hockey players. Med. Sci. Sports Exerc. 33, pp. 201–207.

Nahum, A., Gatts, J.D., Gadd, C.W., Danforth, J.P., 1968. Impact tolerance of the skull and face. Proc. 12th Stapp Car Crash Conf.

Nahum, A.M., Smith, R., 1976. An experimental model for closed head impact injury. 20th Stapp Car Crash Conf.

Nahum, A.M., Smith, R.W., Ward, C.C., 1977. Intracranial pressure dynamics during head impact, in: Proceedings of the 21st Stapp Car Crash Conference.

National Centre For Catastrophic Sports Injury Research, 2002. 19th annual report: Fall 1982-Spring 2001.

Nayaran, A., 2016. Boundaries Galore.URL: https://www.espncricinfo.com/story/_/id/17231837/analysis-boundary-hitting-trends-cricket. Accessed 24/04/2020

NCAA, 2010. Field Hockey Injuries: Data from the 2004/05 - 2008/09 Seasons.

Newman, J.A., 1986. A generalized model for brain injury threshold. Int. IRCOBI Conf. Biomech. Impact pp. 121–131.

Newman, J.A., Barr, C., Beusenberg, M., Fournier, E., Shewchenko, N., Welbourne, E., Withnall, C., 2000a. A new biomechanical assessment of mild traumatic brain injury, part 2: results and conclusions. Proc. 2000 Int. Conf. Biomech. Impact pp. 223–233.

Newman, J.A., Shewchenko, N., Welbourne, E., 2000b. SAE TECHNICAL A Proposed New Biomechanical Head Injury Assessment Function - The Maximum Power Index. Stapp Car Crash J. 44.

News - BBC., 2019. "A stray baseball cracked my skull". URL https://www.bbc.co.uk/news/world-us-canada-50017844 (accessed 11.23.19).

Ni Annaidh, A., Bruyere, K., Destrade, M., Gilchrist, M.D., Ottenio, M., 2012. Characterization of the anisotropic mechanical properties of exercised human skin. J. Mech. Behav. Biomed. Mater. 5, pp. 139–148.

Nicholls, R., Elliot, B., Miller, K., 2004. Impact Injuries in Baseball: Prevalence, Aetiology and the Role of Equipment Performance. Sport. Med. 34, pp. 17–25.

Nishizaki, K., Marino, W., Hoshizaki, T.B., Post, A., Oeur, R.A., Walsh, E.S., Gilchrist, M.D., Kendall, M., 2014. Evaluation of dynamic response and brain deformation metrics for a helmeted and non-helmeted Hybrid III headform using a monorail centric/non-centric protocol. Mech. Concussion Sport. pp. 171–186.

NOCSAE, 2016. Standard Performance Specification for Newly Manufactured Ice Hockey Helmets - ND030-11m16.

NOCSAE, 2015a. Standard Performance Specification for Newly Manufactured Football Helmets - ND002-13m15.

NOCSAE, 2015b. Standard Performance Specification for Newly ManufacturedBaseball/Softball Batter's Helmets - ND022-10m15.

Nuscholtz, G., Lux, P., Kaiker, P., Janicki, M., 1984. Head impact response - skull deformation and angular acceleration. 28th Stapp Car Crash Conf.

Oeur, A., 2012. An analysis of head impact angle on the dynamic response of a hybrid III headform and brain tissue deformation. University of Ottawa.

Oeur, A., Gilchrist, M.D., Hoshizaki, T.B., 2019. Parametric study of impact parameters on peak head acceleration and strain for collision impacts in sport. Int. J. Crashworthiness.

Oeur, R.A., Gilchrist, M.D., Hoshizaki, T.B., 2019. Interaction of impact parameters for simulated falls in sport using three different sized Hybrid III headforms. Int. J. Crashworthiness 24.

Oeur, R.A., Gilchrist, M.D., Hoshizaki, T.B., 2019. Interaction of external head impact parameters on region and volume of strain for collisions in sport. Proc IMechE Part P J. Sport. Eng. Technol. 233, pp. 258–267.

Omalu, B., DeKosky, S., Minster, R., Kamboh, M., Hamilton, R., Wecht, C., 2005. Chronic traumatic encephalopathy in a National Football League player. Neurosurgery 57, pp. 128–134.

Orchard, J., James, T., Kountouris, A., Portus, M., 2006. Changes to injury profile (and recommended cricket injury definitions) based on the increased frequency of Twent20 cricket matches. J. Sports Med. 1, pp. 63–76.

Pang, T.Y., Subic, A., Takla, M., 2013. Impact energy attenuation performance of cricket helmets : standard 2-wire drop test vs . pitching machine impact test. Procedia Eng. 60, pp. 143–150. doi:10.1016/j.proeng.2013.07.013

Paun, M., Sallese, J., Kayal, M., 2013. Hall effect sensor design, integration andbehavior analysis. J. Sens. Actuator Networks 2, pp. 85–97.

Payne, T., 2015. Improved human soft tissue thigh surrogates for superior assessment of sports personal protective equipment. Loughborough University.

Payne, T., Mitchell, S., Bibb, R., Water, M., 2014. Initial Validation of a Relaxed Human Soft Tissue Simulant for Sports Impact Surrogates. Procedia Eng. 72, pp. 533–538.

Payne, T., Mitchell, S., Bibb, R., Waters, M., 2015a. Development of novel synthetic muscle tissues for sports impact surrogates. J. Mech. Behav. Biomed. Mater. 41, pp. 357–373.

Payne, T., Mitchell, S., Halkon, B., Bibb, R., Waters, M., 2015b. Development of an anatomical synthetic human thigh impact surrogate for sports personal protective equipment testing. IMechE, Part P J. Sport. Eng. Technol. 230, pp. 5–16.

Payne, W., Hoy, G., Laussen, S., Carlson, J., 1987. What research tells the cricket coach. Sport Coach 10, pp. 17–22.

Peebles, L., Norris, B., 1998. Adult Data. The Handbook of Adult Anthropometric and Strength Measurements Dept of Trade and Industry, London.

Pellman, E., Viano, D., Tucker, A., Casson, I., Waeckerle, J., 2003. Concussions in Professional Football:

Reconstruction of Game Impacts and Injuries. Neurosurgery 53, pp. 799–814.

Pellman, E.J., Viano, D.C., Casson, I.R., Arfken, C.A., Feuer, H., 2005. Concussion in professional football: Players returning to the same-game - Part 7. Neurosurgery 56, pp. 79–92.

Penrose, T., Foster, D., Blanksby, B., 1976. Release velocities of fast bowlers during a cricket test match. Aust. J. Heal. Phys. Educ. Recreat. 71, pp. 2–5.

Petrone, N., Carraro, G., Dal Castello, S., Broggio, L., Koptyug, A., Backstrom, M., 2018. A novel instrumented human head surrogate for the impact evaluation of helmets, in: Proceedings of the 12th Conference on the Engineering of Sport, ISEA.

Pieter, W., Ryssegem, G., R, L., 1995. Injury situation and injury mechanisms at the 1993 European Taekwondo cup. J. Hum. Mov. Stud. 28, pp. 1–24.

Post, A., Hoshizaki, T.B., 2012. Mechanisms of brain impact injuries and their prediction : A review 0, pp. 1–23. doi:10.1177/1460408612446573

Post, A., Hoshizaki, T.B., Gilchrist, M.D., 2012. Finite element analysis of the effect of loading curve shape on brain injury predictors. J. Biomech. 45, pp. 679–683.

Post, A., Hoshizaki, T.B., Gilchrist, M.D., Cusimano, M.D., 2017. Peak linear and rotational acceleration magnitude and duration effects on maximum principal strain in the corpus callosum for sports impacts. J. Biomechancis 16, pp. 183–192.

Post, A., Karton, C., Hoshizaki, T.B., Gilchrist, M.D., Bailes, J., 2016. Evaluation of the protective capacity of baseball helmets for concussive impacts. Comput. Methods Biomech. Biomed. Engin. 19, 366–375.

Post, A., Oeur, A., Hoshizaki, T.B., Gilchrist, M.D., 2013. The influence of velocity on injury risk in American Football, in: Helmet Performance and Design.

Prange, M., Meaney, D., Margulies, S., 2000. Defining brain mechanical properties: effects of region,direction, and species. Stapp Car Crash J. 44, pp. 205–213.

Prasad, P., Mertz, H., 1985. The position of the United States delegation to the ISO working group 6 on the use of HIC in the automotive environment. Society of Automotive Engineers.

Ranson, C., Peirce, N., Young, M., 2013. Batting head injury in professional cricket : a systematic video analysis of helmet safety characteristics Batting head injury in professional cricket : a systematic video analysis of helmet safety characteristics. Br. J. Sports Med. 0, pp. 1–5. doi:10.1136/bjsports-2012-091898

Rashid, B., Destrade, M., Gilchrist, M.D., 2012. Mechanical characterization of brain tissue in compression at dynamic strain rates. J. Mech. Behav. Biomed. Mater. 10, pp. 23–38.

Raymond, D., 2008. Biomechanics of blunt ballistic tempero-parietal head impact. PhD Thesis. Wayne State University.

Raymond, D.E., van Ee, C., Crawford, G., Bir, C., 2008. Biomechanics of blunt ballistic tempo-parietal head impact. Wayne State University.

Reilly, D.T., Burnstein, A.H., 1974. The mechanical properties of cortical bone. J. Bone Jt. Surgery, pp. 56.

RFU, 2015. England Professional Rugby Injury Surveillance Project.

Robbins, D., Wood, J., 1969. Determination of mechanical properties of the bones of the skull. Exp. Mech. 9, pp. 236–240.

Roberts, J.C., Merkle, A.C., Carneal, C.M., Voo, L.M., Johannes, M.S., Paulson, J.M., Tankard, S., Manny Uy, O., 2013. Development of a human cranial bone surrogate for impact studies. Front. Bioeng. Biotechnol. 1, pp. 13.

Robinovitch, S., McMahon, T., Hayes, W., 1995. Force attenuation in trochanteric soft tissues during impact from a fall. J. or Orthop. Res. 13, pp. 956–962.

Rodriguez-Panes, A., Gil, J.C., Camacho, A.M., 2018. The influence of manufacturing parameters on the mechanical behaviour of PLA and ABS pieces manufactured by FDM: A comparative analysis. Materials2 11, pp. 1–21.

Rogers, S., Trickey, A., 2017. Classification of traumatic brain injury severity using retrospective data. J. Nurs. Educ. Pract. 7, pp. 23–29.

Rutherford, G., Kennedy, J., McGhee, L., 1984. Hazard analysis: base and softball related injuries to children 5-14 years of age. Washingt. DC US Consum. Prod. Saf. Commision, Epidemiol. Heal. Serv. Div. Hazard Anal.

SAE, 1995. SAE J211-1 (1995): Instrumentation for Impact Test, Part 1, Electronic Instrumentation.

Saraf, H., Ramesh, K.T., Lennon, A.M., Merkle, A.C., Roberts, J.C., 2007. Mechanical properties of soft human tissues under dynamic loading. J. Biomech. 40, pp. 1960–1967.

Schneider, D.., Nahum, A.M., 1972. Impact Studies of the facial bones and skull. Proc. 16th Stapp Car Crash Conf.

Shergold, O., Fleck, N., Radford, D., 2006. The uniaxial stress versus strain response of pig skin and silicone rubber at low and high strain rates. Int. J. Impact Eng. 32, pp. 1384–1402.

Shirani, G., Motamedi, M., Ashuri, A., Eshkevari, P., 2010. Prevalence and patterns of combat sport related maxillofacial injuries. J. Emergencies, Truama, Shock 3, pp. 314–317.

Shuaeib, F., Hamouda, A., Radin Umar, R., Hamdan, M., Hashmi, M., 2002. Motorcycle helmet - Part I. Biomechanics and computational issues. J. Mater. Process. Technol. 123, pp. 406–421.

Smith, L. V., 2008. Measuring the hardness of softballs, in: IMAC-XXVI. Orlando.

Smith, L. V., Duris, J.G., 2009. Progress and challengers in numerically modelling solid sports balls with application to softballs. J. Sports Sci. 27, pp. 353–360.

Smith, L. V., Faber, W., 2011. The effect of temperature and humidity on the performance of baseballs and softballs, in: 5th Asia-Pacific Congress on Sports Technology (APCST). pp. 200–206.

Smith, L. V., Nathan, A.M., Duris, J.G., 2010. A determination of the dynamic response of softballs. Sport. Eng. 12, pp. 163–169. doi:10.1007/s12283-010-0041-4

Snell, R., 2003. Clinical anatomy, 7th ed. Lippincott Williams & Wilkins.

Stalhammar, D., Olsson, Y., 1975. Experimental brain damage fromfluid pressures due to impact acceleration - 3. Morphological observations. Acta Neurol. Scand. 52, pp. 38–55.

Standring, S., Borley, N., Gray, H., 2008. Gray's Anatomy, 40th ed. Churchill Livingston/Elsevier.

Stern, R.A., Riley, D.O., Daneshvar, D.H., Nowinski, C.J., Cantu, R.C., McKee, A.C., 2011. Long-term consequences of repetitive brain trauma: Chronic Traumatic Encephalopathy. PM&R 3, pp. 460–467.

Stockill, N., Bartlett, R.M., 1992. A three-dimensional cinematographical analysis of the techniques of International and English county cricket fast bowlers, in: Rodano, R., Ferrigno, G., Santambrogio, G. (Eds.), Proceedings of the Xth Symposium of the International Society of Biomechanics in Sports. Milan, pp. 52–55.

Stone, B.W., Harland, A.R., Mitchell, S.R., Jones, J.A., Sherratt, P.J., Ranson, C.A., Halkon, B.J., 2017. On the dynamic response of an instrumented headform for alternative mounting stiffnesses when subjected to ballistic impacts. Proc IMechE Part P J. Sport. Eng. Technol. pp. 1–12. doi:10.1177/1754337117703574

Stretch, R.A., 2001. Incidence and nature of epidemiological injuries to elite South African cricket players. South African Med. Journal2 91, pp. 336–339.

Stretch, R.A., 2000. The impact absorption characteristics of cricket batting helmets. J. Sports Sci. 18, pp. 959–964. doi:10.1080/026404100446766

Stretch, R.A., 1995. The incidence and nature of injuries in schoolboy cricketers. 1South African Med. J. 85, pp. 1182–1184.

Stretch, R.A., 1993. The incidence and nature of injuries in club and provincial cricketers. South African Med. J. 83.

Stretch, R.A., 1989. Injuries to South African Cricketers playing at first-class level. J. South African Sport. Med. Assoc. 4.

Subic, A., Takla, M., Kovacs, J., 2005. Modelling and analysis of alternative face guard designs for cricket using finite element modelling. Sport. Eng. 8, pp. 209–222.

Takhounts, E., Crandall, J., Darvish, K., 2003. On the importance of nonlinearity of the brain tissue under large deformations. Stapp Car Crash J. 47, pp. 79–92.

Takhounts, E., Ridella, S., Hasija, V., Tannous, R., Campbell, J.Q., Malone, D., Danelson, K.A., Stitzel, J., Rowson, S., Duma, S.M., 2008. Investigation of traumatic brain injuries using the next generation of simulated injury monitor (SIMon) finite element head model. Stapp Car Crash J. 52, pp. 1–31.

Takhounts, E.G., Craig, M.J., Moorhouse, K., McFadden, J., Asija, V., 2013. Development of brain injury criteria (BrIC). Stapp Car Crash J. 57, pp. 243–266.

Temple, R., 1982. Cricket injuries: fast pitches change the gentleman's sport. Physician Sport. Med. 10, pp. 186–192.

Thali, M.J., Kneubuehl, B.P., Zollinger, U., Dirnhofer, R., 2002. The "Skin-skull-brain model": a new instrument for the study of gunshot effects. Forensic Sci. Int. 125, pp. 178–189.

Theilen, T.-M., Mueller-Eising, W., Wefers Bettink, P., Rolle, U., 2016. Injury data of major international field hockey tournaments. Br. J. Sports Med. 50, pp. 657–660. doi:10.1136/bjsports-2015-094847

Thomas, L.M., Hodgson, V.R., 1969. Mechanisms of head and neck injury.

Urbin, M.A., Fleisig, G.S., Abebe, A., Andrews, J.R., 2013. Associations between timing in the baseball pitch and shoulder kinetics, elbow kinetics and ball speed. Am. J. Sports Med. 41, pp. 336–342.

van Dommelem, J., van der Sande, T., Hrapko, M., Peters, G., 2010. Mechanical properties of brain tissue by indentation: interregional variation. J. Mech. Behav. Biomed. Mater. 3, pp. 158–166.

van Lierde, C., Depreitere, B., Vander Sloten, J., van Auderkercke, R., Van der Perre, G., Goffin, J., 2003. Skull biomechanics: The energy absorbability of the human skull frontal bone during fracture under quasi-static loading. J. Appl. Biomater. Biomech. 1, pp. 194–199.

van Sint Jan, S., 2007. Colour atlas of skeletal landmark definitions. Elsevier.

Versace, J., 1971. A review of the Severity Index. Proc. 15th Stapp Car Crash Conf. SAE Technical Paper 710881. doi:10.4271/710881

Viano, D.C., Casson, I.R., Pellman, E.J., Bir, C.A., Zhang, L., Sherman, D.C., Boitano, M.A., 2005a. Concussion in professional football: Comparison with boxing head impacts - Part 10. Neurosurgery 57, pp. 1154–1170. doi:10.1227/01.NEU.0000187541.87937.D9

Viano, D.C., Casson, I.R., Pellman, E.J., Zhang, L., King, A.I., Yang, K.H., 2005b. Concussion in professional football: Brain responses by finite element analysis: Part 9. Neurosurgery 57, pp. 891–915. doi:10.1227/01.NEU.0000186950.54075.3B

Viano, D.C., McClearly, J.D., Andrzejak, D. V, Janda, D., 1993. Analysis and comparison of head impacts using baseballs of various hardness and a Hybrid III dummy. Clin. J. Sport Med. pp. 217-228.

Walilko, T.J., Viano, D., Bir, C.A., 2005. Biomechanics of the head for Olympic boxer punches to the face. Br. J. Sports Med. 39, pp. 710–719.

Walker, L.B., Harris, E.H., Pontius, U., 1973. Mass, volume, center of mass, and mass moment of inertia of head and head and neck of human body, in: Stapp Car Crash Conference. pp. 525–538.

Walsh, E.S., Rousseau, P., Hoshizaki, T.B., 2011. The influence of impact location and angle on the dynamic impact response of a Hybrid III headform. Sport. Eng. 13, pp. 135–143. doi:10.1007/s12283-011-0060-9

Weightman, D., Browne, R., 1971. Injuries in eleven selected sports. Br. J. Sports Med. pp. 136-141

Wilberger, J.E., 1993. Minor Head Injuries in American Football. Sport. Med. 15, pp. 338–343. doi:10.2165/00007256-199315050-00005

Winter, D.A., 1990. Biomechanics and motor control of human movement. John Wiley & Sons, New York.

Wood, J.I., 1971. Dynamic response of human cranial bone. J. Biomech. 4, pp. 1–12.

Wu, J., Dong, R., Smutz, W., Schopper, A., 2003. Nonlinear and viscoelastic characteristics of skin under compression: experiment and analysis. Bio-Medical Mater. Eng. 13, pp. 373–385.

Yang, N., Rodowicz, K., Dainty, D., 2014. Baseball Head Impacts to the Non-Helmeted and Helmeted Hybrid III ATD, in: ASME 2014 International Mechanical Engineering Congress and Exposition. Montreal, Canada.

Yeni, Y., Brown, C., Norman, T., 1998. Influence of bone composition and apparent density on fracture toughness of the human femur and tibia. Bone 22, pp. 79–84.

Yoganandan, N., Pintar, F.A., Zhang, J., Baisden, J.L., 2009. Physical properties of the human head: Mass, center of gravity and moment of inertia. J. Biomech. 42, pp. 1177–1192. doi:10.1016/j.jbiomech.2009.03.029

Zagelbaum, B., Hersh, O., Donnenfeld, D., Perry, H., Hochman, M., 1994. Ocular trauma in Major League Baseball players. N. Engl. J. Med. 330, pp. 1021–1023.

Zanetti, K., Post, A., Karton, C., Kendall, M., Hoshizaki, T.B., Gilchrist, M.D., 2013. Identifying injury characteristics for three player positions in American Football using physical and finite element modelling reconstructions, in: IRCOBI 2013.

Zazryn, T., Finch, C., McCrory, P., 2003a. A 16-year study ofinjuries to professional boxers in the state of Victoria, Australia. Br. J. Sports Med. 37, pp. 321–324.

Zazryn, T., Finch, C., McCrory, P., 2003b. A 16-year study of injuries to professional kickboxers in the state of Victoria, Australia. Br. J. Sports Med. 37, pp. 448–451.

Zhang, J., Yoganandan, N., Pintar, F.A., Gennarelli, T.A., 2006. Role of translational and rotational accelerations on brain strain in lateral head impact. Biomed. Sci. Instrum. 42, pp. 501–506.

Zhang, L., Yang, K.H., King, A.I., 2004. A proposed injury threshold for mild traumatic brain injury. J Biomech Eng 126, pp. 226–236. doi:10.1115/1.1691446

Zhang, L., Yang, K.H., King, A.I., 2001. Comparison of brain responses between frontal and lateral impacts by finite element modelling. J. Neurotrauma 18.

Zou, H., Kleiven, S., Schmiedeler, J., 2007. The effect of brain mass and moment of inertia on relative brain-skull displacement during low-severity impacts. Int. J. Crashworthiness2 12, pp. 341–353.